

**Analysis of the interaction between
the 2C protein of parechoviruses
and lipid droplets**

Ali Aidarous Khrid

A thesis submitted for the degree of Doctor of Philosophy

School of Biological Sciences

University of Essex

October 2016

ABSTRACT

Picornaviruses are non-enveloped, positive sense single-stranded RNA viruses which cause many diseases ranging from slight illness to fatal meningitis and encephalitis. There are no vaccines against most picornaviruses so drugs need to be developed. Human parechoviruses (HPeVs) are being increasingly recognised as important human pathogens, but are genetically diverse from other picornaviruses. We therefore need to understand the details of virus replication to improve the opportunities to develop antiviral drugs. Viruses often rearrange the ER, ERGIC and Golgi to give a new membrane structures involved in viral replication and/or assembly. To improve our understanding of HPeV replication, we first studied the secretory pathway compartments and we found in HPeV-infected cells that the Golgi was rearranged and became more concentrated near to the replication complex. ER seemed to disappear almost completely. In terms of HPeV non-structural proteins, 2C had a major effect on the compartments and also co-localised and aggregated lipid droplets. Many viruses such as hepatitis C virus (HCV) and Dengue virus recruit lipid droplets to replication complexes. We found that lipid droplets became larger in HPeV-infected cells, but do not co-localise with replication complexes. To investigate the interaction between 2C and lipid droplets we made several 2C mutants. Mutation of NTPase domain of 2C did not change the interaction with lipid droplets. Instead we found that other domains, including a novel amphipathic helix are important. The results suggest that lipid droplets play a role in HPeV replication and so we investigated the effect of drugs which target lipid droplet formation and lipid homeostasis on HPeV replication. We demonstrated that drugs which target the enzyme DGAT1, which is involved in lipid droplet formation, have a potent effect on HPeV replication. Our results suggest that blocking lipid droplet formation is could be an important strategy for the treatment of HPeV infection.

ACKNOWLEDGEMENTS

All praise is due to Almighty ALLAH, whose mercy and knowledge surround every single known matter and even those beyond our perception in this universe. Then peace and blessing be upon Prophet Muhammad (peace be upon him).

I would like to express my sincere gratitude to my supervisors Prof. Glyn Stanway for his guidance, patience, motivation, support and helped all the time throughout this study. Very warm thanks to DR. Metodi Metodiev for his invaluable advice and comments.

I would like to express my deepest appreciation to all of the people who have provided me with helpful advice and support, especially to virology lab colleagues Dr. Shaia Al Malki, Dr. Arsalan Salimi, Dr Naseebah Baeshen, Dr Ashjan Shami, Miss Cheryl Eno-Ibanga, Miss Marina Ioannou, Mr Osamah Abdullah, Mrs Natalie Gray and Mrs. Hannah Adams. Thanks also go to Mrs Rana Al Ghamdi for her help with the confocal microscopy.

My heartfelt gratitude goes to the most loving people in my life, my parents for giving me generous care and support in each stage of my life. I would like to extend my sincerest thanks to my wife and children, my brothers and my sister for their sincere prayers and support.

As this project was generously funded by the government of the Kingdom of Saudi Arabia through Ministry of Health, I am sincerely grateful to them for the financial support throughout my study.

Table of Contents

ABSTRACT	i
ACKNOWLEDGEMENTS	ii
LIST OF TABLES	IX
TABLE OF FIGURES	X
LIST OF ABBREVIATIONS	XIII
CHAPTER ONE	1
INTRODUCTION	1
1.1 Picornaviruses	1
1.1.1 Classification	1
1.1.2 Medical importance	2
1.1.2.1 Human picornavirus	2
1.1.2.1.1 Poliovirus (PV)	2
1.1.2.1.2 Coxsackievirus and Echovirus	2
1.1.2.1.3 Enterovirus 71 (EV71)	3
1.1.2.1.4 Human Rhinovirus (HRV)	3
1.1.2.1.5 Hepatovirus	4
1.1.2.1.6 Parechoviruses	4
1.1.2.1.7 Other human viruses	5
1.1.2.2 Non-human picornavirus	6
1.1.2.2.1 Foot-and-mouth-disease virus (FMDV)	6
1.1.2.2.2 Other non-human picornaviruses	6
1.1.3 Picornavirus Molecular Biology	6
1.1.3.1 Particle and Genome	6
1.1.3.2 Enteroviruses	9
1.1.3.3 Parechoviruses	10
1.1.4 The picornaviral life cycle	11
1.1.4.1 Summary	11
1.1.4.2 Entry	11
1.1.4.3 Translation	13
1.1.4.4 Polyprotein processing	13

1.1.4.5	Replication.....	14
1.1.4.6	Assembly, Maturation and Release	17
1.1.5	Non-structural proteins	17
1.1.5.1	Genome.....	17
1.1.5.2	2A, 3C and L protein	17
1.1.5.3	2B	19
1.1.5.4	2C and 2BC	19
1.1.5.5	3A and 3AB	20
1.1.5.6	3CD.....	22
1.1.5.7	3Dpol.....	22
1.2	Secretory pathway	23
1.2.1	Introduction.....	23
1.2.2	Endoplasmic reticulum (ER).....	23
1.2.3	Transitional ER (tER) or ER exit sites (ERES).....	24
1.2.4	The ER-Golgi intermediate compartment (ERGIC).....	25
1.2.5	Golgi	25
1.2.5.1	Transport to the Golgi	25
1.2.5.2	Transport through Golgi	26
1.2.5.3	Transport from the Golgi.....	26
1.2.6	Coated vesicles proteins.....	26
1.2.6.1	COPII vesicles.....	26
1.2.6.2	COPI vesicles.....	27
1.3	Lipids	29
1.3.1	Lipid droplets (LDs).....	29
1.3.1.1	Lipid droplets formation.....	32
1.3.1.2	Lipid droplet growth	33
1.3.1.3	Lipid droplet proteins	33
1.3.1.4	Lipid droplet catabolism	36
1.3.1.5	Lipid droplets interact with other organelles	37
1.3.1.5.1	The Endoplasmic Reticulum (ER)	37
1.3.1.5.2	Endosomes	37
1.3.1.5.3	Mitochondria and peroxisomes.....	38
1.3.1.5.4	COPI and COPII	38
1.3.1.6	Lipid droplets and disease	38

1.3.2	Diacylglycerol acyltransferase (DGAT) enzymes	39
1.4	Role of cellular lipid in viral infections	40
1.4.1	Entry	40
1.4.2	Replication.....	41
1.4.3	Assembly	42
1.5	Remodelling of secretory pathway in viral infection	43
1.6	Antiviral Drugs.....	45
1.6.1	Antiviral drugs targeting lipids.....	46
	Aims	49
	CHAPTER TWO.....	50
	MATERIALS AND METHODS	50
2.1	Materials	51
2.1.1	Chemicals and Reagents	51
2.1.1.1	Cell culture	51
2.1.1.2	Virology	51
2.1.1.3	Imaging.....	52
2.1.1.4	Molecular biology.....	53
2.1.2	Solution and buffers	55
2.1.2.1	Phosphate buffered saline buffer	55
2.1.2.2	HEPES buffer.....	55
2.1.2.3	Carboxy methyl cellulose (CMC).....	55
2.1.2.4	Crystal violet solution	59
2.1.2.5	Blocking solution	59
2.1.2.6	Fixing solution	59
2.1.2.7	Permeabilization solution.....	59
2.1.2.8	Antibody diluent solution	59
2.1.2.9	Glycine washing solution	59
2.1.2.10	DNA electrophoresis buffer (ELFO).....	59
2.1.2.11	Clear loading dye for agarose gels	59
2.1.2.12	Mowiol mounting medium	60
2.1.2.13	Isopropyl β -D-thiogalactopyranoside (IPTG) solution.....	60
2.1.2.14	5-Bromo-4-chloro-3-indolyl β -D-galactopyranoside (X-Gal) solution	60
2.1.2.15	Luria-Bertani Broth (LB Broth)	60
2.1.2.16	Luria-Bertani Agar.....	60

2.1.3	Cell lines and viruses	60
2.2	Methods	62
2.2.1	Cell Culture	62
2.2.1.1	Passaging/Splitting Cells	62
2.2.1.2	Cell line storage	62
2.2.2	Molecular biology.....	63
2.2.2.1	Double digestion	63
2.2.2.2	Agarose gels	63
2.2.2.3	Gel extraction	63
2.2.2.4	Ligation of DNA fragments using T4 DNA ligase	64
2.2.2.5	Competent cells.....	64
2.2.2.6	Transformation.....	64
2.2.2.7	Purification of DNA using QIAprep miniprep kit	65
2.2.2.8	Purification of DNA using a Qiagen HiSpeed plasmid midi kit	65
2.2.2.9	Polymerase chain reaction (PCR).....	66
2.2.2.10	Ligation using the pGEM-T Easy vector.....	67
2.2.2.11	Transformation using the pGEM-T Easy vector	67
2.2.2.12	Colony PCR	70
2.2.2.13	Purification of viral RNA using a QIAamp Viral RNA Mini Kit	70
2.2.2.14	Reverse transcription-PCR (RT-PCR)	72
2.2.3	Virus propagation and plaque assays	72
2.2.3.1	Propagation of Viruses	72
2.2.3.2	Plaque assay	72
2.2.4	Drugs and generation of mutants resistant to drugs.....	73
2.2.4.1	Drugs and inhibitors screening study	73
2.2.4.2	Generation of mutants resistant to drugs and inhibitors	73
2.2.4.3	Time-of-addition assay	73
2.2.5	Immunofluorescence.....	74
2.2.5.1	Detection of infected cells and lipid staining.....	74
2.2.5.2	Detection of infected cells and fatty acids staining	74
2.2.5.3	Transfection of fluorescent constructs	75
2.2.5.3.1	Xfect protein transfection reagent	75
2.2.5.3.2	Lipofectin [®] transfection reagent	75
2.2.5.3.3	TurboFect transfection reagent.....	76

2.2.5.4	Confocal microscope	76
2.2.6	Computer analysis	78
	CHAPTER THREE	79
	EFFECT OF HPeV INFECTION AND HPeV PROTEINS ON THE SECRETORY SYSTEM	79
3.1	Introduction	80
3.2	The effect of HPeV1 infection on the secretory pathway	83
3.3	Distribution of HPeV1 non-structural proteins	88
3.4	Non-structural proteins of HPeV1 and the secretory pathway	98
3.4.1	The ER marker (PDI)	98
3.4.2	The ERGIC	98
3.4.3	The Golgi	99
3.4.4	Lysosomes	99
3.4.5	Mitochondria	100
3.4.6	Peroxisomes	100
3.5	Discussion.....	113
	CHAPTER FOUR.....	117
	THE INTERACTION BETWEEN HPeV 2C AND LIPID DROPLETS	117
4.1	Introduction	118
4.2	Fatty acid study	119
4.2.1	Virus and fatty acids	119
4.2.2	Non-structural proteins of HPeV1 and fatty acid.....	120
4.3	Lipid droplets study	125
4.3.1	Lipid Droplets and viruses	125
4.3.2	Non-structural proteins of HPeV1	130
4.4	2C protein and LD	135
4.4.1	2C of other picornaviruses.....	135
4.4.2	ATPase activity site of 2C and LD	138
4.4.3	2C fragment and LDs	138
4.4.4	Location of the LD-interacting region of 2C.....	152
4.4.5	Cav1 and 2C of HPeV1	161
4.4.6	ADRP and 2C of HPeV1	161
4.5	Discussion.....	166
	CHAPTER FIVE.....	170
	ANTIVIRAL DRUGS STUDY	170

5.1	Introduction	171
5.1.1	Itraconazole.....	172
5.1.2	Brefeldin A.....	172
5.1.3	Diacylglycerol acyltransferase inhibitor.....	173
5.1.4	Betulinic acid	173
5.2	Immunofluorescence study	175
5.3	Plaque assay	179
5.4	Screening study of drugs	179
5.5	Time-of-addition study.....	188
5.6	Attempts to generate drug resistant mutants.....	188
5.7	Discussion.....	191
	CHAPTER SIX.....	196
	GENERAL DISCUSSION.....	196
	Future Work.....	201
	REFERENCES	204

LIST OF TABLES

Table 1.1: Summary of potential antiviral drugs which target cellular lipids.....	48
Table 2.1: List of antibodies and labels that were used and their types and supplier.....	54
Table 2.2: List of restriction enzymes that were used and their target sequence and supplier..	56
Table 2.3: List of oligonucleotides used in this project.....	57
Table 2.4: List of EGFP/ m-Cherry fusion constructs used.....	58
Table 5.1: List of all concentration of drugs that used in this study.....	180

TABLE OF FIGURES

Chapter 1

FIGURE 1.1: Structural of picornaviruses.....	7
FIGURE 1.2: 3D structure for some picornaviruses.....	8
FIGURE 1.3: Summary of the life cycle of a typical picornavirus.....	15
FIGURE 1.4: Schematic of a picornavirus genome.....	16
FIGURE 1.5: Schematic diagram of the 2C protein of EV71.....	21
FIGURE 1.6: Schematic of the secretory pathway.....	28
FIGURE 1.7: The structure of a lipid droplet.....	30
FIGURE 1.8: Lipid metabolism and LD formation in mammal and yeast.....	31
FIGURE 1.9: Some of LD formation models.....	34

Chapter 2

FIGURE 2.1: Schematic diagram of the PCR reaction.....	68
FIGURE 2.2: Schematic diagram of overlap PCR.....	69
FIGURE 2.3: Schematic diagram of the Colony PCR reaction.....	71

Chapter 3

FIGURE 3.1: The effect of HPeV1 infection on the Golgi marker GM130.	85
FIGURE 3.2: The effect of CAV9 infection on the Golgi marker GM130.....	85
FIGURE 3.3: The effect of HPeV1 infection on the ER marker PDI	86
FIGURE 3.4: The effect of HPeV1 infection on the ERGIC marker ERGIC-53	87
FIGURE 3.5: Schematic of the HPeV1 genome representing the location of the proteins 2A, 2BC, 2B, 2C, 3A and 3C in the polyprotein.....	90
FIGURE 3.6: The distribution of EGFP expressed from the pEGFP-C1 vector	91
FIGURE 3.7: The distribution of mCherry expressed from the pmCherry-C1 vector.....	91
FIGURE 3.8: The distribution of HPeV1 2A protein.....	92
FIGURE 3.9: The distribution of HPeV1 2B protein.....	93
FIGURE 3.10: The distribution of HPeV1 3A protein.....	94
FIGURE 3.11: The distribution of HPeV1 3C protein.....	95
FIGURE 3.12: The distribution of HPeV1 2C protein.....	96
FIGURE 3.13: The distribution of HPeV1 2BC protein.....	97
FIGURE 3.14: The effect of HPeV1 proteins (fused to mCherry) on the ER marker PDI	101
FIGURE 3.15: The effect of HPeV1 proteins (fused to EGFP) on the ER marker PDI.....	102

FIGURE 3.16: The effect of HPeV1 proteins (fused to mCherry) on the ERGIC	103
FIGURE 3.17: The effect of HPeV1 2BC fused to EGFP on the ERGIC	104
FIGURE 3.18: The effect of HPeV1 proteins (fused to mCherry) on the Golgi	105
FIGURE 3.19 The normal distribution of lysosomes.....	106
FIGURE 3.20: The effect of HPeV1 proteins (fused to mCherry) on lysosomes	107
FIGURE 3.21: The normal distribution of mitochondria.....	108
FIGURE 3.22: The effect of HPeV1 proteins (fused to mCherry) on mitochondria	109
FIGURE 3.23 The normal distribution of peroxisomes.....	110
FIGURE 3.24: The effect of HPeV1 proteins (fused to mCherry) on peroxisomes	111
FIGURE 3.25: The effect of HPeV1 infection on the peroxisomes.....	112
FIGURE 3.26: The effect of CAV-9 infection on the peroxisomes.....	112
Chapter 4	
FIGURE 4.1: The normal distribution of fatty acids (FAs) in GMK cells.....	121
FIGURE 4.2: The effect of CAV9 on fatty acids (FAs)	122
FIGURE 4.3: The effect of HPeV1 on fatty acids (FAs).....	123
FIGURE 4.4: The localisation of fatty acids (FAs) in cells transfected with constructs encoding HPeV1 proteins fused to mCherry	124
FIGURE 4.5: The effect of CAV9 on lipid droplets (LDs) in early stages of infection	126
FIGURE 4.6: The effect of CAV9 on lipid droplets (LDs) in late stage of infection.....	127
FIGURE 4.7: The effect of HPeV1 on lipid droplets (LDs) in early stage of infection.....	128
FIGURE 4.8: The effect of HPeV1 on on lipid droplets (LDs) in late stage of infection.....	129
FIGURE 4.9: Lipid droplets (LDs) and pmCherry-C1 vector.....	131
FIGURE 4.10: The effect of mCherry-2A and mCherry-3C on lipid droplets (LDs).....	132
FIGURE 4.11: The effect of mCherry-2B, mChery-2C and mCherry-3A on lipid droplets (LDs).....	133
FIGURE 4.12: The effect of EGFP-2BC on lipid droplets (LDs).....	134
FIGURE 4.13: A neighbor-joining tree based on 2C nucleotide sequences of some members of the <i>Picornaviridae</i> family.....	136
FIGURE 4.14: Relationship of mCherry-2C of CAV9 and HRV1B with lipid droplets (LDs)	137
FIGURE 4.15: Multiple sequence alignment of the amino acid sequences of 2C in several membrans of the <i>Picornaviridae</i> family using protein BLAST	140
FIGURE 4.16: The effect of Walker A and Walker B mutations in HPeV1 2C on lipid droplets (LDs).....	144
FIGURE 4.17: The effect of combining Walker A and Walker B mutations in HPeV1 2C on lipid droplets (LDs).....	145
FIGURE 4.18: Co-transfection of pmCherry-2CK and pmCherry-2CD mutants with pEGFP-2C.....	146
FIGURE 4.19: Schematic diagram showing the regions of the 2C protein encoded in three mutants.....	147

FIGURE 4.20: The distribution and effect of pmCherry-2C1, pmCherry-2C2 and pmCherry-2C4 deletion mutants on lipid droplets (LDs).....	148
FIGURE 4.21: Co-transfection of pmCherry-2C1, pmCherry-2C2 and pmCherry-2C4 mutants with pEGFP-2C.....	149
FIGURE 4.22: Co-transfection of pmCherry-2C1 and pmCherry-2C2 with pEGFP-2C and pmCherry-2C1 with pEGFP-2C2.....	150
FIGURE 4.23: The effect of pmCherry-2C12 mutant on lipid droplets (LDs)	151
FIGURE 4.24. The predicted region of amphipathic helix in HCV, PV and HPeV1.....	154
FIGURE 4.25. The part of the HPeV1 2C protein located in a set of mCherry-2C deletion mutant.....	155
FIGURE 4.26: The effect of pmCherry-2C7A and pmCherry-2C25A mutants on lipid droplets (LDs) distribution	156
FIGURE 4.27: The effect of pmCherry-2C53A and pmCherry-2C75A mutants on lipid droplets (LDs) distribution	157
FIGURE 4.28: Co-transfection for pmCherry-2C53A and pmCherry-2C75A to pEGFP-2C...	158
FIGURE 4.29: The effect of pmCherry-2C87A and pmCherry-2C129A mutants on lipid droplets (LDs) distribution	159
FIGURE 4.30: A. A predicted amphipathic helix overlapping the region found to be important in HPeV 2C LD localisation.....	160
FIGURE 4.31: The effect of pmCherry-2C87A and pmCherry-2C129A mutants on lipid droplets (LDs) distribution	162
FIGURE 4.32: Co-transfection of pmCherry-Cav1 and pEGFP-2C	163
FIGURE 4.33: pmCherry-ADRP and lipid droplets (LDs).....	164
FIGURE 4.34: Co-transfection of pmCherry-ADRP and pEGFP-2C/pEGFP-2BC	165
Chapter 5	
FIGURE 5.1: Chemical structure of drugs and inhibitor used in this study.....	174
FIGURE 5.2: The effect of drugs and inhibitor on HPeV1 and CAV9 using immunofluorescent microscope.....	176
FIGURE 5.3: The bar chart of microscopy study of HPeV1 treated with drugs.....	177
FIGURE 5.4: The bar chart of microscopy study of CAV9 treated with drugs.....	178
FIGURE 5.5: Plaque assays of CAV9 (GMK cells) and HPeV1 (HT29 cells).....	181
FIGURE 5.6: An example of a plaque assay for HPeV1 treated with DGAT inhibitor A922500.....	182
FIGURE 5.7: An example of a plaque assay for CAV9 treated with DGAT inhibitor A922500.....	183
FIGURE 5.8: Bar chart of plaque assays done to measure the amount of virus produced at different drug concentrations, when the DGAT inhibitor A922500 was used...	184
FIGURE 5.9: Bar chart of plaque assays done to measure the amount of virus produced at different drug concentrations, when the Betulinic acid was used.....	185
FIGURE 5.10: Bar chart of plaque assays done to measure the amount of virus produced at different drug concentrations, when Itraconazole was used.....	186
FIGURE 5.11: Bar chart of plaque assays done to measure the amount of virus produced at different drug concentrations, when Brefeldin A was used.....	187
FIGURE 5.12: Graph of HPeV titre obtained after drug was added at different times before (zero time) or after infection.....	189
FIGURE 5.13: Graph of CAV9 titre obtained after drug was added at different times before (zero time) or after infection.....	190

LIST OF ABBREVIATIONS

(m⁷G) cap structure	the 5` 7-methyl guanosine
2A^{pro}	Protease
3C^{pro}	Protease
3CD^{pro}	Protease
3D^{pol}	RNA polymerase
ACBD3	Acyl-coenzyme A Binding Domain Containing 3
Acyl- CoA	Acyl-coenzyme A
ADRP	Adipose differentiation-related protein
AGPAT2	Acylglycerol-Phosphate Acyltransferase
AiV	Aichi virus
Arf6	ADP-ribosylation factor 6
ATGL	A dipose tissue triacylglycerol lipase
ATPase	Adenosine triphosphatase
BetA	Betulinic acid
BFA	Brefeldin A
BMV	Brome Mosaic virus
CAR	Coxsackie-adenovirus receptor
CAV1	Caveolin 1
CAV9	Coxsackievirus A9
CGN	Cis-Golgi network
CMC	Carboxyl methylcellulose
CNS	Central nervous system
COPD	Obstructive Pulmonary Disease
COPI	Coated vesicles proteins I
COPII	Coated vesicles proteins II
CVB3	Coxsackievirus B3
DAF or CD55	Decay accelerating factor
DAPI	4',6-Diamidino-2-phenylindole dihydrochloride
DCV	Drosophila C virus
DGAT	Diacylglycerol acyltransferase
DGAT inhibitor	Diacylglycerol acyltransferase inhibitor (A922500)
DLP	Double-layer particle
DMEM	Dulbecco's Modified Eagle's Medium
dsRNA	Double-stranded RNA
<i>E.coli</i>	<i>Escherichia coli</i>
EGFP	Enhanced green fluorescent protein

eIF4E	Eukaryotic translation-initiation factor 4E
eIF-4F	Eukaryotic initiation factor 4F
EMCV	Encephalomyocarditis virus
ER	Endoplasmic reticulum
ERES	ER exit sites site
ERGIC	ER-Golgi intermediate compartment
EV	Enterovirus
FASN	Fatty Acid Synthase
FBS	Fetal Bovine Serum
FITM/FIT	Fat storage–Inducing Transmembrane Protein
FMDV	Foot-and-mouth disease virus
GEFs	Guanine nucleotide exchange factors
GMK	Green Monkey Kidney cell line
GTP	Guanosine-5'-triphosphate
GAP	GTPase activating proteins
HAV	Hepatitis A virus
HCMV	Human cytomegalovirus
HCV	Hepatitis C virus
HDL	High-Density Lipoprotein
HFMD	Hand, foot and mouth disease
HIV	Human ImmunoDeficiency virus
HPeV	Human Parechoviruses
HRV	Human Rhinovirus
HSPA5	Heat shock 70-kDa protein 5
HT29	Human colon adenocarcinoma cells
ICAM-1	Intercellular adhesion molecule-1
IFN	Type I interferon responses
IPV	Inactivated Poliovirus vaccines
IRES	Internal ribosome entry site
ITAFS	IRES transacting factors
ITZ	Itraconazole
kD	kilo Daltons
LAMP-1	lysosomal-associated membrane protein 1
LC3-II	LC3-phosphatidylethanolamine conjugate
LDL-R	Low Density Lipoprotein Receptor
LDs	Lipid droplets
MHC-I	Major histocompatibility complex class I
NIH	The National Institutes of Health
NPGP	Asn–Pro–Gly–Pro amino acids
OPV	Oral Poliovirus vaccine
ORF	open-reading frame

OSBP1	Oxysterol-binding protein 1
PABP	Poly (A) binding protein
PC	Phosphatidylcholine
PCBP2	Poly (rC)-binding protein
PCR	Polymerase Chain Reaction
PE	Phosphatidylethanolamine
PI4K	Phosphatidylinositol 4-kinase
PI4P	Phosphatidylinositol-4-phosphate
PM	Plasma membrane
PPARG	Peroxisome Proliferator Activated Receptor
PV	Poliovirus
PVR or CD155	poliovirus receptor
Rab	Membrane-trafficking proteins
RGD	Arginine-glycine-aspartic acid motif
RNA	Ribonucleic Acid
SARS	Severe acute respiratory syndrome
SNARE	Soluble N-Ethylmaleimide-Sensitive Factor Activating Protein Receptor
TG	Triglycerides
TGN	Trans-Golgi network
TIP47	Tail-interacting Protein of 47 kilo Daltons
UTR	Untranslated regions
VCAM-1	Vascular cell adhesion molecule-1
VP	Virus-encoded proteins
VPg	Genome-linked protein
VSV	Vesicular Stomatitis virus
WHO	The World Health Organisation
WNV	West Nile virus
YFV	Yellow Fever Virus
αSNAP	Soluble NSF Attachment Protein

CHAPTER ONE

INTRODUCTION

1.1 Picornaviruses

1.1.1 Classification

Picornaviruses, where Pico refers to ‘small size’ and rna refers to ‘ribonucleic acid’ (RNA), are assigned to class IV in the Baltimore classification (Acheson, 2007; Carter and Saunders, 2007). These small, non-enveloped, single-stranded, positive-sense viruses belong to the family *Picornaviridae* (Knowles *et al.*, 2012). At present, this family groups into 31 genera consisting of 54 species. The genera are: *Aphthovirus*, *Aquamavirus*, *Avihepatovirus*, *Avisivirus*, *Cardiovirus*, *Cosavirus*, *Dicipivirus*, *Enterovirus*, *Erbovirus*, *Gallivirus*, *Hepatovirus*, *Hunnivirus*, *Kobuvirus*, *Kunsagivirus*, *Limnipivirus*, *Megrivirus*, *Mischivirus*, *Mosavirus*, *Oscivirus*, *Parechovirus*, *Pasivirus*, *Passerivirus*, *Potamipivirus*, *Rosavirus*, *Sakobuvirus*, *Salivirus*, *Sapelovirus*, *Senecavirus*, *Sicinivirus*, *Teschovirus* and *Tremovirus* (Adams *et al.*, 2015; Adams *et al.*, 2013; Adams *et al.*, 2014; Adams *et al.*, 2016; Knowles *et al.*, 2012). Some of these genera contain several species, for instance *Enterovirus* has 12. Some species have a single virus serotype while other contain many, for instance the *Enterovirus* species *Rhinovirus A* contains 80 serotypes (Knowles, 2016). This classification was originally based on morphology, physicochemical and biological properties, antigenic structures, genomic sequence and mode of replication although genome sequence is now the only factor considered. Even serotype is usually predicted on the basis of virus sequences (Hyypia *et al.*, 1997).

The genome of members of the *Picornaviridae* family consists of RNA containing a single open reading frame that encodes for a large polyprotein. The polyprotein is processed by virus-encoded proteases to generate individual structural and non-structural proteins, as well as some relatively stable cleavage intermediates (Wessels *et al.*, 2006).

Picornaviruses include many economically and socially important pathogens of humans and animals, such as poliovirus, enterovirus 71, rhinoviruses, hepatitis A virus, foot-and-mouth disease virus and parechoviruses (van der Linden *et al.*, 2015; Whitton *et al.*, 2005).

1.1.2 Medical importance

The *Picornaviridae* family contains a wide variety of human and animal pathogens with varying clinical features including respiratory symptoms, gastroenteritis, myocarditis, rashes and infections of the central nervous system such as meningitis, encephalitis and paralysis (Merilahti *et al.*, 2012).

1.1.2.1 Human picornavirus

1.1.2.1.1 Poliovirus (PV)

The most significant picornavirus is poliovirus (PV). PV belongs to the *Enterovirus* genus and causes poliomyelitis. Poliomyelitis is actually a relatively rare complication of poliovirus infection as only around 1% of infections lead to this condition. Even so, epidemics of poliomyelitis have killed or paralysed many hundreds of thousands of people over the past 200 years before vaccinations became available in the mid-1950s (Jurgeit *et al.*, 2010; Whitton *et al.*, 2005). PV spreads by the faecal–oral route, passes through the stomach and replicates in the intestine. In the case of poliomyelitis, the virus enters the blood stream then infects the anterior spinal cord. The development of both live attenuated oral poliovirus vaccine (OPV) and inactivated poliovirus vaccine (IPV) against the 3 poliovirus serotypes reduced the number of infected patients dramatically. The World Health Organisation (WHO) has been attempting to complete the eradication of poliovirus for a number of years. Currently, wild poliovirus (only serotype 1) is circulating only in Pakistan and Afghanistan but there are also cases of circulating virus which has been derived from the vaccine strains (Dunn *et al.*, 2015; Initiative, 2015).

1.1.2.1.2 Coxsackievirus and Echovirus

A second group of viruses of the *Enterovirus* genus is coxsackievirus (A and B). The first isolation of group A was in Coxsackie, New York, from a young boy suffering from acute flaccid paralysis. Group B was isolated from a patient with aseptic meningitis (Whitton *et al.*, 2005). Many coxsackievirus B infections are mild, but these viruses can also cause serious, even

fatal diseases affecting the heart, central nervous system (CNS) and pancreas, leading to myocarditis meningitis, encephalitis in new-borns and pancreatitis (Hyypia and Stanway, 1993; Stanway *et al.*, 2000; Whitton *et al.*, 2005). Coxsackie A viruses cause respiratory infections, conjunctivitis, rashes, meningoencephalitis, while coxsackievirus A16 causes hand, foot and mouth disease (HFMD) (Hyypia and Stanway, 1993; Stanway *et al.*, 2000).

Echoviruses are another group of viruses in the *Enterovirus* genus and are one of the most frequent causes of aseptic meningitis. They can also be involved in meningoencephalitis, paralysis, neonatal sepsis and gastrointestinal infections. Echovirus 9,11 and 30 are the most commonly isolated enteroviruses in specimens from all patients (Khetsuriani *et al.*, 2006).

1.1.2.1.3 Enterovirus 71 (EV71)

EV71 is another cause of HFMD in young children and infants. EV71 HFMD is usually a mild disease with a localized rash and fever. However, in more severe cases these can be neurological complications, including aseptic meningitis, acute flaccid paralysis, fatal encephalitis, and pulmonary edema (Lei *et al.*, 2011; Shang *et al.*, 2013). The virus was isolated for the first time in 1974 and there have been several large outbreaks since then, particularly in Asia. Epidemic outbreaks of HFMD occur frequently in Singapore, Taiwan, Malaysia and China (Gopalkrishna *et al.*, 2012; Kiener *et al.*, 2012). More than 1,600,000 cases of EV71 infection, with more than 500 deaths, were reported in China in 2011 (Shang *et al.*, 2013).

1.1.2.1.4 Human Rhinovirus (HRV)

HRV is the most frequent cause of the common cold. This disease is usually mild but has an important economic impact. But it is also associated with acute and chronic bronchitis and other respiratory tract illnesses, as well as making asthma symptoms more severe. The National Institutes of Health in the USA, estimate that more than a billion cases of the common cold occur annually, resulting from HRV infections, costing approximately \$40 billion in health care every year (Jurgeit *et al.*, 2010; Whitton *et al.*, 2005). HRV infections also make symptoms worse in

patients with chronic obstructive pulmonary disease (COPD) (Jurgeit *et al.*, 2010; Wanga and Chen, 2007; Whitton *et al.*, 2005). WHO predicts that COPD will become the third leading cause of death worldwide by the year 2030 (van der Schaar *et al.*, 2013).

1.1.2.1.5 Hepatovirus

Hepatitis A virus (HAV) is member of the *Hepatovirus* genus. It is responsible for a relatively mild form of human hepatitis where an acute illness gives symptoms including jaundice or elevated serum transaminase levels (De Palma *et al.*, 2008). HAV does not lead to liver cirrhosis and hepatocellular carcinoma as it gives an acute, not a persistent infections unlike hepatitis B and hepatitis C (Martin and Lemon, 2006). This virus is responsible for more than 7,000 cases of hepatitis in the USA annually (De Palma *et al.*, 2008).

1.1.2.1.6 Parechoviruses

Human Parechoviruses (HPeV) are members of the species *Parechovirus A*, until recently called *Human parechovirus*. 16 types, HPeV1–HPeV16 are known (Knowles, 2016). Human parechovirus infections are common during early childhood. In the USA between 1983 and 2003, a large investigation revealed that 73% of HPeV1 infection and 68% of HPeV2 infections occurred in children less than one year (Chang *et al.*, 2015). Parechoviruses usually cause mild respiratory or gastrointestinal illness but have been reported to sometimes cause severe conditions, such as flaccid paralysis and encephalitis. These serious infections are less frequent than those caused by enteroviruses (Harvala *et al.*, 2014; Merilahti *et al.*, 2012; Seitsonen *et al.*, 2010; Wang *et al.*, 2012a). Parechovirus infections seem to occur relatively frequently, as at least 95% of the adult population in the Netherlands, the USA, Canada and Germany have been infected at some point (Harvala *et al.*, 2008). In many studies, the predominant symptom caused by HPeV1, the most commonly isolated HPeV, is diarrhoea, although two outbreaks of necrotising enterocolitis were reported in 1997. In addition, HPeV1 has been linked with

myocarditis and other diseases, including haemolytic uraemic syndrome and an outbreak of acute flaccid paralysis in Jamaica (Stanway *et al.*, 2000).

Less is known about the impact of the other HPeV types, but except for HPeV3 the symptoms caused are similar to those caused by HPeV1. HPeV6 has been suggested as a causative agent of diarrhoea in children (Harvala *et al.*, 2008). HPeV3 seem to have a different pattern of disease compared to other HPeVs, as it leads sometimes to serious disease in much younger children than most HPeVs. HPeV3 has been isolated from a one year old patient with transient paralysis in Japan and was also found in three patients with neonatal sepsis in Canada (Boivin *et al.*, 2005). Neonatal sepsis caused by HPeV3 been reported in several more recent studies (Benschop *et al.*, 2006; Harvala *et al.*, 2014; Khatami *et al.*, 2014; Kolehmainen *et al.*, 2014). HPeV4 may also be involved in neonatal sepsis (Kolehmainen *et al.*, 2014).

Although HPeV is a widespread pathogen and can cause severe diseases, it is not routinely detected in most laboratories because it often grows poorly in culture and typing reagents are not widely available (Chang *et al.*, 2015).

1.1.2.1.7 Other human viruses

Aichi virus (AiV) represents the *Kobuvirus* genus (*Aichivirus A* species), and the single serotype, AiV-1, is associated with acute gastroenteritis in humans (De Palma *et al.*, 2008). AiV-1 is distributed worldwide and has been detected in human faecal samples in Asia, Europe, South America and Africa. The symptoms of AiV-1 infection vary from diarrhoea, abdominal pain, nausea, vomiting and fever, and it is usually present, together with enteroviruses, in faecal samples of gastroenteritis patients (Kitajima and Gerba, 2015).

1.1.2.2 Non-human picornavirus

1.1.2.2.1 Foot-and-mouth-disease virus (FMDV)

Foot-and-mouth-disease virus (FMDV) is a member of the *Foot-and-mouth-disease virus* species of the *Aphthovirus* genus. This virus causes lesions in cloven-hoof animals such as cattle, swine, goat, sheep and buffalo (Grubman and Baxt, 2004; Jamal and Belsham, 2013). The disease is not usually fatal but reduces productivity and so is economically very important. FMDV caused widespread problems throughout Europe until an inactivated vaccine became commercially available. However, FMDV remains endemic in other parts of the world such as Africa and Asia. A major outbreak of the virus in the UK (2001) led to the slaughter of 6.5 million animals and cost the UK economy around £3 billion (De Palma *et al.*, 2008; Whitton *et al.*, 2005).

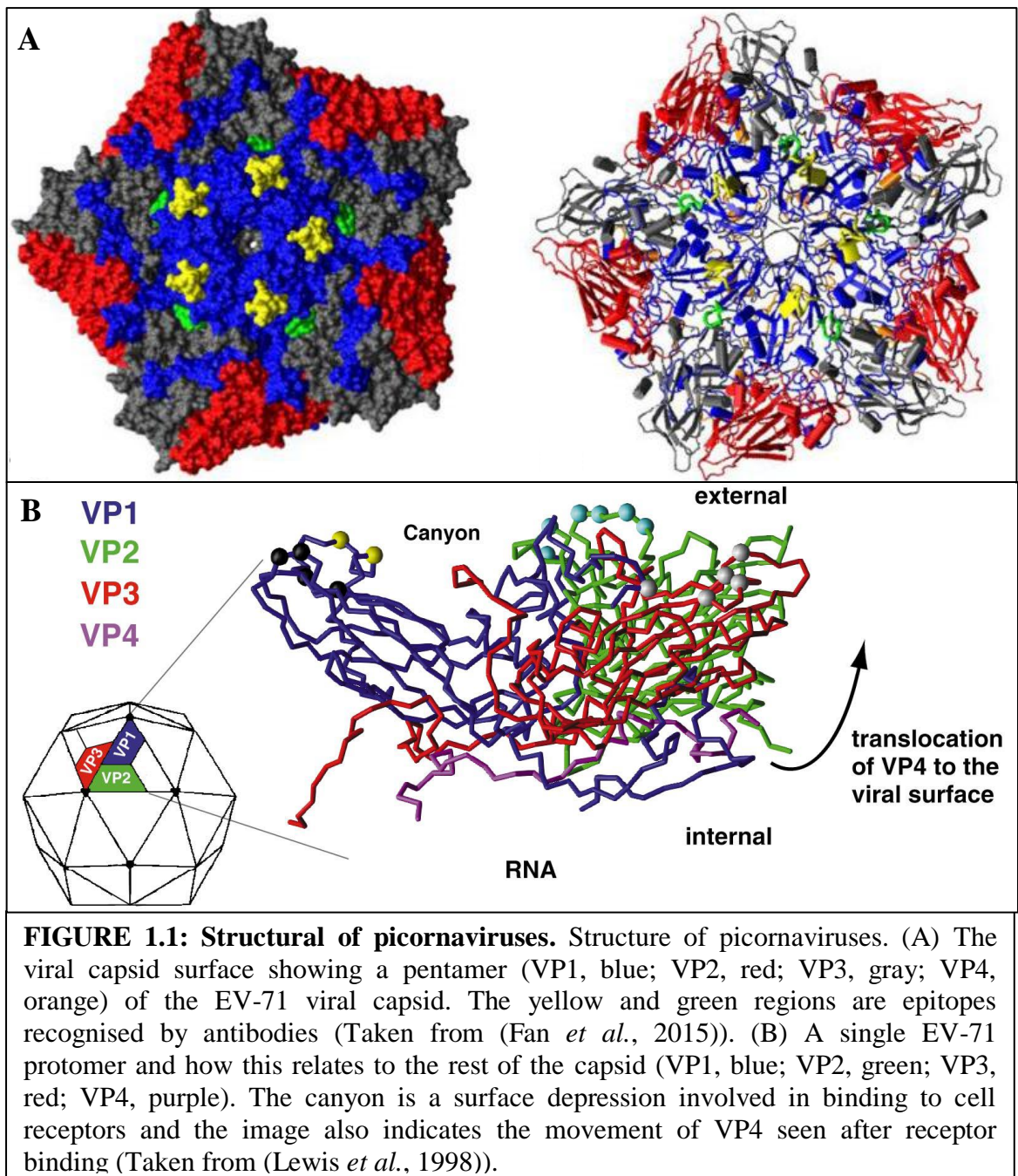
1.1.2.2.2 Other non-human picornaviruses

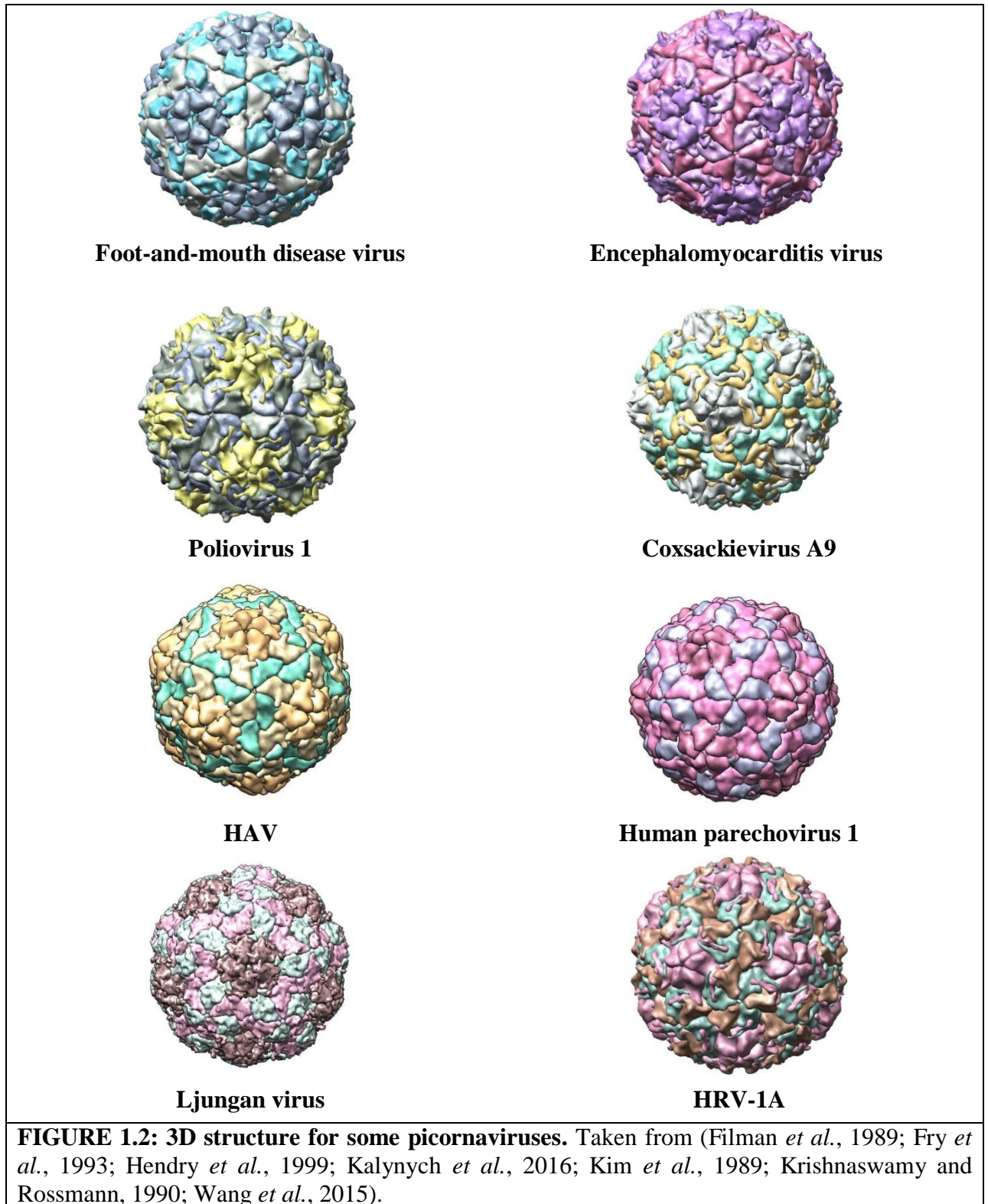
Teschoviruses can affect cattle, usually leading to asymptomatic infections. They can also cause a neurological disorder in pigs, known as Teschen-Talfan disease (De Palma *et al.*, 2008; Whitton *et al.*, 2005). Several outbreaks of ‘teschovirus encephalomyelitis’ were reported in Ukraine in 1996–2005, Russia in 2004, Madagascar in 2004–2005, Belarus in 2005 and Haiti in 2008–2009 (Boros *et al.*, 2012).

1.1.3 Picornavirus Molecular Biology

1.1.3.1 Particle and Genome

Picornaviruses are small, icosahedral, non-enveloped, positive-sense, single stranded RNA viruses of around 28-30 nm in diameter (Jurgeit *et al.*, 2010). Their protein shell is composed of 60 copies of three or four virus-encoded proteins (VP1-4 or VP0, VP1 and VP3) (Figure 1.1). While VP1-3 form the icosahedral shell, VP4 is on the inner surface and is probably partially in contact with the RNA genome (Merilahti *et al.*, 2012) (Figure 1.2). The genomes of picornaviruses are around 7000–9700 nucleotides in length and encode one polyprotein which is





cleaved by virus proteases to give a number of functionally important precursors and individual proteins. These include the capsid protein-encoding P1 region (encoding VP1-VP4) and non-structural protein-encoding P2 and P3 regions (Kitamura *et al.*, 1981; Knowles, 2016). The polyprotein-encoding open-reading frame (ORF) is preceded by a 5' untranslated regions which is covalently linked to a small viral protein (VPg) at the 5' end and followed by a 3' UTR and a poly A tail (Sasaki *et al.*, 2012). The only known exception is the *Dicripivirus* genus where the genome has two open reading frames (Woo *et al.*, 2012). Capsid monomers assemble into pentamers, which form the complete icosahedral shell of the virus from twelve pentamer subunits (Merilahti *et al.*, 2012).

After entry into the cellular cytoplasm, the virus RNA is translated and the polyprotein is cleaved. Following production of proteins required for RNA replication, the input viral RNA also acts as the template for the synthesis of negative-sense transcripts, which are then used to synthesize positive-sense genomes. Picornavirus RNA replication takes place in the cytoplasm, occurs on membrane-bound replication complexes and involves several different viral proteins in addition to the RNA polymerase (3D^{pol}) (Belsham and Normann, 2008; Jurgait *et al.*, 2010).

1.1.3.2 Enteroviruses

The *Enterovirus* genus includes PVs, coxsackie A viruses, coxsackie B viruses, echoviruses and more-recently isolated viruses which are called by species and number e.g. EV-D68 to EV-A121 (Hu *et al.*, 2011; Knowles, 2016). Members of all 12 *Enterovirus* species are closely related and share marked similarities with respect to virus structure, genomic organization and replicative cycle. Differences in tropism are assumed to be based on the ability to bind to specific receptors for cell entry, due to differences in the structural capsid proteins encoded by the P1 region of the genome, and the occurrence of host-species specific cis-acting translational control elements in the genomic RNA (van Kuppeveld *et al.*, 1997a). Some of the non-structural proteins are also involved in defining tropism e.g. the host that can be infected (Harris and Racaniello, 2005).

These viruses possess a deep depression (a 'canyon') around the fivefold axis, which is involved in receptor interactions (Rossmann, 2002).

Enterovirus genomes are between 7200-7500 nucleotides long and the polyprotein is processed to 11 final products. The 5'UTR is around 740 nucleotides long in EV-A to EV-J species and 600 nucleotides in RV-A to RV-C. Processing of the P1 region gives VP1-VP4 and the 2A protein is a protease (Bonderoff *et al.*, 2008; Hughes and Stanway, 2000; Shang *et al.*, 2013).

1.1.3.3 Parechoviruses

Human parechoviruses (HPeVs) are members of the species *Parechovirus A* (originally *Human parechovirus*) of the genus *Parechovirus*. There are two other species *Parechovirus B* (including Ljungan virus) and *Parechovirus C* (including Sebokele virus). A virus which infects ferrets may form another species (Adams *et al.*, 2015). HPeV1 and HPeV2 were isolated in 1956, were thought to be enteroviruses and were called echovirus 22 and 23 (Stanway and Hyypiä, 1999). However, several studies that investigated their molecular characteristics found that these viruses had unusual properties compared to other enteroviruses and the nucleotide sequence was found to be very different (Hyypiä *et al.*, 1992). As a result, they were reclassified as members of a new genus *Parechovirus* in 1999 (Banerjee *et al.*, 2004; Stanway and Hyypiä, 1999; Stanway *et al.*, 1994).

The *Parechovirus* genome is 7300-7600 nucleotides in length. The 5' UTR is 700 nucleotides long. The polyprotein is post-translationally cleaved to give 10 final proteins, structural proteins VP0, VP3 and VP1 derived from P1, and seven non-structural proteins 2A–2C and 3A– 3D (Benschop *et al.*, 2010). The virus only has 3 structural proteins as VP0 is not cleaved to VP4 and VP2 as seen in most picornaviruses (Stanway *et al.*, 1994).

The VP3 protein possesses a unique N-terminal extension of approximately 30 amino acids, which are predominantly positively charged (Al-Sunaidi *et al.*, 2007; Boonyakiat *et al.*, 2001; Stanway *et al.*, 2000; Williams *et al.*, 2009). In addition, the 2A protein is homologous to

cellular proteins that are involved in cell proliferation and contains Hbox and NC motifs (Hughes and Stanway, 2000).

1.1.4 The picornaviral life cycle

1.1.4.1 Summary

A summary of the life cycle is shown in Figure 1.3. The virus attaches to receptors on the cell surface and enters the cell, often in vesicles. The RNA is released and the single open reading frame is translated to give a polyprotein. This is cleaved by virus proteases to give precursors then the final virus proteins. These include non-structural proteins which are needed to make more copies of the RNA genomes, via negative sense RNA copies. Structural proteins and the new RNA copies assemble to give new virus particles, there is often a final maturation step and then the particles leave the cell by lysis (Merilahti *et al.*, 2012; Whitton *et al.*, 2005).

1.1.4.2 Entry

The first stage of the life cycle of most viruses is attachment of the virion onto host cell surface receptor(s), followed by entry through the plasma membrane, usually in endocytic vesicles, into the cell cytosol and subsequent release of the genome. The details of these events probably play an important role in tissue tropism and pathogenesis. In enteroviruses, the virus often attaches to the host cell through binding of receptors to the virus canyon. Other virus/receptor interactions may then occur and open a channel to permit the externalization of VP4 and the amino end of VP1 (Rossmann *et al.*, 2002; Tuthill *et al.*, 2010). It was thought that this channel may allow RNA release, but it now seems likely that RNA leave the capsid at another point, near to the 2 fold axis (Levy *et al.*, 2010).

Many cellular receptors for picornaviruses have been identified and these have a wide variation in their structures and normal physiological functions (Evans and Almond, 1998; Stanway, 2013). Some of them are may be relatively non-specific and low-affinity, such as heparan sulphate, while others bind more tightly and bring about essential conformational changes to the

virion needed for the eventual release of the RNA. Picornavirus receptors include integrins, which are a family of transmembrane glycoproteins that form noncovalent heterodimers between α - and β - subunits and often bind to viruses via a specific arginine-glycine-aspartic acid (RGD) motif; members of the immunoglobulin superfamily such as coxsackie-adenovirus receptor (CAR), intercellular adhesion molecule-1 (ICAM-1 or CD54), the poliovirus receptor (PVR or CD155), vascular cell adhesion molecule-1 (VCAM-1); and the decay accelerating factor (DAF or CD55). β 2-microglobulin (a subunit of major histocompatibility complex class I [MHC-I] complex); and heat shock 70-kDa protein 5 (HSPA5, also known as glucoseregulated protein 78-kDa, or GRP78) have been suggested to be co-receptors or needed for later steps in entry (Joki-Korpela *et al.*, 2001; Merilahti *et al.*, 2012; Rossmann *et al.*, 2002).

Both the enterovirus coxsackievirus A9 (CAV9) and most parechoviruses including HPeV1 possess a receptor-binding motif, RGD, at the C-terminus of the VP1 protein through which they interact with cell surface integrin $\alpha V\beta 3$ and/or $\alpha V\beta 6$ (Heikkila *et al.*, 2009; Joki-Korpela *et al.*, 2001; Merilahti *et al.*, 2012; Seitsonen *et al.*, 2010; Williams *et al.*, 2004). FMDV also has a functional RGD motif but this is located within VP1, not at the C-terminus. Other mechanisms than RGD binding to integrin may occur however, upon infection with different HPeVs, such as HPeV3, HPeV7 and HPeV8, as the RGD motif is absent (Chang *et al.*, 2015). CAV9 can also infect cells via a non-RGD mechanism as mutants with no RGD are infectious (Hughes *et al.*, 1995).

Viruses can enter host cells through different internalization pathways including clathrin-mediated endocytosis, uptake via caveolae, macropinocytosis, phagocytosis and Arf6 (ADP-ribosylation factor 6) dependent mechanisms. For example, HRV-14 and HPeV1 both use the clathrin-dependent endocytotic pathway, whereas PV may release their genome through the plasma membrane directly after attachment to their specific receptor. Caveolae-mediated endocytosis has been demonstrated for echovirus 1 (Merilahti *et al.*, 2012; Sieczkarski and

Whittaker, 2002). RNA release may be triggered by interaction with receptors and/or be a pH-dependent process taking advantage of the low pH of endosomes (Mercer *et al.*, 2010).

1.1.4.3 Translation

Following RNA release, the virus genome is translated. In eukaryotic cells, the 5' 7-methylguanosine (m7G) cap structure at the ends of most cellular mRNAs is recognized by the eukaryotic translation-initiation factor 4E (eIF4E). eIF4E is a component of the cap-binding complex eIF4F, which also includes the RNA helicases eIF4A and eIF4G. These bind several factors and bridge the mRNA and 40S subunit of the ribosome. The complex then moves in a 5' to 3' direction. Usually, when the 40S subunit complex reaches the nearest AUG codon to the 5' end translation begins. Initiation proteins are released, allowing the 60S ribosomal subunit to associate with the 40S and thus forming the 80S ribosome (Pestova *et al.*, 1996; Poulin and Sonenberg, 2000). The m7G cap is absent from the 5' end of picornavirus RNAs, thus they cannot undergo cap-dependent translation. Translational initiation in these viruses instead depends on the internal ribosome entry site (IRES) (Pelletier and Sonenberg, 1988). This is a long (about 400 nucleotides) sequence made up of several RNA structure and translation initiation depends in several initiation factors as well as IRES transacting factors (ITAFS) which are proteins needed for internal initiation, but not for cap-dependent translation (Lin *et al.*, 2009). Each member of the family *Picornaviridae* expresses its viral gene products through the IRES-directed translation of a single ORF that encodes a ~250-kDa polyprotein (Whitton *et al.*, 2005).

1.1.4.4 Polyprotein processing

After the large polyprotein has been translated from the single ORF, the polyprotein is processed by virus-encoded proteases into 10–12 final cleavage products (Figure 1.4). The protease cascade is initiated by one or more primary cleavage events carried out in *cis*. In enteroviruses this is carried out by 2A^{pro}, cleaving at its N-terminus. Several picornaviruses have an NPGP motif at the 2A position and this leads to the polyprotein being made in two pieces, following

termination/reinitiation. A series of *trans* cleavages gives mature polypeptides, as well as several precursor molecules. These cleavages are performed by 3C^{pro} or 3CD^{pro} in all picornaviruses. Often the intermediate cleavage products have different functions from their final products (Ghazi *et al.*, 1998; Sasaki *et al.*, 2012; Whitton *et al.*, 2005).

1.1.4.5 Replication

Picornaviral genome replication takes place in a viral replication complex and depends on the RNA-dependent RNA polymerase 3D^{pol}, which is the most highly conserved polypeptide amongst members of the family *Picornaviridae* (Merilahti *et al.*, 2012; Whitton *et al.*, 2005) (Figure 1.3). The details of the mechanism of replication of picornavirus genomes is poorly understood. Several virus proteins are involved in the replication of viral RNA. The enzyme-dependent RNA polymerase 3D^{pol} plays a central role in RNA replication and *in vitro*, this enzyme is involved in three reactions. First, 3D^{pol} synthesizes its primer by uridylylating the genome-linked protein VPg to VPg-pU(pU) and uses this nucleotide-modified protein to initiate chain elongation, a process that has been called ‘protein priming’. Second, 3D^{pol} transcribes the RNA templates, giving minus- and plus-strand RNA. Third, 3D^{pol} unwinds double-stranded RNA during chain elongation (Pfister *et al.*, 2000). 2C has also been shown to have an RNA helicase and chaperone activity which may be involved in unwinding the virus RNA during replication (Xia *et al.*, 2015).

Some other proteins are involved in RNA replication. One is 3AB (the precursor of VPg), which stimulates RNA polymerase activity of 3D^{pol}. Another is the main protease 3C (or its precursor protein 3CD). Cell proteins such as poly (rC)-binding protein (PCBP2) are also involved. 3CD and PCBP2 interact with a cloverleaf structure at the 5’ end of enterovirus RNA, giving a complex needed for viral RNA replication. The precursor proteins 3AB and 3CD also interact

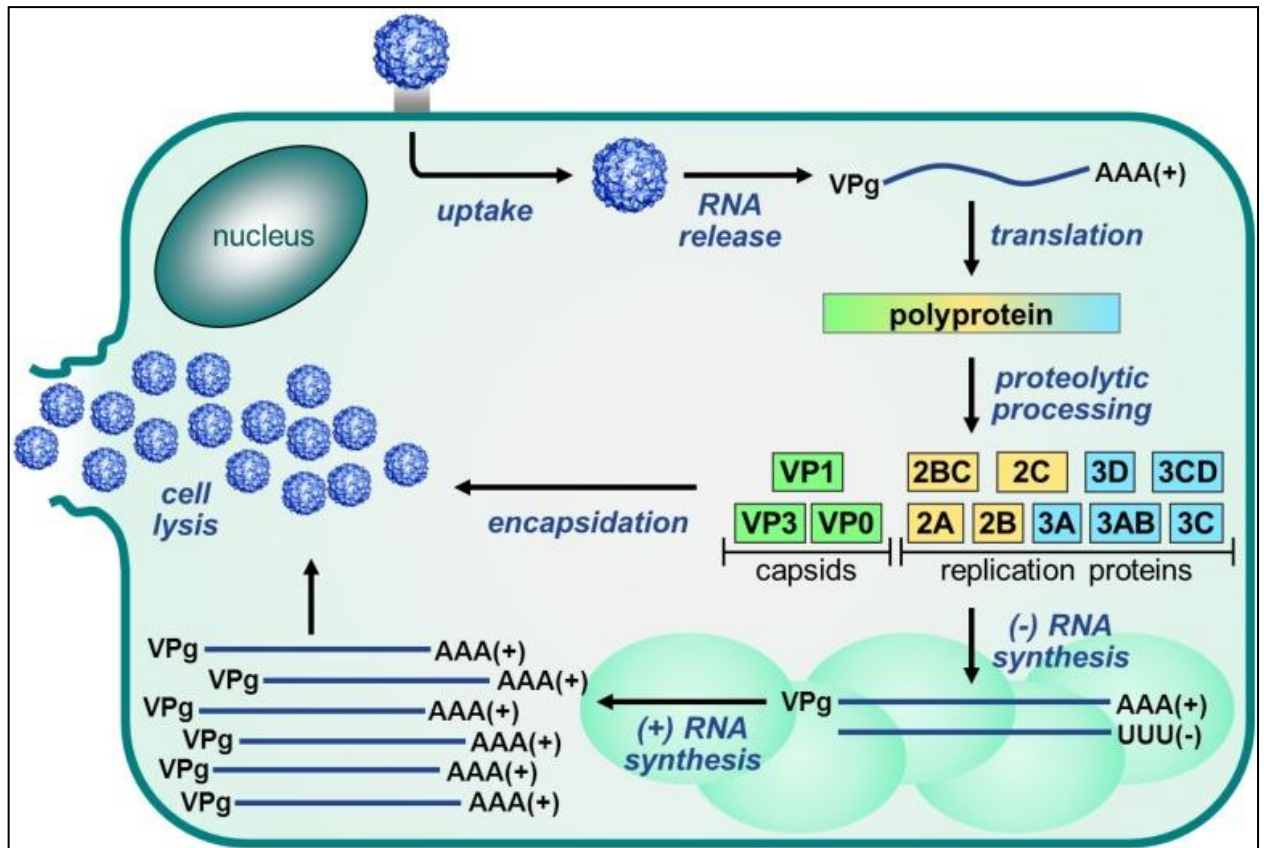


FIGURE 1.3: Summary of the life cycle of a typical picornavirus. The virus attaches to a host cell receptor and this triggers entry, which usually occurs in a vesicle. The RNA is released and translated by host cell ribosomes. The polyprotein produced is processed by proteases. As the level of protein increases there is a switch from translation to replication of (-) strand RNA using the original (+) strand RNA template, followed by (+) strand RNA synthesis. The RNA is packaged to give a particle containing 60 copies of the capsid proteins VP0, VP3 and VP1. In most picornaviruses, VP0 is cleaved during a final maturation step to give VP4 and VP2. The mature viruses leave the cell as it is lysed. Taken from (van der Linden *et al.*, 2015).

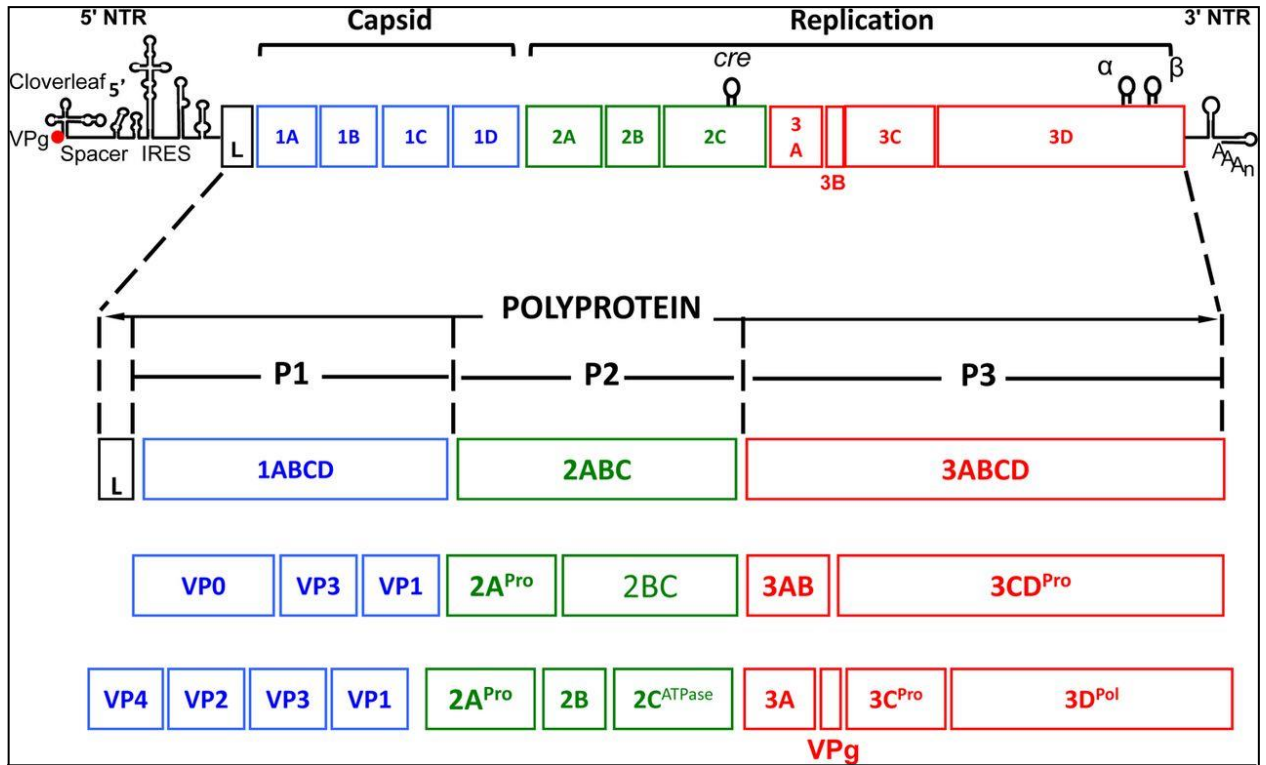


Figure 1.4: Schematic of a picornavirus genome. The diagram also shows the pathway to give the final proteins, via precursors, from the polyprotein. Non-structural proteins are 2A, 2B, 2C, 3A, 3B, 3C^{Pro}, 3D^{Pol}, L. IRES, internal ribosome entry site; NTR, non-untranslated region; VPg, viral protein genome-linked. Taken from (Jiang *et al.*, 2014).

with the 3'-UTR region of viral RNA (Banerjee *et al.*, 2004; Pfister *et al.*, 2000). In addition, cellular factors are thought to be required for membrane reorganization for picornavirus replication (Sasaki *et al.*, 2012).

1.1.4.6 Assembly, Maturation and Release

The details of the assembly process are not clear but 5 protomers, made up of VP0, VP3 and VP1 are thought to assemble into pentamers and 12 pentamers can form empty particles which may then allow the RNA to be packaged (Li *et al.*, 2012). In addition to the RNA and capsid proteins, 2C may have a role in packaging through interactions with VP3 and/or VP3 (Jiang *et al.*, 2014). After assembly, VP0 is cleaved to give VP4 and VP2 in most picornaviruses and this is necessary for the particle to be infectious. The particles are released as the cell lyses, although the details of this process are not well understood (Jiang *et al.*, 2014; van der Linden *et al.*, 2015).

1.1.5 Non-structural proteins

1.1.5.1 Genome

A schematic of the genome is shown in Figure 1.4. Non-structural proteins are encoded downstream of the capsid protein-encoding region.

1.1.5.2 2A, 3C and L protein

The 2A protein sequence, length, and roles vary considerably among the *Picornaviridae* genera (Hughes and Stanway, 2000). In enteroviruses, the polyprotein is processed mainly by 3C^{pro}. However, the primary cleavage event, separating the structural protein precursor from the non-structural one, is performed by 2A^{pro}. 2A^{pro} cleaves the viral polyprotein between the C terminus of VP1 and its own N terminus. The 2A of most other picornaviruses does not carry out such a proteolytic function (Buenz and Howe, 2006). Although not proteolytic, several picornaviruses have a highly conserved Asn-Pro-Gly-Pro (NPGP) motif at the 2A-2B junction which has been linked to a “ribosomal skip” that prevents the formation of the Gly-Pro peptide bond and then

allows translation to continue, so the P1–2A region is made separately from the rest of the polyprotein (Donnelly *et al.*, 2001; Funston *et al.*, 2008; Hughes and Stanway, 2000; Stanway *et al.*, 2000; Whitton *et al.*, 2005). The 2A proteins of many picornaviruses, including parechoviruses, show homology to cellular proteins involved in the control of cell proliferation, and do not seem to have a protease activity (Hughes and Stanway, 2000; Stanway *et al.*, 2000). Several other picornaviruses have multiple 2A proteins and there is little information on their function.

The enterovirus 2A^{pro} cleaves eIF4G and eIF3, which are involved in cap-dependent translation initiation, and prevents the infected cell translating its own capped mRNA. As IRES-dependent translation is not cap-dependent virus translation is not inhibited. Another protein involved in cellular translation, poly (A) binding protein (PABP), is also cleaved by enterovirus 2A^{pro}, as well as 3C^{pro} (Bonderoff *et al.*, 2008; Deszcz *et al.*, 2006; Yin *et al.*, 2007). 3C^{pro} has also been shown to cleave and inactivate several transcription factors and this leads to inhibition of cellular transcription (Banerjee *et al.*, 2004). 3C of enteroviruses also induces apoptosis by activating caspases and can block type I interferon (IFN) responses. 3C is related to the chymotrypsin family of proteases, but its active site is cysteine not the serine usually seen in this family of proteases. The enterovirus 2A^{pro} also has a chymotrypsin-like fold, but is more related to smaller serine proteases such as α -lytic proteinase (Seipelt *et al.*, 1999).

The third picornaviral protease is the *Aphthovirus* L protein, a cysteine protease related to papain (Seipelt *et al.*, 1999). This releases itself from the P1 region of the polyprotein and also cleaves the eIF4G subunit of eukaryotic initiation factor 4F (eIF-4F) leading to shutoff of cap-dependent host cell protein synthesis (Piccone *et al.*, 1995). Most other L proteins in the subset of picornaviruses which have this protein are not proteolytically active and are released from the P1 region of the polyprotein by 3C. One L protein which has been studied extensively is that in

cardioviruses and this seems to have an effect on host antiviral defences by preventing apoptosis and affecting interferon induction (Whitton *et al.*, 2005).

1.1.5.3 2B

The 2B protein is a small, hydrophobic, membrane protein that is responsible for blocking cellular secretory transport, disrupting Golgi membranes and membrane permeabilisation (de Jong *et al.*, 2008; van Kuppeveld *et al.*, 1997b; Yin *et al.*, 2007). It can release Ca^{2+} and H^+ from organelles by forming pores (de Jong *et al.*, 2008), although HAV 2B had little effect on ER and Golgi complex Ca^{2+} concentrations (de Jong *et al.*, 2008). The accumulation of 2B or 2BC proteins in the Golgi causes cell lysis by changing the permeability of the plasma membrane causing disassembly of the Golgi complex (Lin *et al.*, 2009; Sweeney *et al.*, 2010).

1.1.5.4 2C and 2BC

The poliovirus 2C protein is a 37.5 kDa protein containing 329 amino acids. This protein is one of the most highly conserved picornavirus proteins and has several functions such as host cell membrane rearrangement and virus RNA encapsidation. The protein includes regions which interact with other viral and cellular proteins. In RNA replication, 2C has two functions, a *cis*-acting guanidine-sensitive function required for initiation and a *trans*-acting function required for elongation, but the exact role of 2C is unknown (Banerjee *et al.*, 2004; Belsham and Normann, 2008). In addition, sequencing analysis of 2C shows similarity to several known ATPase, ATP- and GTP-binding proteins and viral helicases present in plus-strand RNA viruses. Both 2C and its precursor 2BC appear to be associated with viral RNA in infected cells *in vitro* (Banerjee *et al.*, 2004; Teterina *et al.*, 1997).

On the basis of several sequence motifs and its structure, 2C is considered to be a member of the superfamily III helicases group of the AAA+ ATPase (Belsham and Normann, 2008; Sweeney *et al.*, 2010). 2C has both ATPase and GTPase activities and 2BC is also capable of selectively hydrolysing ATP. However, only one study (Xia *et al.*, 2015) has demonstrated any helicase

activity for a picornavirus 2C (in EV-71 and the closely related virus CAV16). The study also found that 2C acts as an RNA chaperone to destabilize helices from either direction and facilitates RNA:RNA interactions. This seems to be independent of ATP.

A schematic of 2C is shown in Figure 1.5. 2C has a predicted N-terminal membrane-binding amphipathic helix, in addition to the main ATPase domain, and the ability to bind to membranes seems to partially correspond to this region. The AAA⁺ protein superfamily III helicase motifs in 2C are the ‘Walker’ motif A, which is thought to participate in binding the phosphate moiety of NTP, ‘Walker’ motif B, which may chelate magnesium ions involved in NTP hydrolysis, and motif C (Figure 1.5) (Sweeney *et al.*, 2010; Teterina *et al.*, 1997).

2C ATPase activity is inhibited by low concentrations of guanidine hydrochloride and this drug blocks negative strand RNA synthesis in poliovirus (Rightsel *et al.*, 1961). The enterovirus 2C also contains a zinc-binding cysteine-rich motif reported to be involved in RNA replication (Banerjee *et al.*, 2004; Belsham and Normann, 2008; Pfister *et al.*, 2000). This motif is not present in many picornavirus 2C proteins and is absent in FMDV, the structure of which has been solved (Sweeney *et al.*, 2010). Sequence analysis of 2C reveals homology to protease inhibitors, particularly serine protease inhibitors or ‘serpins’, which inhibit protease activity by binding to the catalytic pocket of proteases and blocking their ability to associate with specific substrates. In addition, 2C was found to be homologous to proteasome regulatory subunits from various organisms. This may be why 2C can regulate 3C^{pro} activity both *in vitro* and *in vivo* (Banerjee *et al.*, 2004; Teterina *et al.*, 1997).

1.1.5.5 3A and 3AB

3AB is a small, basic protein with multiple functions in viral RNA replication. *In vitro*, 3AB was found to stimulate the polymerase activity of 3D^{pol} as well as the self-cleavage of 3CD^{pro}. 3AB may also form a complex with both 3CD^{pro} and the 5’ enterovirus cloverleaf RNA structure involved in RNA replication and act to anchor 3D^{pol} in the replication complex. 3AB has also

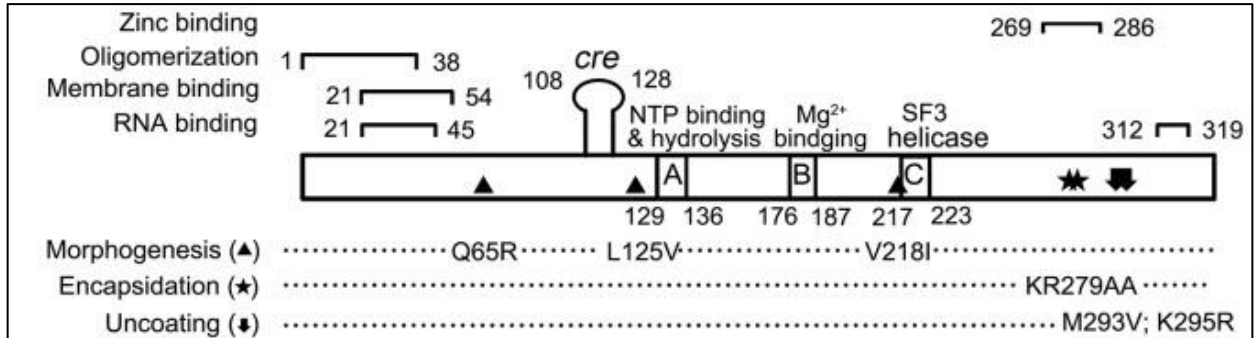


FIGURE 1.5: Schematic diagram of the 2C protein of EV71. Showing the Walker A and B motifs and motif C, found in the AAA+ protein superfamily III helicases. Regions of 2C involved with different functions are shown above the bar and mutations affecting the virus lifecycle are shown below the bar. 2C consists of 319 amino acid. In enteroviruses the 2C-encoding region is the location of the RNA structure the cre. Taken from (Xia *et al.*, 2015).

been shown to be the substrate for 3Dpol VPg uridylylation and involved in delivering VPg to replication complexes for VPg uridylylation (Lin *et al.*, 2009; Yin *et al.*, 2007).

Viral proteins 3A, as well as 2B and 2C, contains an amphipathic helix and these proteins and their precursors bind membranes directly (Teterina *et al.*, 2011; Wessels *et al.*, 2006). Cleavage of 3AB occurs only when the precursor is bound to membranes. The C-terminus of 3A also has 22 amino acid hydrophobic domain involved in membrane association and this has been shown to be important for poliovirus replication (Teterina *et al.*, 2011). Amino acid changes in the 3A protein have been shown to alter host range and tropism in rhinoviruses (Harris and Racaniello, 2005). The enterovirus 3A proteins inhibits endoplasmic reticulum (ER)-to-Golgi transport and is involved in replication complex formation (Lin *et al.*, 2009; Wessels *et al.*, 2006; Yin *et al.*, 2007).

1.1.5.6 3CD

3CD^{pro} (the precursor of mature 3C^{pro} and 3D^{pol}) is the protease involved in processing of the capsid proteins (Ypma-Wong *et al.*, 1988). 3CD^{pro} is also an RNA-binding protein that binds to the 5' cloverleaf of the PV RNA genome, which is needed for viral replication. In addition, 3CD^{pro} binds *in vitro* to the cre structure in the 2C-encoding region in enteroviruses, which is the template for the uridylylation of VPg by 3Dpol (Lin *et al.*, 2009; Yin *et al.*, 2007).

1.1.5.7 3Dpol

The viral RNA-dependent RNA polymerase 3D^{pol} is needed for viral RNA replication. 3D^{pol} is a template- and primer-dependent RNA polymerase with RNA binding activity. It can also unwind dsRNA during RNA replication. 3D polymerase can also uridylylate VPg and use VPg-pUpU as a primer during viral RNA replication (Lin *et al.*, 2009; Yin *et al.*, 2007).

1.2 Secretory pathway

1.2.1 Introduction

Most positive-strand RNA viruses use host intracellular membranes of the early secretory pathway or structures such as mitochondria or lysosomes to make replication complexes for genome replication (Midgley *et al.*, 2013; Sasaki *et al.*, 2012). The secretory pathway involves the endoplasmic reticulum (ER), the ER-Golgi intermediate compartment (ERGIC) and the Golgi. Coronavirus replicates on a reticulovesicular network derived from the ER, Semliki Forest virus uses endolysosomes and lysosomes, Flock House virus genome replication takes place next to mitochondria. For hepatitis C virus, RNA replication takes place at ER membranes and lipid droplets (Inoue and Tsai, 2013; Quiner and Jackson, 2010).

These virus-induced membrane structures help to increase the concentrations of components required for virus replication, provide a scaffold for anchoring the replication complexes, prevent the activation of host defence mechanisms that recognise dsRNA produced during virus RNA replication, tether viral RNA during unwinding and provide certain lipids that are required for genome synthesis (Miller and Krijnse-Locker, 2008; Sasaki *et al.*, 2012).

1.2.2 Endoplasmic reticulum (ER)

The ER is a dynamic cytoplasmic membrane system and is the largest organelle in a cell. It is a major site of synthesis of secreted and membrane proteins, protein transport, protein folding, lipid and steroid synthesis, carbohydrate metabolism and calcium storage (Romero-Brey and Bartenschlager, 2016). The ER is a continuous membranous system including the nuclear envelope and structures made up of branched sheets and tubules. The rough ER, with ribosomes attached, corresponds to membrane sheets and the smooth ER is made of tubules (Inoue and Tsai, 2013). The rough ER is the site of translation of secretory and transmembrane proteins and the smooth ER has functions related to lipid and glycogen metabolism (Inoue and Tsai, 2013).

ER sheets are a series of stacked flat cisternae which are connected by helicoidal ramps, which are twisted flat membrane surfaces. This means that the packing of the sheets is very efficient (English and Voeltz, 2013).

ER tubules are constantly changing shape and size. The membranes are generally more curved than ER sheets and have fewer ribosomes associated with them than sheets. Membrane proteins play a major role in the formation, maintenance and branching of both sheets and tubules (Schwarz and Blower, 2016).

In addition to its role in the synthesis, modification and transport of secretory and membrane proteins and the synthesis and transport of several lipids, the ER interacts with many other organelles, such as lipid droplets, mitochondria, endosomes, peroxisomes, and phagophores generated during autophagy (Romero-Brey and Bartenschlager, 2016).

Contact sites between the ER and mitochondria are involved in Ca^{2+} signalling, lipid biosynthesis and mitochondrial division, including Ca^{2+} entry into mitochondria and biosynthesis of phosphatidylcholine (PC). ER interactions with endosomes allow the exchange of lipids and sterols and may regulate cholesterol levels in the endocytic pathway. In addition, peroxisomes are made from components from the ER. A pool of vesicles containing peroxisomal proteins bud from the ER close to peroxisomes (English and Voeltz, 2013; Raychaudhuri and Prinz, 2008).

1.2.3 **Transitional ER (tER) or ER exit sites (ERES)**

ERES are projections of the ER, which lack ribosomes and are coated with COPII components. They seem to be involved in the selection and packaging of cargo (e.g. proteins) leaving the ER, as well as ensuring that ER resident proteins and other non-cargo materials remain in the ER. COPII vesicles bud off from ERES and form the next compartment in the secretory pathway, the ERGIC (Barlowe and Helenius, 2016; Gillon *et al.*, 2012).

1.2.4 The ER-Golgi intermediate compartment (ERGIC)

The ERGIC (also known as vesicular-tubular clusters or pre-Golgi intermediates) is a complex membrane system between the rough ER and the Golgi. ERGIC-53, a 53 kDa non-glycosylated type I membrane protein, localises to the ERGIC and is often used as a marker for this compartment (Appenzeller-Herzog and Hauri, 2006; Hauri *et al.*, 2000; Szul and Sztul, 2011). The ERGIC is made up of two types of vesicles. One is used for anterograde transport from ER to Golgi when COPII-coated vesicles bud from the ERES and are transported along the microtubule to the cis-Golgi. There they can fuse with the first cisterna of the cis-Golgi or form a new cis-Golgi cisterna by fusion with Rab1. The other is due to retrograde movement from the Golgi back to ER, which involves COPI-coated vesicles. Recycled proteins are sent back to the ER and resident ERGIC proteins are retained within the ERGIC (Appenzeller-Herzog and Hauri, 2006; Szul and Sztul, 2011).

1.2.5 Golgi

The main functions of the Golgi are sorting macromolecules for delivery to structures such as endosomes and plasma membrane or the cell exterior, as well as protein glycosylation (Midgley *et al.*, 2013). The Golgi complex is made up of one or more stacks of disk-shaped cisternae that are connected by tubulovesicular regions (Glick and Nakano, 2009; Nakamura *et al.*, 2012). Each stack of cisternae has two faces, the cis-Golgi network (CGN) which faces the ER and the trans-Golgi network (TGN), which faces the opposite side. The CGN receives protein and lipid cargos from the ER and cargo is sorted and directed to different cellular compartments in the TGN (Jackson, 2009; Nakamura *et al.*, 2012).

1.2.5.1 Transport to the Golgi

As already described, secretory cargo proteins bud off from the ERES in COPII-coated vesicles. They pass through the vesicular-tubular membrane of the ERGIC to the CGN. COPI-coated

vesicles then bud off from the ERGIC elements to recycle components of the transport and sorting machinery back to the ER (Glick, 2000).

1.2.5.2 Transport through Golgi

Two main mechanisms are proposed for the movement of secretory cargo through the Golgi (Barlowe and Helenius, 2016). The stable compartments model proposes that anterograde COPI vesicles specifically recognise secretory cargo, transport it forward and exclude proteins that need to be resident in the Golgi. The cisternal maturation model proposes that both resident proteins and cargo are transported forward, but retrograde COPI vesicles recycle resident Golgi proteins back to the Golgi (Glick *et al.*, 1997). A third model, rapid-partitioning, suggests that cargo can move in a bidirectional manner, in both cis-to-trans and trans-to-cis directions (Jackson, 2009).

1.2.5.3 Transport from the Golgi

Multiple types of vesicles form at the TGN. Clathrin-coated vesicles bud from the TGN and deliver material to the endosomal/lysosomal/vacuolar system and immature secretory granules detach from the TGN and then mature (Glick, 2000).

1.2.6 Coated vesicles proteins

Vesicles with different coats are formed in a similar way, involving coat complexes, Sar1/ARF GTPases, guanine nucleotide exchange factors (GEFs), and GTPase activating proteins (GAPs).

1.2.6.1 COPII vesicles

Budding of COPII-coated vesicles depends on the active GTP-bound form of the small GTPase Sar1-specific guanine nucleotide exchange factor and this process is catalyzed by the Sec12 GEF, which is a membrane protein found in the ER. Sec12 controls Sar1 and active Sar1 directly binds Sec23/Sec24 to the inner heterodimeric sub-complex of the COPII coat. This then recruits the outer coat components (Sec13/Sec31) to the Sec23/Sec24 core and the mature coated vesicles bud from the ER (Midgley *et al.*, 2013). Sar1, Sec23/24 and Sec13/31 are necessary to generate

COPII vesicles in vitro. At least some cargo is exported from the ER by binding to cargo receptors of the ERGIC-53 family that facilitate sorting into COPII vesicles (D'Arcangelo *et al.*, 2013; Gillon *et al.*, 2012; Szul and Sztul, 2011). Sar1 is converted to its inactive GDP-bound form and COPII coats rapidly dissociate from the vesicles, which then acquire COPI (“COPII/COPI exchange”) before fusion with the ERGIC (Stephens *et al.*, 2000) (Figure 1.5).

1.2.6.2 COPI vesicles

COPI appears to be required at more than one stage of ER-to-Golgi transport. For example, COPI is involved in anterograde transport after COPII/COPI exchange, movement within the Golgi and in the retrograde movement of components from the Golgi back to the ER. COPI is also required for lipid storage and lipid homeostasis (Szul and Sztul, 2011; Wang *et al.*, 2012b). COPI is composed of seven coatomer subunits and an ADP ribosylation factor (ARF)-dependent GTPase. The subunits of COPI are α COP, β COP, β' COP, γ COP, δ COP, ϵ COP and ζ COP (Wang *et al.*, 2012b). ‘Thin’ COPI vesicles are found close to the cis-Golgi and between the cis-Golgi and the ERES, suggesting that they recycle materials from the cis-Golgi to the ER. ‘Thick’ COPI vesicles are found close to medial- and trans-Golgi, suggesting that they are involved in retrograde trafficking within the Golgi (Szul and Sztul, 2011).

COPI coat formation requires ARF1, which is activated on the Golgi by two related GEF, GBF1 and BIGs. GBF1 (ARF1-GEF) is present in the cis-Golgi and BIG is located in the trans-Golgi (Midgley *et al.*, 2013).

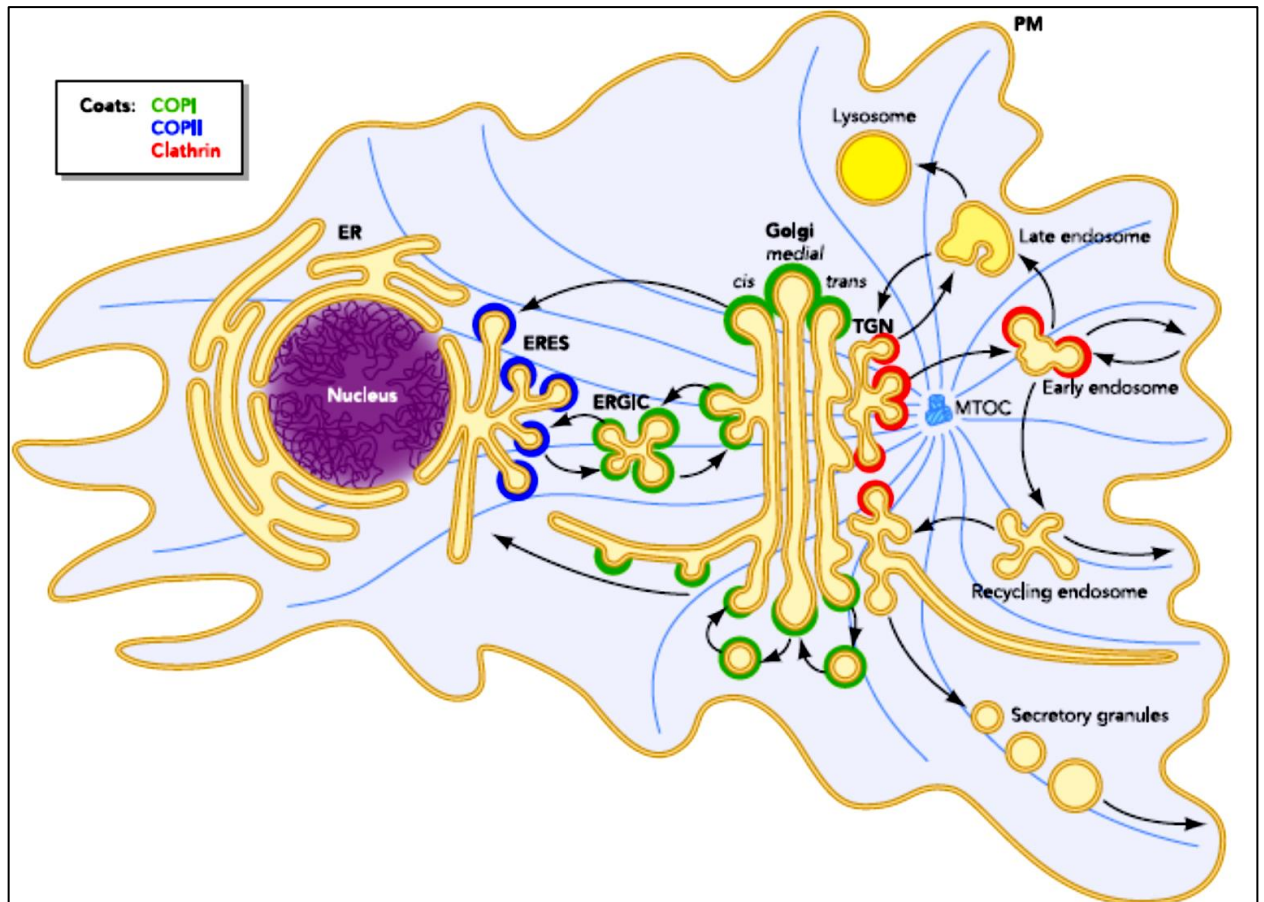


FIGURE 1.6: Schematic of the secretory pathway. Secretory cargos are synthesized in the ER, exit the ER at ERES in COPII-coated vesicles, and are transported to ERGIC. Cargos are sorted from the ERGIC and move to the Golgi. Cargos are sorted at the TGN (trans Golgi network) for delivery to the plasma membrane (PM) and early and late endosomes. Colours indicate the known coats: COPII (blue), COPI (green), and clathrin (red). Taken from (Szul and Sztul. 2011).

1.3 Lipids

Many viruses interact with and exploit host cell lipids at different stages of the virus replication including entry, nucleic acid replication and budding of new enveloped particles (Martin-Acebes *et al.*, 2013). The effects on lipids include changes to the composition, fluidity, and curvature of membrane compartments. Particularly extensive changes are seen in cells infected with positive sense RNA viruses where specific membrane compartments are induced by viruses and used to generate replication complexes (Chukkapalli *et al.*, 2012).

1.3.1 Lipid droplets (LDs)

LDs are dynamic cytoplasmic organelles present in most cells and are the most important storage organelles for neutral lipids. The size and number of LDs varies between cell types, for example up to 100 μm in diameter in white adipocytes but only up to 100–200-nm in many other cells. LDs consist of a hydrophobic core of neutral lipids (triglycerides (TG) and cholesterol esters (CE), surrounded by a phospholipid monolayer, embedded in which are several associated proteins (Guo *et al.*, 2009; Herker and Ott, 2012; Walther and Farese, 2012) (Figure 1.7). LDs interact with several amphipathic molecules (Walther and Farese, 2012).

LDs can have several functions, apart from lipid storage for future energy generation. The stored lipids can also be the raw materials for making new membranes and the starting point for making specific lipids. CEs in steroidogenic cell LDs are used for steroid synthesis, and arachidonic acid esters present in mast cell LDs are used in eicosanoid synthesis. In hepatocytes, the lipid ester in LDs is utilized for lipoprotein formation (Fujimoto *et al.*, 2008). LDs are reported to be involved in esterification of excess free fatty acids (FAs) and free CEs, which prevents toxicity of these molecules (Fujimoto *et al.*, 2008; Suzuki *et al.*, 2011). Lipid synthesis is summarised in Figure 1.8.

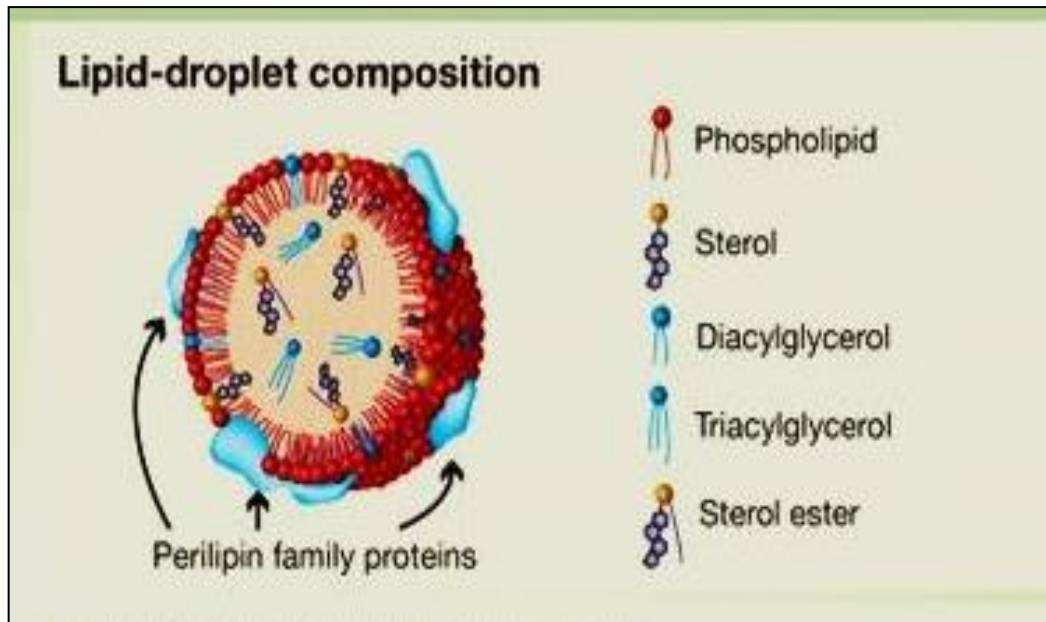


FIGURE1.7: The structure of a lipid droplet. A hydrophobic core of neutral lipids (triglycerides and sterol esters) is surrounded by a phospholipid monolayer which interacts with proteins, particularly members of the perilipin family. Taken from (Guo *et al.*, 2009).

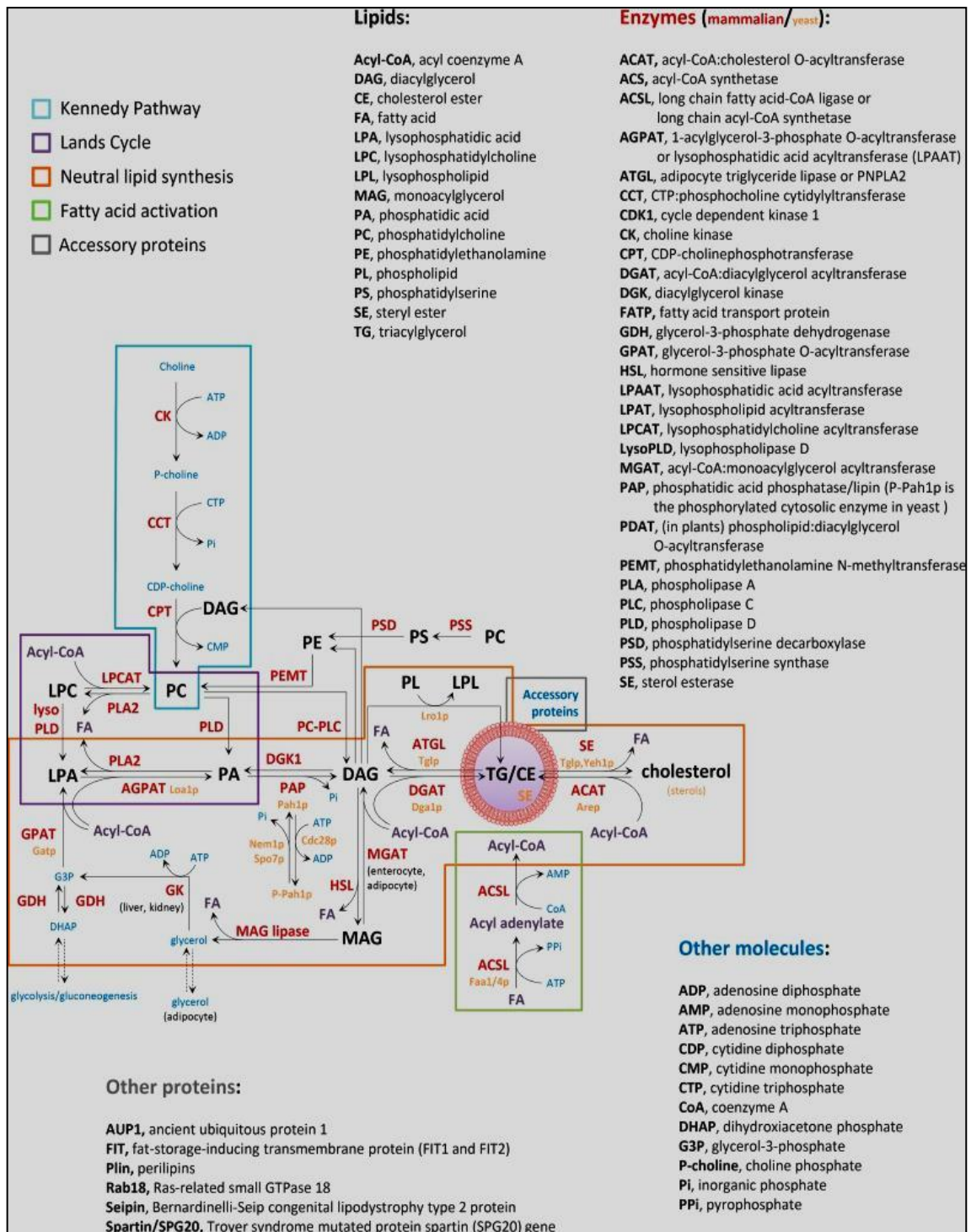


FIGURE 1.8: Lipid metabolism and LD formation in mammal and yeast. LD biogenesis requires coordination of acyl-CoA synthetases (green box), neutral lipids (orange box), phospholipid remodeling (purple box), phospholipid synthesis (blue box), and the function of accessory proteins (grey box). The enzymes involved in these pathways are indicated with red (mammal) and yellow letters (yeast). Taken from (Pol *et al.*, 2014).

Proteins can also be stored temporarily in LDs, for example some membrane proteins targeted for degradation (Fujimoto *et al.*, 2008; Guo *et al.*, 2009; Walther and Farese, 2012). Lipidated apolipoprotein B-100 and α -synuclein (which contribute to Lewy bodies in Parkinson's disease) accumulates on LDs when proteasomal degradation or autophagy are inhibited. This suggests that LDs may sequester these proteins to prevent them from forming insoluble aggregates before they can be effectively degraded (Suzuki *et al.*, 2011).

Enzymes involved in LD formation are mainly found in the ER, but not diacylglycerol acyltransferase 2 (DGAT2), which localised to LDs. Examples of these enzymes are acyl-coenzyme A (acyl-CoA) and DGAT 1 and 2, which synthesize TG and acyl-CoA cholesterol acyltransferase (ACAT) 1 and 2 that generate SEs. Other hydrophobic lipids found in LDs include retinyl esters (in LDs of hepatic stellate cells and in the retina), wax esters and ether lipids and long-chain isoprenoids (Walther and Farese, 2012).

The main surface phospholipids of LDs are phosphatidylcholine (PC), phosphatidylethanolamine (PE) and phosphatidylinositol. LDs have much less phosphatidylserine and phosphatidic acid than other membranes but more lyso-PC and lyso-PE. LDs of white adipocytes contain large amounts of free cholesterol as they acts as a cholesterol sink for the whole body (Fujimoto *et al.*, 2008; Walther and Farese, 2012).

Several kinds of proteins are present on the LD surface. These are structural proteins (e.g. perilipin family members), lipid-synthesis enzymes [e.g. acetyl coenzyme A (CoA) carboxylase, acyl-CoA synthetase and acyl-CoA], lipases [e.g. adipose tissue triacylglycerol lipase (ATGL)] and membrane-trafficking proteins (e.g. Rab5, Rab18 and ARF1) (Guo *et al.*, 2009).

1.3.1.1 Lipid droplets formation

Formation of LDs take place in the ER (Guo *et al.*, 2009; Pol *et al.*, 2014). How they form is not fully understood. ER budding, where LDs grow from the ER bilayer and either remain connected or bud off, is one possibility; bicelle formation, in which neutral lipids accumulate between the

leaflets of the ER membrane and nascent LDs are excised from the membrane is another suggestion. Vesicular budding, in which a bilayer vesicle forms, followed by filling of the space between the bilayers with neutral lipids, could also occur. Finally, 'eggcup' model has been proposed in which a LD grows within a concave depression of the ER through transport of neutral lipids from the ER (Robenek *et al.*, 2006) (Figure 1.9).

1.3.1.2 Lipid droplet growth

If LDs remain attached to the ER, newly synthesized lipids and proteins can diffuse to them, but if they are detached they need to be transported through membrane connections or via vesicles. Neutral lipids can be made in LD cores by enzymes such as DGAT2 which catalyzes the final step of TG synthesis. Sterolesters are made in the ER. The increase in the volume of neutral lipids in LD cores requires more phospholipids at the surface and so there needs to be a lot of coordination of processes during LD growth (Guo *et al.*, 2009; Walther and Farese, 2012).

Fusion of LDs can also occur and lead to an increase in size. Soluble N-ethylmaleimide-sensitive factor activating protein receptor (SNARE) proteins are found in LDs and are required for fusion. In LD fusion, the total volume of lipid esters appears to remain constant and the resulting LD regains the spherical shape immediately, suggesting that these are highly dynamic structures (Bostrom *et al.*, 2007).

1.3.1.3 Lipid droplet proteins

LD proteins can be classified into five groups: (i) small GTPases that regulate vesicle formation and movement; (ii) motor proteins that move vesicles on the cytoskeleton (kinesin and myosin); (iii) N-ethylmaleimide-sensitive factor (NSF), soluble NSF attachment protein (α SNAP), the SNARE and SNAP23 are needed for LD docking and fusion; (iv) vesicular traffic proteins that regulate cargo sorting and vesicle budding such as ARF1, membrane, Sar1, Sec21, COPs, and Sec22; and (v) unknown function membrane traffic proteins (VAT1, Rap1, P22, and TIP47) (Zehmer *et al.*, 2009).

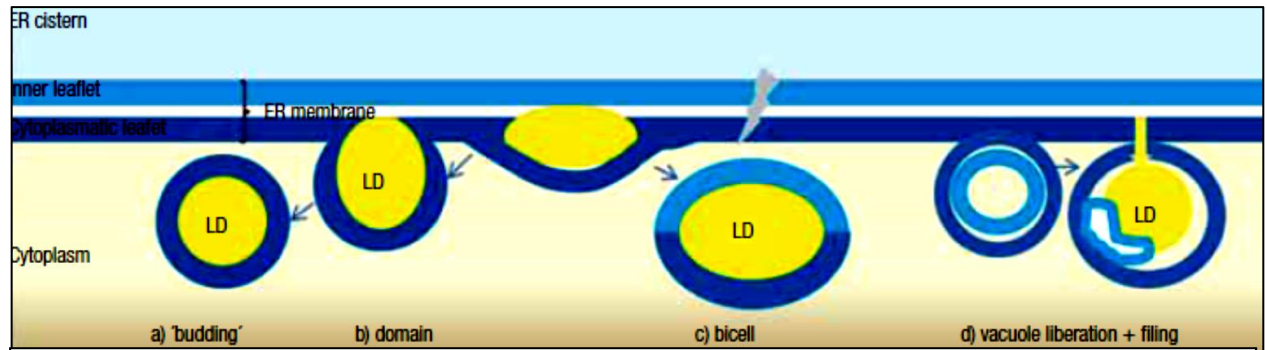


FIGURE 1.9: Some of LD formation models. These include ER budding, bicelle formation and vesicular budding. Taken from (Meester *et al.*, 2011).

The best studied are PAT proteins, which include perilipin, adipose differentiation-related protein (ADRP), tail-interacting protein of 47 kD (TIP47), S3-12 and MLDP/OXPAT/PAT-1 (Fujimoto *et al.*, 2008). Perilipins are not essential for LD formation, but are important for regulating lipid metabolism at LDs (Listenberger *et al.*, 2007; Walther and Farese, 2012). Unphosphorylated perilipin protects the lipid droplet from lipase activity (Beller *et al.*, 2008).

ADRP is present on the surface of LDs from the earliest time of their synthesis and helps to regulate lipid storage during LD formation. Over-expression of ADRP causes an increase in neutral lipid mass and LD accumulation, showing an important function in LD regulation. This is related to reduced TAG turnover and TAG secretion in cells over-expressing ADRP. Suppression of ADRP expression in mice significantly reduces hepatic TAG accumulation (Listenberger *et al.*, 2007).

TIP47 may also protect against lipolysis by affecting the LD surface (Suzuki *et al.*, 2011; Beller *et al.*, 2008; Bickel *et al.*, 2009; Fujimoto *et al.*, 2008; Vogt *et al.*, 2013).

Other proteins such as Rab18 (a small GTPase) localize to LDs and influence interactions with the ER. MLDP/OXPAT/PAT-1 also inhibits lipolysis in LDs, and S3-12 (which may be related to lipid storage) is expressed almost exclusively in the adipocyte (Fujimoto *et al.*, 2008).

The movement of LDs is driven by microtubule motor proteins, kinesin and dynein. Erk-mediated phosphorylation of dynein increases the association of this motor protein with LDs. The ability of LDs to form and grow is dependent on motor proteins and microtubules and dynein neutralizing antibodies and the microtubule inhibitor nocodazole inhibit fusion of LDs (Zehmer *et al.*, 2009).

Caveolins, which form the coats of caveolae, play a role in cholesterol trafficking (Fujimoto *et al.*, 2008; Le Lay *et al.*, 2006). In adipocytes, caveolae seem to produce TGs and caveolae can bud and transport to LDs. PTRF/cavin-1, a peripheral membrane protein essential for caveolae

formation, is also thought to be linked with LD functions and lipid storage in adipocytes (Suzuki *et al.*, 2011). Caveolin-1 binds glycolipids and fatty acids and contributes to intracellular lipid transport. As well as caveolae, Caveolin-1 localises to the Golgi, but in the presence of excess lipid it is endocytosed and translocates to the LD. Rab18 is thought to regulate the interaction between LDs and the ER and overexpression of Rab18 expels ADRP from the LD and brings LDs closer to the ER (Fujimoto *et al.*, 2008). ARF1/COPI proteins are required for LD localization of the major TG lipase ATGL (Wilfling *et al.*, 2014).

There are various different mechanisms to explain how proteins target LDs. These include long membrane-embedded domains that enter and exit the membrane on the same side of the lipid monolayer; embedding an amphipathic helix internal protein domain that penetrates the LD with hydrophobic spans; lipid anchors; and interaction with other LD-bound proteins (Guo *et al.*, 2009; Walther and Farese, 2012).

1.3.1.4 Lipid droplet catabolism

Lipolysis is the process of breaking down LDs to form FAs and lipids. In adipocytes it is initiated by hormonal, nutritional or inflammatory (such as tumor necrosis factor- α) signals. Firstly, catecholamines bind to β -adrenergic G-protein-coupled receptors at the plasma membrane and stimulate adenylyl cyclase. This generates cAMP which activates protein kinase A, then phosphorylates perilipin A. Perilipin A activates adipose triglyceride lipase (ATGL) and recruits phosphorylated HSL to the LD surface. ATGL and HSL then hydrolyze triacylglycerols to FAs and monoacylglycerols, which are further broken down to glycerol and FAs (Guo *et al.*, 2009; Herker and Ott, 2012; Suzuki *et al.*, 2011; Walther and Farese, 2012). During lipolysis, LDs shrink as the core lipids are broken down. The surface then needs to shrink but it is unknown if excess proteins and phospholipids are resorbed into the ER or degraded. The released FAs can be used in several ways, including being incorporated into new TGs, broken

down to provide energy by β -oxidation, used to make membrane lipids, exported or become involved in cell signalling (Guo *et al.*, 2009; Walther and Farese, 2012).

Lipids in LDs can also be degraded by lipases within lysosomes during macroautophagy, induced by nutrient deprivation or hormonal signals. LDs are surrounded by a membrane bilayer containing the activated LC3-II protein (Walther and Farese, 2012). Regulation of lipolysis seems to be the primary function of perilipins by recruiting or preventing the access of lipases to LDs (Pol *et al.*, 2014).

1.3.1.5 Lipid droplets interact with other organelles

LDs often interact with the ER, mitochondria and peroxisomes, both in adipocytes and in non-adipocytes.

1.3.1.5.1 The Endoplasmic Reticulum (ER)

LD biogenesis takes place in the ER membrane and LDs form and grow by incorporating lipid esters synthesized in the ER (Suzuki *et al.*, 2011; Zehmer *et al.*, 2009). There are also other interactions not related to the ER origin of LDs. LD-ER contacts induced by the GTP/GDP state of Rab18 or knockdown of ADRP bring about the reverse movement of lipids from LDs to ER, which can presumably occur naturally (Suzuki *et al.*, 2011; Zehmer *et al.*, 2009). LD-ER contact sites seem to be involved in replication of some viruses, possibly by allowing lipid movement between these organelles (Zehmer *et al.*, 2009).

Seipin and the fat storage-inducing transmembrane protein (FITM/FIT) are two ER resident proteins involved in LD formation, possibly through membrane-spanning helices which could interact with LDs. Removal of seipin in yeast and in fibroblasts results caused a large variation in size of LDs (Pol *et al.*, 2014).

1.3.1.5.2 Endosomes

The interaction between LDs and endosomes seems to be important for normal membrane traffic and several proteins involved in trafficking are found in LDs. Endosome carrying high-density

lipoprotein (HDL) associate with LDs and Rab5/Rab11. Rab GTPases may therefore regulate interactions between LDs and endosomes. LDs also contain proteins known to mediate SNARE-dependent membrane-membrane fusion (Zehmer *et al.*, 2009).

1.3.1.5.3 Mitochondria and peroxisomes

A physical link between mitochondria/peroxisomes and LDs allows the import of fatty acids for β -oxidation (Suzuki *et al.*, 2011). LDs and mitochondria co-localise in skeletal muscle cells, which have a high lipid requirement for energy production. This interaction is enhanced when energy requirements are increased. Caveolae protein, caveolin-1, plays a role in maintaining the interaction between LDs and mitochondria (Zehmer *et al.*, 2009).

In some cases, peroxisomes in contact with LDs form structures called “gnarls” that push into the LD core. This association may allow the products of lipolysis to be fed into the β -oxidation pathway in peroxisomes (Zehmer *et al.*, 2009). LDs and phagosomes may interact by a briefer, kiss-and-run type contact and this could be important for supplying phagosomes with lipids (Suzuki *et al.*, 2011).

1.3.1.5.4 COPI and COPII

COPI protein, but not COPII, is needed to use lipid stores in LDs. Presumably there is some trafficking between ER and LDs using COPI vesicles. Blocking this pathway changes the levels of TIP47 and ATGL on the LD surface implying that it is a specific process (Beller *et al.*, 2008).

1.3.1.6 Lipid droplets and disease

Excessive lipid storage in LDs is associated with many metabolic diseases as cells cannot store enough lipid to prevent a toxic effect by some lipid precursors. Unesterified lipids, such as cholesterol or FAs, can trigger inflammatory responses that result in tissue damage, fibrosis, scarring and potentially organ failure. Obesity involves excess lipid storage in LDs in the adipose tissue and complications such as type 2 diabetes mellitus seem to be one problem of this excess storage. Therapies that target LDs could block lipid absorption in the small intestine and so LD

formation, enhance breakdown rather than storage of lipids or, alternatively, increase LD capacity in adipocytes or macrophages to store toxic lipids and prevent associated inflammation and tissue damage (Krahmer *et al.*, 2013).

Atherosclerosis is associated with deposition of lipids in tissues, specifically cholesterol derived from apo B-containing lipoproteins in arterial walls. Excess cholesterol is taken up and esterified by macrophages. Cholesterol esters are stored in LDs until they can be mobilized and sent to high-density lipoproteins, which are transported to the liver for clearance of cholesterol from bile. Excess lipid overloads this system (Krahmer *et al.*, 2013; Walther and Farese, 2012).

Absence or deficiency of white adipose tissue (lipodystrophy) results in LD deficiency and there are a number of genetic causes such as mutations in genes that encode acylglycerol-phosphate acyltransferase (AGPAT2), seipin (BCSL2) or caveolin 1 (CAV1). Partial lipodystrophy can be caused by defective lamin A/C (LMNA), peroxisome proliferator-activated receptor- γ (PPARG), Akt2/protein kinase B (AKT2) and endoprotease Face-1 (ZMPSTE24) (Garg and Agarwal, 2009).

Some tumor cells and associated inflammatory cells have prominent LDs, which could be related to increased FA synthesis or impairments in FA oxidation (Pan *et al.*, 2012). Clinical studies suggest that chronic HCV infection is associated with various disorders of lipid metabolism resulting in accumulation of LDs in the liver (steatosis) and reduced serum beta-lipoprotein levels (Fukasawa, 2010).

1.3.2 Diacylglycerol acyltransferase (DGAT) enzymes

Acyl CoA diacylglycerol acyltransferase (DGAT; EC 2.3.1.20) is a microsomal enzyme involved in the metabolism of cellular glycerolipids. Its substrates are diacylglycerol (DAG) and fatty acyl CoAs (Camus *et al.*, 2013). DGAT is involved in a number of lipid-related processes (Cases *et al.*, 1998). Both DGAT1 and DGAT2 are essential in LD biogenesis. Both enzymes are

found in the ER and when cells take up of fatty acids, DGAT2 (but not DGAT1) localizes to LDs (Herker *et al.*, 2010).

1.4 Role of cellular lipid in viral infections

Among the cellular factors required by viruses, lipids play an important role in both enveloped and non-enveloped virus infections. Cellular lipids are important to viral infection particularly for membrane fusion during the entry process, replication and budding of the virus. Exploitation of host cell lipids plays an important role in efficient replication of RNA viruses (Chukkapalli *et al.*, 2012; Heaton and Randall, 2011).

1.4.1 Entry

The first step of a viral infection is entry into a host cell and involves attachment of the virus particle to a specific receptor(s) located on the cell surface (Martin-Acebes *et al.*, 2013). Several viruses bind to lipid molecules, including members of the *Polyomaviridae* family which bind directly to ganglioside. Influenza virus and human immunodeficiency virus also bind to gangliosides (Ewers and Helenius, 2011; Izquierdo-Useros *et al.*, 2012; Meisen *et al.*, 2012). The rhabdovirus vesicular stomatitis virus (VSV) interacts with negatively charged phospholipids during entry (Schlegel *et al.*, 1983) and HCV requires lipid trafficking receptors such as low density lipoprotein receptor (LDL-R) as indirect viral receptor (Agnello *et al.*, 1999). Influenza A virus, human West Nile virus (WNV) and herpes virus 6 require cholesterol in the virus envelope for efficient entry (Heaton and Randall, 2011; Martin-Acebes *et al.*, 2013). In addition, lipid rafts have been associated with various endocytic mechanisms exploited by viruses. These include the coronavirus SARS virus, murine leukemia virus, herpes simplex virus, Japanese encephalitis virus, SV40 and echovirus 1. Foot-and-mouth disease virus (FMDV) and human rhinovirus type 2 also require cholesterol for efficient entry (Martin-Acebes *et al.*, 2013). The use of cholesterol and lipid rafts for viral entry into cells has also been documented for coxsackievirus B3 (CVB3) infection (Coyne and Bergelson, 2006).

Many viruses depend on phosphatidylinositol (PI)-3 kinase signaling for internalization. This sorts the virus particles into an endosomal compartment which is then endocytosed. Specific lipids may influence the compartment of entry and uncoating, for instance dengue virus (DENV) fuse with late endosomes containing the late endosome-specific lipid species bis (monoacylglycero) phosphate (Heaton and Randall, 2011; Martin-Acebes *et al.*, 2013).

The plasma membrane also exhibits clusters of other lipids like phosphatidylinositol 4,5-bisphosphate (PI(4,5)P₂), which has an important role in clathrin-mediated endocytosis and also plays a role in HIV-1 entry (Barrero-Villar *et al.*, 2008). FMDV require this phospholipid in the plasma membrane for internalization (Martin-Acebes *et al.*, 2007).

1.4.2 Replication

Cell membranes from the ER, Golgi, endosomes, lysosomes, peroxisomes and mitochondria can be used to form replication complexes for positive-stranded RNA viruses. These viruses can also exploit LDs for their replication (Heaton and Randall, 2011; Martin-Acebes *et al.*, 2013). Viral and cell proteins are needed to recruit these membranes. Host proteins may be involved through biosynthesis of membrane components or providing the support for the membranes. Brome mosaic virus (BMV) replication requires the host gene OLE1, which affects membrane fluidity. BMV also utilize ACB1-encoded acyl CoA binding protein (ACBP), which promotes lipid synthesis for efficient replication (Lee *et al.*, 2001; Zhang *et al.*, 2012).

Many viruses require cholesterol and FAs for their RCs. For example, WNV manipulates a cholesterol biosynthesis pathway by 3-hydroxymethylglutaryl-CoA reductase, redistributes cellular cholesterol to replication sites and reduces cholesterol at the plasma membrane to deactivate antiviral signalling (Mackenzie *et al.*, 2007). Furthermore, yellow fever virus (YFV) and DENV proteins bind to fatty acid synthase (FASN) and relocalizes it to sites of viral replication (Heaton *et al.*, 2010; Perera *et al.*, 2012).

Specific phospholipids also play a key role in viral replication. For example, HCV NS5A expression stimulates cellular phosphatidylinositol-4-phosphate (PI4P) production by ER-associated phosphatidylinositol-4 kinases (PI4K) III-alpha. Enterovirus, 3A protein recruits the Golgi isoform PI4-kinase III-beta. Viral proteins of Aichivirus interact with acyl-coenzyme A binding domain containing 3 (ACBD3), which can interact with and recruit PI4KB to RCs. Further, the PV RNA polymerase 3D^{pol} physically binds PI4P, which could influence both its association with cellular membranes and its ability to synthesize RNA (Reiss *et al.*, 2011; Sasaki *et al.*, 2012).

DENV infection consumes LDs and stimulates β -oxidation (Heaton and Randall, 2010). The FA oxidation enzyme dodecenoyl coenzyme A delta isomerase is essential for HCV replication (Rasmussen *et al.*, 2011). On the other hand Human cytomegalovirus (HCMV) appears to reduce β -oxidation (Seo *et al.*, 2011). Several viruses also manipulate peroxisomes during replication, either for β -oxidation of fatty acids or for other purposes (Chukkapalli *et al.*, 2012).

1.4.3 Assembly

Many enveloped viruses acquire their lipid membrane by budding through a cellular membrane. For example, DENV and WNV acquire an envelope through budding into the ER, whilst influenza and HIV acquire an envelope by budding from the plasma membrane. Synthesis of fatty acids has also been associated with envelope formation in viruses (Martin-Acebes *et al.*, 2013). HCMV stimulates fatty acid synthesis in order to enhance the assembly of infectious HCMV virions (Munger *et al.*, 2008).

Lipid signalling also helps organize HIV budding sites by recruiting the major HIV structural protein, Gag. The localization of Gag to lipid rafts at the plasma membrane is dependent on the interactions of Gag with the lipid signalling molecule PI-(4,5)-bisphosphate, which is enriched at the plasma membrane (Chukkapalli *et al.*, 2008). Similarly, the trafficking of influenza virus

glycoproteins to the plasma membrane and subsequent budding, depends on the interaction of virus components with lipid rafts (Nayak *et al.*, 2009).

In some viruses, LDs contribute towards the assembly. DENV and HCV are good illustrations of this. HCV core protein enhances the accumulation of LDs in the perinuclear region, potentially enhancing an interaction between the HCV core and DGAT-1, and as result promotes LD formation (Heaton and Randall, 2011; Martin-Acebes *et al.*, 2013). In non-enveloped viruses, myristoylation of VP4 protein in PV and FMDV has been shown necessary for correct capsid assembly (Goodwin *et al.*, 2009; Moscufo *et al.*, 1991).

1.5 Remodelling of secretory pathway in viral infection

Several enveloped and non-enveloped viruses, belonging to both RNA and DNA virus families, rearrange cell compartments to generate novel structures for replication and assembly (Inoue and Tsai, 2013). The ER is often involved and there can be a great change in ER morphology. (Pierini *et al.*, 2009). Other targeted membranes include the Golgi apparatus and mitochondria. These membranes may provide a structural framework for replication, and different compartments may be important for some viruses if they produce both genomic and sub-genomic RNA or positive and negative sense RNA. In some viruses the replication complex may be generated by a cellular autophagic process (Cherry *et al.*, 2006).

HCV promotes the formation of an ER-derived membranous matrix (membranous web) that is important for viral replication and assembly. DENV generates vesicle packets and complex membranes to facilitate genome replication and virus assembly (Inoue and Tsai, 2013).

In HCV, web formation is thought to initiate when the ER membrane-bound viral non-structural protein NS5A recruits and activates PI4KIII α , thus increasing the local concentration of PI4P which might itself be an important membrane constituent that supports membranous web structural integrity. It is thought that PI4P may recruit downstream effector proteins such as

oxysterol-binding protein 1 (OSBP1) to form a sterol-rich environment surrounding the membranous web, that is essential for HCV replication. Moreover, DENV's non-structural protein NS4A rearranges the ER membrane, leading to the formation of vesicle packets and convoluted membranes. It also uses LDs for particle formation. In rotavirus, the ER also supports virus assembly during the late stage of this process. A viral intermediate containing the core shell and middle layer is called a double-layer particle (DLP), and a mature infectious particle harbouring all three layers is referred to as a triple-layer particle (TLP). DLP-to-TLP morphogenesis is intimately associated with the ER (Inoue and Tsai, 2013).

Enteroviruses utilize ER exit sites to form tubular structures that extend into the cytoplasm to anchor the viral replication machinery on the cytoplasmic membrane of the ER. The formation of enterovirus replication organelles also specifically requires COPI, which is recruited to replication complexes via inhibition of ARF1 GTPase by the virally-encoded 3A protein (Morosky *et al.*, 2016). PV 3A protein binds GBF1 and modulates recruitment of ARF1 effectors to favour phosphatidylinositol 4-kinase (PI4K) over COPI components. It may also inhibit ER-to-Golgi transport by stabilizing ARF1-GDP-GBF1 complexes, reducing the supply of Arf1-GTP for COPI coats. This creates membranes lacking COPI and enriched for PI4P, which promotes membrane binding of viral RNA-dependent RNA polymerases and formation of the viral replication complex (Midgley *et al.*, 2013; Pierini *et al.*, 2009).

PV-induced membrane vesicles have also been linked to COPII-dependent vesicle trafficking. The 2B, 2C and 3A proteins interact with each other and the other replication proteins and bring about membrane association of RNA replication proteins (den Boon *et al.*, 2010). In FMDV, secretion is blocked by the 2BC protein rather than 3A. The 2B and 2BC of enteroviruses also slow secretion when expressed alone in cells. These proteins can therefore affect membrane traffic and for 2C, this may involve binding to ER membrane protein reticulon 3, which is involved in ER-to-Golgi trafficking and is required for replication (Pierini *et al.*, 2009).

COPI activity is required for EV11 and HCV replication. The COPI inhibitor Brefeldin A (BFA) inhibits RNA replication in PV and EV11, but not FMDV and encephalomyocarditis virus (EMCV) infection and only partially inhibits HPeV1. Genome-wide RNA interference screening revealed that picorna-like virus, Drosophila C virus (DCV), also recruited COPI proteins to achieve viral replication (Wang *et al.*, 2012b). For enterovirus 71 (a BFA-sensitive picornavirus), COPI but not COPII has been shown to be required for infection (Midgley *et al.*, 2013).

1.6 Antiviral Drugs

The use of vaccines to prevent disease, or drugs to inhibit viral replication, are the two main strategies currently used to combat viral infections (van der Schaar *et al.*, 2013). For viruses with multiple serotypes, vaccines are not useful and antiviral drugs are required. Many targets have been studied as antiviral treatments. Traditionally, viral proteins such as proteases, polymerases and integrases have been targets for classical anti-viral agents. Enterovirus inhibitors have been developed against the HRV protease 3C (Jurgeit *et al.*, 2010).

Despite considerable research, there are no clinically-used antivirals against picornaviruses (van der Schaar *et al.*, 2013; Whitton *et al.*, 2005; Zuo *et al.*, 2016). Pleconaril is an example of a drug that has the potential to treat acute and chronic picornavirus infections. This compound binds to a hydrophobic pocket of the enteroviral and rhinoviral capsids, inducing conformational changes that alter binding to the cognate viral receptor. Furthermore, it has shown promise against neonatal enteroviral hepatitis and multisystem CVB infection in preterm newborns, and was used to successfully treat enterovirus infection in two infants with severe combined immunodeficiency. The drug was under investigation in a phase II clinical trial, but the emergence of drug-resistant viral variants was a problem (Whitton *et al.*, 2005). Targeting host cell proteins is an attractive strategy as it is thought that drug resistant mutants would be less of a problem than drugs which target virus proteins. A potential disadvantage of host-targeting

compounds is that interference with a cellular target may be associated with toxic side effects. Alisporivir is a compound that binds to the host factor cyclophilin, and is an example of a safe host-targeting antiviral agent that has successfully passed phase II clinical trials for treatment of HCV (van der Schaar *et al.*, 2013).

1.6.1 Antiviral drugs targeting lipids

Different strategies can be used to disrupt viral infection, for example targeting one of the many specific lipids used in the viral replication cycle. Chemical compounds, or even antibodies, can be used to target lipids integrated into the viral particle, in order to inhibit enveloped virus replication Table 1.1 (Martin-Acebes *et al.*, 2013). In addition, inhibitors of enzymes that catalyse lipid metabolic fluxes in viral infections can be used to target lipid metabolism as an antiviral strategy (Munger *et al.*, 2008).

An example of these inhibitors is statins, which are cholesterol biosynthetic pathway inhibitors. Statins are commonly used in the treatment of cardiovascular disease and the treatment of patients with different statins (i.e. lovastatin, simvastin or fluvastin) has significantly decreased the level of viremia, of IL-6 and TNF-alpha in the patients with chronic HCV (Mihaila *et al.*, 2009). A combination of statin/caffeine effectively ameliorated lung damage and inhibited viral replication in influenza virus (Liu *et al.*, 2009). Lovastatin also inhibits Respiratory syncytial virus (RSV) infection both in cultured cells and in mice (Gower and Graham, 2001). Another antiviral that targets cholesterol is U18666A, which suppressed HCV replication in the replicon cell lines (Takano *et al.*, 2011). Using U18666A with DENV infection retarded viral trafficking in the cholesterol-loaded late endosomes/lysosomes and suppressed de novo sterol biosynthesis in treated infected cells (Poh *et al.*, 2012).

Many drugs target fatty acid biosynthesis, such as 5-tetradecyloxy-2-furoic acid (TOFA). TOFA inhibits the biosynthesis of fatty acids acetyl-CoA carboxylase (ACC) and has been shown to block replication of HCMV and influenza A virus. Treatment with trans-4-carboxy-5-octyl-3-

methylene-butyrolactone (C75), an inhibitor of FASN (the key enzyme of fatty acid biosynthetic pathway), also resulted in inhibition of the replication in HCMV, influenza A virus, DENV, yellow fever virus (YFV), WNV, HCV CVB3 and PV (Martin-Acebes *et al.*, 2013).

PIK93 is an inhibitor of PI4KIII β and has been shown to impair replication of enteroviruses (van der Schaar *et al.*, 2013). Enviroxime-like compounds (e.g. T-00127-HEV1 and GW5074) are a group of antivirals that inhibit enterovirus replication, for which mutations conferring drug resistance mapped to the same region of the enteroviral protein 3A (Arita *et al.*, 2011). However, a recent study has associated the antiviral activity of a representative 4-anilino quinazoline (AL-9) with the inhibition of PI4KIII α during HCV infection (Bianco *et al.*, 2012).

Table 1.1: Summary of potential antiviral drugs which target cellular lipids*.		
Target lipid	Inhibitor	Antiviral activity against
Cholesterol	Statins	HIV, HCV, influenza
	U18666A	DENV, HCV
Fatty acids	TOFA	HCMV, Influenza
	C75	HCMV, DENV, YFV, WNV, Influenza, HCV, CVB3
	Cerulenin	DENV, WNV, PV, CVB3
	Arachidonate	HCV
	Oleic acid	PV
PI4P	Enviroxime-like	PV, AiV
	PIK93	PV, CVB3, CVB5
	AL-9	HCV
Sphingolipids	Myriocin	Hepatitis B virus, HCV
Multiple	Valproic acid	VACV, WNV, SFV, SINV, ASFV, VSV, LCMV, USUV
*Taken from (Martin-Acebes <i>et al.</i> , 2013).		

Aims

Human parechoviruses (HPeVs) are important pathogens which can cause serious diseases, but have been studied relatively little. They are also relatively different from better-studied human and animal pathogens, such as enteroviruses and FMDV, and identifying similarities and differences from these viruses may identify potential targets for antiviral agents which could be effective against many different picornaviruses. The aim of the work described in this thesis was to understand the changes to the host cell which occur during HPeV infection, particularly the secretory system which is modified by picornaviruses to generate replication complexes.

The specific objectives were:

To find which components of the secretory system were affected by infection and identify the virus proteins involved in the changes.

To study further a previously observed interaction between HPeV 2C and lipid droplets to define which regions of the protein are involved.

To investigate if drugs which target cellular lipid metabolism can inhibit HPeV infection.

CHAPTER TWO

MATERIALS AND METHODS

2.1 Materials

2.1.1 Chemicals and Reagents

Many chemicals and other reagents were used during this project for the cell culture, virology, imaging and molecular biology experiments that were performed. These chemicals and reagents are listed here to enable other researchers to be able to identify exactly which materials were used.

2.1.1.1 Cell culture

- Dulbecco's Modified Eagle's Medium high glucose (DMEM, Sigma-Aldrich).
- McCoy's 5A Medium (Life Technologies).
- Opti-MEM Reduced Serum Medium (Life Technologies).
- Phosphate buffered saline Dulbecco A tablets (PBS, Oxoid Limited).
- MEM non-essential amino acid 100x Solution (Sigma-Aldrich).
- Penicillin-streptomycin with 10,000 units penicillin and 10 mg streptomycin per ml (Sigma-Aldrich).
- Fetal bovine serum (FBS, Sigma-Aldrich).
- Trypsin-EDTA (0.25%) (Gibco, by Life Technologies).
- Accutase solution (Sigma-Aldrich).
- Dimethyl sulfoxide minimum $\geq 99.5\%$ (DMSO, Sigma-Aldrich).
- 4-(2-hydroxyethyl)-1-piperazineethanesulfonic acid) HEPES (Sigma-Aldrich).

2.1.1.2 Virology

- Carboxymethylcellulose sodium (CMC, Sigma-Aldrich).
- Ethanol, absolute (Fisher BioReagents).
- Crystal violet, pure, indicator (ACROS Organics).
- Itraconazole $\geq 98\%$ (TLC) (Sigma-Aldrich).

- Betulinic acid $\geq 98\%$ (HPLC) (Sigma-Aldrich).
- Brefeldin A from *Penicillium brefeldianum*, $\geq 99\%$ (HPLC and TLC) (Sigma-Aldrich).
- DGAT-1 Inhibitor, A 922500 (Sigma-Aldrich).

2.1.1.3 Imaging

- Triton X-100 (Sigma-Aldrich).
- Saponin (Sigma-Aldrich).
- Glycine (Fisher BioReagents).
- Tween 20 (Sigma-Aldrich).
- Albumin, from bovine serum (Sigma-Aldrich).
- Formaldehyde, 37% by weight (Fisher Chemical).
- Vectashield hard set, antifade mounting medium with DAPI (1.5 $\mu\text{g/ml}$) (H-1500, Vector laboratories).
- Hoechst 33342, trihydrochloride, trihydrate (Invitrogen).
- Analytical grade glycerol (Sigma-Aldrich).
- Mowiol 488 reagent (Calbiochem).
- Xfect protein transfection reagent (Clontech Laboratories).
- Lipofectin reagent (Invitrogen).
- TurboFect transfection reagent (Thermo Scientific).
- HCS (high content screening) LipidTOX (Deep Red neutral, Invitrogen).
- BODIPY 500/510 C4, C9 (5-butyl-4,4-difluoro-4-bora-3a,4a-diaza-s-indacene-3-nonanoic acid) (Life Technologies).
- BODIPY 493/503 (4,4-difluoro-1,3,5,7,8-pentamethyl-4-bora-3a,4a-diaza-s-indacene) (Molecular probes).
- LysoTracker DNA 26 (Life Technologies).
- Mitotracker (green) (Molecular probes).

- All antibodies used are listed in Table 2.1.

2.1.1.4 Molecular biology

- Agarose (Protein Electrophoresis Grade) (Fisher BioReagents).
- Calcium chloride dihydrate, $\geq 99\%$ (CaCl_2 , Sigma-Aldrich).
- Tris base (Fisher BioReagents).
- Ethylenediamine-N, N,N',N',-tetraacetic acid (EDTA, Surechem Products).
- Isopropanol (Fisher BioReagents).
- Ampicillin sodium salt (Sigma-Aldrich).
- Kanamycin sulfate from *Streptomyces kanamyceticus* (Sigma-Aldrich).
- Water, nuclease-free (Thermo Scientific).
- SafeView nucleic acid stain (NBS biologicals).
- Isopropyl β -D-thiogalactopyranoside solution (IPTG, Sigma-Aldrich).
- 5-Bromo-4-chloro-3-indolyl β -D-galactopyranoside (X-Gal, Sigma-Aldrich).
- Agar bacteriological (Oxoid Limited).
- dNTP mix (10mM) (Fermentas Life Sciences).
- T4 DNA ligase (5 weiss u/ μ l) (Thermo Scientific).
- pEGFP-C1 vector (Chemicon).
- pmCherry-C1 (Clontech).
- Dimethylformamide (Sigma-Aldrich).
- Sodium chloride (NaCl , Sigma-Aldrich).
- Tryptone (Sigma-Aldrich).
- Yeast extract (Sigma-Aldrich).
- QIAprep spin miniprep kit (Qiagen).
- HiSpeed plasmid midi Kit (Qiagen).
- QIAquick gel extraction kit (Qiagen).

Table 2.1: List of antibodies and labels that were used and their types and supplier.		
Antibody/ label	Type	Supplier
Anti-CAV9 450-11G-8A-5E	Mouse monoclonal primary antibody	Millipore
Anti-HPeV particles	Rabbit polyclonal primary antibody	Gift from Prof. T. Hyypiä
Anti-PDI* RL90	Mouse monoclonal primary antibody	abcam
Anti-GM130* EP892Y	Rabbit polyclonal primary antibody	abcam
Anti-ERGIC-53 B-9	Mouse monoclonal primary antibody	Santa Cruz Biotechnology
Anti-dsRNA J2*	Mouse monoclonal primary antibody	English & Scientific Consulting Kft., Hősök tere 2, 3044 Szirák, Hungary
Alexa Fluor 405	Goat polyclonal secondary antibody to mouse IgG	Life technologies
Alexa Fluor 405	Goat polyclonal secondary antibody to rabbit IgG	Life technologies
Alexa Fluor 488	Goat polyclonal secondary antibody to mouse IgG	Life technologies
Alexa Fluor 488	Goat polyclonal secondary antibody to rabbit IgG	Life technologies
Alexa Fluor 555	Goat polyclonal secondary antibody to mouse IgG	Life technologies
Alexa Fluor 568	Goat polyclonal secondary antibody to rabbit IgG	Life technologies

PDI: Protein disulfide isomerase an ER marker

GM130: cis-Golgi Marker

dsRNA: double strand RNA

- QIAamp Viral RNA Mini Kit (Qiagen).
- Taq DNA polymerase (Thermo Scientific).
- Pfu DNA polymerase (Thermo Scientific).
- pGEM-T easy vector system I (Promega).
- SuperScript III One-Step RT-PCR System with Platinum Taq DNA Polymerase (Invitrogen).
- All restriction enzymes used are listed in Table 2.2.
- All oligonucleotides used are listed in Table 2.3. They were custom-made by Fisher or Sigma and were dissolved in DNase free water to a final concentration of 100 μ M.
- All constructs encoding the protein of interest fused to a fluorescent protein are listed in Table 2.4

2.1.2 Solution and buffers

2.1.2.1 Phosphate buffered saline buffer

Tablets of PBS (6) were added to 600 ml of deionized water (DI water) to prepare 1X PBS buffer, and then autoclaved.

2.1.2.2 HEPES buffer

To prepare a HEPES solution (500 mM), HEPES (12 g) was dissolved in 100 ml DI water and was adjusted to pH 7.4 with 10N NaOH. The solution then was autoclaved.

2.1.2.3 Carboxy methyl cellulose (CMC)

To prepare a 2% CMC solution, 2 g of CMC was dissolved in 100 ml of DI water then autoclaved.

Table 2.2: List of restriction enzymes that were used and their target sequence and supplier.		
Enzyme	Target and cleavage	Supplier
XhoI (10 U/ μ l)	5`..C↓TCGAG..3` 3`..GAGCT↑C..5`	Thermo Fisher Scientific
SalI (10 U/ μ l)	5`..G↓TCGAC..3` 3`..CAGCT↑G..5`	Thermo Fisher Scientific
EcoRI (10 U/ μ l)	5`..G↓AATTC..3` 3`..CTTAA↑G..5`	Thermo Fisher Scientific
HindIII (10 U/ μ l)	5`..A↓AGCTT..3` 3`..TTCGA↑A..5`	Thermo Fisher Scientific
BamHI (10 U/ μ l)	5`..G↓GATCC..3` 3`..CCTAG↑G..5`	Thermo Fisher Scientific

Table 2.3: List of oligonucleotides used in this project. The oligonucleotides were used to make HPeV1 constructs unless stated otherwise.

Primers	Name	Sequence 5' to 3'
Forward	HRV1B2C	AGAATTCATCTGATTCATGGCTCAAGAAATT TACTG
Reverse	HRV1B2C	TGGATCCTATTGGAAAATTGCAGACATTACA TCTAC
Forward	2C K146	AGGTGAGCCAGGACAAGGAGCATCTTTCTTG ACCCACA
Reverse	2C K146	TGTGGGTCAAGAAAGATGCTCCTTGTCTGG CTCACCT
Forward	2C D188	GATAATCAGGACATTCATTTGATTGCTGACTT GGGTCAAACAAGA
Reverse	2C D188	TCTTGTTTGACCCAAGTCAGCAATCAAATGA ATGTCCTGATTATC
Reverse	2BC	GTCGACTTACTGATTTTCCAATTGTTGTTTCC AAGC
Forward	2C	GAATTCTGGACCTTTTAAAGGATTCAATG
Forward	2C 7A	AGAATTCTGAAGTTTCCACAGCATTTAGGCA TATAGACT
Forward	2C 25A	AGAATTCTATCAAAGATATGGTTCTTAGTGTT TTCAAACCCA
Forward	2C 53A	GAATTCTTGTAGTATCCTTGATTATGCCTC
Forward	2C 75A	GAATTCTCAAGATTTCTACCAAAGGTATTC
Forward	2C 87A	GAATTCTGCCAAGTTCAAGCCAATCATG
Forward	2C 129A	GAATTCTAGAATTGAGCCCATTGGCATTTG
Reverse	2C C1	GTCGACGTAGAAATCTTGAGTCTTCATCTTAG
Reverse	2C C2	GTCGACTTTTTGTAATTGTCTGGAGAGGGTG
Forward	2C Internal	CTTGACCCACACCCTCTCCAGAC
Forward	CAV92A	GTGTCATAGGCATCGTAACCATGGGAG
Reverse	CAV92C	AGGAGACTCTTTTCCATCAGGGTTCTG
Forward	CAV92C	CAGACCCAGATCACTTTGATGGCTAC
Reverse	CAV93C	AGTTTCTCTTCATCATTGCAACGGCGA
Forward	Peroxisome	AGCTACCAGGATCACTGGGAAGACCAAGCTG TAA
Reverse	Peroxisome	GATCTTACAGCTTGGTCTTCCCAGTGATCCTG GT

Table 2.4: List of EGFP/ m-Cherryfusion constructs used. cDNA encoding virus proteins 2A, 2B, 2BC, 2C, 3A or 3C, from either HPeV1 or CAV-9, were provided within vectors encoding EGFP or mCherry. 2C1, 2C2 and 2C4 refer to different parts of the HPeV1 2C protein. Constructs encoding the cellular proteins caveolin 1 (fused to mCherry) or ADRP (fused to RFP) were also used.

Construct	Provided by
pEGFP- 2A HPeV1	Prof. Glyn Stanway and Arsalan Salimi
pEGFP- 2B HPeV1	Prof. Glyn Stanway and Arsalan Salimi
pEGFP- 2C HPeV1	Prof. Glyn Stanway and Arsalan Salimi
pEGFP- 2BC HPeV1	Prof. Glyn Stanway and Arsalan Salimi
pEGFP- 3A HPeV1	Prof. Glyn Stanway and Arsalan Salimi
pmCherry- 3C HPeV1	Prof. Glyn Stanway and Arsalan Salimi
pmCherry- 2C1 HPeV1	Prof. Glyn Stanway and Arsalan Salimi
pmCherry- 2C2 HPeV1	Prof. Glyn Stanway and Arsalan Salimi
pmCherry- 2C4 HPeV1	Prof. Glyn Stanway and Arsalan Salimi
pEGFP- 2BC CAV9	Prof. Glyn Stanway and Arsalan Salimi
pEGFP- 2C CAV9	Prof. Glyn Stanway and Arsalan Salimi
pEGFP- 2B CAV9	Prof. Glyn Stanway and Arsalan Salimi
pEGFP- 3A CAV9	Prof. Glyn Stanway and Arsalan Salimi
pEGFP- 3C CAV9	Prof. Glyn Stanway and Arsalan Salimi
pmCherry- CaV1(dog caveolin 1)	Addgene
pADRP-RFP (Adipose differentiation-related protein)	Addgene

2.1.2.4 Crystal violet solution

To prepare a 0.5% crystal violet solution, 0.5 g of crystal violet was added to 495 ml DI water and 5 ml of absolute ethanol.

2.1.2.5 Blocking solution

To prepare a 1% blocking solution, 0.1 g of BSA and 200 μ l FBS were added to 10 ml of 1X PBS buffer and mixed well. 65 μ l of Tween 20 was then added.

2.1.2.6 Fixing solution

To prepare a 4% formaldehyde fixing solution, 5 ml of 37% formaldehyde was added to 50 ml of 1X PBS buffer.

2.1.2.7 Permeabilization solution

Triton X-100 (125 μ l) of was added to 50 ml of 1X PBS buffer and 65 μ l of Tween 20 to give a final concentration of Triton of 0.25%. In the case of lipid staining, a 0.1% solution of saponin was made, by adding 0.1 g of saponin to 100 ml of 1X PBS.

2.1.2.8 Antibody diluent solution

Bovine serum albumin (BSA, 0.1 g) was added to 10 ml 1X PBS buffer and 65 μ l Tween 20.

2.1.2.9 Glycine washing solution

Glycine (0.375 g) was added to 50 ml 1X PBS and mixed well until it dissolved.

2.1.2.10 DNA electrophoresis buffer (ELFO)

For a 50X ELFO stock, 242 g of Tris and 100 ml of 0.5 M EDTA (pH 8.0) were added to approximately 600 ml of DI water. The pH was adjusted to 7.7 with glacial acetic acid then the solution was made up to 1 l. 1X ELFO was used to make agarose gels and running buffer and was made by diluting the 50X stock.

2.1.2.11 Clear loading dye for agarose gels

Glycerol (50 ml) was added to 200 μ l of 0.5 M EDTA (pH 8.0) and 49.8 ml DI water.

2.1.2.12 Mowiol mounting medium

Analytical grade glycerol (6 g) and Mowiol (2.4 g) were added to 6 ml distilled water and stirred with a clean stir bar, then 12 ml of 2 M Tris buffer (pH 8.5) were added and incubated in a water bath at 50-60°C for 10 minutes until the Mowiol powder went into solution. The solution was centrifuged at 4000 rpm for 15 minutes to pellet any undissolved Mowiol and the supernatant was carefully removed without disturbing the pellet. The supernatant was aliquoted into 1.5 ml centrifuge tubes, covered with aluminium foil and stored at -20°C.

2.1.2.13 Isopropyl β -D-thiogalactopyranoside (IPTG) solution

IPTG (1.2 g) was added to 50 ml DI water then the solution was filter-sterilized, aliquoted into 1.5 ml centrifuge tubes and stored at -20°C.

2.1.2.14 5-Bromo-4-chloro-3-indolyl β -D-galactopyranoside (X-Gal) solution

X-Gal (100 mg) was dissolved in 2 ml dimethyl-formamide. The tube was covered with aluminium foil and was stored at -20°C.

2.1.2.15 Luria-Bertani Broth (LB Broth)

LB Broth powder (20 g) was dissolved in 1 l distilled water. The solution was adjusted to pH 7.0 with 5 M NaOH then autoclaved.

2.1.2.16 Luria-Bertani Agar

Agar (1.48 g) was dissolved in 100 ml of LB broth and was autoclaved. To produce antibiotic plates, the agar was melted in a boiling water bath, allowed to cool to 50°C and stock ampicillin or kanamycin solutions were added to give a final concentration of 100 μ g/ml and 50 μ g/ml respectively.

2.1.3 Cell lines and viruses

African green monkey kidney epithelial (GMK) and human prostate cancer (PC3) cells were provided by Prof. Glyn Stanway. The human colon adenocarcinoma cell line (HT29) was

provided by Dr Ralf Zwacka. Human parechovirus (HPeV1), Harris strain, was recovered from the cDNA clone pHPeV1 (Nateri *et al.*, 2000). Coxsackievirus A9 (CAV9), Griggs strain, was recovered from the cDNA clone pCAV9 (Hughes *et al.*, 1995).

2.2 Methods

2.2.1 Cell Culture

2.2.1.1 Passaging/Splitting Cells

Cells were observed using a microscope to ensure they were confluent and healthy. The old-medium was discarded and cells washed twice with 1X PBS for 2 minutes. Then 500 μ l of 0.25% trypsin-EDTA was added and the flask was placed on a rocking platform for 5 minutes. The flask was tapped and checked under the microscope to ensure cells detached. DMEM (20 ml containing 10% FBS, 1% MEM non-essential amino acid and 1% Penicillin-Streptomycin) was added to the flask and the cell suspension was divided into 4 new 50 ml flasks (25 cm²). These were incubated in a 5% CO₂ incubator at 37°C. Cells were passaged weekly.

2.2.1.2 Cell line storage

Old medium of a confluent cell line was discarded and the cells were washed twice with 1X PBS. Trypsin-EDTA (500 μ l of a 0.25% solution) was added and the flask was placed on a rocking platform for 5 minutes. The flask was tapped to detach the cell and 1 ml of FBS was added and mixed. A 1 ml aliquot of the mixture was placed in a cryo tube and 111 μ l of DMSO was added. The tube was placed in an insulated container, to ensure slow freezing, for three day at -80°C, then stored at -80°C.

To recover the cells, the tube was thawed and the cell suspension was transferred to a flask containing 4 ml of new medium and 500 μ l FBS and incubated in a 5% CO₂ incubator at 37°C. The medium was changed next day and the cells observed until they became confluent. The cells were then propagated as described in section 2.2.1.1.

2.2.2 Molecular biology

2.2.2.1 Double digestion

The two restriction enzymes (2 μ l of each) were added to 5 μ l of suitable buffer (one where enzymes cut efficiently). DNA (5 μ l, 1 μ g) and DNase free water (36 μ l) were added and incubated for one hour at 37°C. The reaction were separated on a 1% agarose gel and the correct band was cut from the gel and extracted using a Qiaquick gel extraction kit gel (QIAGEN).

2.2.2.2 Agarose gels

Agarose gel electrophoresis was used to size DNA fragments and purify them. Agarose powder (0.5 g) was added to 50 ml of 1X ELFO buffer and melted in a microwave until the agarose completely dissolved and the solution become clear. The agarose solution was allowed to cool down for 5 minutes then SafeView (2 μ l) was added just before pouring into the casting tray. The gel tray had a comb to form the wells. After the gel had set it was placed in the electrophoresis unit which was filled with enough 1X ELFO to cover it. The comb was removed and 5 μ l (for analysis or 50 μ l for purification) of each sample was loaded onto the gel. The gel was run at 80-150V for 10-15 minutes and the DNA was observed using a blue light LED transilluminator. A scalpel was used to cut out bands from agarose gels and purify the DNA for cloning.

2.2.2.3 Gel extraction

Extraction of DNA from agarose gel slices was performed using a QIAquick gel extraction kit according to the manufacturer instructions. Buffer QG (300 μ l) was added to a slice of agarose gel containing the DNA in a 1.5 ml microcentrifuge tube and was incubated at 50°C for 10 minutes. The tube was vortexed every 2-3 minutes until the gel slice completely dissolved. Isopropanol (100 μ l) was added to the tube and was mixed, then the solution was transferred to the QIAquick column and was centrifuged for one minute at 13000 rpm. The flow-through was discarded and the QIAquick column placed back into the same tube. For washing 750 μ l of buffer PE was added and was re-centrifuged and the flow-through was discarded. The QIAquick column was placed

into a clean 1.5 ml microcentrifuge tube and 50 μ l of buffer EB was added to elute the DNA. The column was left for one minute and was then centrifuged at 13000 rpm for one minute. The tube was labelled and stored at -80°C .

2.2.2.4 Ligation of DNA fragments using T4 DNA ligase

In a 1.5 ml microcentrifuge tube on ice, 2 μ l of T4 ligase buffer, 1 μ l of T4 DNA ligase, 3 μ l of the vector (50 ng pmCherry-C1/ pEGFP-C1/ pGEM-T easy), up to 9 μ l of insert DNA (1:3 molar ratio of vector to insert) and DNase-free water to the final volume 50 μ l were mixed gently by pipetting. The mixture was incubated overnight in 4°C then a 5 μ l aliquot of the mixture was used for transformation.

2.2.2.5 Competent cells

A frozen stock of Top10 *E.coli* was streaked out onto an LB plate without antibiotics and incubated overnight at 37°C . A single colony was picked and was grown in 10 ml of LB broth overnight in a shaking incubator at 37°C .

An aliquot (200 μ l) of the overnight culture was added to 10 ml LB broth Top10 and grown for 2 hours in a shaking incubator at 37°C . The cells were centrifuged for 10 minutes at 4,000 rpm and the supernatant was discarded and resuspended in 5 ml ice-cold 0.1 M CaCl_2 for 30 minutes. Then the cells were recentrifuged, the supernatant was discarded and resuspended in 500 μ l ice-cold CaCl_2 for an hour. At this point the competent cells were ready to use in transformation.

2.2.2.6 Transformation

An aliquot (5 μ l) of the transforming DNA construct was added to 100 μ l of competent cells in a 1.5 ml microcentrifuge tube on ice and was incubated for 30 minutes. Then the tube was incubated in a water bath at 42°C for one minute (heat shock) and then was placed back in ice for 2 minutes. LB broth (250 μ l) was added and incubated for one hour at 37°C in a shaking incubator. A 100 μ l aliquot of the mixture was spread on LB plates (with appropriate antibiotic added, 100 $\mu\text{g/ml}$ ampicillin or 50 $\mu\text{g/ml}$ kanamycin).

2.2.2.7 Purification of DNA using QIAprep miniprep kit

A single colony was picked from the transformation plate and was incubated in 10 ml LB medium with antibiotic overnight in a 37°C shaking incubator. Then it was centrifuged at 3000 rpm for 10 minutes and the pellet was resuspended in 250 µl of buffer P1 and was transferred to a 1.5 ml microcentrifuge tube. Buffer P2 (250µl) was added and the tube was inverted 4-6 times to mix. Buffer N3 (350 µl) was added and the tube was inverted immediately 4-6 times, then centrifuged for 10 minutes at 13000 rpm. The supernatant was applied to a QIAprep column in a 1.5 ml microcentrifuge tube and re-centrifuged for 60 seconds and the flow-through was discarded. The QIAprep spin column was washed with 750 µl of PE buffer and centrifuged for 60 seconds. The flow-through was discarded and the column re-centrifuged for 60 seconds to remove residual wash buffer. The QIAprep column was placed in a clean 1.5 ml microcentrifuge tube and the DNA was eluted by adding 50 µl of buffer EB and after one minute was centrifuged for one minute. The purified DNA was stored at -80°C.

2.2.2.8 Purification of DNA using a Qiagen HiSpeed plasmid midi kit

A single colony was picked from a plate and was incubated in 10 ml LB medium containing the appropriate selective antibiotic for 6 hours at 37°C in a shaking incubator. The culture was transferred to 200 ml LB medium containing the appropriate selective antibiotic and was incubated overnight. The bacterial cells were harvested by centrifugation at 6000 rpm for 15 minutes at 4°C and the supernatant was discarded and the pellet was resuspended in 6 ml of buffer P1 by vortexing until no cell clumps remain. Buffer P2 (6 ml) was added and mixed thoroughly by vigorously inverting the sealed tube 4–6 times and incubated at room temperature for 5 minutes. During the incubation the cap was screwed onto the outlet nozzle of the QIAfilter Midi cartridge. Buffer P3 (6 ml) was added, mixed immediately then the sample was poured into the barrel of a QIAfilter cartridge and was incubated at room temperature for 10 minutes. During the incubation a HiSpeed column was equilibrated with 4 ml buffer QBT and the column was

allowed to empty by gravity flow. The cap was removed from the QIAfilter outlet nozzle and the plunger was gently inserted into the cartridge. The lysate was then filtered into the HISpeed tip. The HISpeed tip was washed with 20 ml buffer QC and the DNA was eluted with 5 ml buffer QF and was precipitated by adding 3.5 ml isopropanol and incubating for 5 minutes. During the incubation the plunger from a 20 ml syringe was removed and attached to the QIAprecipitator Midi Module. The QIAprecipitator was placed over a waste bottle and the eluate/isopropanol mixture was transferred into the 20 ml syringe then the plunger was inserted. By using constant pressure the eluate/isopropanol mixture was filtered through the QIAprecipitator. The QIAprecipitator was removed from the 20 ml syringe and the plunger was pulled out, then it was re-attached and 2 ml of 70% ethanol was added to wash the DNA. The QIAprecipitator was removed from the 20 ml syringe and the plunger pulled out and reattached again and the membrane was dried by pressing air through the QIAprecipitator quickly and forcefully. The outlet nozzle of the QIAprecipitator was dried with absorbent paper to prevent ethanol carryover. The plunger from a new 5 ml syringe was removed and attached to the QIAprecipitator onto the outlet nozzle. Over a 1.5 ml microcentrifuge tube 1 ml of buffer TE was added to the 5 ml syringe and the plunger was inserted and the DNA was eluted into a 1.5 ml microcentrifuge tube. The DNA was stored at -80°C .

2.2.2.9 Polymerase chain reaction (PCR)

For each 50 μl PCR reaction 1 μl of DNA template (10 ng), 1 μl of each forward and reverse primer (at a concentration of 100 μM), 5 μl MgSO_4 buffer (final concentration 2 mM), 1 μl dNTP (final concentration 0.2 mM), 1 μl of pfu DNA polymerase and 40 μl DNase free water were placed in PCR machine. The thermocycling profile of the PCR reaction consisted of an initial denaturation step at 95°C for 5 minutes, followed by 35 cycles of denaturation (95°C for one minute), annealing (45°C - 55°C for one minute) and extension (72°C for 1-3 minutes). A final extension step of 72°C for 5 minutes was included to complete the PCR (Figure 2.1). In the final

stage, 2 μl of Taq DNA polymerase was added for 15 min at 72°C to add an A residue to the 3' terminus of the PCR product, so it can be ligated to pGEM-T-Easy. The reaction products were run on a 1% (w/v) agarose gel and extracted using Qiaquick Gel extraction kit gel.

Single mutations were achieved by performing PCR with a pair of overlapping oligonucleotide primers that include a mutation in their sequence together with two other primers. As a result, two fragments were produced. These fragments were fused together by overlapping PCR (Figure 2.2).

2.2.2.10 Ligation using the pGEM-T Easy vector

The purified PCR product were ligated into the pGEM-T Easy cloning vector using the reagent provided by the manufacturers. A 10 μl final reaction volume consisted of 1 μl (50 ng) of pGEM-T Easy DNA, 2 μl of the purified PCR product (20-50 ng), 1 μl T4 DNA ligase, 5 μl of 2x rapid ligation buffer and 1 μl DI water. The reaction was mixed and incubated at room temperature for one hour.

2.2.2.11 Transformation using the pGEM-T Easy vector

An aliquot of the pGEM-T Easy ligation reaction (5 μl) was added to 100 μl of competent cells in a 1.5 ml microcentrifuge tube on ice and was incubated for 30 minutes. Then the tube was incubated in a water bath at 42°C for one minute (heat shock) and then was placed back in ice for 2 minutes. LB broth (250 μl) was added and incubated for one hour at 37°C in a shaking incubator. An aliquot (100 μl) of the mixture was spread on LB plates containing 100 $\mu\text{g/ml}$ ampicillin, 100 mM IPTG and 50 mg/ml X-Gal. The plates were incubated overnight and 3-5 white colonies were picked for DNA purification or colony PCR.

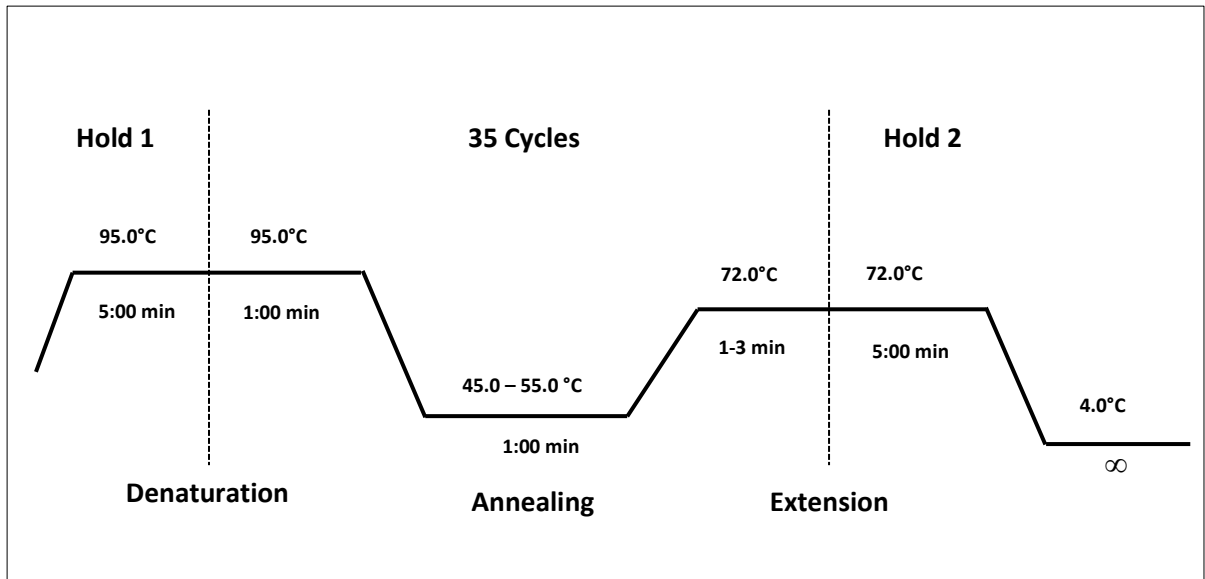


FIGURE 2.1: Schematic diagram of the PCR reaction using pfu polymerase. An initial denaturation step at 95°C for 5 minutes to activate the polymerase enzyme was followed by 35 cycles of denaturation (94°C for one minute), annealing (45°C - 55°C for one minute) and extension (72°C for 2 minutes). A final extension step of 72°C for 5 minutes was included to complete the PCR. The annealing temperature depends on the melting temperature of the primers and the length of the 72°C extension may vary based on the length of the amplified DNA fragment.

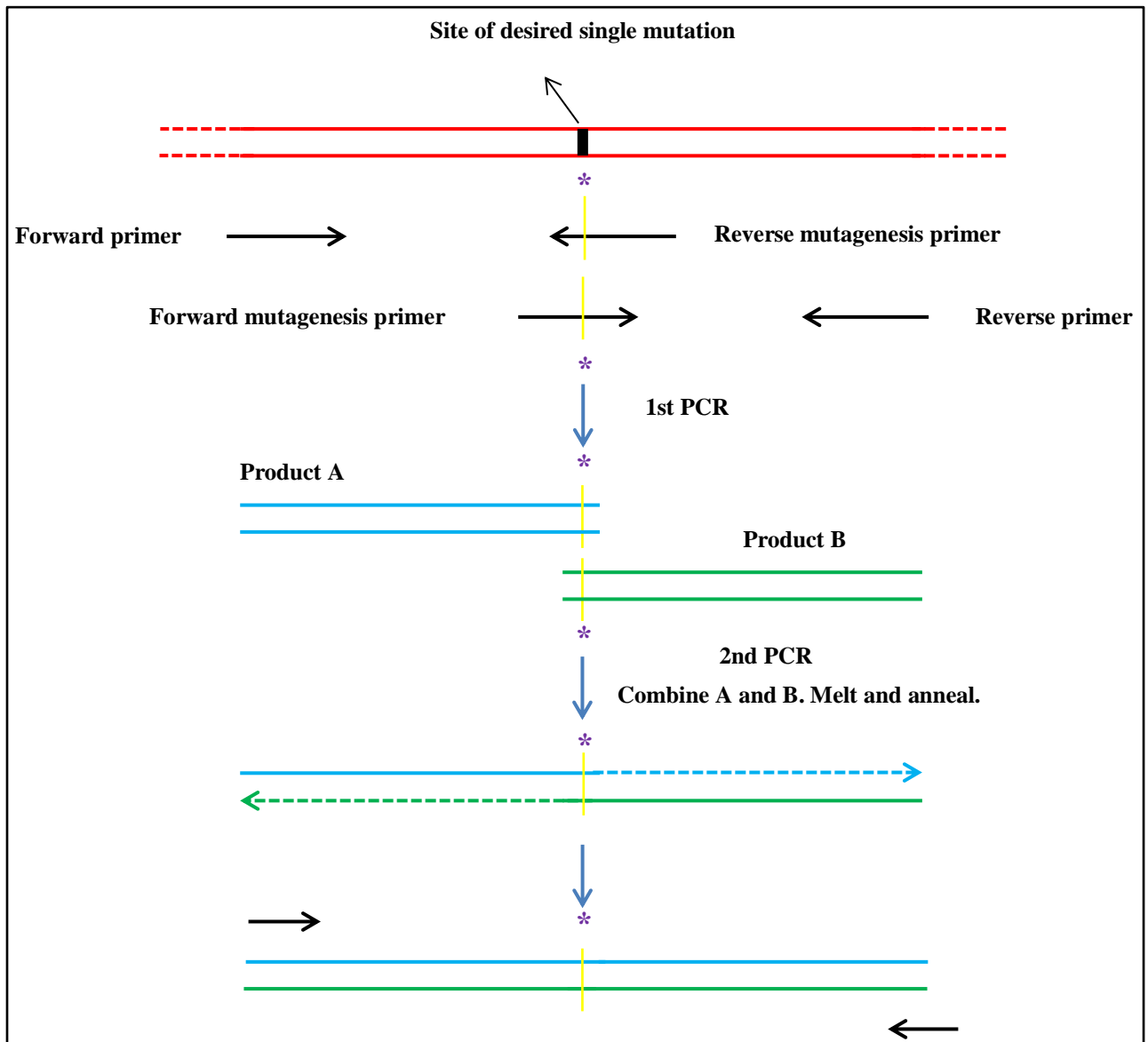


FIGURE 2.2: Schematic diagram of overlap PCR. Designed overlapping oligonucleotide primers (Forward and Reverse primers) include a mutation in their sequence. Two separate PCR reactions are performed. One has Forward primer + Reverse mutagenesis primer (A) and other has Forward mutagenesis primer + Reverse primer (B). As a result two fragments are produced. These fragments are fused together by overlapping PCR. A and B are combined and are melted and annealed in the first cycle of the second PCR. One of the results is an overlap between the top strand of product A and the bottom strand of product B. The overlap region acts as primers which can be extended to complete the dsDNA and "fuse" the two products, containing the mutation (*). The PCR reaction contains Forward and Reverse primers which lead to the amplification of the correct product during the rest of the PCR reaction.

2.2.2.12 Colony PCR

Colony PCR was used as a preliminary screen to identify colonies transformed with the correctly constructed DNA. In a PCR tube, 5 μ l of 10x reaction buffer, 3 μ l $MgCl_2$ (final concentration 2.5 mM), 1 μ l dNTPs (final concentration 0.2 mM), 1 μ l of each desired primer (100 μ M), 0.5 μ l DNA Taq polymerase and 38 μ l of DNase free water were mixed. One colony was touched with a yellow tips and swirled in the PCR mixture which was then placed in the PCR machine. The thermocycling profile of the PCR reaction consisted of an initial denaturation step at 95°C for 2 minute, followed by 30 cycles of denaturation (94°C for one minute), annealing (50°C for one minute) and extension (72°C for 2 minutes). A final extension step of 72°C for 5 minutes was included to complete the PCR (Figure 2.3).

2.2.2.13 Purification of viral RNA using a QIAamp Viral RNA Mini Kit

Buffer AVL (560 μ l) containing carrier RNA was pipetted into a 1.5 ml microcentrifuge tube and 140 μ l supernatant of virus-infected cells was added. The tube was mixed by pulse-vortexing for 15 seconds and was incubated at room temperature for 10 minutes. The tube was briefly centrifuged to remove drops from the inside of the lid and 560 μ l of ethanol (96–100%) was added, mixed by pulse-vortexing for 15 seconds and was briefly centrifuged. Half of the solution (630 μ l) was added to the QIAamp Mini column and centrifuged for 1 minute at 8000 rpm. The QIAamp Mini column was placed into a clean 2 ml collection tube and another 630 μ l of the solution was added and recentrifuged. Buffer AW1 (500 μ l) was added to the QIAamp Mini column and centrifuged for 1 minute at 8000 rpm. The QIAamp Mini column was placed in a clean 2 ml collection tube, 500 μ l of buffer AW2 was added and the column was centrifuged for 3 minutes at 14,000 rpm. The QIAamp Mini column was placed in a clean 1.5 ml microcentrifuge tube and 60 μ l of buffer AVE was added and centrifuged for 1 minute at 8000 rpm to elute the DNA. The DNA was stored at -80°C.

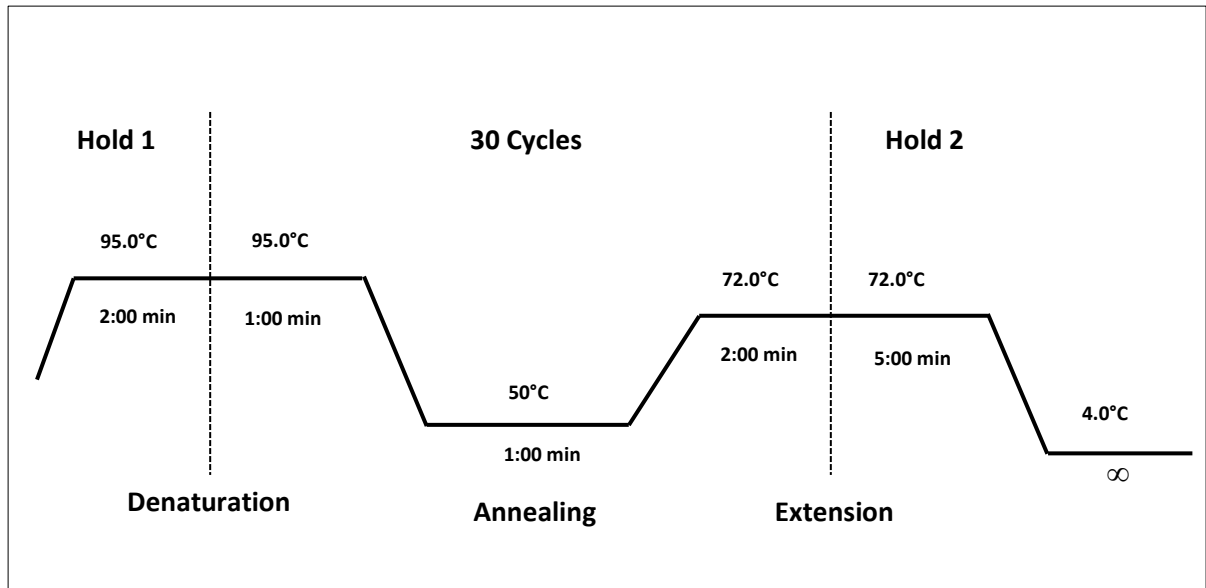


FIGURE 2.3: Schematic diagram of the Colony PCR reaction. An initial denaturation step at 95°C for 2 minutes, was followed by 30 cycles of denaturation (94°C for one minute), annealing at 50°C for one minute and extension 72°C for 2 minutes. A final extension step of 72°C for 5 minutes was included to complete the PCR.

2.2.2.14 Reverse transcription-PCR (RT-PCR)

Per 50 µl PCR reaction 5 µl of RNA, 1 µl of forward and reverse primers (100 µM), 25 µl reaction mix, 1 µl RT/Taq and 17 µl DNase free water were mixed and placed in a PCR machine. The machine was programmed to give an initial RT step of 30 minutes. The thermocycling profile of the PCR reaction consisted of an initial denaturation step at 94°C for 2 minutes, followed by 35 cycles of denaturation (94°C for 30 seconds), annealing (45°C for one minute) and extension (68°C for 2 minutes). A final extension step of (68°C for 5 minutes) was included to complete the PCR. The reaction products were run on a 1% (w/v) agarose gel and extracted using Qiaquick Gel extraction kit gel. The products were sequenced, using the same primers used for RT-PCR, by Source Bioscience.

2.2.3 Virus propagation and plaque assays

2.2.3.1 Propagation of Viruses

Confluent cells in a flask were infected by adding 10 µl of stock virus to the medium and were placed on a rocking platform for 45 minutes then incubated at 37°C for 2-3 days. The flask was frozen and thawed three times then the supernatant stored at -80°C in 500 µl aliquots in 1.5 ml microcentrifuge tubes.

2.2.3.2 Plaque assay

The medium from a confluent monolayer of cells was removed and replaced with 1 ml of fresh medium. Serial 10-fold dilutions of CAV9 and HPeV1 virus were made (10^2 , 10^3 and 10^4) using DMEM medium. Aliquots (100 µl) of each dilution was added to the cell monolayer in a 25 cm² flask or a 6 well plate and the flask or plate was placed on a rocking platform for 45 minutes at room temperature. CMC solution (2%) was melted in a microwave, added to medium (1 ml CMC : 2 ml medium) and incubated in a water bath 45°C to keep it liquid. Part of the mixture (4 ml) was added to the flask (or 2 ml to each well of a 6 well plate), mixed and kept at room temperature until set. The flask or plate was incubated at 37°C for 4-5 days. The flask or plate

was washed with 1 ml of 1X PBS then cells were stained with 0.1% crystal violet for 10 minutes. Finally, cells were washed with 1X PBS.

2.2.4 Drugs and generation of mutants resistant to drugs

2.2.4.1 Drugs and inhibitors screening study

Confluent cells at the time of infection in 6 well plates were used. Different serial concentration of drugs or inhibitors in culture medium were prepared and incubated with cells for 30 minutes before infection. Cells were infected with CAV9 or HPeV1 (MOI 10) and the plate was placed on a rocking platform for 45 minutes then incubated at 37°C for 36 or 42 hours. The cells were frozen and thawed three times and stored at -80°C. A plaque assay were applied to quantify the level of virus. In other experiments, cells were pre-treated with the drugs and then plaque assays were performed as described 2.2.3.2.

2.2.4.2 Generation of mutants resistant to drugs and inhibitors

An attempt was made to generate drug-resistant mutants by passaging virus on cells line in the presence of the drugs or inhibitors. For each round of passaging, cells in 6 well plates were infected with (10 µl of previous passaging for HPeV1 and 100 µl of a 10² dilution of CAV9) in the presence of increasing concentrations of drugs or inhibitors. In the first round of infection 0.1 MOI was used. Viral RNAs from passage 6 were extracted from the culture supernatants using a QIAamp viral RNA minikit. The RNAs were subjected to amplification using SuperScript III one-step reverse transcription-PCR (RT-PCR) kits.

2.2.4.3 Time-of-addition assay

A time-of-addition assay was performed to study the mechanism of drugs and inhibitors. Cells were seeded in a 6 well plate 24 hours before the experiment. Old medium was removed and 0.5 ml of fresh medium was added. The drugs or inhibitor was added to one well which was the zero time point, and incubated for 30 minutes. All the cells were infected with virus and the plate were placed on a rocking platform for 45 minutes. The drugs or inhibitors were added at 1, 3, 5

and 8 hours post- infection. The plate was incubated at 37°C incubators for (36 hours for CAV9 and 42 hours for HPeV1). The plate was frozen-then-thawed three times and a plaque assay was applied.

2.2.5 Immunofluorescence

2.2.5.1 Detection of infected cells and lipid staining

A suspension of GMK or HT29 cells (2 ml) was seeded into each well of a 6 well plate containing a glass coverslip 24 hours before the experiment. After 24 hours, 1.5 ml of the medium was removed and cells were infected with 100 µl CAV9 or HPeV1 (MOI 10) and were placed on a rocking platform for 45 minutes then incubated for 8 hours at 37°C. Cells were fixed with 4% formalin for 20 minutes at room temperature and were washed with glycine washing solution for 5 minutes and permeabilized with Saponin 0.1% for 20 minutes. They were washed with PBS for 10 minutes and blocked with blocking solution for 30 minutes, then washed with PBS for 10 minutes. Primary antibodies to CAV9 or HPeV-1 (50 µl of a 1:100 dilution of primary antibody) was placed onto the coverslip, covered by parafilm and kept overnight at 4°C. Secondary antibody (50 µl of a 1:200 dilution of secondary antibody) was added and incubated for 2 hours at 4°C, then the cells were washed with PBS for 10 minutes. For lipid staining, cells were incubated with BODIPY 493/503 for 10 min then cells were washed twice with PBS. The coverslips were mounted with hard set mounting medium containing DAPI (1.5 µg/ml).

2.2.5.2 Detection of infected cells and fatty acids staining

Cells were seeded to 6 well plates containing glass coverslips 24 hours before the experiment as described in section 2.2.4.1. Cells were washed with DMEM serum-free medium and infected with 50 µl of virus in serum-free medium with 50 mM HEPES. The plate was placed on a rocking platform for 30 minutes then incubated in a 37°C incubator. After 2, 6, or 8 hours, in one well was the medium was replaced with fresh pre-warmed medium containing 0.4 µM BODIPY 500/510 for 30 minutes. Cells were fixed with 4% formalin for 20 minutes at room temperature

and were washed with glycine washing solution for 5 minutes and permeabilized with Saponin 0.1% for 20 min. They were washed with PBS for 10 minutes, blocked by blocking solution for 30 minutes and washed in PBS for 10 minutes. Antibody staining was carried out as described in section 2.2.5.1.

2.2.5.3 Transfection of fluorescent constructs

Three different transfection reagents were used to study the distribution of the fluorescent protein functions and gave similar transfection rates.

2.2.5.3.1 Xfect protein transfection reagent

In a 1.5 ml microcentrifuge tube 5 μ l (5 μ g) of the constructs was added to 100 μ l Xfect reaction buffer and mixed. Xfect Polymer (1.5 μ l) was added to the reaction and incubated for 10 minutes at room temperature. The tube was centrifuged briefly to collect the contents at the bottom of the tube. The solution was added to 50–70% confluent cells at the time of transfection in wells of a 6 well plate containing glass coverslips and placed on a rocking platform for 5 minutes then incubated at 37°C incubator for 4 hours. The solution was replaced with 2 ml fresh DMEM medium, and the plate was returned to the 37°C incubator until the time of analysis. If live cells were visualized, cells were stained with 0.5 μ l Hoechst 33342 per 1 ml of warm DMEM medium and incubated at 37°C for 20 minutes then washed twice with 1X PBS and coverslips were mounted using Mowiol mounting medium. If fixed cells were visualized, the cells were fixed with 4% formalin for 20 minutes at room temperature and were washed with glycine washing solution for 5 minutes. The coverslips were mounted with hard set mounting medium with DAPI (1.5 μ g/ml).

2.2.5.3.2 Lipofectin[®] transfection reagent

Opti-MEM reduced serum medium (100 μ l) was added to two 1.5 ml microcentrifuge tubes (tube A and tube B). In tube A 1-2 μ g of the construct were added and in tube B 2-20 μ l of Lipofectin[®] reagent was added. Both tubes were incubated for one hour at room temperature

then the contents of tube B were combined with tube A, mixed gently and incubated for 20 minutes at room temperature. During the incubation, 50–70% confluent cells, at the time of transfection, in a 6 well plate containing glass coverslips were washed once with Opti-MEM reduced-serum medium. Opti-MEM reduced-serum medium (800 μ l) was added to the tube A+B and the whole sample transferred to one of the wells. The plate was incubated at 37°C for 24 hours then the medium was replaced with 2 ml DMEM medium and was incubated for another 24 hours until time of analysis. Cell visualizing was carried out as described in section 2.2.5.3.1.

2.2.5.3.3 TurboFect transfection reagent

In a 1.5 ml microcentrifuge tube 1 μ g of the construct was added to Opti-MEM reduced serum medium (100 μ l), 2 μ l of TurboFect transfection reagent was added and the tube was mixed. The tube was incubated for 20 minutes at room temperature. The mixture was added to 900 μ l of medium. 50–70% confluent cells, at the time of transfection, in a 6 well plate containing glass coverslips were covered with the mixture. The plate was placed on a rocking platform for 5 minutes and was then incubated in a 37°C incubator for 24-48 hours. Cells were fixed with 4% formalin for 20 minutes at room temperature and were washed with glycine washing solution for 5 minutes. The coverslips were mounted with hard set mounting medium with DAPI (1.5 μ g/ml).

2.2.5.4 Confocal microscope

To record several probes in a single specimen, multichannel fluorescence microscopy using multiple fluorochromes of different excitation and emission wavelengths were used (Landmann, 2002).

Cells were visualized using a Nikon A1si confocal microscope used with a plan apochromatic VC1.4 N.A. 60x magnifying oil-immersion objective. Images were acquired in three channels, using one-way sequential line scans. The emission for DAPI was collected at 450/50 nm with a PMT gain of 118 and the excitation at 400 nm with laser power 7.2 arbitrary units. GFP was excited at 488 nm with laser power 5.8 and the emission was collected at 525/50 nm with a PMT

gain of 90. mCherry was excited at 560 nm with laser power 3.2, and collected at 595/50 nm with a PMT gain of 121. The pinhole size was 47.5 μm , approximating 1.2 times the Airy disk size of the 1.4 N.A. objective at 525 nm. Scan speed was $\frac{1}{4}$ frames/s (galvano scanner). Scanner zoom was centred on the optical axis and set to a lateral magnification of 60 nm/pixel. Axial step size was 105 nm, with 80-100 image planes per z-stack. Identical settings were used for all acquired datasets, Following Nyquist–Shannon reconstruction theorem (Nyquist, 1928; Shannon, 1949).

A minimum of 4 cells were imaged for each experiment, taken from 10 fields-of-view. For localisation studies, each experiment was repeated at least twice and representative images have been chosen. For 2C mutants, three dimensional (3D) images were acquired in three channels, using one-way sequential line scans. In some images, the DAPI stain was faint or lost due to technical problem with the DAPI filter of the confocal microscope.

Colocalisation experiments are based on the detection of the spatial overlap of one fluorescently-labelled molecule e.g. a protein, with another molecule tagged with a fluorophore emitting at a different wavelength. There are two ways to assess colocalization between fluorescence channels (Dunn et al., 2011; Adler and Parmryd, 2010). The co-occurrence method simply considers the presence of both fluorophore signals in individual pixels. For a more quantitative analysis of colocalisation, there are statistical methods to determine the overlap globally, including the use of advanced intensity-based correlation coefficients (Obara et al., 2013).

In the work described in this thesis, colocalisation was usually assessed qualitatively, using overlaid images from green and red channels, which show overlapping regions as yellow, allowing colocalisation to be inferred. In several cases, including all the analysis of the HPeV1 2C mutants, colocalization was characterized more quantitatively by calculating the Pearson's correlation coefficient, using NIS-Elements AR 4.13.01 (Build 916) software to analyse the degree of colocalization.

2.2.6 Computer analysis

NIS-Elements AR 4.13.01(Build 916) software was used for image acquisition. EXCEL 2010 from Microsoft was used to analyse data and graphs. ExPASy - Translate tool <https://www.expasy.org/translate/> and Multiple Sequence Alignment by CLUSTALW <http://www.genome.jp/tools/clustalw/> were used to analyse the sequencing results. NetWheels (<http://lbqp.unb.br/NetWheels/>) was used to produce helical wheel projections of potential amphipathic helices.

CHAPTER THREE
EFFECT OF HPeV INFECTION AND
HPeV PROTEINS ON THE
SECRETORY SYSTEM

3.1 Introduction

In mammalian cells, there is extensive trafficking of proteins and lipids between intracellular compartments (Watson and Stephens, 2005). The early secretory pathway consists of the endoplasmic reticulum (ER), the ER–Golgi intermediate compartment (ERGIC) and the Golgi as well as the transport vesicles that shuttle between them (Midgley *et al.*, 2013). The ER is the first compartment and is the largest organelle in a cell. It is a highly dynamic membrane system and is the major site of many processes such as protein synthesis and transport, protein folding, lipid and steroid synthesis, carbohydrate metabolism and calcium storage (Romero-Brey and Bartenschlager, 2016). The ERGIC is the second compartment and is the initial site of protein sorting. The Golgi is important for sorting and packaging of macromolecules for delivery to endosomes, the plasma membrane or the cell exterior (Barlowe and Helenius, 2016).

Vesicles carry cargos through the early secretory pathway and their formation is dependent on the function of two membrane coat complexes, COPI and COPII, and requires the GTPase Sar1, Arf1 and Rab proteins. Cargo traffic from the ER to Golgi (anterograde) through the ERGIC is due to COPII-coated vesicles, which form at ER exit site (ERESs), then COPI-coated vesicles (Gazina *et al.*, 2002; Sharp *et al.*, 2010).

COPI-coated vesicles are also involved in retrograde trafficking from the ERGIC and Golgi to the ER. COPI coat formation requires the GTPase ADP-ribosylation factor 1 (Arf1) which is activated on the Golgi by two related GEFs called GBF1 and BIGs (Sharp *et al.*, 2010). Rab proteins also regulate the secretory pathway and are involved in vesicle formation, transport, tethering, docking and membrane fusion (Gazina *et al.*, 2002; Midgley *et al.*, 2013).

Lysosomes are organelles found in the cytoplasm of most cells. Lysosomes degrade macromolecules or infecting pathogens from the secretory, endocytic, autophagic, and phagocytic membrane-trafficking pathways, which are essential for innate immunity recognition, antigen presentation, and pathogen elimination (Ju *et al.*, 2015; Luzio *et al.*, 2007).

Mitochondria are involved in many cellular metabolic processes including ATP production, calcium homeostasis, cell proliferation, programmed cell death, and the synthesis of amino acids, nucleotides, and lipids. Mitochondria play a central role in host antiviral responses, and a number of viral proteins localise in mitochondria and interact with mitochondrial proteins (Ohta and Nishiyama, 2011).

Peroxisomes are found in almost all eukaryotic cells and are surrounded by a single membrane (Baker *et al.*, 2015). Functionally and morphologically, peroxisomes are complex organelles that play a central role in diverse metabolic processes and interact with other organelles such as the ER, mitochondria and lipid droplets. One important function of peroxisomes is β -oxidation where a very long fatty acid chain and dicarboxylic acids is degraded (Baker *et al.*, 2015; Odendall and Kagan, 2013).

In positive-strand RNA viruses, RNA synthesis involves cytoplasmic membranes, but different cellular membranes can be used by different viruses. The ER, trans-Golgi, endosomes, mitochondria or lysosomes are known as sources for virally induced membranes (Suhy *et al.*, 2000). These membrane structures are used for several reasons, such as concentrating components needed for virus replication, providing a scaffold to anchor replication complexes, hiding dsRNA and so avoiding host defence mechanisms which respond to dsRNA, tethering viral RNA during unwinding and providing lipids needed for genome synthesis (Miller and Krijnse-Locker, 2008; Sasaki *et al.*, 2012). Hepatitis E virus may utilize modified early secretory pathway membranes for replication (Perttilä *et al.*, 2013). Dengue virus non-structural protein NS4A rearranges the ER membrane, leading to the formation of vesicle packets and convoluted membranes (Inoue and Tsai, 2013).

Remodelling of the secretory system seems to depend on different non-structural proteins in different viruses. 2B, 2BC, or 3A (but *not* 2C) of PV disrupt protein trafficking and cell surface protein expression. Expression of 2B *and* 2C or of the 2BC precursor (but *not* 3A) is sufficient to

inhibit trafficking between the ER and Golgi in FDMV (Sweeney *et al.*, 2010). In FMDV-infected cells, the ER remained largely intact but the Golgi and ERGIC was disrupted (Midgley *et al.*, 2013).

Not much is known about the effect of HPeV infection on the secretory system. It has been reported that none of the HPeV1 non-structural proteins studied was able, alone or when combined, to induce changes in the intracellular morphology similar to those seen in HPeV infected cells (Krogerus *et al.* 2007). The individual distribution of the proteins was also not affected when they combined.

The effects of picornavirus infection on structure such as the mitochondria, lysosome and peroxisomes have not been studied extensively. In this study we looked at the effect of human parechovirus infection on the secretory system and re-investigated the role of the non-structural proteins in these effects as well as the effects on mitochondria, lysosome and peroxisomes.

3.2 The effect of HPeV1 infection on the secretory pathway

We studied the effect of HPeV1 infection on the ER, ERGIC, and Golgi using antibodies against dsRNA (mouse monoclonal) or HPeV1 (rabbit polyclonal) to identify infected cells. Antibodies against the marker proteins PDI (ER marker, mouse monoclonal antibody), ERGIC-53 (ERGIC marker, mouse monoclonal antibody) and GM130 (cis Golgi marker, rabbit polyclonal antibody) were used to mark the compartments. Confluent HT29 cells at the time of infection were prepared in 6 well plates containing glass coverslips. The cells were infected with HPeV1 (MOI 10) for 8 hours at 37°C and were fixed, followed by permeabilization and blocking and a double antibody labelling stain were used. All primary antibodies were incubated overnight at 4°C. The cells were washed and treated with the appropriate secondary antibody (1:500) and incubated for 2 hours at 4°C. The cells were washed again and incubated with polyclonal antibody against HPeV1 (1:50) or monoclonal antibody against dsRNA (1:100) overnight then were washed and treated with secondary antibody (1:500). Slides were then visualized using a Nikon A1 si confocal microscope. At least 10 fields were observed for each slide and 4 typical cells were imaged. The images presented are the most representative of the cells observed.

In HPeV-infected cells dsRNA, presumably in replication complexes, accumulated near the nucleus and was concentrated in large foci. Whereas the anti-HPeV1 antibody gives staining throughout the cytoplasm. The GM130 seems to distribute mostly to one side of the nucleus in uninfected cells (Figure 3.1), while in infected cells it seems to redistribute and become more concentrated near to, but largely separate from replication complexes. To compare with another relatively diverse picornavirus, coxsackievirus A9 (CAV9) was used. GMK cells were used as CAV9 does not infect HT29 cells. The GM130 distribution was different from that seen in uninfected HT29 cells where it was more localised in one perinuclear region (Figure 3.2). Infection with CAV9 caused a large reduction in the intensity of GM130 staining, with just a few

spots around the nucleus. The CAV9 replication complexes were seen as dots through the cytoplasm and did not seem to co-localise with the GM130 (Figure 3.2).

PDI seems to be distributed around the nucleus in uninfected cells (Figure 3.3). Interestingly, in some cells infected with HPeV1 the stain almost completely disappears, while in others it is reduced. The ERGIC-53 appears as dots in the cytoplasm in uninfected cells. In cells infected with HPeV1 the stain is slightly weaker and the number of dots is reduced in some cells as the staining is more diffuse (Figure 3.4). Infection with HPeV1 therefore changes the distribution of the Golgi, ERGIC and the ER markers, suggesting these structures are altered.

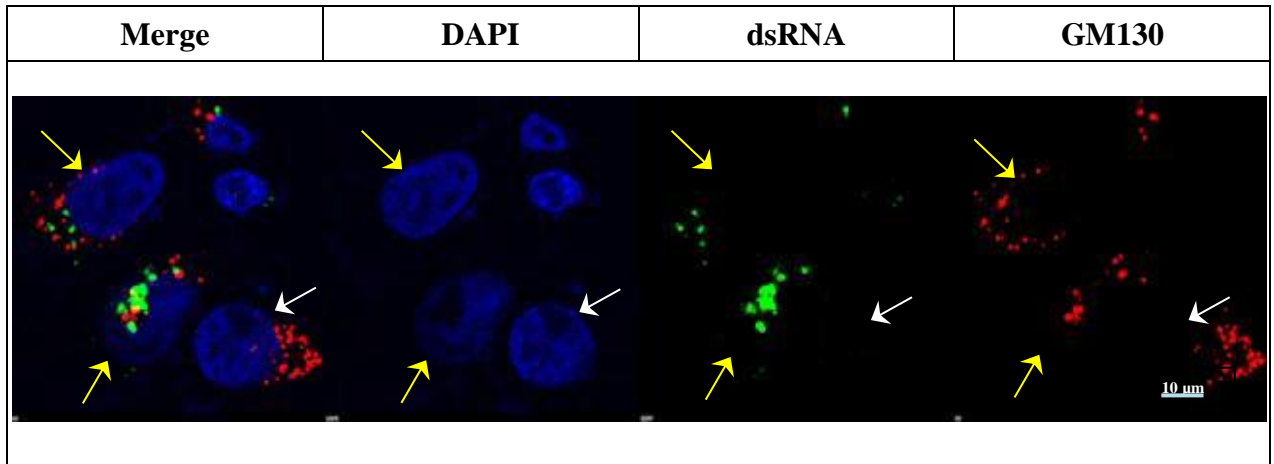


FIGURE 3.1: The effect of HPeV1 infection on the Golgi marker GM130. HT29 cells were grown on coverslips and infected with HPeV1 for 8 hr. Double staining with antibody was used. The polyclonal rabbit antibody to GM130 was recognised with a red secondary antibody labelled with Alexa Fluor 568. The mouse monoclonal antibody to dsRNA was recognised with a green secondary antibody labelled with Alexa Fluor 488. Nuclei were stained with DAPI in the mounting medium. Images were visualized using a Nikon A1 confocal microscope. The blue filter detects the nucleus, the green filter detects dsRNA in infected cells and the red filter detects GM130. The white arrow indicates an uninfected cell and the yellow arrows indicate infected cells (identified by the presence of dsRNA in replication complexes). Compared to uninfected cells, the GM130 is redistributed in infected cells and is concentrated near to replication complexes. The scale bar shown is 10 μm .

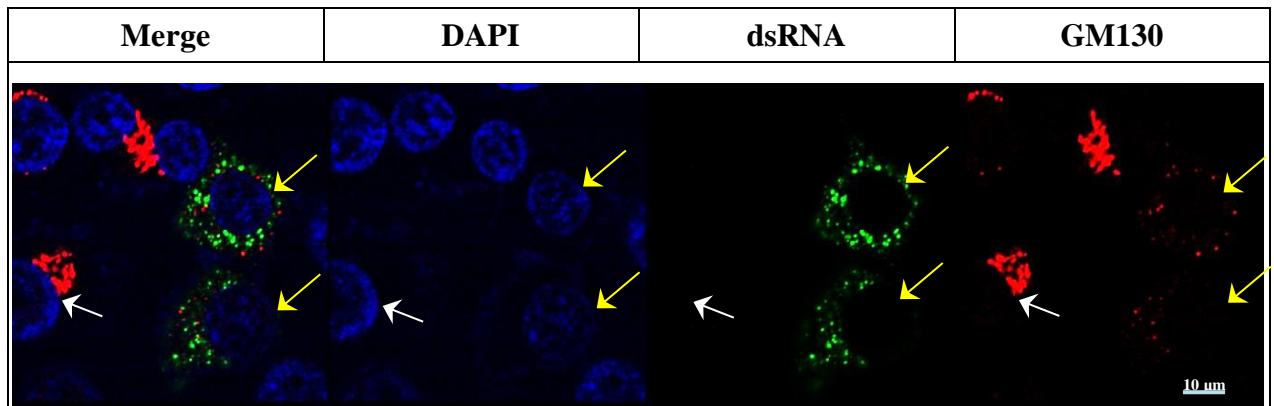


FIGURE 3.2: The effect of CAV9 infection on the Golgi marker GM130. GMK cells were grown on coverslips and infected with CAV9 for 8 hr. Double staining with antibody was used. The polyclonal rabbit antibody to GM130 was recognised with a red secondary antibody labelled with Alexa Fluor 568. The mouse monoclonal antibody to dsRNA was recognised with a green secondary antibody labelled with Alexa Fluor 488. Nuclei were stained with DAPI in the mounting medium. Images were visualized using a Nikon A1 confocal microscope. The blue filter detects the nucleus, the green filter detects dsRNA in infected cells and the red filter detects GM130. The white arrow indicates an uninfected cell and the yellow arrows indicate infected cells (identified by the presence of dsRNA in replication complexes). Compared to uninfected cells, the GM130 staining is reduced to just a few relatively weak spots in infected cells. The scale bar shown is 10 μm .

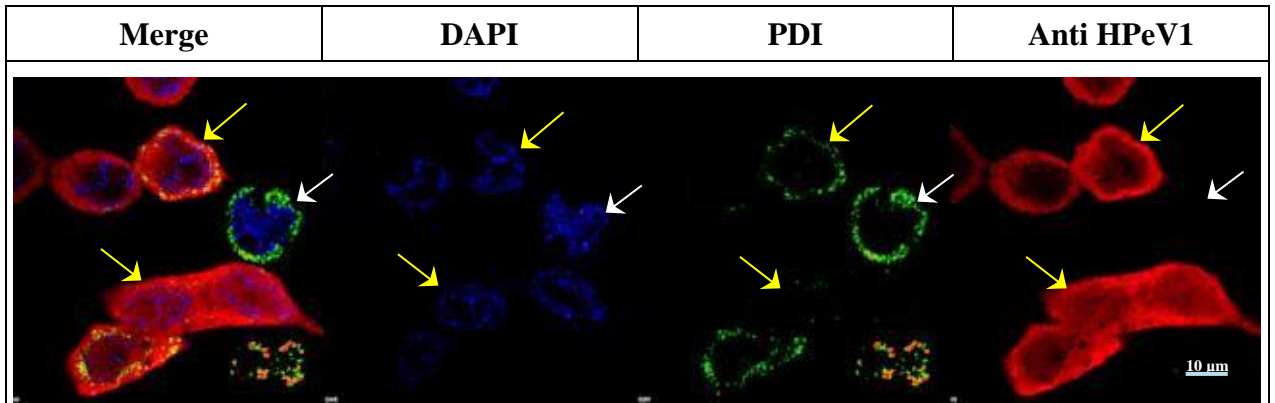


FIGURE 3.3: The effect of HPeV1 infection on the ER marker PDI. HT29 cells were grown on coverslips and infected with HPeV1 for 8 hr. Double staining with antibody was used. The mouse monoclonal antibody to PDI was recognised with a green secondary antibody labelled with Alexa Fluor 488. The rabbit polyclonal antibody to HPeV1 was recognised with a red secondary antibody labelled with Alexa Fluor 568. Nuclei were stained with DAPI in the mounting medium. Images were visualized using a Nikon A1 confocal microscope. The blue filter detects the nucleus, the green filter detects PDI and the red filter detects cells infected with HPeV1. The white arrow indicates an uninfected cell and the yellow arrows indicate infected cells (identified by the presence of HPeV proteins). Compared to uninfected cells, the PDI staining is greatly reduced or completely lost in infected cells. The scale bar shown is 10 μm .

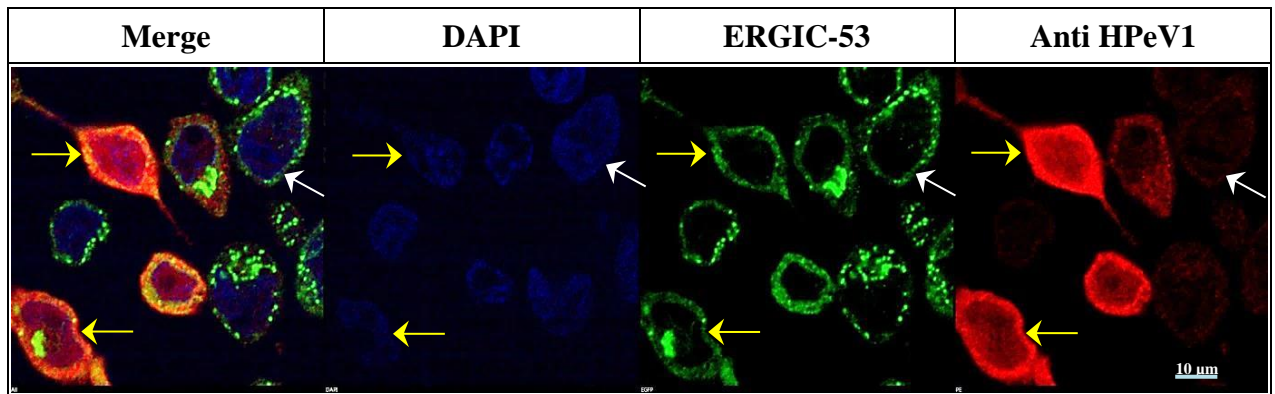


FIGURE 3.4: The effect of HPeV1 infection on the ERGIC marker ERGIC-53. HT29 cells were grown on coverslips and infected with HPeV1 for 8 hr. Double staining with antibody was used. The mouse monoclonal antibody to ERGIC-53 was recognised with a green secondary antibody labelled with Alexa Fluor 488. The rabbit polyclonal antibody to HPeV1 was recognised with a red secondary antibody labelled with Alexa Fluor 568. Nuclei were stained with DAPI in the mounting medium. Images were visualized using a Nikon A1 confocal microscope. The blue filter detects the nucleus, the green filter detects PDI and the red filter detects infected cells with HPeV1. The white arrow indicates an uninfected cell and the yellow arrows indicate infected cells (identified by the presence of HPeV proteins) with slightly weaker, more diffuse ERGIC-53 staining. The scale bar shown is 10 µm.

3.3 Distribution of HPeV1 non-structural proteins

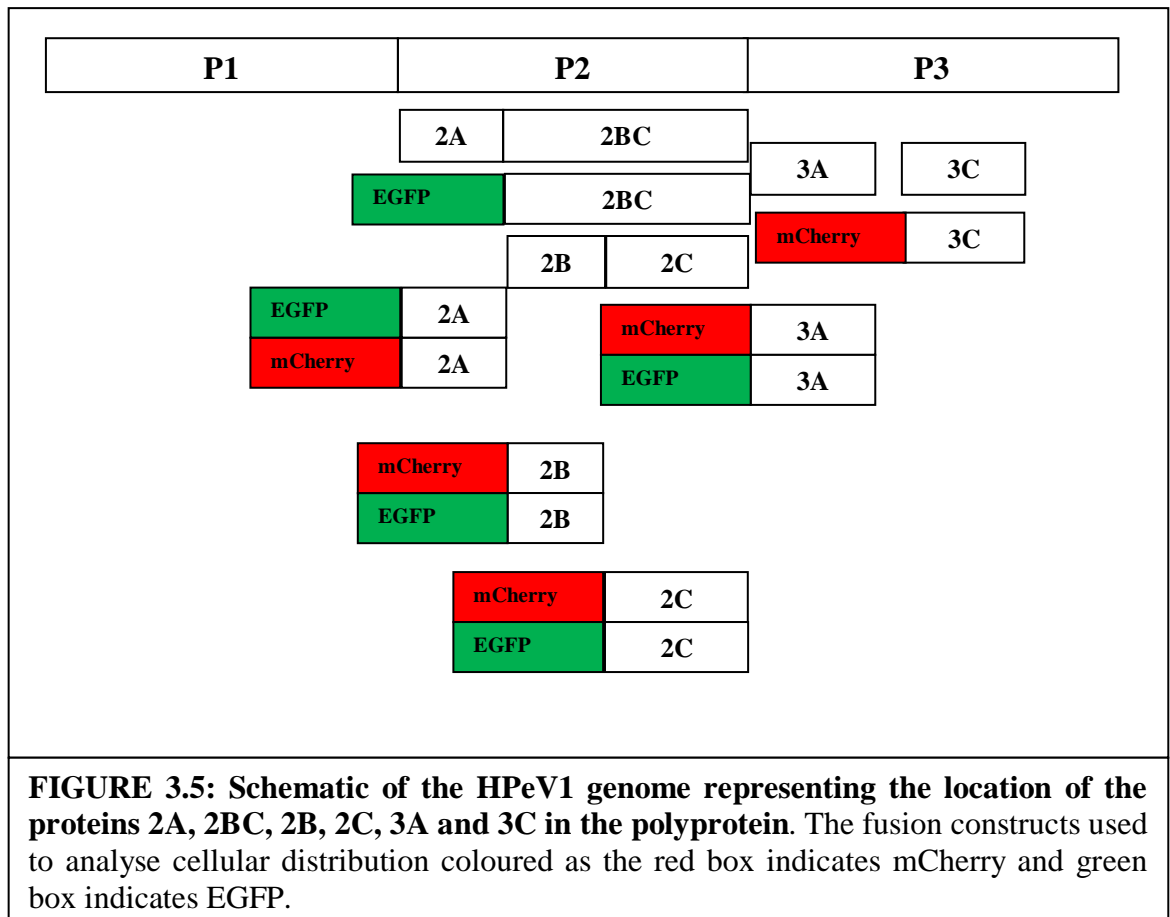
To investigate which HPeV non-structural proteins could be involved in the changes to the Golgi, the ER and ERGIC, several EGFP/ mCherry fusions were used to confirm the results (Figure 3.5). EGFP constructs of 2A, 2B, 2C, and 3A were available (Salimi, 2015). mCherry constructs of these proteins were made by using double digestion with appropriate restriction enzymes. EGFP-2BC and mCherry-3C were produced by amplifying these coding regions from a HPeV1 clone and ligating into pEGFP-C1 or pmCherry-C1.

First we studied the distribution of the non-structural proteins alone in GMK cells line. 50–70% confluent cells were used for transfection in 6 well plates containing glass coverslips. They were transfected with non-structural protein constructs using X-fect or Lipofectin transfection reagents (the same reagent for each set of experiments). The results were visualised using a Nikon A1 si confocal microscope.

The distribution of EGFP expressed from pEGFP-C1 vector and mCherry expressed from pmCherry-C1 vector is shown in Figure 3.6. and Figure 3.7. Both of them are diffuse in the cytoplasm and the nucleus. mCherry-2A and EGFP-2A were also seen diffusely in the cytoplasm and nucleus (Figure 3.8). mCherry-2B, EGFP-2B (Figure 3.9), mCherry-3A and EGFP-3A (Figure 3.10) formed a reticular pattern in the cytoplasm. In some cells these also accumulated in perinuclear locations (data not shown). mCherry-3C caused major change to the cells, including rounding of the cell and contraction of the nucleus as seen in Figure 3.11. In some cells the nuclear staining was lost or was dispersed through the cell. These changes are possibly due to apoptosis.

The most interesting distribution was shown by both EGFP-2C and mCherry-2C (Figure 3.12). The fluorescence was mainly localised in a few large and bright spots in the cytoplasm. The distribution of EGFP-2BC was variable. In some cells, it was very similar to the 2C distribution,

but in others it had a more diffuse, dot-like or reticular appearance in the cytoplasm (Figure 3.13).



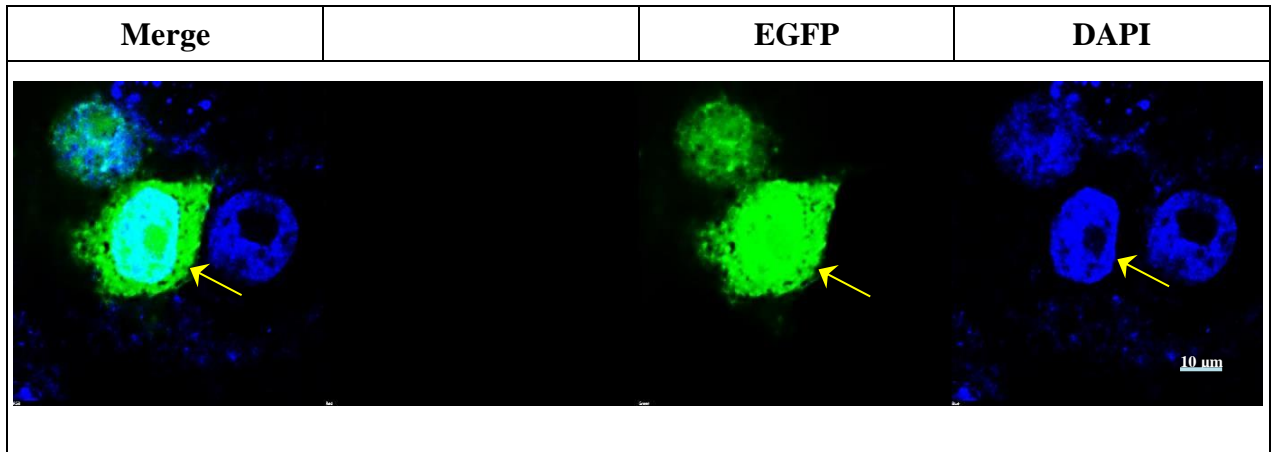


FIGURE 3.6: The distribution of EGFP expressed from the pEGFP-C1 vector. GMK cells were transfected with pEGFP-C1 using Xfect. Cells were visualized after fixation with formalin of 24 hours after transfection. Images were obtained with a Nikon AR Confocal Fluorescence Microscope. The blue filter detects the nucleus and the green filter detects EGFP. The yellow arrow indicates a cell transfected with pEGFP-C1, showing diffuse EGFP staining in the cytoplasm and the nucleus. The scale bar shown is 10 μm .

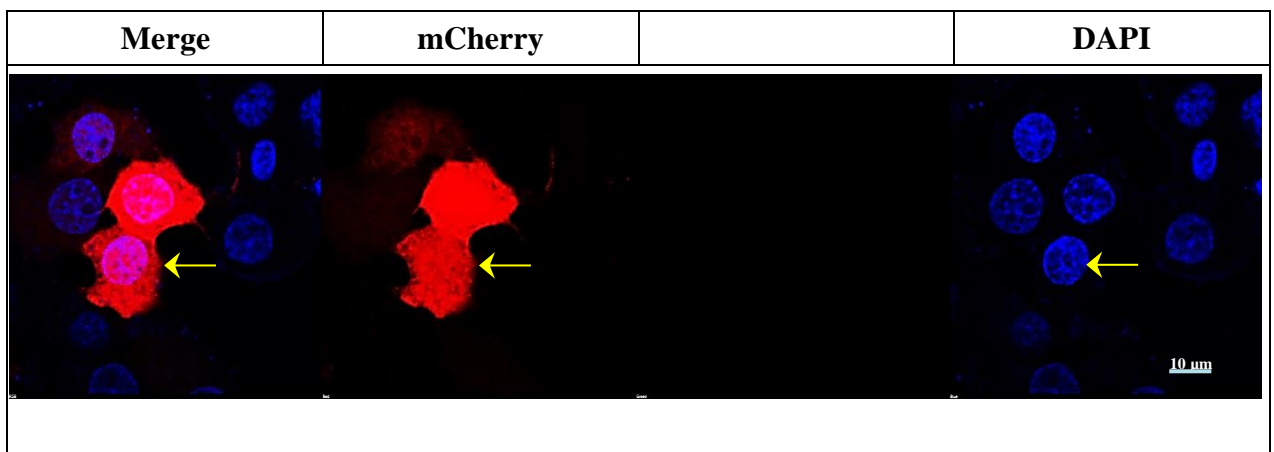


FIGURE 3.7: The distribution of mCherry expressed from the pmCherry-C1 vector. GMK cells were transfected with mCherry using Xfect. Cells were visualized after fixation with formalin 24 hours after transfection. Images were obtained with a Nikon AR Confocal Fluorescence Microscope. The blue filter detects the nucleus and the red filter detects mCherry. The yellow arrow indicates a cell transfected with pmCherry-C1 showing diffuse mCherry staining in the cytoplasm and the nucleus. The scale bar shown is 10 μm .

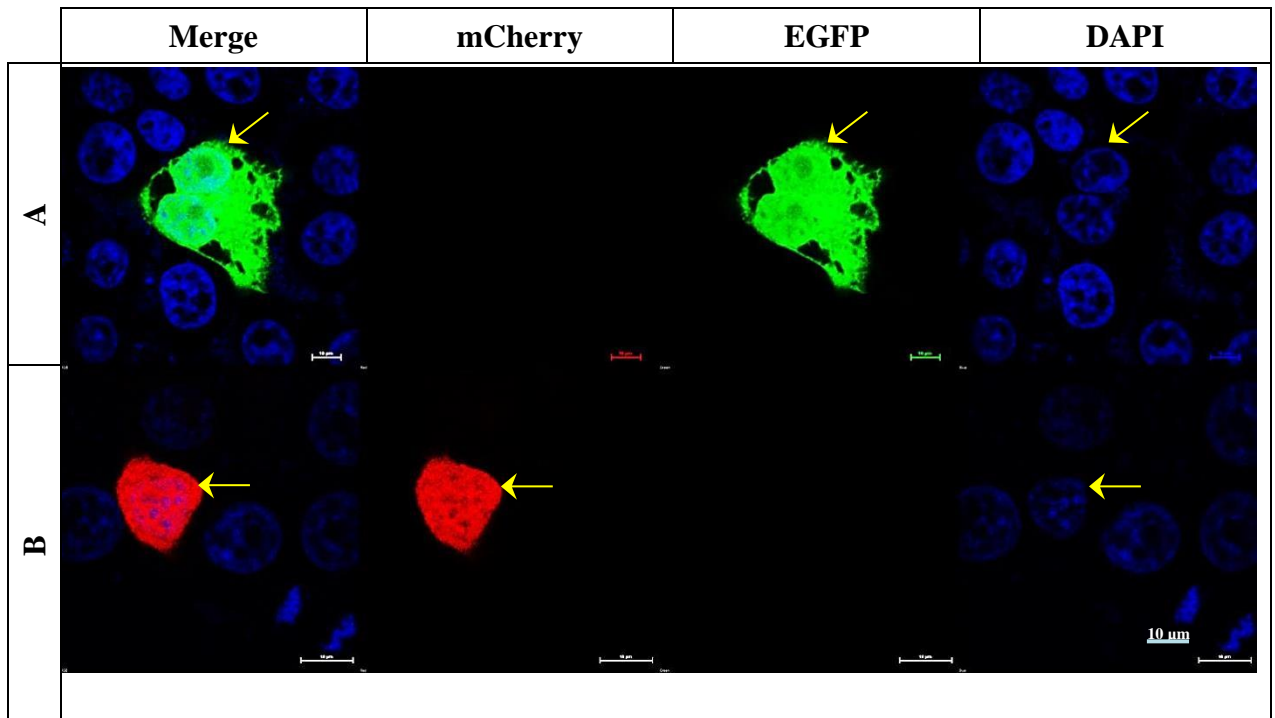


FIGURE 3.8: The distribution of HPeV1 2A protein. GMK cells were transfected with A) pEGFP-2A and B) pmCherry-2A from HPeV1 using Xfect. Cells were visualized after fixation with formalin 24 hours after transfection. Images were obtained with Nikon AR Confocal Fluorescence Microscope. The blue filter detects the nucleus, the green filter detects EGFP-2A and the red filter detects mCherry-2A. The yellow arrows indicate transfected cells. Both EGFP-2A and mCherry-2A show a diffuse staining pattern in the cytoplasm and nucleus. The scale bar shown is 10 μm .

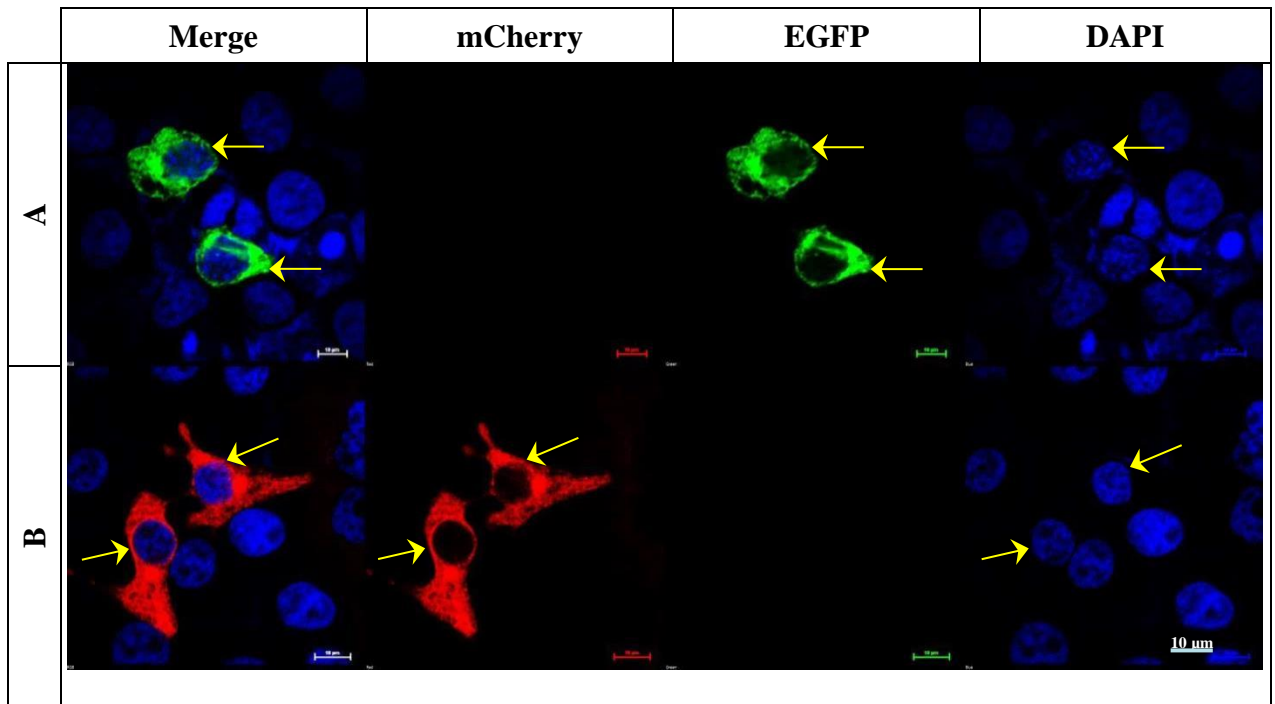


FIGURE 3.9: The distribution of HPeV1 2B protein. GMK cells were transfected with A) pEGFP-2B and B) pmCherry-2B from HPeV1 using Xfect. Cells were visualized after fixation with formalin 24 hours after transfection. Images were obtained with Nikon AR Confocal Fluorescence Microscope. The blue filter detects the nucleus, the green filter detects EGFP-2B and the red filter detects mCherry-2B. The yellow arrows indicate transfected cells. Both EGFP-2B and mCherry-2B show a reticular staining pattern in the cytoplasm. The scale bar shown is 10 μm .

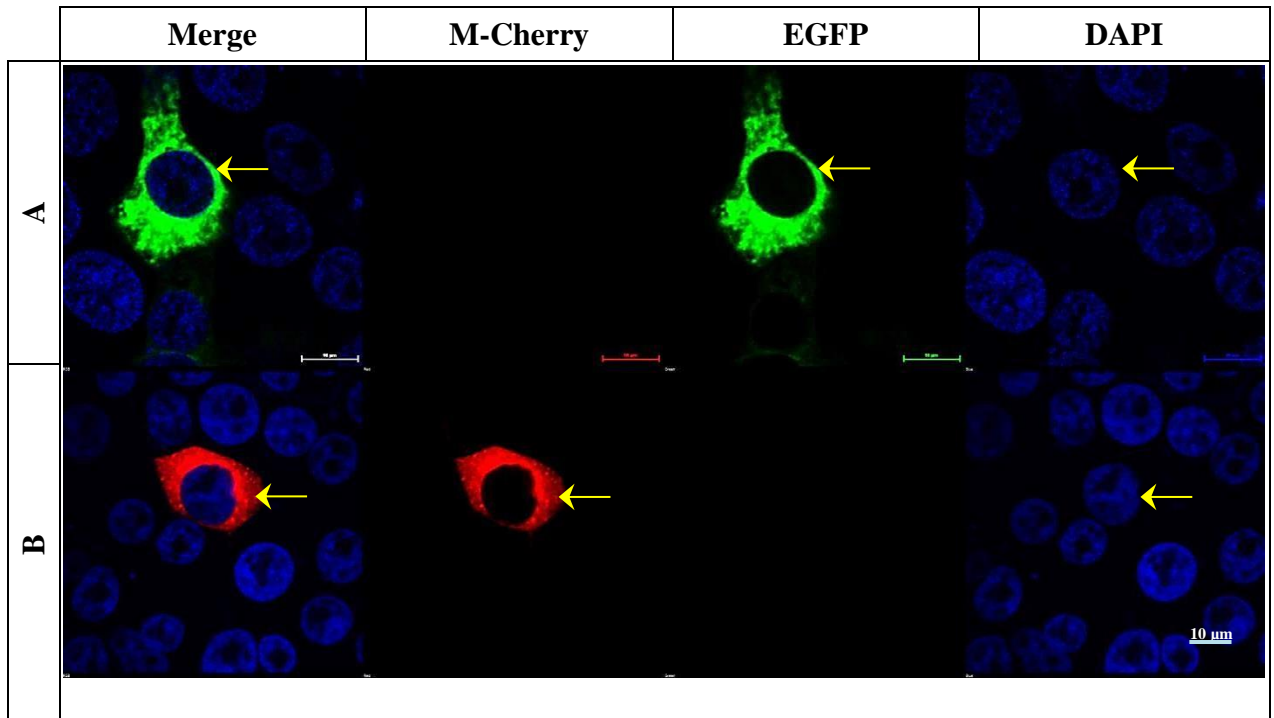


FIGURE 3.10: The distribution of HPeV1 3A protein. GMK cells were transfected with A) pEGFP-3A and B) pmCherry-3A from HPeV1 using Xfect. Cells were visualized after fixation with formalin 24 hours after transfection. Images were obtained with Nikon AR Confocal Fluorescence Microscope. The blue filter detects the nucleus, the green filter detects EGFP-3A and the red filter detects mCherry-3A. The yellow arrows indicate transfected cells. Both EGFP-3A and mCherry-3A show a reticular staining pattern in the cytoplasm. The scale bar shown is 10 μm .

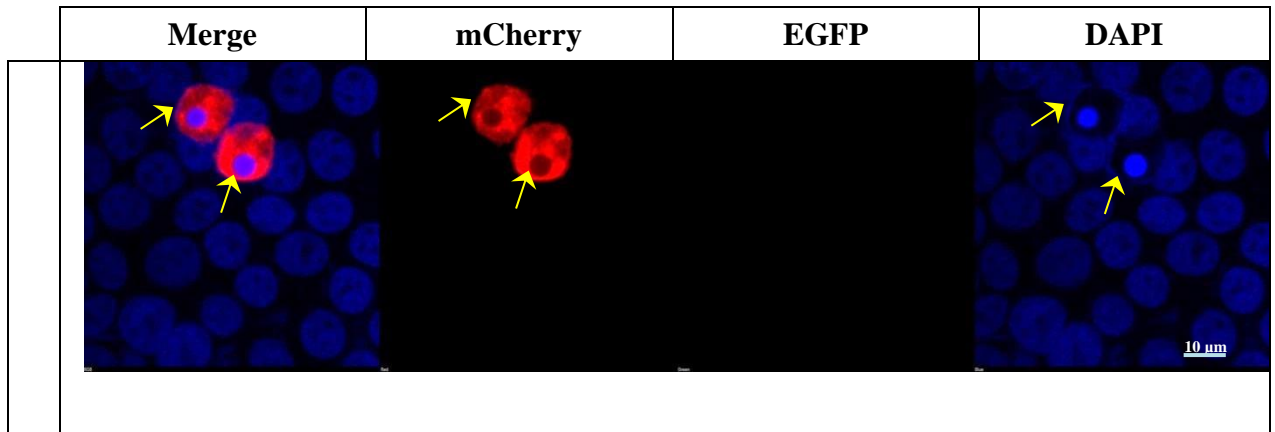


FIGURE 3.11: The distribution of HPeV1 3C protein. GMK cells were transfected with pmCherry-3C from HPeV1 using Xfect. Cells were visualized after fixation with formalin 24 hours after transfection. Images were obtained with Nikon AR Confocal Fluorescence Microscope. The blue filter detects the nucleus and the red filter detects mCherry-3C. The yellow arrows indicate transfected cells. mCherry-3C causes a major change to the cells, including rounding of the cell and contraction of the nucleus. The scale bar shown is 10 μm .

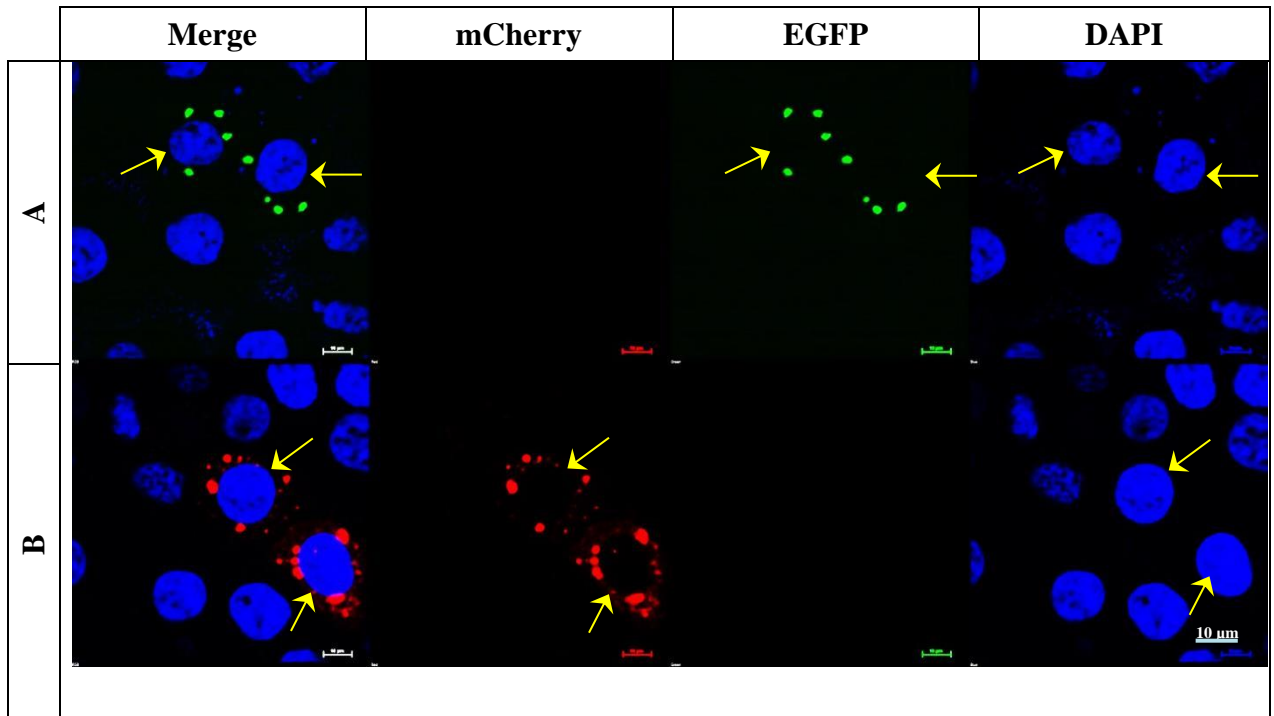


FIGURE 3.12: The distribution of HPeV1 2C protein. GMK cells were transfected with A) pEGFP-2C and B) pmCherry-2C from HPeV1 using Xfect. Cells were visualized after fixation with formalin 24 hours after transfection. Images were obtained with Nikon AR Confocal Fluorescence Microscope. The blue filter detects the nucleus, the green filter detects EGFP-2C and the red filter detects mCherry-2C. The yellow arrows indicate transfected cells. Both EGFP-2C and mCherry-2C are located in a few large and bright spots in the cytoplasm. The scale bar shown is 10 μm .

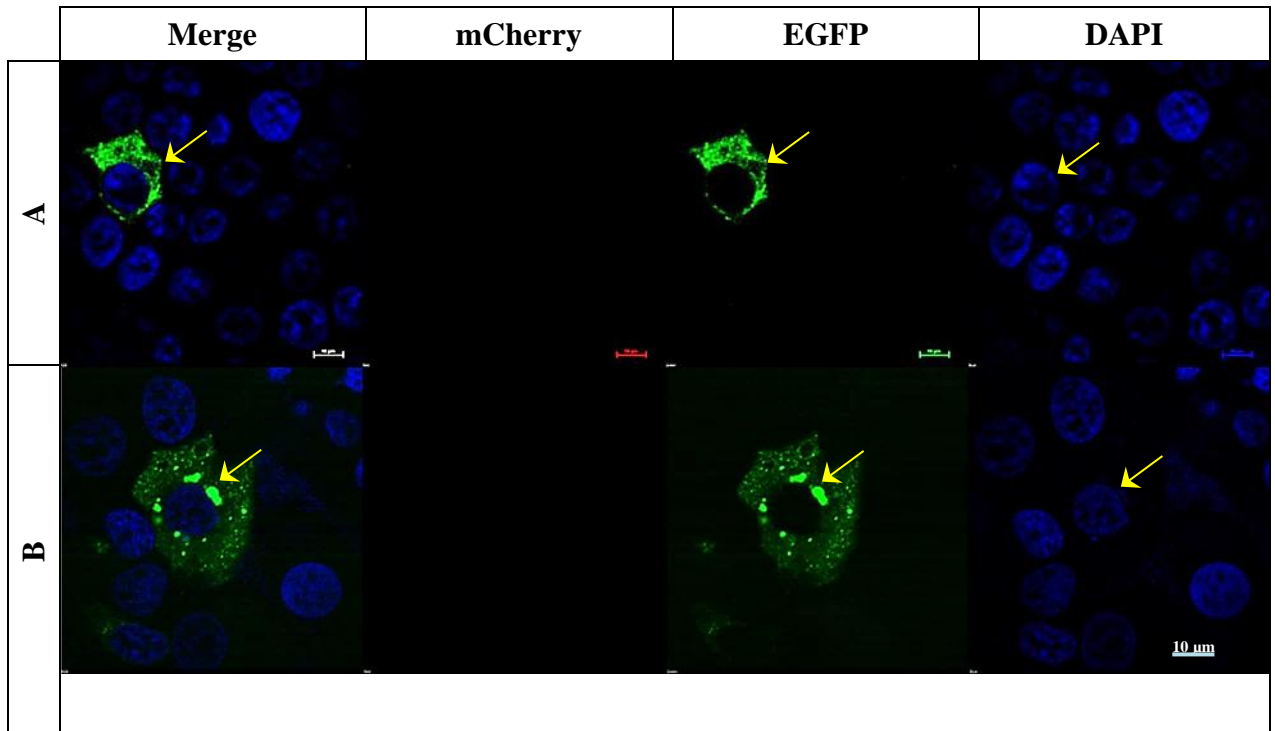


FIGURE 3.13: The distribution of HPeV1 2BC protein. GMK cells were transfected with pEGFP-2BC from HPeV1 using Xfect. Cells were visualized after fixation with formalin of 24 hours after transfection. Images were obtained with Nikon AR Confocal Fluorescence Microscope. The blue filter detects the nucleus and the green filter detects EGFP-2BC. The yellow arrows indicate transfected cells. EGFP-2BC shows two different patterns A) a reticular staining pattern in the cytoplasm, B) a few large spots, similar to the 2C staining pattern seen in Figure 3.12. The scale bar shown is 10 μm .

3.4 Non-structural proteins of HPeV1 and the secretory pathway

After we studied the distribution of the HPeV1 non-structural proteins in GMK cells, we investigated the effect of these proteins on the ER, ERGIC and Golgi and any co-localisation. 50–70% confluent GMK cells were used and transfected with non-structural proteins using Turbofect transfection reagent. The cells were fixed after 24-48 hours then stained with monoclonal anti-PDI or ERGIC antibody or polyclonal antibody to GM130.

3.4.1 The ER marker (PDI)

For some non-structural proteins we used both EGFP and mCherry constructs. PDI seems to have a perinuclear distribution in un-transfected cells and no change in this distribution was caused by mCherry-2A and EGFP-2A (Figure 3.14 and 3.15). In some cells transfected with mCherry-2B and EGFP-2B the PDI stain has a lower concentration than untransfected cells but there was not much effect. mCherry-2C has a large effect on the PDI marker in some cells the ER seemed to be almost completely destroyed (Figure 3.14). In other cells the effect was less (data not shown) and EGFP-2C also has less effect, although EGFP-2BC also caused loss of the PDI stain in some cells (Figure 3.15). m-Cherry-3A seems to change the distribution of PDI and partly co-localise to it. m-Cherry-3C shows a possible apoptosis affect to transfected cell which have very condensed nuclei. This affects PDI distribution, but the effect may not be specific as the cell morphology is badly disrupted (Figure 3.14). The results show that 2C or 2BC can cause similar changes to the ER seen in HPeV1-infected cells (Figure 3.3).

3.4.2 The ERGIC

The ERGIC marker ERGIC-53 seems to be located through the cytoplasm but is clustered into many clear dots in cells that are untransfected (Figure 3.16). No change in this structure in cell was seen when cells were transfected with mCherry-2A. mCherry-2B partly co-localises to

ERGIC in transfected cells but causes no clear difference to ERGIC structure. mCherry-2C does not cause any clear difference to the ERGIC and does not colocalise. mCherry-3A seems to change the distribution of ERGIC by condensing it close to the nucleus. There is also some co-localisation between mCherry-3A and the ERGIC marker. mCherry-3C has a major effect on the ERGIC, which seem to completely disappear in transfected cells. However, this may not be specific as the cell morphology is badly disrupted (Figure 3.16). EGFP-2BC also seemed to cause disruption of the ERGIC (Figure 3.17).

3.4.3 The Golgi

This cis-Golgi marked GM130 distributes mostly to one side of the nucleus in untransfected (Figure 3.18). mCherry-2A has little effect on the distribution of GM130. On other hand, mCherry-2B seems to cause the loss of most of the Golgi marker. mCherry-2C seems to cause collapse of the Golgi to a small number of structures near to the nucleus. mCherry-3A seems to cause the loss of most of the Golgi marker. The marker is also not seen in cells transfected with mCherry-3C, but again these cells show major changes in morphology.

Overall, all the non-structural proteins except 2A seem to have a large effect on Golgi structure (Figure 3.18).

3.4.4 Lysosomes

For more investigation on secretory pathways, we studied the effect of non-structural proteins on lysosomes. In this investigation the fluorescence intensities recorded for the non-structural protein fusions were decreased to clearly observe the interactions. In addition, live cells were imaged, rather than fixed ones. Under these conditions, the distribution recorded for 2B and 3A fusions was much more punctate than that seen in the work shown in Figures 3.9-3.18. The lysosome stain shows foci throughout the cytoplasm (Figure 3.19). There are fewer foci in cells transfected with mCherry-2A. The foci seem larger and more intense in cells transfected with mCherry-2B. mCherry-2C causes a reduction in number and intensity of foci. mCherry-3A

causes an increase in the intensity and number of foci and like mCherry-2B, there seems to be some co-localisation. mCherry-3C has little effect (Figure 3.20).

3.4.5 Mitochondria

Mitotracker 20 ng/ml was used to visualise mitochondria. Again, in this investigation the fluorescence intensities recorded for the non-structural protein fusions were decreased to clearly observe the interactions and live cells were imaged. In transfected cells mitochondria were localised in a network of foci throughout the cytoplasm (Figure 3.21). None of the HPeV1 proteins had a significant effect on this distribution apart from 2A and 3C (Figure 3.22). mCherry-2A seemed to reduce the size of the network, while the network was broken down into more individual foci by mCherry-3C, but again the cells were highly disrupted by mCherry-3C and so the effect on mitochondria may not be specific.

3.4.6 Peroxisomes

An EGFP-peroxisome construct was made by cutting pEGFP-C1 with HindIII and BamHI and ligating in a pair of overlapping oligonucleotides. These changed the C-terminal sequence of EGFP to TKL, which is a peroxisomes target sequence (Brocard and Hartig, 2006). The constructs gave the expected punctate distribution in the cytoplasm (Figure 3.23), but some nuclear staining was seen in some cells and this complicated the results when it was co-transfected with HPeV1 mCherry constructs (Figure 3.24). mCherry-2C seemed to increase the size and intensity of the peroxisome spots (Figure 3.24). mCherry-2B had little effect and mCherry-2A, -3A and -3C caused some disruption to the pattern but this was unclear. None of the proteins co-localised with the peroxisomes.

Interestingly, infection with both HPeV1 and CAV9 seems to disrupt the peroxisomes pattern (Figure 3.25 and 3.26).

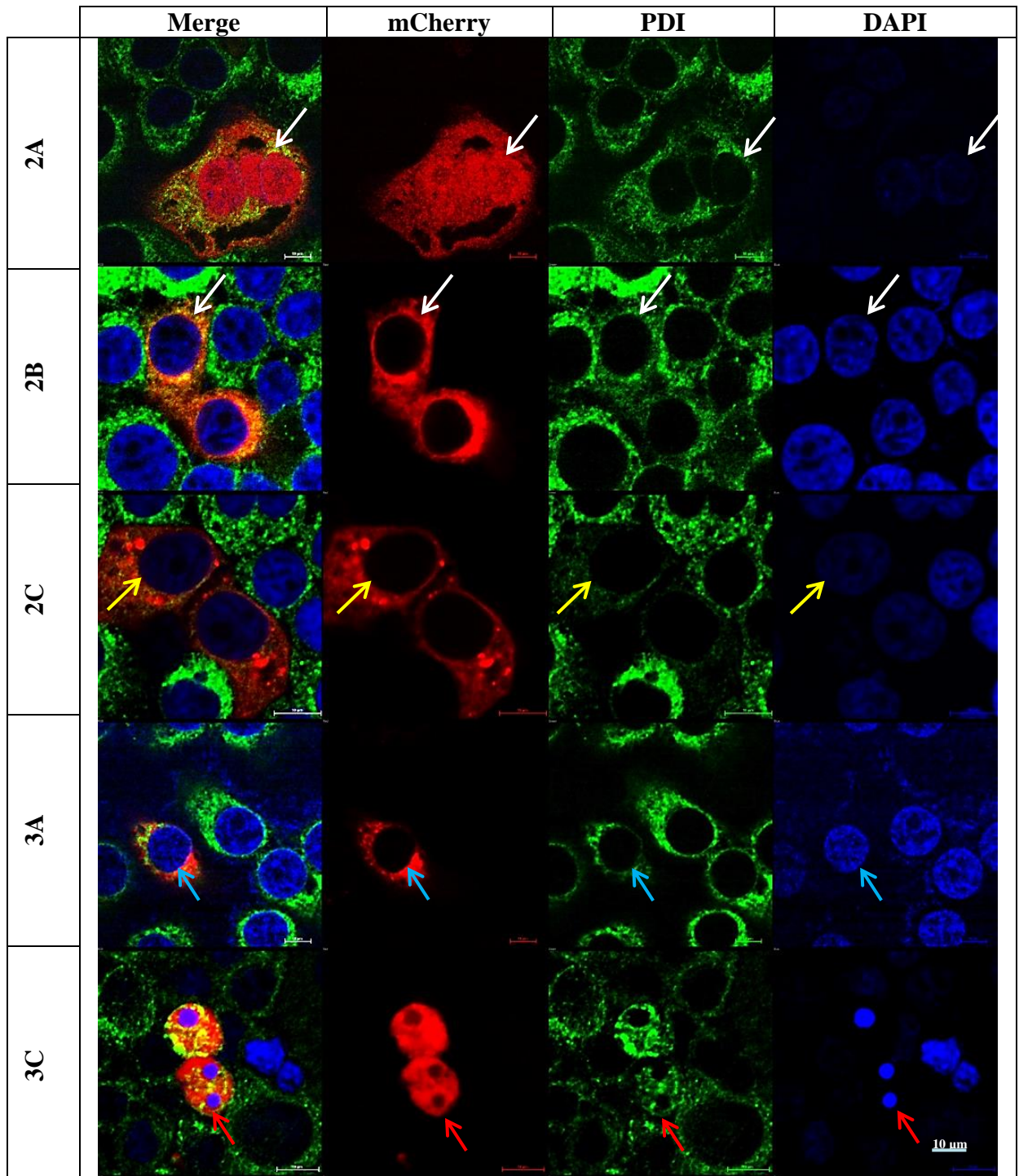


FIGURE 3.14: The effect of HPeV1 proteins (fused to mCherry) on the ER marker PDI. GMK cells were grown on coverslips and transfected with mCherry fusion constructs using Turbofect. 48 hours after transfection, a monoclonal antibody to PDI and a green secondary antibody labelled with Alexa Fluor 488 were used to observe the ER. Nuclei were stained with DAPI in the mounting medium. Images were visualized using a Nikon A1 confocal microscope. The blue filter detects the nucleus, the red filter detects mCherry fused to 2A, 2B, 2C, 3A or 3C and the green filter detects PDI/secondary antibody. The arrows indicate transfected cells (which show an mCherry signal). mCherry-2A and mCherry 2B (white arrows) have little effect on PDI staining compared to non-transfected cells in the field. Staining is almost completely destroyed by mCherry-2C (yellow arrow). The PDI distribution is changed by mCherry-3A (blue arrow), which also partly co-localises to it. mCherry-3C (red arrow) causes major disruption to the cell structure, including nuclear condensation. The scale bar shown is 10 μm .

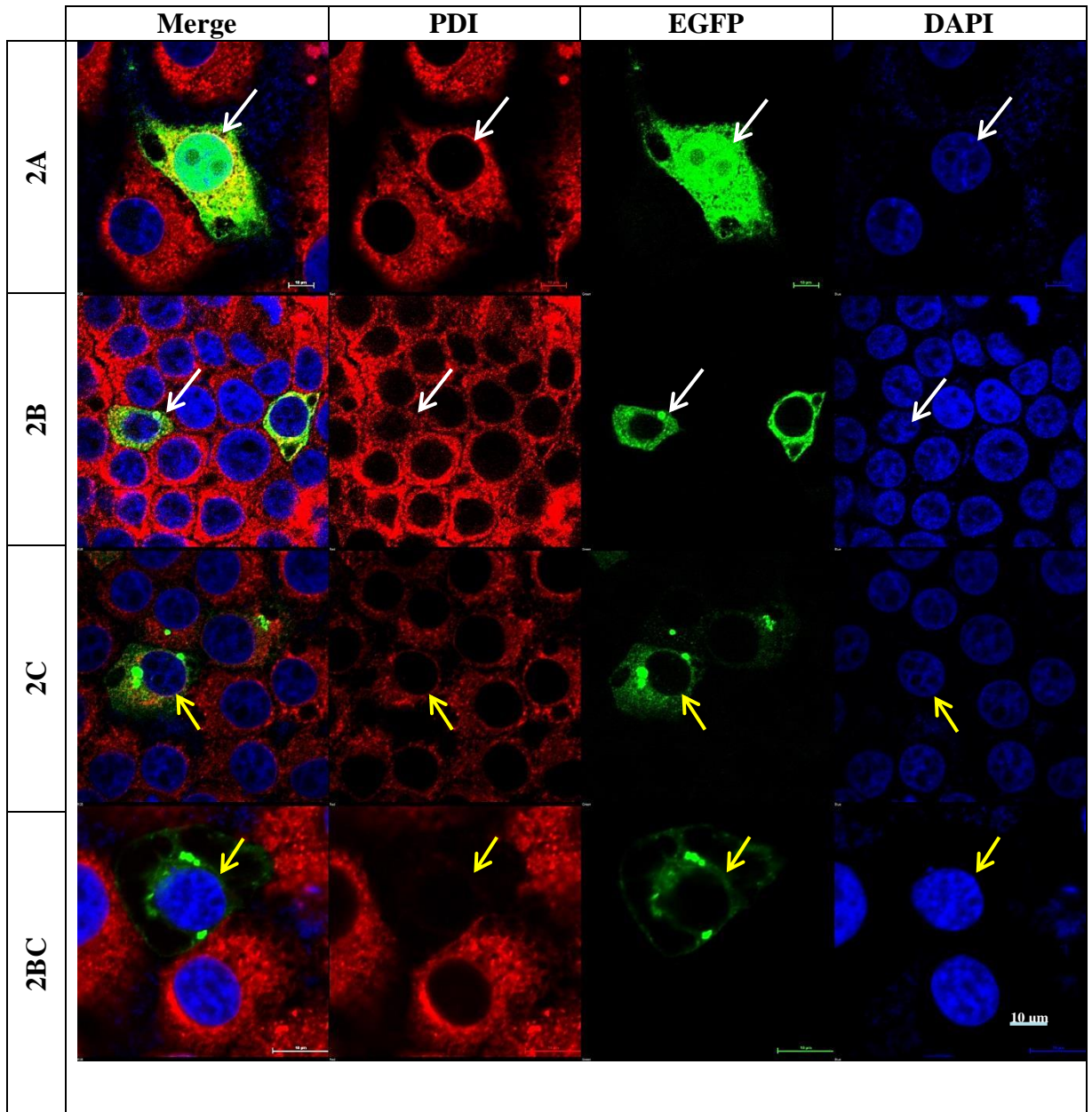


FIGURE 3.15: The effect of HPeV1 proteins (fused to EGFP) on the ER marker PDI. GMK cells were grown on coverslips and transfected with EGFP fusion constructs using Turbofect. 48 hours after transfection, a monoclonal antibody to PDI and a red secondary antibody labelled with Alexa Fluor 568 were used to observe the ER. Nuclei were stained with DAPI in the mounting medium. Images were visualized using a Nikon A1 confocal microscope. The blue filter detects the nucleus, the red filter detects PDI/ secondary antibody, and the green filter detects EGFP fused to 2A, 2B, 2C, and 2BC. The arrows indicate transfected cells (which show an EGFP signal). EGFP-2A and EGFP-2B (white arrows) have little effect on PDI staining compared to non-transfected cells in the field. Staining is almost completely destroyed by EGFP-2C and EGFP-2BC (yellow arrows). The scale bar shown is 10 μ m.

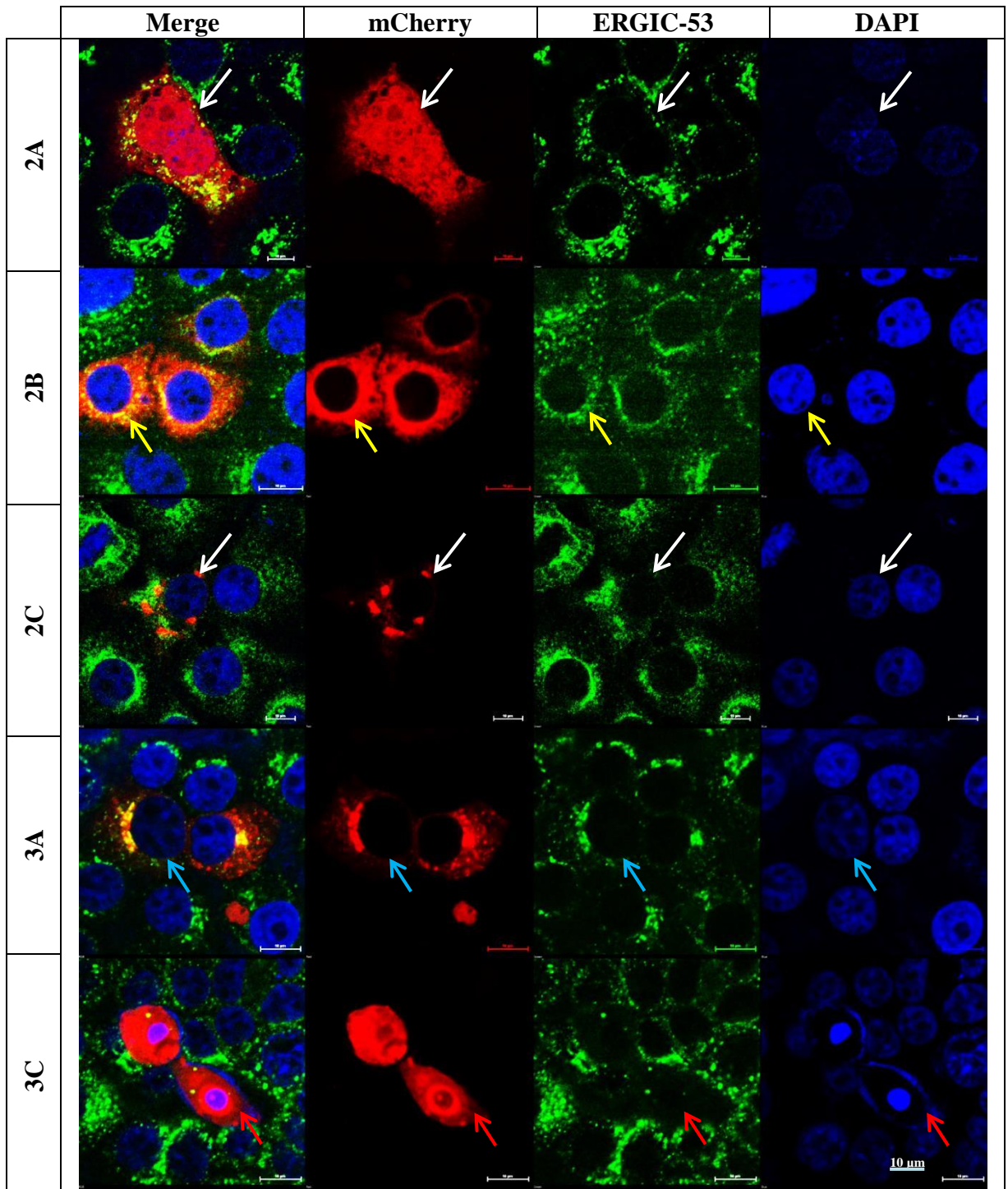


FIGURE 3.16: The effect of HPeV1 proteins (fused to mCherry) on the ERGIC. GMK cells were grown on coverslips and transfected with mCherry fusion constructs using Turbofect. 48 hours after transfection, a monoclonal antibody to ERGIC and a green secondary antibody labelled with Alexa Fluor 488 were used to observe ERGIC. Nuclei were stained with DAPI in the mounting medium. Images were visualized using a Nikon A1 confocal microscope. The blue filter detects the nucleus, the red filter detects mCherry fused to 2A, 2B, 2C, 3A and 3C the green filter detects ERGIC/ secondary antibody. The arrows indicate transfected cells (which show an mCherry signal). mCherry-2A and mCherry-2C (white arrows) have little effect on PDI staining compared to non-transfected cells in the field. mCherry-2B has a slight effect on ERGIC (yellow arrow). The ERGIC distribution is changed by mCherry-3A (blue arrow), which also partly co-localises to it. mCherry-3C (red arrow) causes major disruption to the cell structure, including nuclear condensation. The scale bar shown is 10 μm .

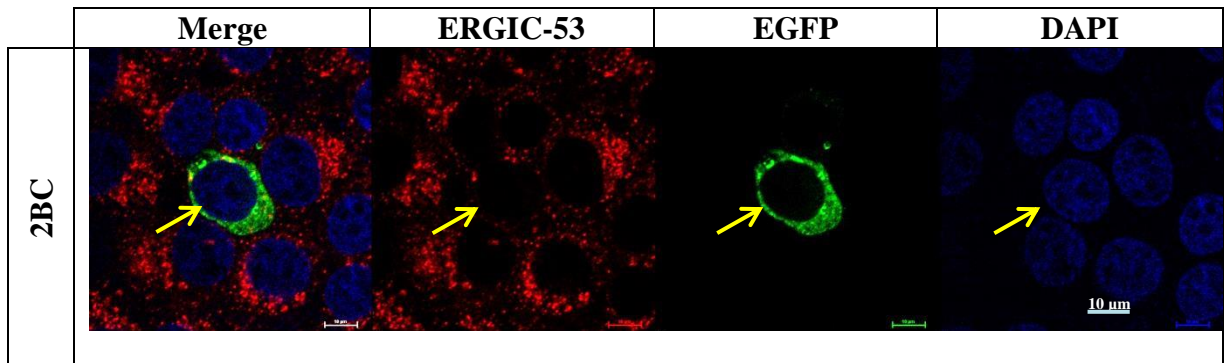


FIGURE 3.17: The effect of HPeV1 2BC fused to EGFP on the ERGIC. GMK cells were grown on coverslips and transfected with EGFP fusion construct using Turbofect. 48 hours after transfection, a monoclonal antibody to ERGIC and a red secondary antibody labelled with Alexa Fluor 568 were used to observe ERGIC. Nuclei were stained with DAPI in the mounting medium. Images were visualized using a Nikon A1 confocal microscope. The blue filter detects the nucleus, the red filter detects ERGIC/ secondary antibody and the green filter detects EGFP fused to 2BC. The arrow indicates a transfected cell (which shows an EGFP signal). The transfected cell has a much weaker ERGIC staining than the untransfected cells in the field and the distribution is changed. The scale bar shown is 10 μm .

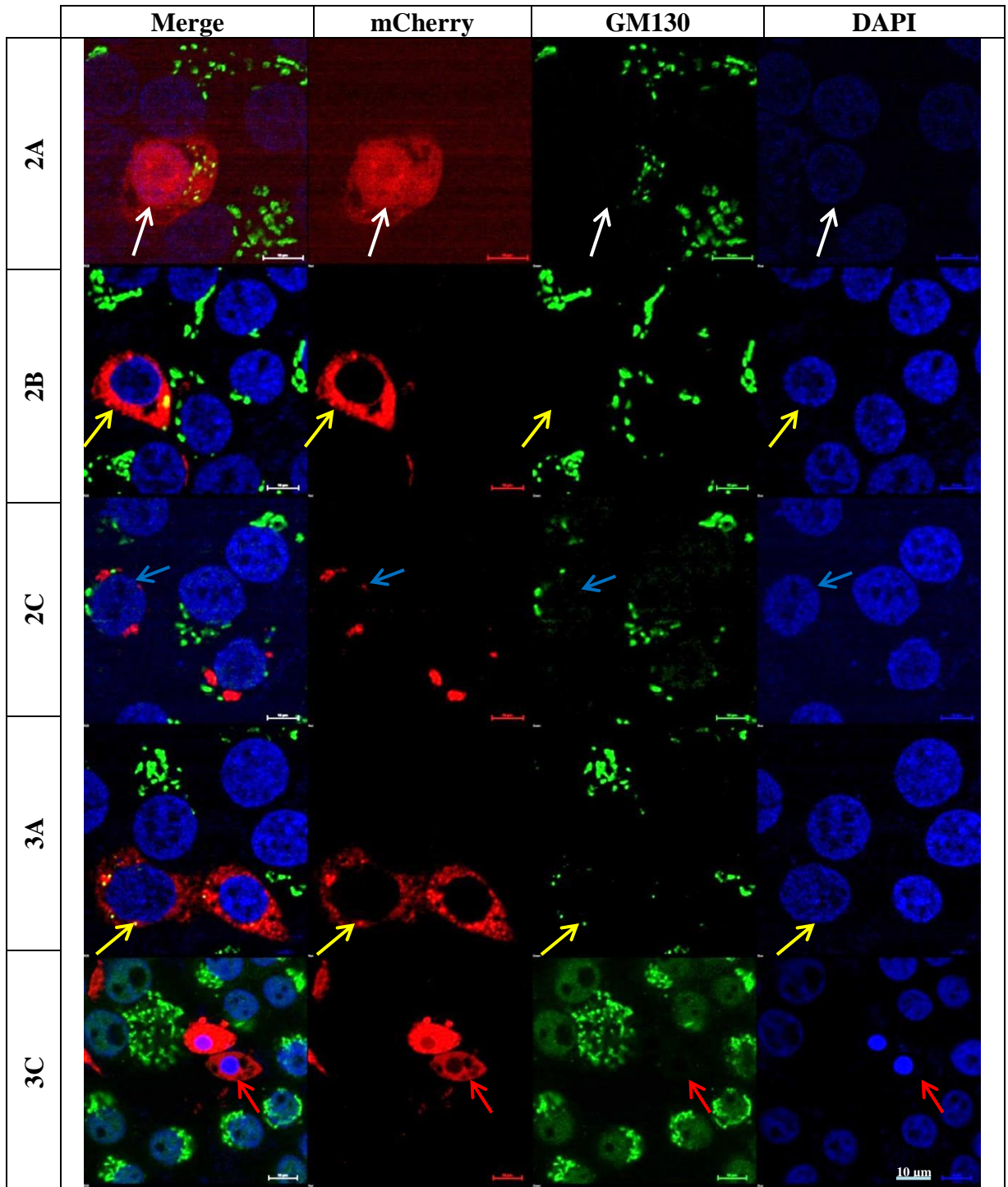


FIGURE 3.18: The effect of HPeV1 proteins (fused to mCherry) on the Golgi. GMK cells were grown on coverslips and transfected with mCherry fusion constructs using Turbofect. 48 hours after transfection, a polyclonal antibody to GM130 and a green secondary antibody labelled with Alexa Fluor 488 were used to observe Golgi. Nuclei were stained with DAPI in the mounting medium. Images were visualized using a Nikon A1 confocal microscope. The blue filter detects the nucleus, the red filter detects mCherry fused to 2A, 2B, 2C, 3A and 3C the green filter detects GM130/ secondary antibody. The arrows indicate transfected cells (which show an mCherry signal). mCherry-2A (white arrow) has little effect on GM130 staining compared to non-transfected cells in the field. The GM130 distribution is mostly lost by mCherry-2B or mCherry-3A (yellow arrows). mCherry-2C changed the distribution to a small number of structures near to the nucleus (blue arrow). mCherry-3C (red arrow) causes major disruption to the cell structure, including nuclear condensation. The scale bar shown is 10 μm .

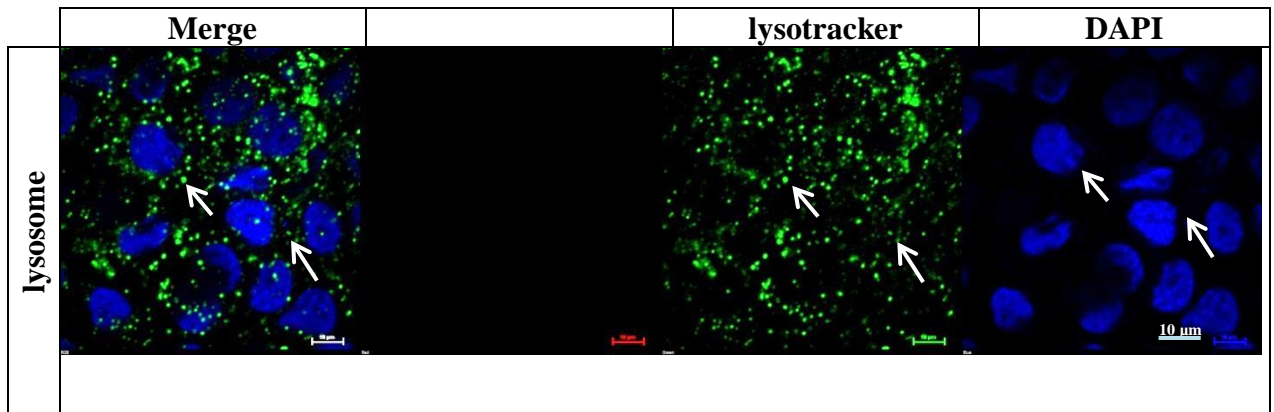


FIGURE 3.19 The normal distribution of lysosomes. GMK cells were grown on coverslips and stained with green lysotracker. Nuclei were stained with Hoechst 33342. Images were visualized using a Nikon A1 confocal microscope. The blue filter detects the nucleus and the green filter detects lysosomes. The white arrows indicate the distribution of lysosome stain as foci throughout the cytoplasm. The scale bar shown is 10 μm .

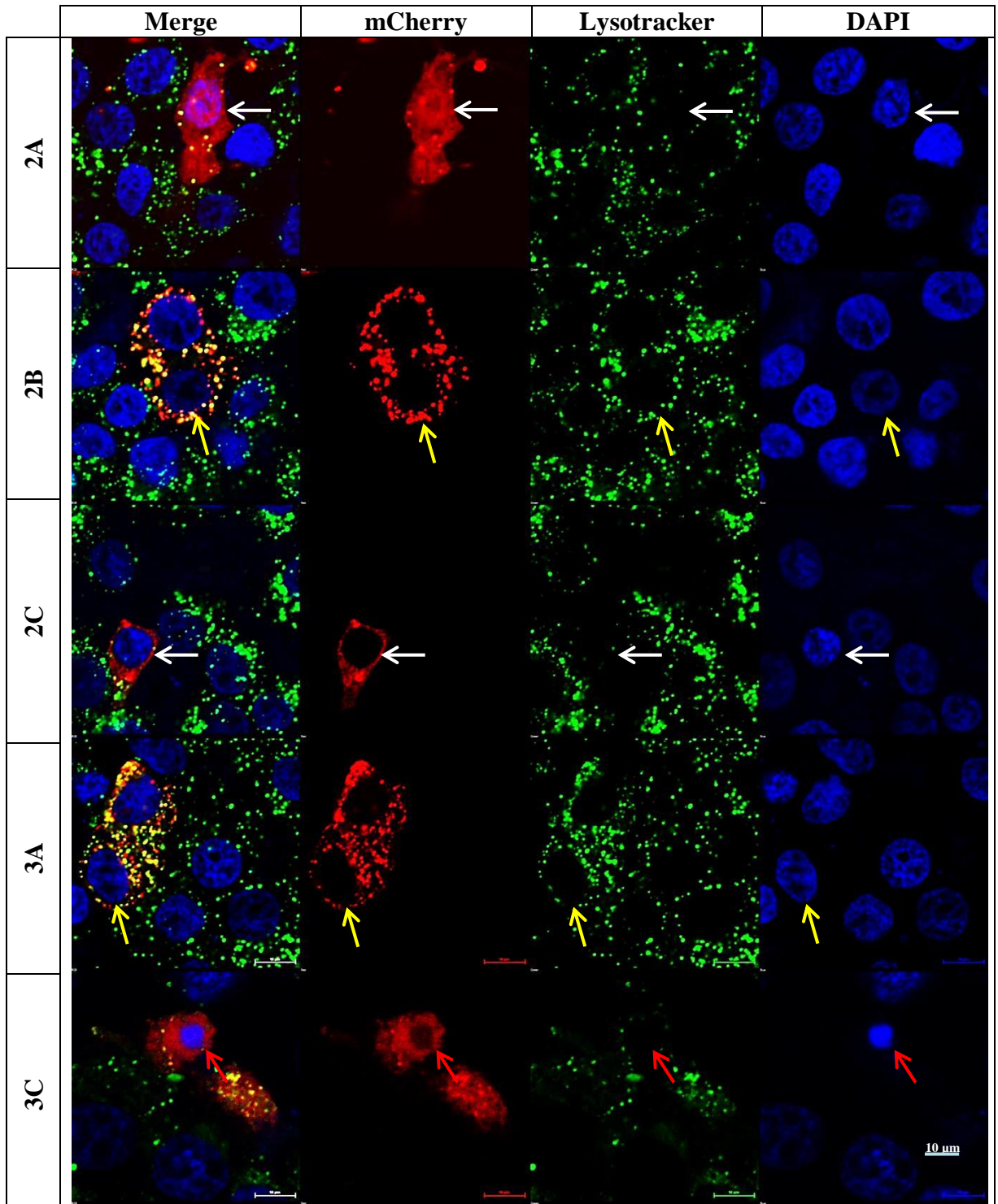


FIGURE 3.20: The effect of HPeV1 proteins (fused to mCherry) on lysosomes. GMK cells were grown on coverslips and transfected with mCherry fusion constructs using Turbofect. A green lysotracker stain was used and the nuclei were stained with Hoechst 33342. Live images were visualized using a Nikon A1 confocal microscope. The blue filter detects the nucleus, the red filter detects mCherry fused to 2A, 2B, 2C, 3A and 3C and the green filter detects lysosomes. The arrows indicate transfected cells (which show an mCherry signal). mCherry-2A and mCherry 2C (white arrows) have some effect on lysosome staining and the number of foci are less compared to non-transfected cells in the field. The stain distribution is changed by mCherry-2B and mCherry-3A (yellow arrows) to larger and more intense, which also partly co-localises to both of them. mCherry-3C (red arrow) causes major disruption to the cell structure, including nuclear condensation. The scale bar shown is 10 μm .

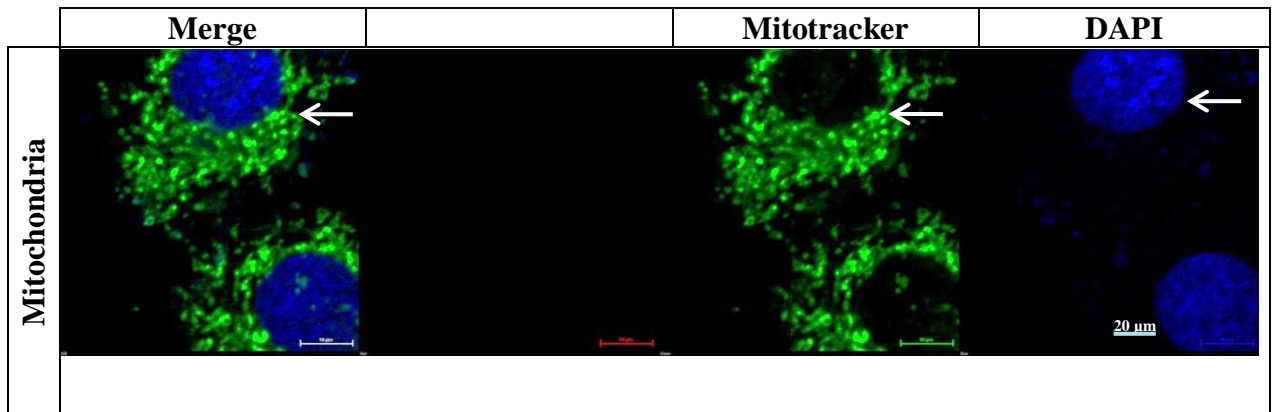


FIGURE 3.21: The normal distribution of mitochondria. GMK cells were grown on coverslips and stained with green mitotracker. Nuclei were stained with Hoechst 33342. Live images were visualized using a Nikon A1 confocal microscope. The blue filter detects the nucleus and the green filter detects mitochondria. The white arrows indicate the distribution of mitochondria stain as a network of foci throughout the cytoplasm. The scale bar shown is 20 μm .

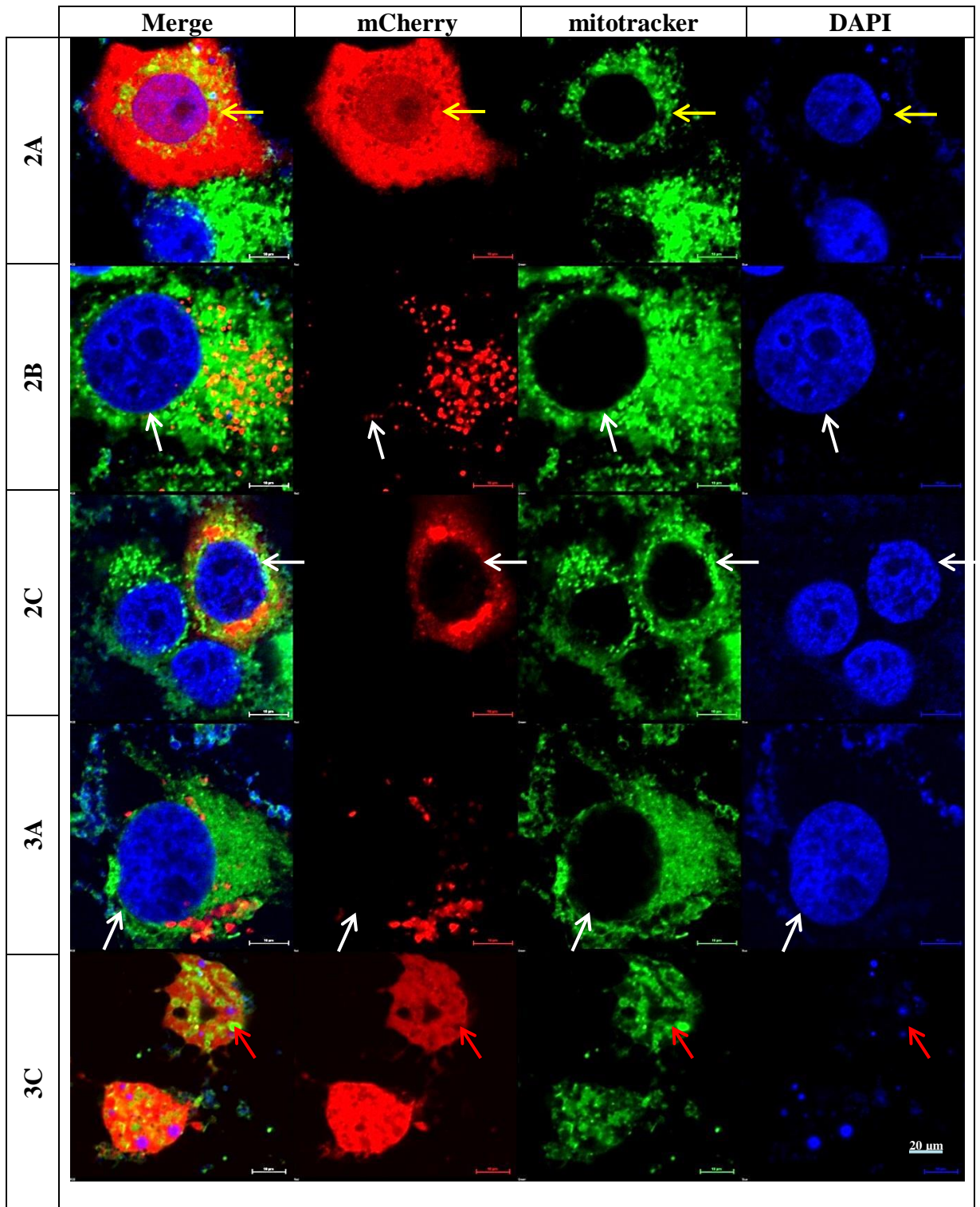


FIGURE 3.22: The effect of HPeV1 proteins (fused to mCherry) on mitochondria. GMK cells were grown on coverslips and transfected with mCherry fusion constructs using Turbofect. A green mitotracker stain were used and the nuclei were stained with Hoechst 33342. Live images were visualized using a Nikon A1 confocal microscope. The blue filter detects the nucleus, the red filter detects mCherry fused to 2A, 2B, 2C, 3A and 3C and the green filter detects mitochondria. The arrows indicate transfected cells (which show an mCherry signal). mCherry-2A shows a reduced of the size of the network (yellow arrows). mCherry 2B, mCherry-2C and mCherry-3A (white arrows) have little effect on mitochondria staining compared to non-transfected cells in the field. mCherry-3C (red arrow) causes major disruption to the cell structure, including nuclear condensation. The scale bar shown is 20 μm .

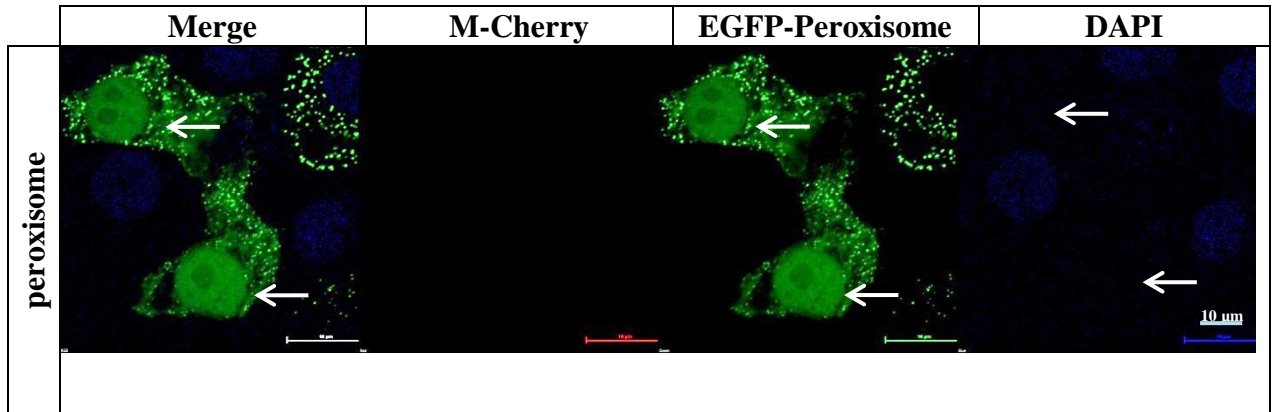


FIGURE 3.23: The normal distribution of peroxisomes. GMK cells were grown on coverslips and transfected with EGFP-peroxisome using Turbofect. Nuclei were stained with DAPI in the mounting medium. Images were visualized using a Nikon A1 confocal microscope. The blue filter detects the nucleus and the green filter detects peroxisome. The white arrows indicate the distribution of peroxisomes construct as a punctate distribution in the cytoplasm. The scale bar shown is 10 μm .

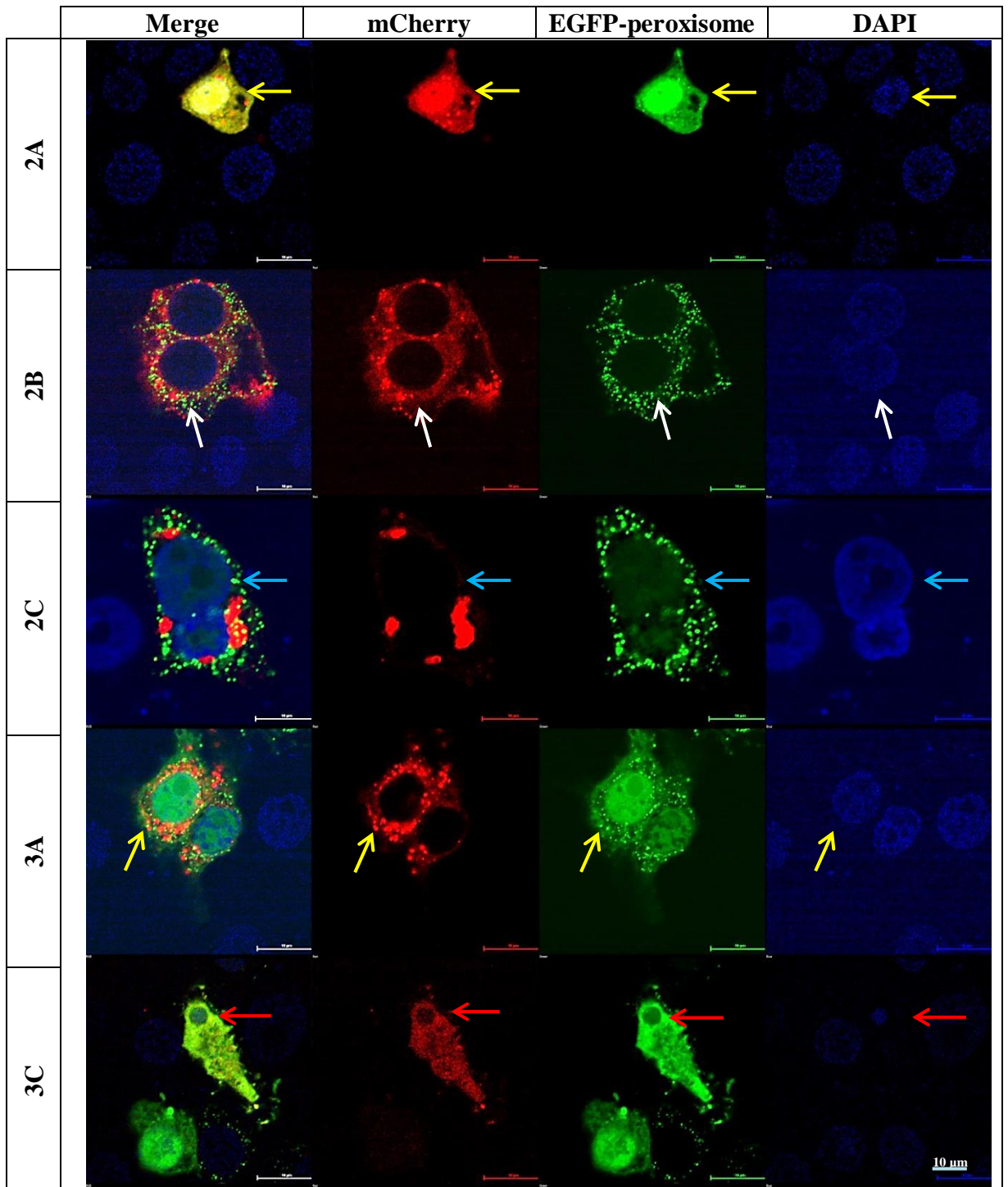


FIGURE 3.24: The effect of HPeV1 proteins (fused to mCherry) on peroxisomes. GMK cells were grown on coverslips and co-transfected with mCherry fusion constructs and EGFP-peroxisome using Turbofect. Nuclei were stained with DAPI in the mounting medium. Images were visualized using a Nikon A1 confocal microscope. The blue filter detects the nucleus, the red filter detects mCherry fused to 2A, 2B, 2C, 3A and 3C and the green filter detects EGFP-peroxisome. The arrows indicate transfected cells (which show an mCherry signal). The peroxisome distribution is changed by mCherry-2A and mCherry-3A (yellow arrows). mCherry 2B, (white arrow) has no effects on peroxisomes distribution compared to non-transfected cells in the field. mCherry-2C seemed to increase the size and intensity of the spots (blue arrow). mCherry-3C (red arrow) causes major disruption to the cell structure, including nuclear condensation. The scale bar shown is 10 μm .

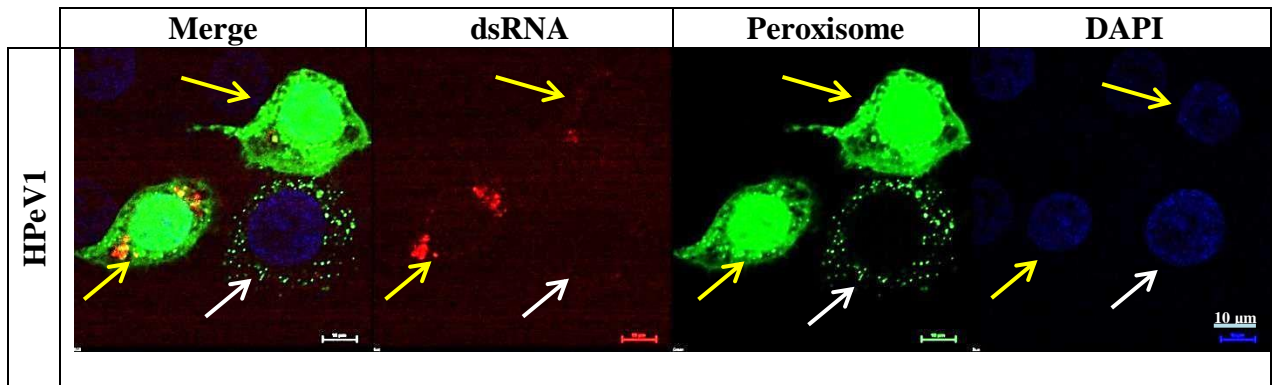


FIGURE 3.25: The effect of HPeV1 infection on the peroxisomes. HT29 cells were grown on coverslips and transfected with EGFP-peroxisome using Lipofectin reagent and then infected with HPeV1 for 8 hr. A monoclonal antibody against dsRNA was used and recognised with a secondary antibody labelled with Alexa Fluor 555. Nuclei were stained with DAPI in the mounting medium. Images were visualized using a Nikon A1 confocal microscope. The blue filter detects the nucleus, the green filter detects EGFP-peroxisome and the red filter detects dsRNA HPeV1 replication complexes. The white arrow indicates an uninfected cell and the yellow arrows indicate infected cells (identified by the presence of dsRNA in replication complexes). Compared to uninfected cells, HPeV disrupts the peroxisome pattern. The scale bar shown is 10 μm .

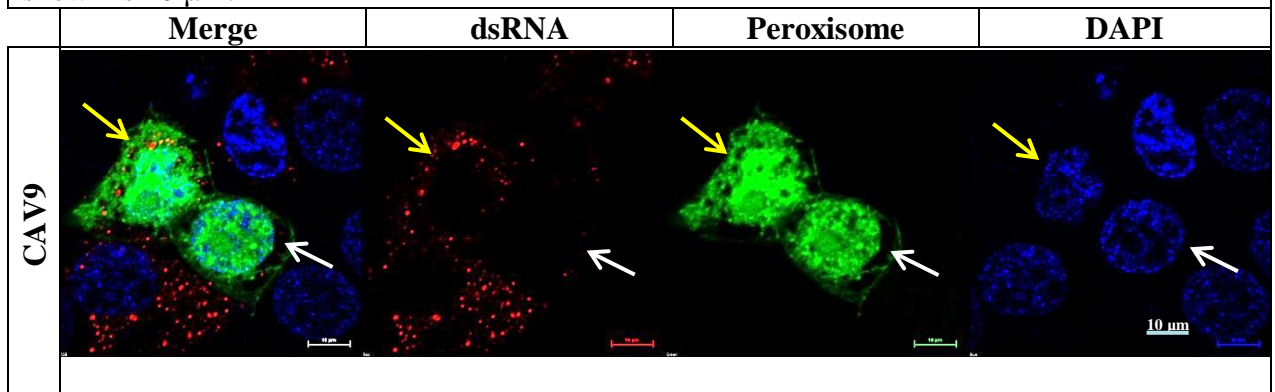


FIGURE 3.26: The effect of CAV9 infection on the peroxisomes. GMK cells were grown on coverslips and transfected with EGFP-peroxisome using Turbofect reagent and then infected with CAV-9 for 8 hr. A monoclonal antibody against dsRNA was used and recognised with a secondary antibody labelled with Alexa Fluor 555. Nuclei were stained with DAPI in the mounting medium. Images were visualized using a Nikon A1 confocal microscope. The blue filter detects the nucleus, the green filter detects EGFP-peroxisome and the red filter detects dsRNA of CAV9 replication complexes. The white arrow indicates an uninfected cell and the yellow arrow indicates an infected cell (identified by the presence of dsRNA in replication complexes). Compared to uninfected cells, CAV9 disrupts the peroxisome pattern. The scale bar shown is 10 μm .

3.5 Discussion

Cells transfer protein, lipid and other components between intracellular compartments using the early secretory pathway which consists of the ER, the ERGIC and the Golgi as well as the transport vesicles (coated with COPI or COPII) that shuttle between them (Midgley *et al.*, 2013; Watson and Stephens, 2005).

Viruses often rearrange cell compartments to give new membrane structures involved in viral replication and/or assembly (Inoue and Tsai, 2013). This concentrates materials needed for virus replication, holds replication complexes in place, and in the case of RNA viruses prevents dsRNA being recognised by the cell and so preventing defence responses triggered by dsRNA (Miller and Krijnse-Locker, 2008; Sasaki *et al.*, 2012).

Studies of several different positive-strand RNA viruses have suggested the ER, Golgi, endosomes or lysosomes as sources for these structures needed for replication (Salonen *et al.*, 2005; Suhy *et al.*, 2000). The use of cellular membranes from the secretory system for generating replication complexes also potentially affects protein secretion and cell-surface protein expression. Preventing MHC class 1 expression at the cell surface could be one way that the virus avoids host cell defence mechanisms (Belov, 2014).

HPEVs are being increasingly recognised as important human pathogens, but are genetically diverse from several picornaviruses. We therefore need to understand the details of virus replication to improve the opportunities to develop antiviral drugs. In this study, we first investigated the effect of HPEV1 infection on some compartments of the secretory pathway.

Our results agreed with previous work on HPEV infection which showed that infection has a large effect on the ER (Krogerus *et al.*, 2003). These authors also found that HPEV infection caused Golgi fragmentation, as observed in our study. Our study used HT29 cells (human colon carcinoma), while the previous work used A549 cells (human lung carcinoma) and as similar results were obtained, it suggests that loss of the ER and Golgi fragmentation are key features of

HPeV infection. In cells infected with CAV9 the Golgi marker GM130 was generally reduced and dispersed. This pattern seen was similar to that in previous work on enteroviruses (Cornell *et al.*, 2006; Mousnier *et al.*, 2014).

Infection with another picornavirus, FMDV, has little effect on the ER, but again leads to Golgi disruption and also causes a change to the distribution of the ERGIC. Even cells with low levels of FMDV infection showed these changes, suggesting that the ERGIC and Golgi are disrupted early after infection and before major changes are detected in the ER (Midgley *et al.*, 2013; Wang, 2012). These observations and analysis of cell proteins involved in the secretory pathway suggest that ER exit sites are important in replication complex formation (Midgley *et al.*, 2013). The difference between FMDV infection (ER remains intact) and HPeV infection (ER disrupted) suggests that HPeV replication complexes are produced from different components of the secretory pathway and it would be interesting to identify the source and mechanism, as they do not seem to contain ER, ERGIC or Golgi markers.

The origin of the poliovirus replication complex is not entirely clear and may involve lysosome, ER, and Golgi components (Schlegel *et al.*, 1996; Suhy *et al.*, 2000). There are many hypotheses for the formation of these structures during poliovirus infection (Reid *et al.*, 2015). Autophagic vesicles is one suggestion as early PV infection show 2BC and 3A proteins co-localise with lysosomal-associated membrane protein 1 (LAMP-1) and LC3-phosphatidylethanolamine conjugate (LC3-II) (Jackson *et al.*, 2005). Inhibiting autophagy decreases the amount of virus produced during infection with the related viruses, HRV-2 and HRV-14 (Klein and Jackson, 2011). It is interesting that in our experiments, both HPeV1 2B and 3A seemed to partially co-localise with lysosomes and this may suggest some involvement of these structures in replication complex formation.

During early infection, COPII-coated vesicles may be used to generate replication complexes by blocking anterograde transport and accumulating and relocating these vesicles. Infection with

poliovirus and expression of 3A blocks ER-Golgi protein transport (Choe *et al.*, 2005; Richards *et al.*, 2014). Poliovirus 2B has been found to co-localise with Sec13 and Sec31, which are components of the COPII vesicles and it was shown that infection with poliovirus results in a transient increase in COPII vesicles (den Boon *et al.*, 2010). However, other work shows no co-localisation between dsRNA and Sec31 (Richards *et al.*, 2014). In EV-71 COPI, but not COPII, is required for replication and EV-71 2C protein might locate COPI to the viral replication complex (Wang *et al.*, 2012b). Poliovirus replication complexes may also originate from the COPI secretory pathway as poliovirus infection is sensitive to brefeldin A (BFA). BFA inhibits the activation of the small GTPase Arf1 by interacting with specific guanine nucleotide exchange factors (GEFs) (Behnia and Munro, 2005; Irurzun *et al.*, 1992). Poliovirus 3A protein binds GBF1 and recruits it to virus-induced vesicles but does not recruit Arf1 (Belov *et al.*, 2008). 3A protein of CVB3 also induces the recruitment of GBF1 to membranes (Richards *et al.*, 2014; Sharp *et al.*, 2010). HRV-2 or HRV-14 3A recruited PI4KIII β to replication sites but do not bind to GBF1 (Dorobantu *et al.*, 2015). This suggests that even very similar viruses may use different host factors for replication. Viruses could possibly switch between these factors as brefeldin A resistant mutants of poliovirus can be generated easily and these presumably do not require GBF1 (Crotty *et al.*, 2004; Viktorova *et al.*, 2015). HPeV infection is only partially blocked by brefeldin A, while EMCV infection is resistant, again emphasizing that there are differences in host factor requirements between different picornaviruses (Gazina *et al.*, 2002).

To understand which virus proteins were responsible for the changes to the secretory pathway seen in infected cells, individual HPeV proteins were expressed as fusions with mCherry or EGFP. There was no difference in the localization regarding the fluorescent protein used (EGFP or mCherry). This suggests that the fluorescent proteins are not affecting the distribution of the virus proteins. 2C has the most distinctive distribution, large spots in the cytoplasm and this was previously suggested to be due to localisation to lipid droplet (Krogerus *et al.*, 2007). We

confirmed this using a different lipid droplet dye, which also revealed that the lipid droplets were greatly increased in size in the presence of HPeV 2C. The distributions of the other HPeV1 non-structural proteins was similar to that previously reported. 2A, 2B, 2C, 2BC, and 3A non-structural proteins previously (Krogerus *et al.*, 2003).

In FMDV, 2B plus 2C, or the 2BC precursor (but not 3A) can block trafficking of proteins between the ER and Golgi and their expression on the cell surface in FDMV (Sweeney *et al.*, 2010). We did not study the effect on secretion, but 2C/2BC seemed to affect all the compartments, especially the ER and this suggests that it would have a strong effect on secretion as in FMDV, rather than 3A as in enteroviruses. However, fragmentation of the Golgi without blocking of protein secretion in HRV-1A and HRV-16 have been reported and so the effect of our observed changes on secretion may not be predictable (Mousnier *et al.*, 2014; Quiner and Jackson, 2010).

In conclusion, some picornaviruses change the distribution of secretory pathway compartment and we found in this study that HPeV1 infection affects the Golgi and ERGIC, and almost completely destroys the ER in the HT29 cell line. 2B, 2BC/2C and 3A are the main non-structural proteins that affect the secretory pathway in picornaviruses. For HPeV1 we found that 2C affects all these compartments and 3A also has an effect on some of them.

It would be interesting to investigate the basis of changes to understand HPeV infections more fully and possibly identify new targets for antiviral drugs.

CHAPTER FOUR
THE INTERACTION BETWEEN
HPeV 2C AND LIPID DROPLETS

4.1 Introduction

2C protein is relatively highly conserved among picornaviruses and has been implicated in replication complex formation and several steps during viral replication. These include host cell membrane rearrangement and encapsidation. 2C includes regions which interact with other viral and cellular proteins (Banerjee *et al.*, 2004; Belsham and Normann, 2008). 2C has been assigned as a member of the superfamily III helicases group of the AAA+ ATPases although no helicase activity has been shown for picornavirus 2C proteins except EV-71 and the closely related virus CAV16 (Belsham and Normann, 2008; Sweeney *et al.*, 2010; Xia *et al.*, 2015). It has a predicted N-terminal membrane-binding amphipathic helix and nucleoside triphosphate (NTP) binding protein motifs, found in the central portion of 2C, including the ‘Walker’ motif A, involved in binding the phosphate to NTP, ‘Walker’ motif B, which may chelate Mg^{+2} involved in NTP hydrolysis, and motif C (Sweeney *et al.*, 2010; Teterina *et al.*, 1997).

In enterovirus-infected cells, 2C protein is associated with vesicles surrounding the viral RNA replication complexes and may be involved in the formation of the replication complex. During poliovirus infection, 2C and its precursor 2BC, migrate to the ER where they induce the formation of vesicles that bud off and become the site of viral RNA synthesis (Palmenberg *et al.*, 2010; Teterina *et al.*, 1997).

Lipids and associated molecules and structures such as fatty acids, lipid droplets and phosphoinositide are being increasingly recognised to be involved in many stages of the viral life cycle such as entry, replication, assembly and exit by budding (Chukkapalli *et al.*, 2012; Martin-Acebes *et al.*, 2013; van der Schaar *et al.*, 2016).

Lipid droplets (LD) are dynamic cytoplasmic organelles found in most cells. They are the most important storage site for neutral lipids. They consist of a hydrophobic core of neutral lipids (triglycerides (TG) and cholesterol esters (CE)), surrounded by a phospholipid monolayer (Guo *et al.*, 2009; Herker and Ott, 2012; Walther and Farese, 2012). Lipid stored in LDs have several

functions, including energy generation, providing building components for membrane synthesis and being the starting point to synthesize specific lipids. LDs can also be used for protein storage, for example to temporarily store unfolded membrane proteins before proteasomal degradation (Fujimoto et al., 2008; Guo et al., 2009; Walther and Farese, 2012). LDs also contain their own specific proteins on the surface including structural proteins (e.g. proteins of the perilipin family), lipid-synthesis enzymes, lipases and membrane-trafficking proteins (e.g. Rab5, Rab18 and ARF1) (Guo et al., 2009).

Many viruses including hepatitis C virus (HCV), Dengue virus, West Nile virus and Rotavirus (RV) have been reported to use LDs in replication complexes formation (Gaunt *et al.*, 2013). The core protein of HCV was reported to localise to LDs and the capsid protein of Dengue virus also associates to LDs, which is necessary for efficient viral replication (Saka and Valdivia, 2012). It was previously reported that HPeV 2C, interacts with LDs (Krogerus *et al.*, 2007) and this observation was confirmed in our laboratory (Salimi, 2015). Expression of individual HPeV non-structural proteins described in chapter 3, shows that 2C localises in large perinuclear foci, presumably lipid droplets. The aims of this work described in this chapter is to understand the basis of this interaction, how it plays a role in HPeV infection and if this interaction occurs in related viruses.

4.2 Fatty acid study

4.2.1 Virus and fatty acids

Firstly, we analysed the effect of HPeV1 or CAV9 infection on intracellular lipid using the lipid marker BODIPY 500/510 C4-C9. GMK or HT29 cells were seeded in 6 well plates containing glass coverslips 24 hours before the experiment and were confluent before the start of the experiment. Cells were infected with CAV9 or HPeV1 at MOI 10. At time intervals (2, 6, 8 hours) the medium was replaced with fresh pre-warmed medium with 0.4 μ M BODIPY 500/510 C4-C9 for 30 minutes (Nchoutmboube *et al.*, 2013). Cells were fixed and virus infected cells

were identified with a dsRNA antibody. The results are shown in Figures 4.1- 4.3. There seem to be no consistent differences between uninfected and infected cells.

4.2.2 **Non-structural proteins of HPeV1 and fatty acid**

We next investigate if the non-structural proteins of HPeV1 interact with fatty acids. Cells were transfected with Turbofect, then stained with BODIPY 500/510 C4- C9. The results are shown in Figure 4.4. There seemed to be some co-localisation between FA and HPeV 2B and 3A. In the case of 2C, some of the FA stain is located in foci and these correspond to the concentrations of 2C. This suggests that 2C is associating with fatty acid/lipid structures.

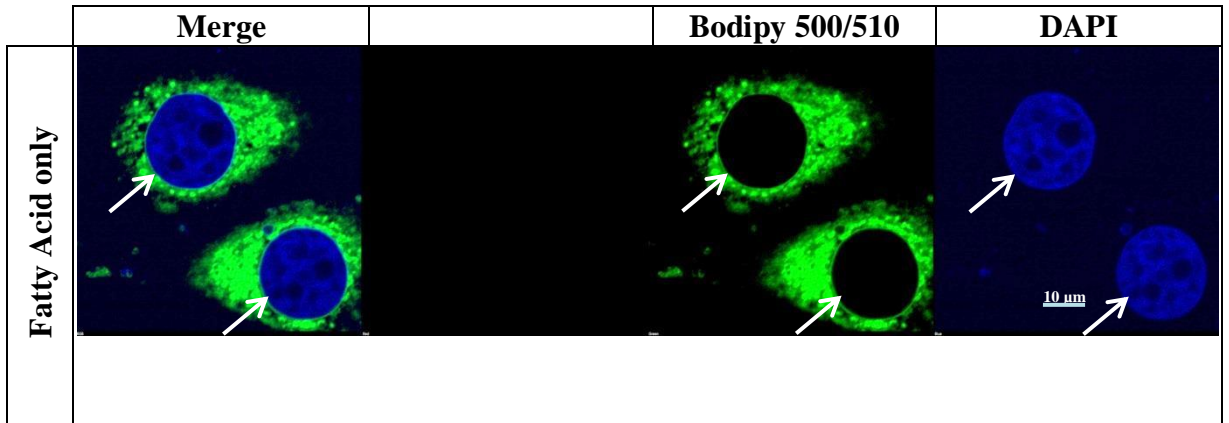


FIGURE 4.1: The normal distribution of fatty acids (FAs) in GMK cells. GMK cells were grown on coverslips and washed with DMEM serum-free medium. Cells were grown in serum-free medium with 50mM HEPES for 30 minutes then the medium was replaced with fresh pre-warmed medium with 0.4 μ M BODIPY 500/510 for 30 minutes. Cells were fixed and washed with glycine and permeabilized with Saponin then blocked. The coverslips were mounted with hard set mounting medium with DAPI. Images were visualized using a Nikon A1 confocal microscope. The blue filter detects the nucleus and the green filter detects FAs. The white arrows show the normal distribution of FAs as a diffuse staining pattern in the cytoplasm. The scale bar shown is 10 μ m.

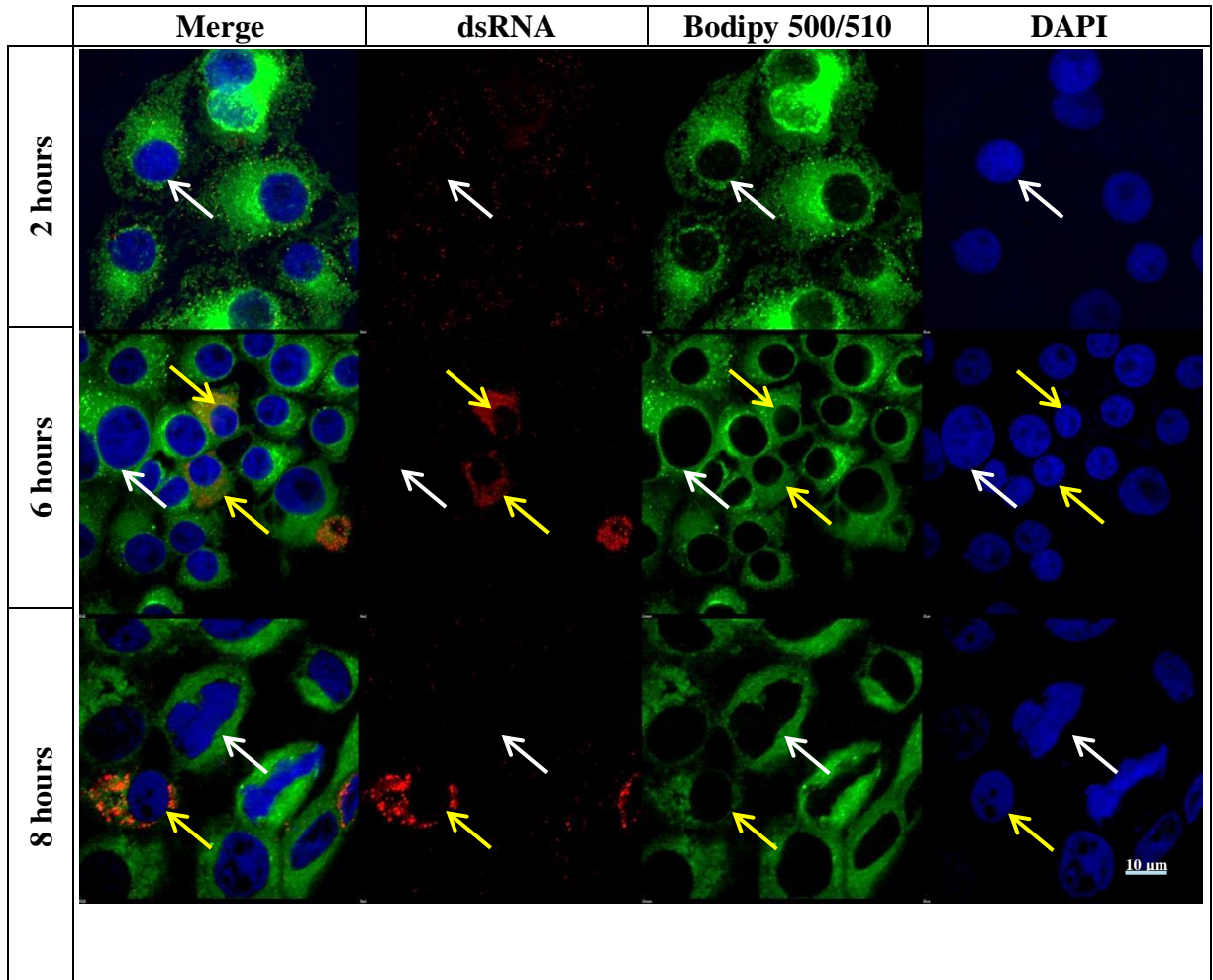


FIGURE 4.2: The effect of CAV9 on fatty acids (FAs). GMK cells were seeded in 6 well plates containing glass coverslips and were confluent before the start of the experiment. Cells were washed with DMEM serum-free medium and infected with CAV9 (MOI 10) in serum-free medium with 50mM HEPES. At 2, 6, or 8 hours the medium was replaced with fresh pre-warmed medium with 0.4 μ M BODIPY 500/510 for 30 minutes. Cells were fixed, permeabilized and blocked. dsRNA monoclonal antibody, followed by secondary antibody labelled with Alexa Fluor 555 was used to identify infected cells. The coverslips were mounted with hard set mounting medium with DAPI. Images were visualized using a Nikon A1 confocal microscope. The blue filter detects the nucleus, the green filter detects FAs and red filter detects dsRNA. The white arrows indicate uninfected cells and the yellow arrows indicate infected cells (identified by the presence of dsRNA in replication complexes). Compared to uninfected cells, there is no consistent difference between uninfected and infected cells at 2, 6 and 8 hours post infection. The scale bar shown is 10 μ m.

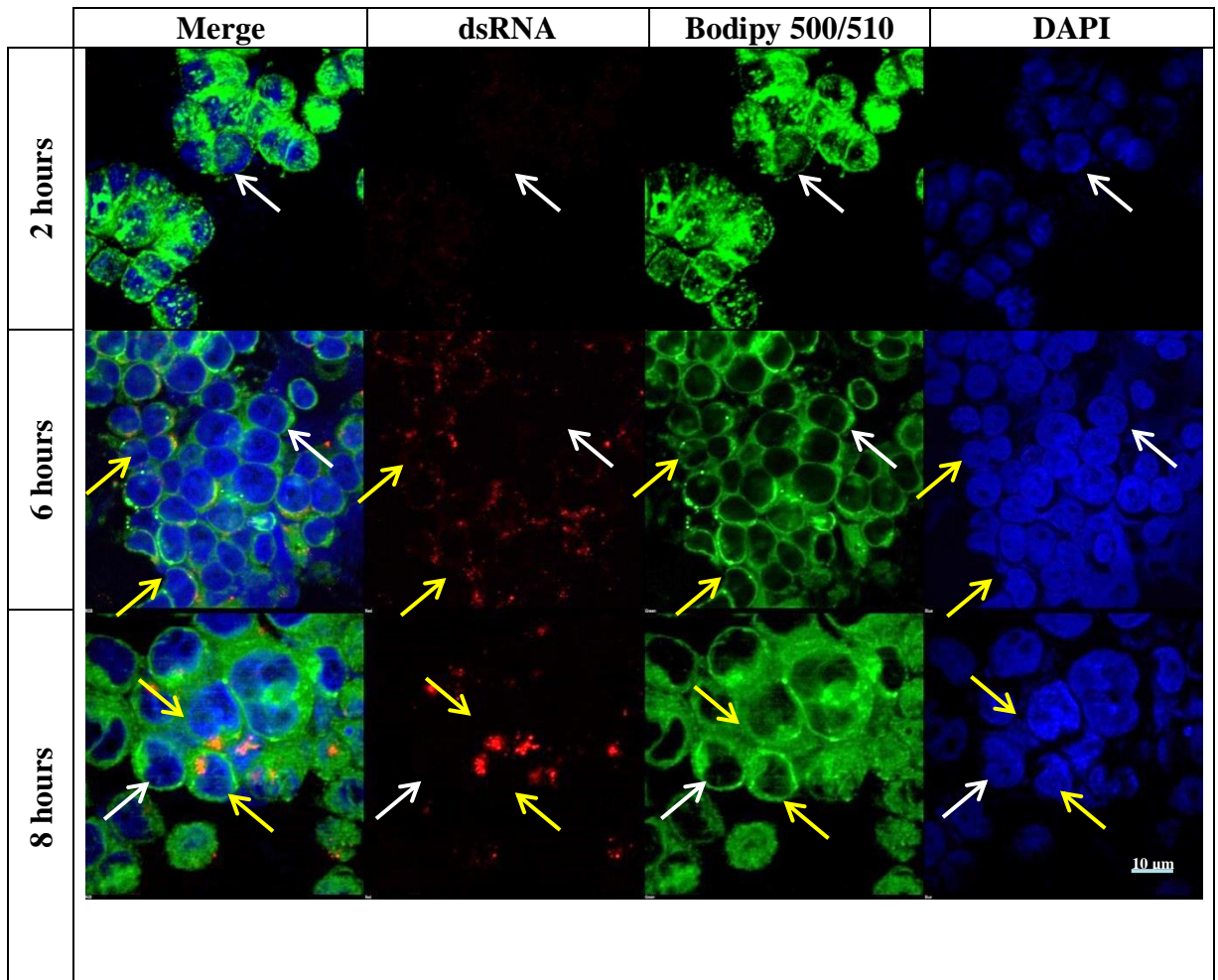


FIGURE 4.3: The effect of HPeV1 on fatty acids (FAs). HT29 cells were seeded in 6 well plates containing glass coverslips and were confluent before the start of the experiment. Cells were washed with DMEM serum-free medium and infected with HPeV1 (MOI 10) in serum-free medium with 50mM HEPES. At 2, 6, or 8 hours the medium was replaced with fresh pre-warmed medium with 0.4 μ M BODIPY 500/510 for 30 minutes. Cells were fixed, permeabilized and blocked. dsRNA monoclonal antibody, followed by secondary antibody labelled with Alexa Fluor 555 was used to identify infected cells. The coverslips were mounted with hard set mounting medium with DAPI. Images were visualized using a Nikon A1 confocal microscope. The blue filter detects the nucleus, the green filter detects FAs and red filter detects dsRNA. The white arrows indicate uninfected cells and the yellow arrows indicate infected cells (identified by the presence of dsRNA in replication complexes). Compared to uninfected cells, there is no consistent difference between uninfected and infected cells at 2, 6 and 8 hours post infection. The scale bar shown is 10 μ m.

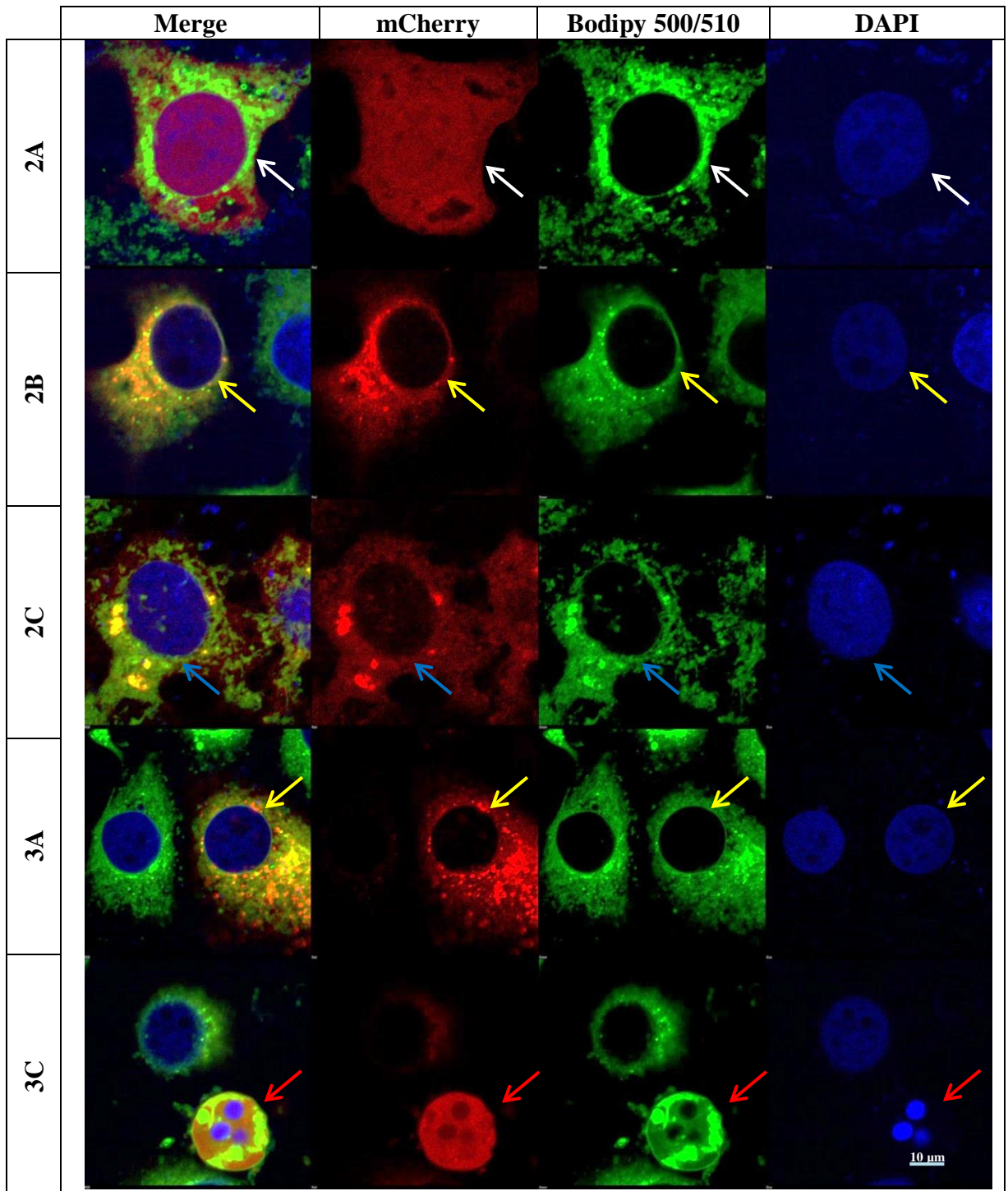


FIGURE 4.4: The localisation of fatty acids (FAs) in cells transfected with constructs encoding HPeV1 proteins fused to mCherry. GMK cells were grown on coverslips and transfected with HPeV1 constructs for 24-48 hours using Turbofect. A fresh pre-warmed medium with 0.4 μM BODIPY 500/510 was added for 30 minutes and washed twice with PBS. The coverslips were mounted with hard set mounting medium with DAPI. Images were visualized using a Nikon A1 confocal microscope. The blue filter detects the nucleus, the red filter detects mCherry of 2A, 2B, 2C, 3A and, 3C and the green filter detects FAs. The arrows indicate transfected cells (which show an mCherry signal). mCherry-2A (white arrow) has no effect on FAs staining compared to non-transfected cells in the field. mCherry 2B, and mCherry-3A (yellow arrows) seemed to be co-localised with FA. Some of the FA stain is located in foci by mCherry-2C (blue arrow), and these correspond to the concentrations of 2C. mCherry-3C (red arrow) causes major disruption to the cell structure, including nuclear condensation. The scale bar shown is 10 μm .

4.3 Lipid droplets study

4.3.1 Lipid Droplets and viruses

We then investigated LDs in infected cells. Cells were infected for 0, 2, 4, 6, 8, or 10 hours then fixed. LDs were identified by staining with BODIPY 493/503 at a final concentration of 10 mg/ml (Wolins *et al.*, 2001) and infected cells by using dsRNA antibody.

LDs show spherical structures in the cytoplasm in uninfected GMK cells and cells in the early stage of infection with CAV9 (0, 2 and 4 hours post infection) (Figure 4.5). CAV9 replication complexes are visible at 4 hours and do not co-localise with LDs. Later post-infection (6, 8, and 10 hours) this distribution seem to be less in infected cells and no LDs are visible 10 hours post-infection (Figure 4.6).

LDs show spherical structures in the cytoplasm in the HT29 cell line and are brighter than those seen in GMK cells. The LDs distribution become less 4 hours post-infection (Figure 4.7). LDs become more concentrated near to the dsRNA 6, 8, and 12 hours post-infection in some cells but seem not to be present in some infected cells (Figure 4.8). Again the LDs do not co-localise with replication complexes although they tend to be close.

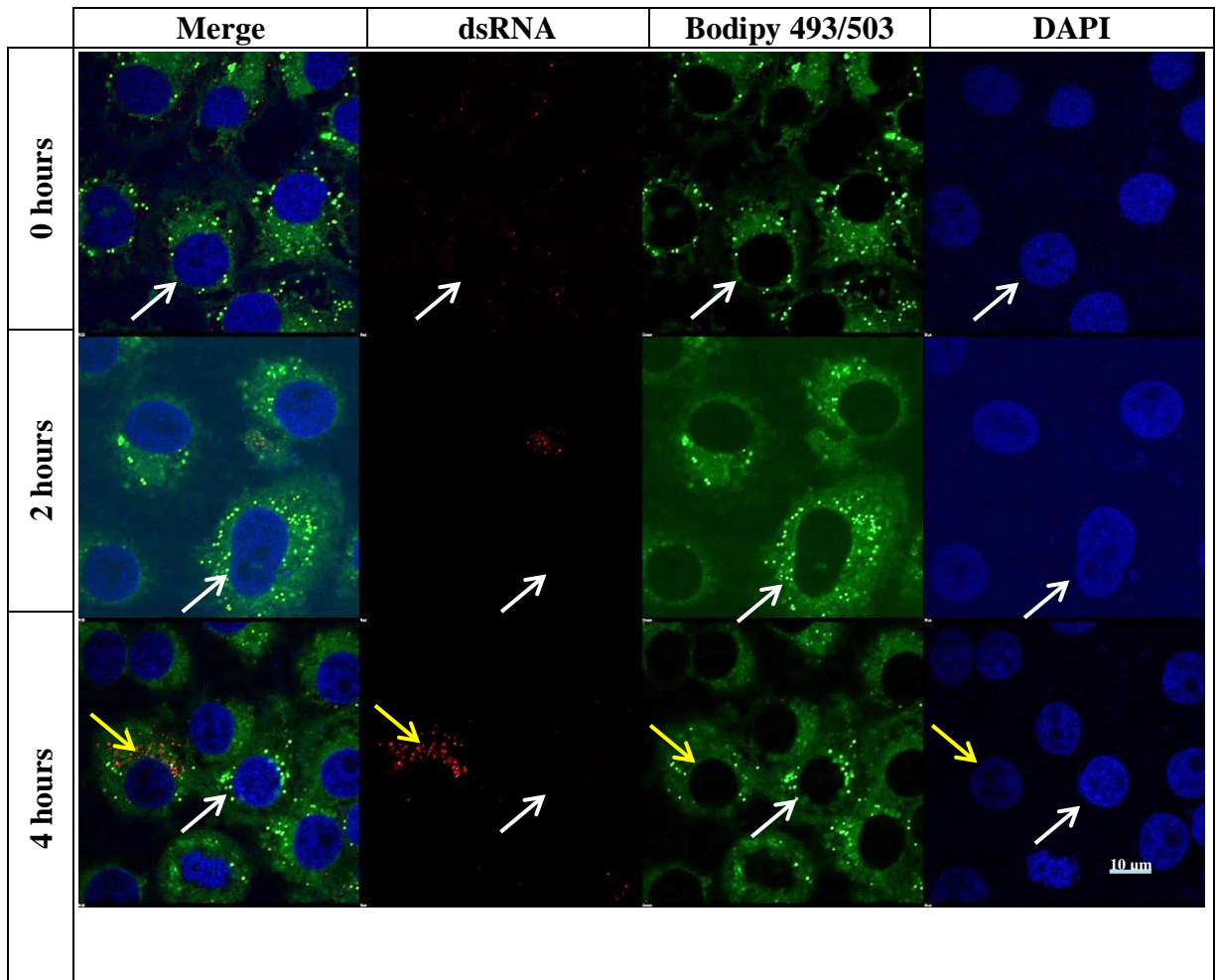


FIGURE 4.5: The effect of CAV9 on lipid droplets (LDs) in early stages of infection. GMK cells were seeded in 6 well plates containing glass coverslips and were confluent before the start of the experiment. Cells were infected with 50 μ l of CAV9 (MOI 10) and incubated for 0, 2, 4 hours and after each incubation the cells were fixed, permeabilized and blocked. dsRNA monoclonal antibody was added after incubation overnight and washing, this was detected with secondary antibody labelled with Alexa Fluor 555. Cells were stained with BODIPY 493/503 for 10 min at a final concentration of 10 mg/ml then cells were washed twice with PBS. The coverslips were mounted with hard set mounting medium with DAPI. Images were visualized using a Nikon A1 confocal microscope. The blue filter detects the nucleus, the green filter detects neutral lipids in LDs and red filter detects dsRNA. The white arrows indicate uninfected cells and the yellow arrow indicates an infected cell (identified by the presence of dsRNA in replication complexes). Compared to uninfected cells, there is no consistent difference in LD distribution in infected cells at 4 hours post infection. The infected cells only become visible 4 hours after infection. The scale bar shown is 10 μ m.

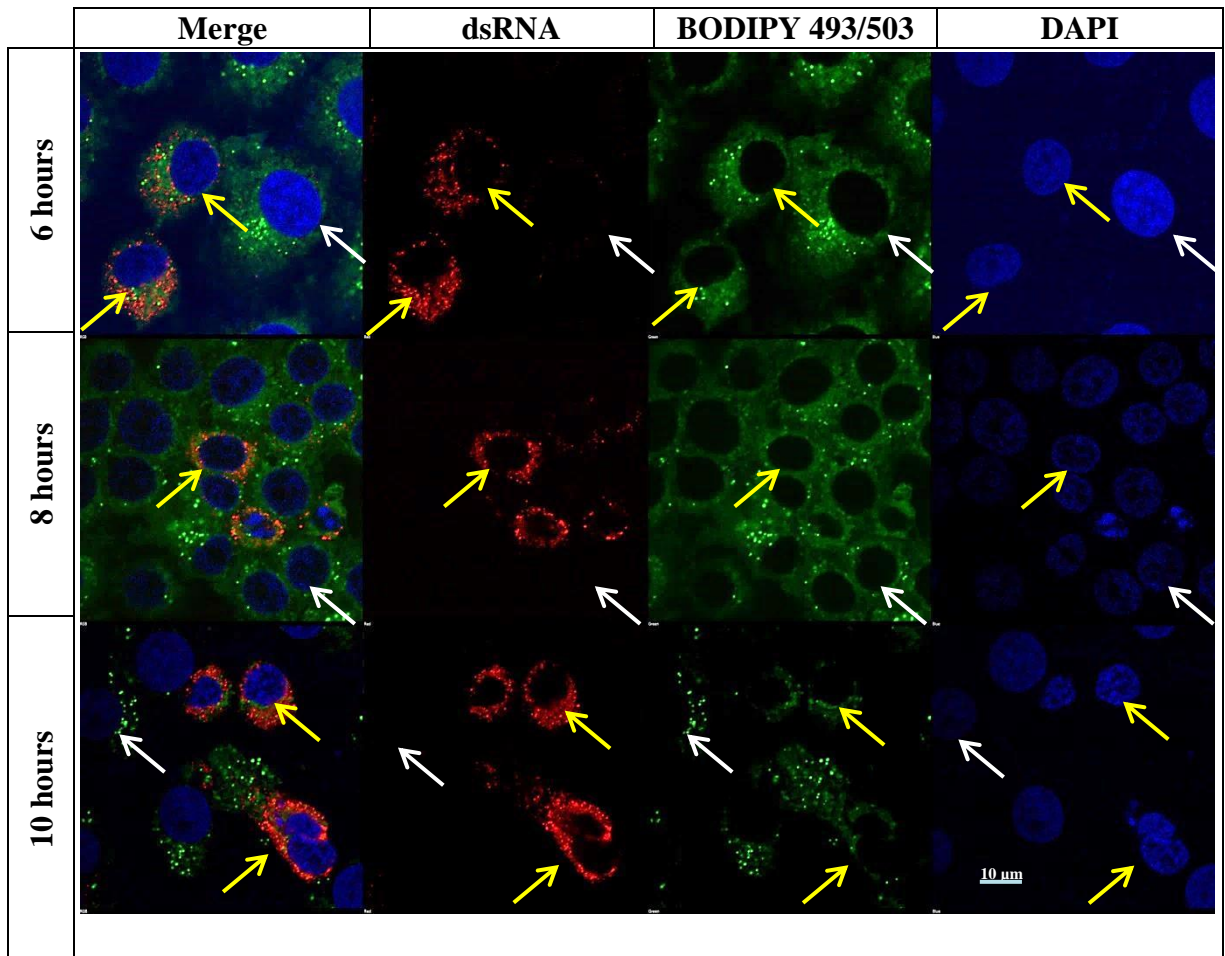


FIGURE 4.6: The effect of CAV9 on lipid droplets (LDs) in late stages of infection. GMK cells were seeded in 6 well plates containing glass coverslips and were confluent before the start of the experiment. Cells were infected with 50 μ l of CAV9 (MOI 10) and incubated for 6, 8, 10 hours and after each incubation the cells were fixed, permeabilized and blocked. dsRNA monoclonal antibody was added after incubation overnight and washing, this was detected with secondary antibody labelled with Alexa Fluor 555. Cells were stained with BODIPY 493/503 for 10 min at a final concentration of 10 mg/ml then cells were washed twice with PBS. The coverslips were mounted with hard set mounting medium with DAPI. Images were visualized using a Nikon A1 confocal microscope. The blue filter detects the nucleus, the green filter detects neutral lipids in LDs and red filter detects dsRNA. The white arrows indicate uninfected cells and the yellow arrows indicate infected cells (identified by the presence of dsRNA in replication complexes). Compared to uninfected cells in the field, the LD distribution seems to be less in infected cells than in uninfected cells at 6 and 8 hours post infection. No LDs are visible at 10 hours post-infection. The scale bar shown is 10 μ m.

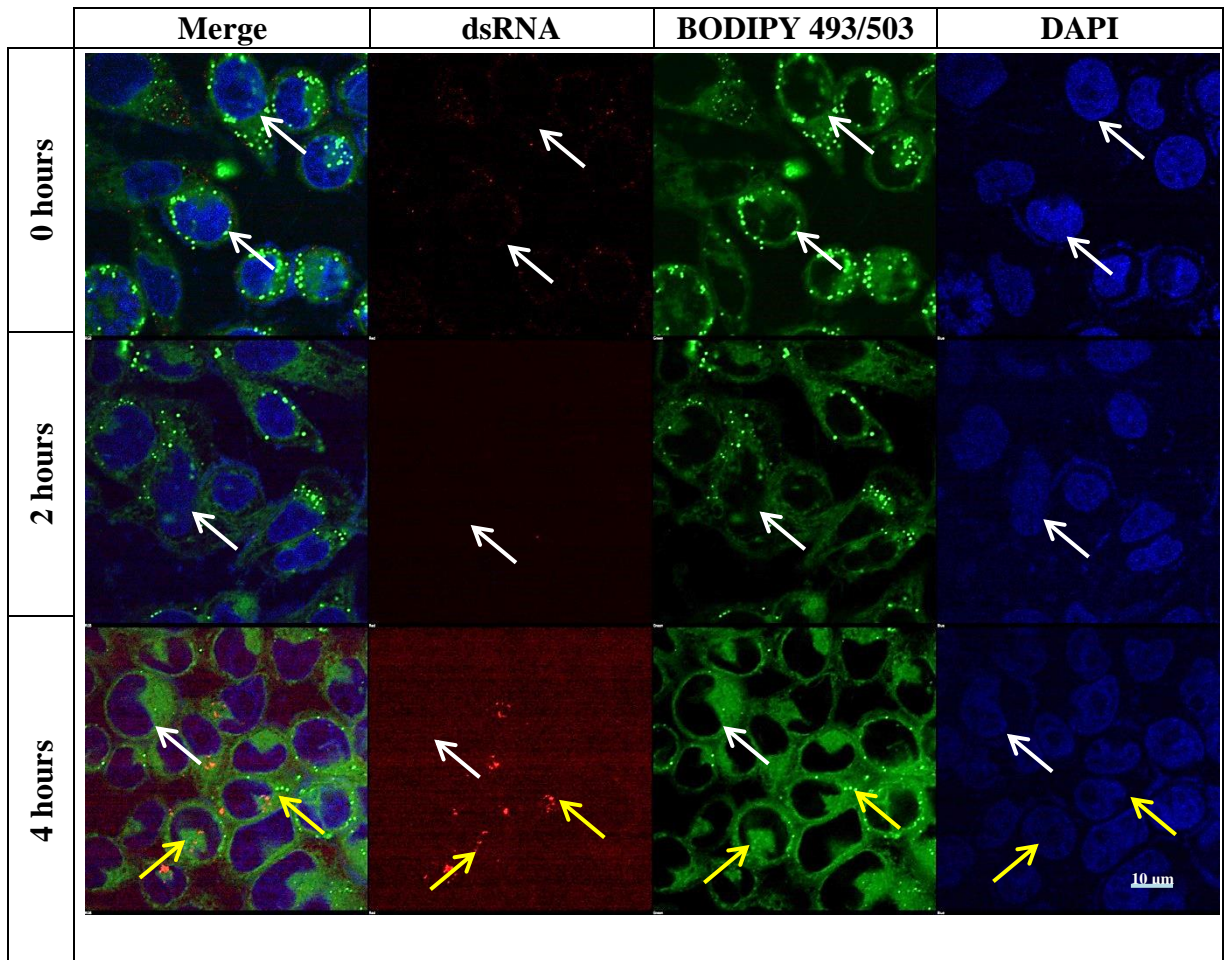


FIGURE 4.7: The effect of HPeV1 on lipid droplets (LDs) in early stages of infection. HT29 cells were seeded in 6 well plates containing glass coverslips and were confluent before the start of the experiment. Cells were infected with 50 μ l of HPeV1 (MOI 10) and incubated for 0, 2, 4 hours and after each incubation the cells were fixed, permeabilized and blocked. dsRNA monoclonal antibody was added after incubation overnight and washing, this was detected with secondary antibody labelled with Alexa Fluor 555. Cells were stained with BODIPY 493/503 for 10 min at a final concentration of 10 mg/ml then cells were washed twice with PBS. The coverslips were mounted with hard set mounting medium with DAPI. Images were visualized using a Nikon A1 confocal microscope. The blue filter detects the nucleus, the green filter detects neutral lipids in LDs and red filter detects dsRNA. The white arrows indicate uninfected cells and the yellow arrows indicate infected cells (identified by the presence of dsRNA in replication complexes). Compared to uninfected cells, there is no consistent difference in LD distribution in infected cells at 4 hours post infection. The infected cells only become visible 4 hours after infection. The scale bar shown is 10 μ m.

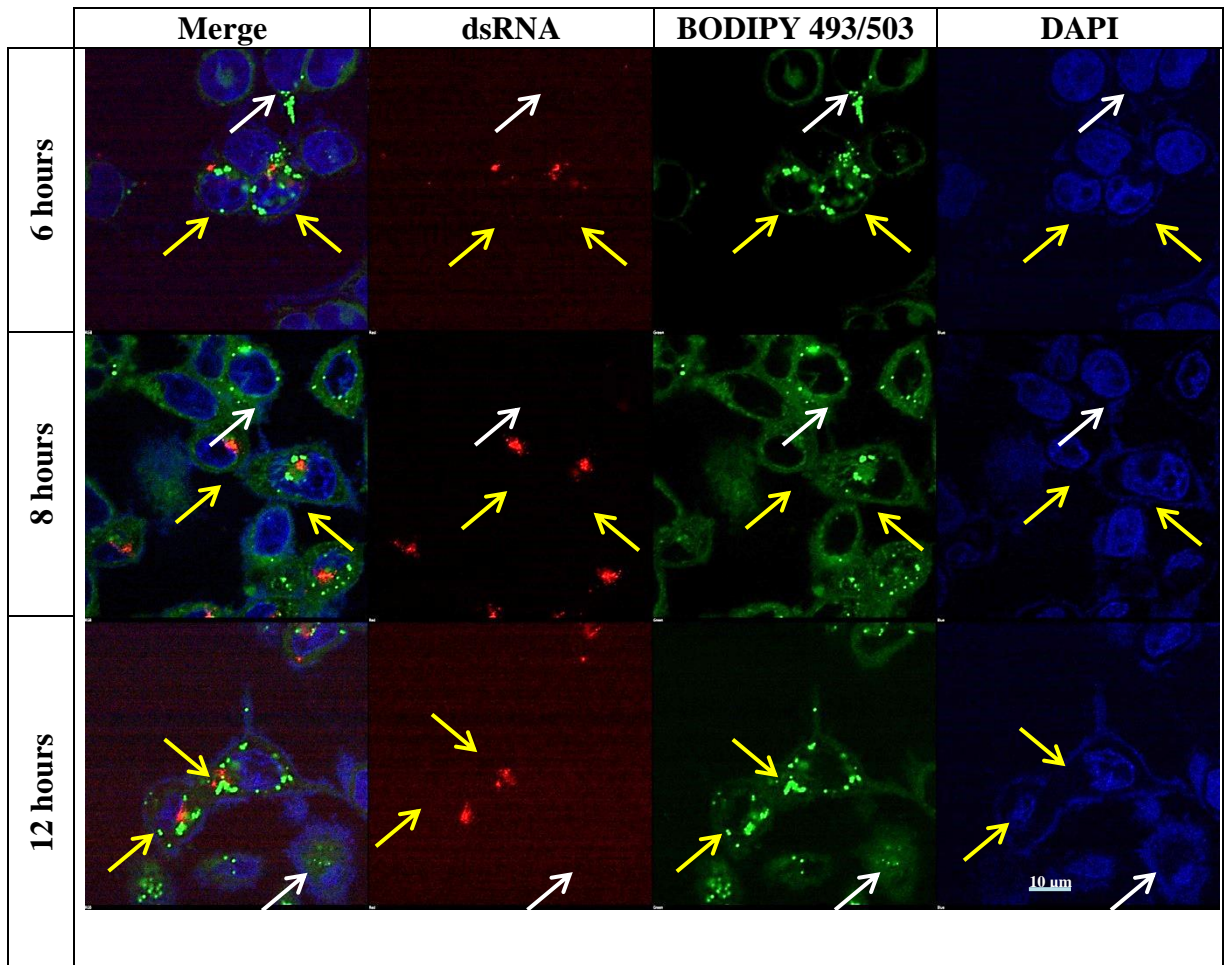


FIGURE 4.8: The effect of HPeV1 on lipid droplets (LDs) in late stages of infection. HT29 cells were seeded in 6 well plates containing glass coverslips and were confluent before the start of the experiment. Cells were infected with 50 μ l of HPeV1 (MOI 10) and incubated for 6, 8, 12 hours and after each incubation the cells were fixed, permeabilized and blocked. dsRNA monoclonal antibody was added after incubation overnight and washing, this was detected with secondary antibody labelled with Alexa Fluor 555. Cells were stained with BODIPY 493/503 for 10 min at a final concentration of 10 mg/ml then cells were washed twice with PBS. The coverslips were mounted with hard set mounting medium with DAPI. Images were visualized using a Nikon A1 confocal microscope. The blue filter detects the nucleus, the green filter detects neutral lipids in LDs and red filter detects dsRNA. The white arrows indicate uninfected cells and the yellow arrows indicate infected cells (identified by the presence of dsRNA in replication complexes). Compared to uninfected cells, LDs become more concentrated and located near to the dsRNA 6, 8, and 12 hours post-infection. The scale bar shown is 10 μ m.

4.3.2 Non-structural proteins of HPeV1

To continue our investigation with LDs, we examined the effect of HPeV1 non-structural proteins. The constructs shown in (Figure 3.5) were used and were transfected into GMK cells using TurboFect. GMK cells were used as they have a better transfection efficiency and morphology for imaging than HT29 cells. LDs were detected with BODIPY 493/503.

We first examined BODIPY 493/503 and pmCherry-C1 vector as a control. The LD stain showed spherical structures in the cytoplasm. mCherry is diffuse in the cytoplasm and nucleus and there is no change in the distribution of LDs compared with untransfected cells (Figure 4.9).

The distribution and/or the number of LDs in cells transfected with mCherry-2A or mCherry-3C were similar to untransfected cells (Figure 4.10). mCherry-2B and mCherry-3A show slight co-localisation with LDs but LDs have the typical distribution (Figure 4.11). Clear co-localisation was seen between mCherry-2C and LDs. In addition, the LDs were aggregated into punctate structures (Figure 4.11). EGFP-2BC co-localised with another LD stain, Lipotox, but did not seem to cause the same amount of LD aggregation (Figure 4.12).

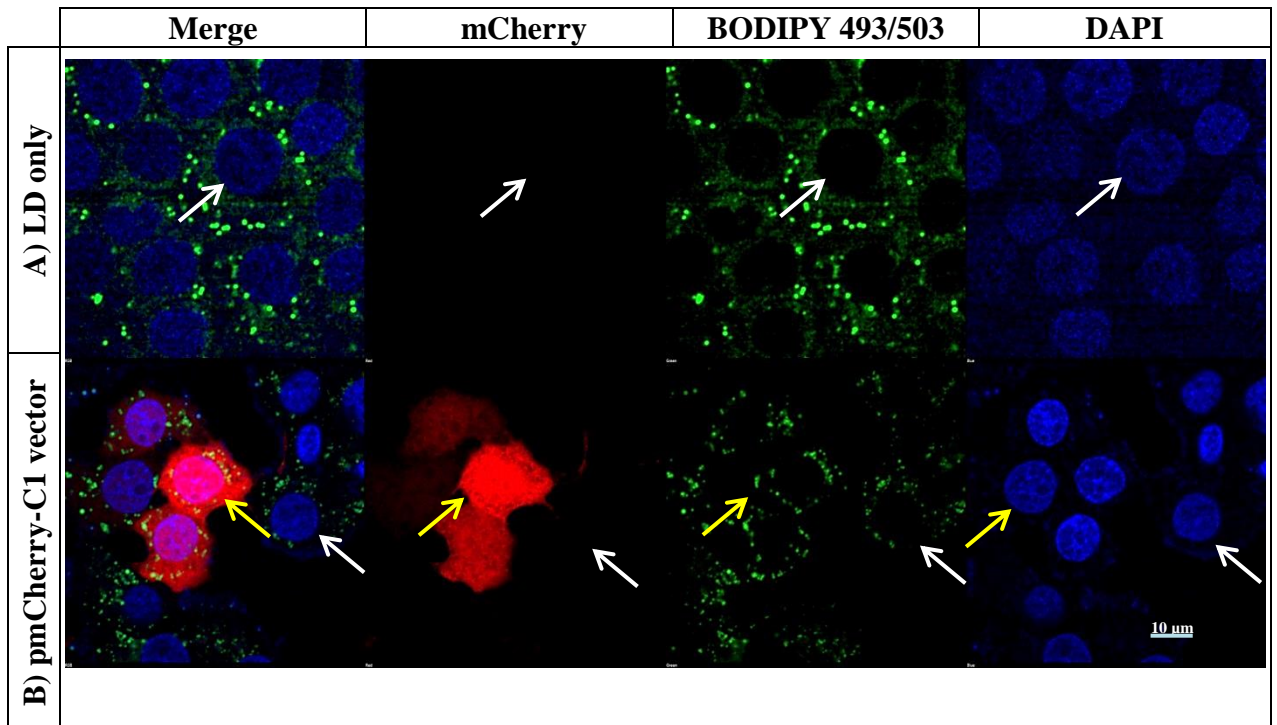


FIGURE 4.9: Lipid droplets (LDs) and pmCherry-C1 vector. GMK cells were grown on coverslips and one sample was transfected with pmCherry-C1 using Turbofect. Cells were fixed and stained with BODIPY 493/503 for 10 min at a final concentration of 10 mg/ml then cells were washed twice with PBS. The coverslips were mounted with hard set mounting medium with DAPI. Images were visualized using a Nikon A1 confocal microscope. The blue filter detects the nucleus, the red filter detects mCherry vector and the green filter detects neutral lipids in LDs. A) Untransfected cells. The white arrow indicates a cell showing the normal distribution of LDs as spherical structures in the cytoplasm. B) Cells transfected with pmCherry-C1. The yellow arrow shows a transfected cell (which shows an mCherry signal). There is no difference in the LD distribution between the transfected cell and an untransfected cell (white arrow) in the same field. The scale bar shown is 10 μ m.

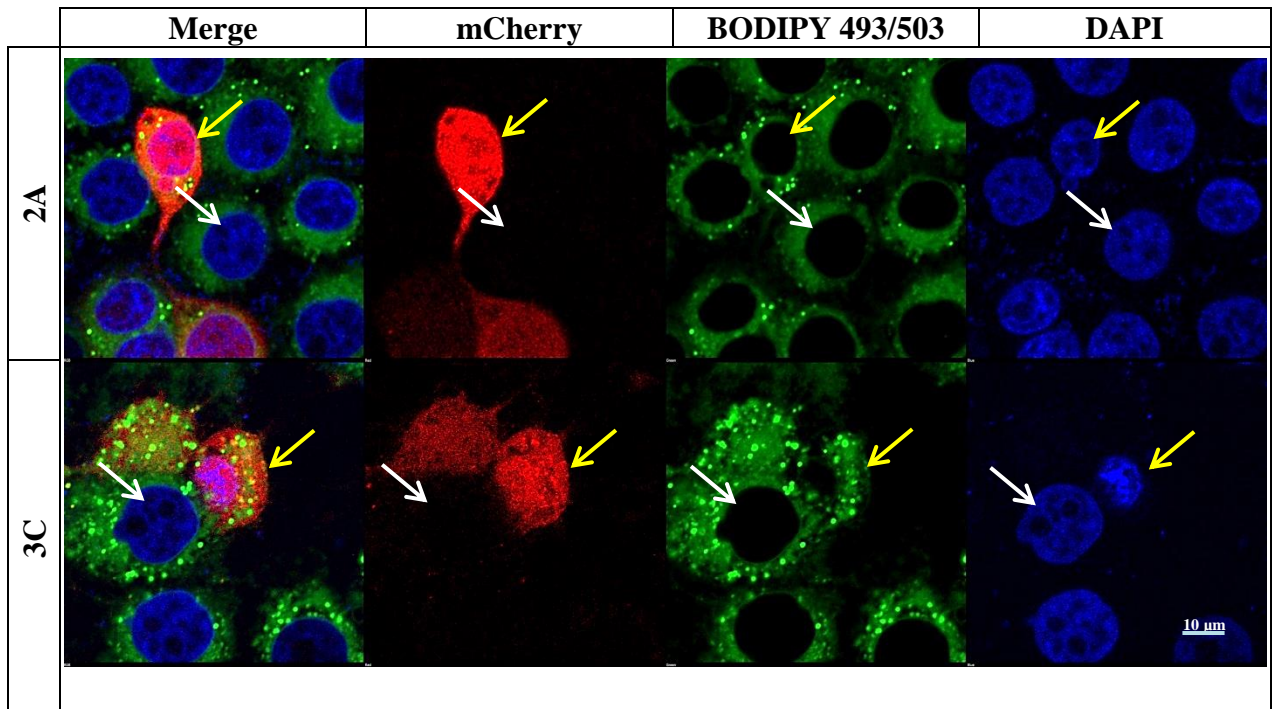


FIGURE 4.10: The effect of mCherry-2A and mCherry-3C on lipid droplets (LDs). GMK cells were grown on coverslips and transfected with the HPeV1 non-structural protein constructs pmCherry-2A or pmCherry-3C using Turbofect. Cells were fixed and stained with BODIPY 493/503 for 10 min at a final concentration of 10 mg/ml then cells were washed twice with PBS. The coverslips were mounted with hard set mounting medium with DAPI. Images were visualized using a Nikon A1 confocal microscope. The blue filter detects the nucleus, the red filter detects mCherry-2A and mCherry-3C and the green filter detects neutral lipids in LDs. The yellow arrows indicate transfected cells (which show an mCherry signal). mCherry-2A and mCherry-3C (yellow arrows) have no effect on LD staining compared to non-transfected cells in the field (white arrows). The scale bar shown is 10 μm .

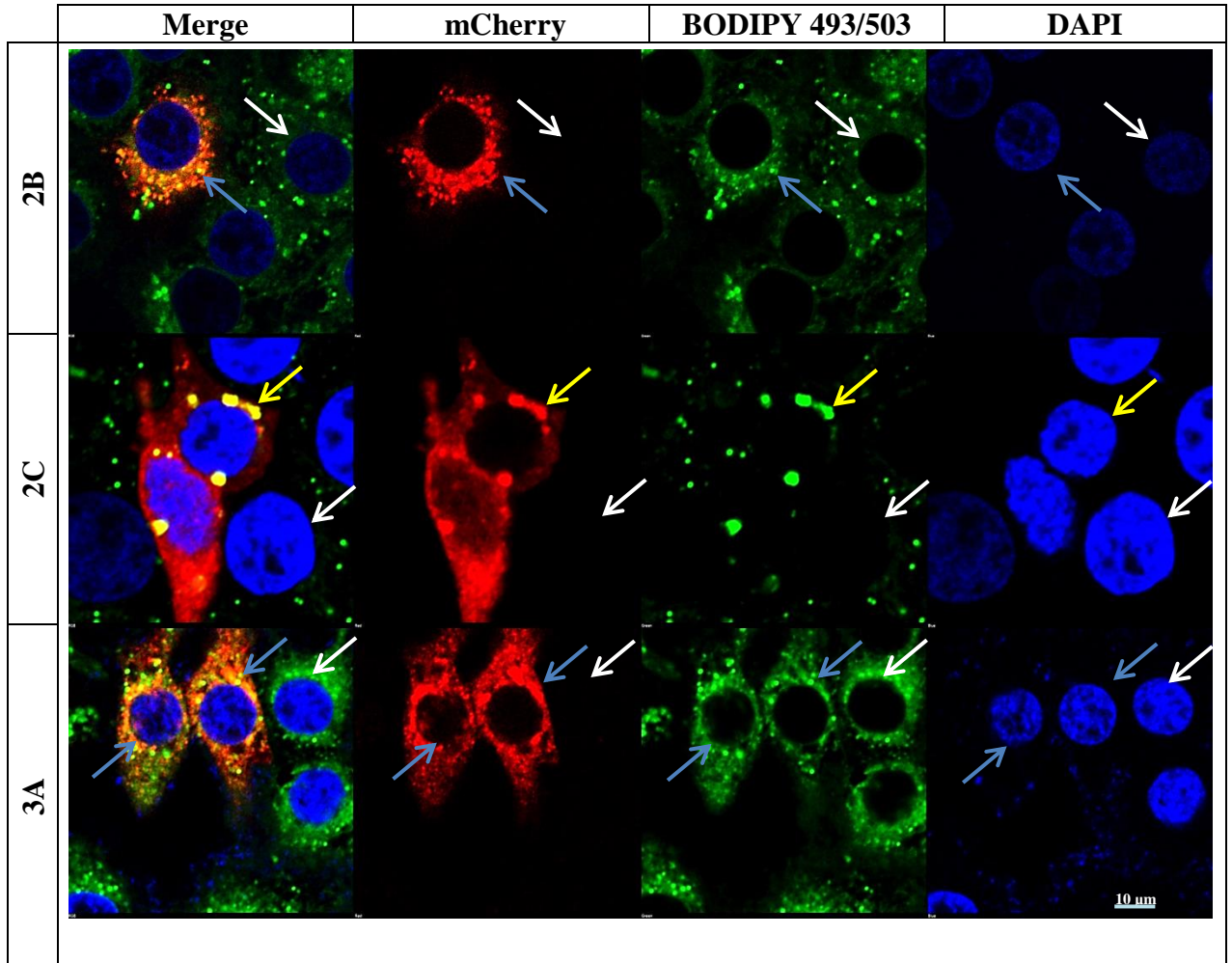


FIGURE 4.11: The effect of mCherry-2B, mCherry-2C and mCherry-3A on lipid droplets (LDs). GMK cells were grown on coverslips and transfected with HPeV1 non-structural protein constructs pmCherry-2B, pmCherry-2C or pmCherry-3A using Turbofect. Cells were fixed and stained with BODIPY 493/503 for 10 min at a final concentration of 10 mg/ml then cells were washed twice with PBS. The coverslips were mounted with hard set mounting medium with DAPI. Images were visualized using a Nikon A1 confocal microscope. The blue filter detects the nucleus, the red filter detects mCherry-2B, mCherry-2C and mCherry-3A and the green filter detects neutral lipids in LDs. The blue or yellow arrows indicate transfected cells (which show an mCherry signal). mCherry-2B and mCherry-3A (blue arrows) show slight co-localisation with LDs but LDs have the typical distribution. There is a co-localisation between mCherry-2C (yellow arrow) and LDs. The LDs are greatly expanded compared to non-transfected cells (white arrows). The scale bar shown is 10 μ m.

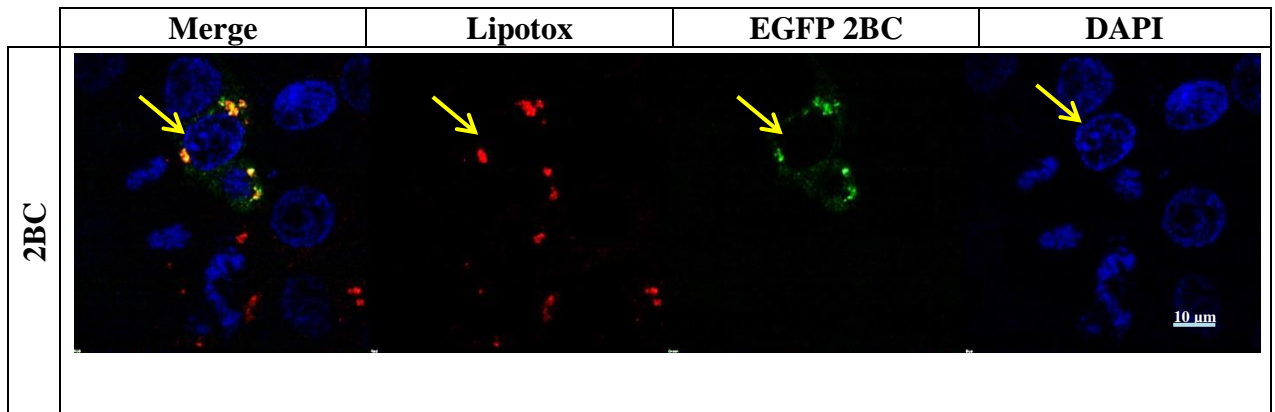


FIGURE 4.12: The effect of EGFP-2BC on lipid droplets (LDs). GMK cells were grown on coverslips and transfected with HPeV1 non-structural protein constructs pEGFP-2BC using Turbofect. Cells were fixed and stained with BODIPY 493/503 for 10 min at a final concentration of 10 mg/ml then cells were washed twice with PBS. The coverslips were mounted with hard set mounting medium with DAPI. Images were visualized using a Nikon A1 confocal microscope. The blue filter detects the nucleus, the red filter detects neutral lipids in LDs the green filter detects EGFP-2BC. The yellow arrow indicates transfected cells (which show an EGFP signal). EGFP-2BC co-localised with the Lipotox LD stain in this cell. The scale bar shown is 10 μ m.

4.4 2C protein and LD

4.4.1 2C of other picornaviruses

The results show co-localisation between HPeV1 2C and LDs. Although 2C is relatively well conserved among picornaviruses, there is some variation. A neighbour-joining tree of 2C sequence shows that the HPeV 2C is part of a distinct cluster from that containing enteroviruses (Figure 4.13). To compare the HPeV1 result with other 2Cs of picornaviruses we fused the 2C-encoding region of CAV9 and HRV1B (*Enterovirus* genus) to the mCherry gene.

mCherry-2C of CAV9 gave a rather diffuse distribution, with a few regions where it is more concentrated (Figure 4.14). Compared to untransfected cells the LD stain was more concentrated and there was some co-localisation with mCherry-2C. mCherry-2C of HRV1B was again more diffuse than mCherry-2C of HPeV1 (Figure 4.14). Several distinct spots were seen however. The LD stain was more concentrated in transfected cells than in the surrounding non-transfected cells and there was clear co-localisation with some of the mCherry-2C fluorescence. The results show that 2C from CAV9 and HRV1B (two highly similar picornaviruses) behave slightly differently. However, there seems to be some interaction with LDs, similar to, but not as clear as, that seen for 2C from the divergent picornavirus HPeV1. This suggests that LDs may play some role in infection by many picornaviruses.

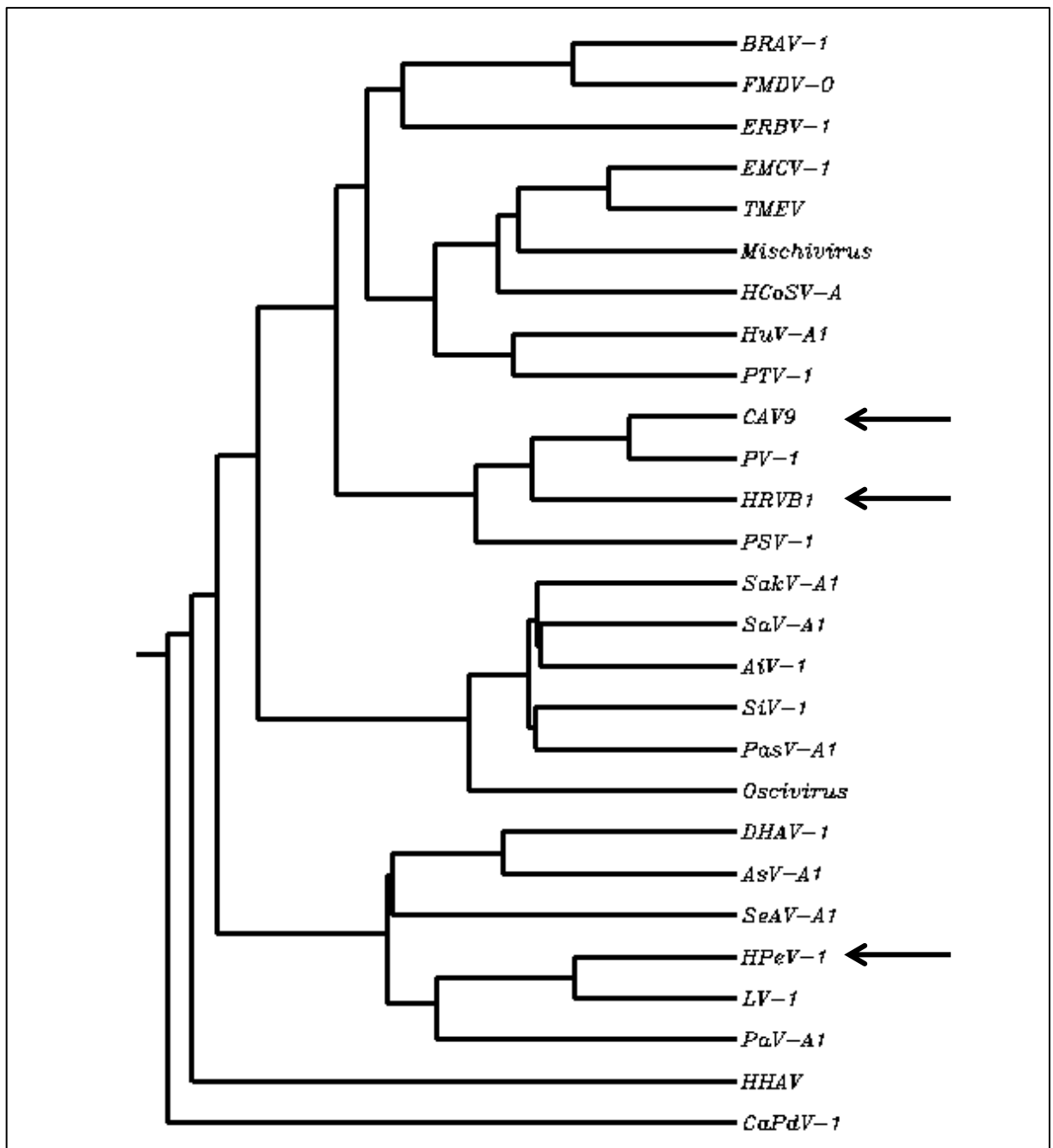


FIGURE 4.13: A neighbor-joining tree based on 2C nucleotide sequences of some members of the *Picornaviridae* family. Bovine rhinitis A virus 1 (BRAV-1), Foot-and-mouth disease virus O (FMDV-O), Seal aquamavirus A1 (SeAV-A1), Duck hepatitis A virus 1 (DHAV-1), Avisivirus A1 (AsV-A1), Encephalomyocarditis virus 1 (EMCV-1), Theiler's murine encephalomyelitis virus (TMEV), Human cosavirus A (HCoSV-A), Canine picodistovirus 1 (CaPdV-1), Coxsackievirus A9 (CAV9), Poliovirus 1 (PV-1), Human rhinovirus 1B (HRVB1), Equine rhinitis B virus 1 (ERBV-1), Human hepatitis A virus (HHAV), Hunnivirus A1 (HuV-A1), Aichi virus 1 (AiV-1), Mischivirus A1, Oscivirus A1, Human parechovirus 1 (HPeV-1), Ljungan virus 1 (LV-1), Pasivirus A1 (PaV-A1), Passerivirus A1 (PasV-A1), Sakobivirus A1 (SakV-A1), Salivirus A1 (SaV-A1), Porcine sapelovirus 1 (PSV-1), Sicinivirus A1 (SiV-1) and Porcine teschovirus 1 (PTV-1). The arrows show different 2C proteins analysed in this thesis.

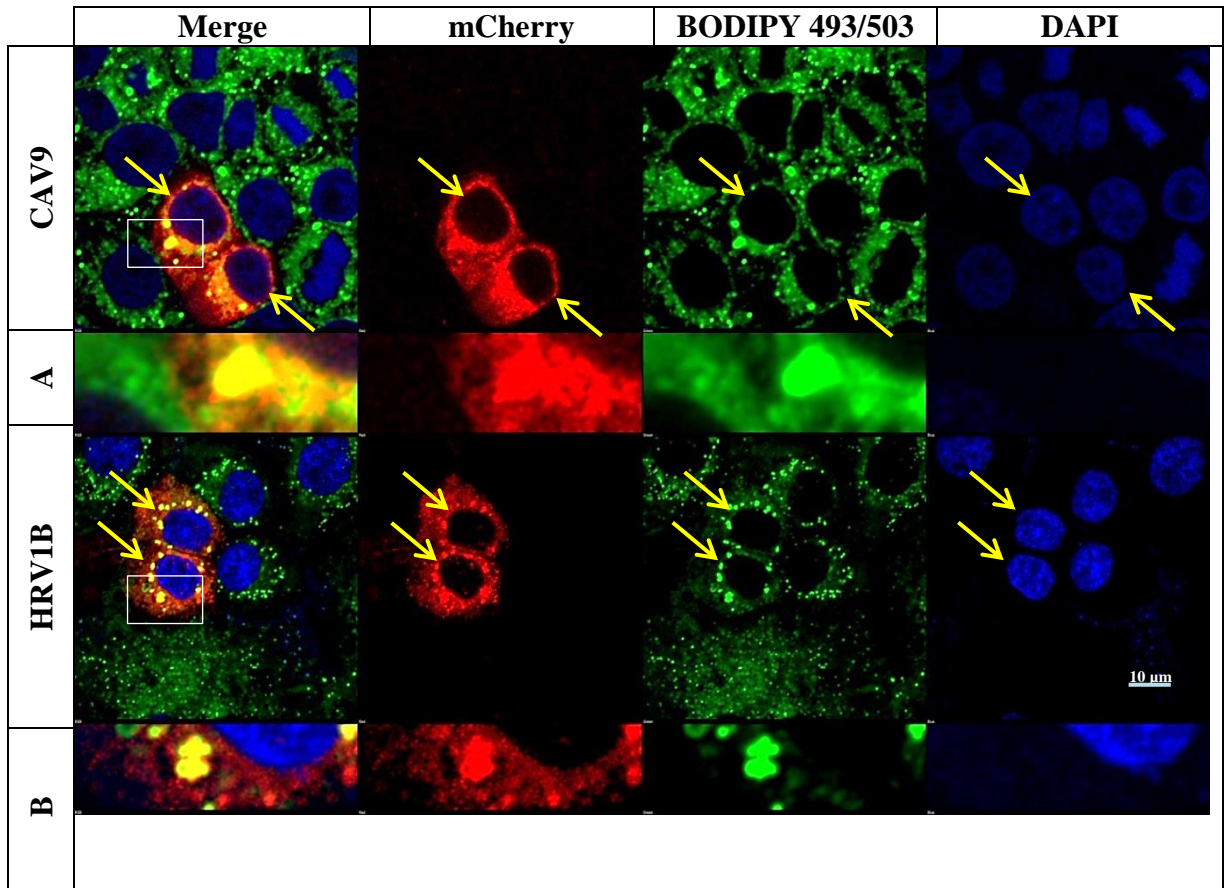


FIGURE 4.14: Relationship of mCherry-2C of CAV9 and HRV1B with lipid droplets (LDs). GMK cells were grown on coverslips and transfected with constructs of mCherry fused to the 2C protein from either CAV9 or HRV1B (pmCherry-2C) using Turbofect. Cells were fixed and stained with BODIPY 493/503 for 10 min at a final concentration of 10 mg/ml then cells were washed twice with PBS. The coverslips were mounted with hard set mounting medium with DAPI. Images were visualized using a Nikon A1 confocal microscope. The blue filter detects the nucleus, the red filter detects mCherry-2C of CAV9 and mCherry-2C of HRV1B and the green filter detects neutral lipids in LDs. The yellow arrows indicate transfected cells (which show an mCherry signal). There is some co-localisation between LDs and the 2C protein of both viruses and also some expansion of LDs compared to non-transfected cells in the field. A and B show close-up images of areas marked with white boxes to illustrate the co-localisation. The scale bar shown is 10 μ m.

4.4.2 ATPase activity site of 2C and LD

2C of all picornaviruses contains 3 perfectly conserved motifs (Figure 4.15). The Walker A and Walker B motifs are needed for NTPase activity. To investigate if these motifs are involved in the co-localisation of LDs to 2C, we used overlap PCR mutagenesis to make a K144A Walker A mutant (pmCherry-2CK) and a D188A Walker B mutant (pmCherry-2CD) fused to mCherry. These were transfected into GMK cells. Both mutants have punctate distribution and co-localise to LDs (Figure 4.16). Further investigation was carried out by combining these mutations (mutant KD) and the same results were found when transfected into GMK cells (Figure 4.17). In all cases, the mutants caused aggregation of the LDs into large clusters, as seen for the original mCherry-2C. This implies that the co-localisation and the ability to aggregate the LDs does not depend on the NTPase activity of 2C. We co-transfected pEGFP-2C with pmCherry-2CK and 2CD and both mutants co-localise with EGFP-2C (Figure 4.18).

4.4.3 2C fragment and LDs

To investigate the distribution of 2C, a further 3 (2C1, 2C2 and 2C4 mutants) were used. These were originally produced by Arsalan Salimi as EGFP fusions and the mutant 2C DNA was transferred to mCherry (Figure 4.19). The three mutants were transfected into GMK cells to define which parts of 2C interact with LDs. mCherry-2C1 and mCherry-2C2 gave similar results, with most of the protein located around the nucleus. The distribution is not as punctate as mCherry-2C, but there are some spots and these partly co-localise to LD. Both mutants seemed to cause some clustering of LDs. The mCherry-2C4 protein is mainly localised in the nucleus and has no clustering effect on the LD distribution (Figure 4.20), in fact LDs appeared very dispersed in transfected cells. pmCherry-2C1, pmCherry-2C2 and pmCherry-2C4 were co-transfected with pEGFP-2C into GMK cells, to define if the proteins co-localised. It can be seen that there is some similarity in the distribution of EGFP-2C with mCherry-2C1 and mCherry-2C2, but the bright punctuate spots seen in EGFP-2C are not present in cells transfected with two

mutants (Figure 4.21). To investigate if combinations of these two mutants give the same distribution as EGFP-2C, a co-transfection was performed. The two deletion mutants had a similar distribution (Figure 4.22). Surprisingly, the combination of two mutants had a very similar distribution to EGFP-2C.

To further investigate, a new mutant was made with mCherry fused to 2C1+2C2 i.e the part of 2C from position 1 to 160 (2C12). The distribution of the new mutant mCherry-2C12 protein was mainly punctate and mostly co-localises to LDs (Figure 4.23). There was no clear clustering of LD compared to untransfected cells, suggesting that other regions participate in clustering.

BRAV-1	-----FSMKRLNDIFSFLKNGEWLIKFFLSIRSWSVRTWLKQEETVMS-----
FMDV-O	-----LKARDINDIFAILKNGEWLVKLI LAIRDWIKAWIASEEKFVT-----
CAV9	-----NDSWLKKFTEMTNACKRMEWIAIKIQKFIEWLKVKILPEVREKHEFLNRLKQPL
PV-1	-----GDSWLKKFTEACNAAKGLEWVSNKISKFIDWLKEKIIPQARDKLEFVTKLKQLEM
HRVB1	-----SDSWLKKFTEMCNAARGLEWIGNKISKFIDWMKS-MLPQAQLKVKYLNEIKKLSL
PSV-1	-----GPSDWLKDFNIAINSKGFDFLCSKLMQLIEWIKQFFQORVEPEYKYFKELLESWPK
EMCV-1	-----SPLKQVNDIFS LAKNLDWAVKTVEKVVDWFGTWVQEEKEQT--LDQLLQR--
TMEV	-----GPLREANEGETFAKNIEWATKTIQSIVNWLTSWFQEEEDHPQSKLDKLLME--
Mischivirus	--GDGFVKRAQDANHTFNFLKNLEWLTNLI TKLFNWISSWFAPKPEATKHEILDNKMKL--
HCoSV-A	-----GPDLRDFVTFNAARCAQWMLDSLKALITWIKQWLELEEENEAVQLEKMLID--
HuV-A1	-----GPIMSEINQVVLVLCRNAQWLAQQLQKILGWLGVWVQEEEDASEERFRERMV--
PTV-1	-----GPMQDVSSLINILKGAEWIYHQFEKVIKWLKTWRTAEYEVSSDYLQNMKN--
ERBV-1	-----GISSTLSVLNGFNLFKNVQWFLDFLKSCYGLSKLQKPMQSLRD-----
SakV-A1	-----AGVDDFNKWSLAAKNADWLFDRMLSCLKQLLDWVGLRVREDPRSEIWANHDKV
SaV-A1	-----GVRDYNDIMSALRNTDWF FEKIMTHIKNLEWLVKLVKDDPRTKLNGQHEKI
AiV-1	-----GLKDFNDGALAMRNVEWIGETAWKWAHRLLDWI PGKAKTDPQAKLADVHDEI
SiV-1	-----GPMRDYNDCMNALKNTDWLLHRI LDLARILCEWLTKRSKEDPAAKLDELHQLV
PasV-A1	-----GVKEYNDGVNALKNTIEWLIKKIFEYIKDLEWLVGRVAKSEPSAQLAQSHDTI
Oscivirus	-----AFKPKDFNDWANFFKNI DWAVTRLVVLIEKLIKQIQQA-AKANPEIGISWYHDDI
DHAV-1	---SGKTTSPKSFNDWTTCAKNVQWVWLESFVKVNVNWLKEKIFPSKTDPTLQWLQDHEEHI
AsV-A1	----GPDATGKSFNTWTLVAKNLEWVVDKQFINWIRTKLFPDARDKIEAMESVRDRM
HPeV-1	-----GPFKGFNEVSTAFRHDIDWIIHTLLKIKDMVLSVFKPSIESKAIQWLERNKHEV
LV-1	-----GWREFNDVSMSEFRHEVWVWLTMFKKVYNVLSIFAPSIEQKAVDWIDRNQEYI
PaV-A1	-----SLAAFNALSLSARNCTWWIIELFQKLHTFVRDLLKPDTSAKFHEWCRKNKMLI
SeAV-A1	-----GFASFTSALRACEWVIKTIKAFVSVWVKTTCFSN-----PLVGEARDQL
CaPdV-1	DLFAKATKGVKLINDTATAVKNVKMFIDLIMWLLDEIKKWRKVEDTKPYFVESNKDKVF
HHAV	----SFSNWLRLDICSGITIFKNFKDAIYWLYTKLKDFYEVNNGKKKDI LNILKDNQOKIE
:	
BRAV-1	-----YNDLVPKIIQKQLELKEPSTFAQAKNWLVRQREILLTAG--QKDLAQLCEVKVK
FMDV-O	-----MTDLVPGILEKQRDLNDPSKYKEAKEWLDNARQACLKSG--NVHIANLCKVVAP
CAV9	LESQIATIEQSAPSQ---SDQEQLFSNVQYFAHYCRKYAPLYAAEAKRVFSLEKKMSNYIQ
PV-1	LENQISTIHQSCPSQ--EHQEILFNVRWLSIQSKRFAPLYAVEAKRIQKLEHTINNYIQ
HRVB1	LEKQIENLRAADN----ATQEKIKCEIDTLHDLSCKFLPLYAHEAKRIKVLNKCNSIIK
PSV-1	VCAKVFLEFKNCKTTLGQEDICQIKVYIDKLIELGNKYGHKFNLQMSQLLQCSNI INKAYS
EMCV-1	-----FPEHAKRISDLRNGMAAYVECKESDFDFFEKLYNQAVKEKRTGIAAVCEKFRQKH
TMEV	-----FPDHCNIMDMRNGRKAYCECTASFKYFDDLYNLAVTCKRIPLASLCEKFKNRH
Mischivirus	-----FAAAVDEIQSYRSGESNTFPETS-VALVKEVFTLASETGKTLANLASKYMITR
HCoSV-A	-----SPRHCKAINDYNRGSFQRPNTS-FEFMDRLVECATKLGKVIATYFRNFITAD
HuV-A1	-----YPQMMEQYEQYKN-SPRHQKWNDCKTWFDDEMRLKAVLHDPKLVN--LFPNMASI
PTV-1	-----YPHYHRKYKECAN-NYRHPDRTEVANYFKKMRKCAAHVNPRLMG--MFPEFDPS
ERBV-1	-----KVLQTYADSI AEFMTPSAQKKELYLQNHYDAVEAGLNSIAAAWKDLANK
SakV-A1	EKLYEDSISATTS-AKPPDSQAVQANLSIARALLETAGRASSLSHTSMLQRAISNYTSVL
SaV-A1	LELYTDSVTASSTPPSELSADAIRSNLDLAKQLLTLSHAANSVTHIQLCRAITNYSTAL
AiV-1	MLHYSDSILALGS--EKLPI DHITKISIRCRELVSIAQEAKSGPHSSFLNQAVKNYTLAI
SiV-1	TQLYSDSVDVLTAA--PRVMRSAVEENLSRARAALPTASELRSPPHTTMLLRAITNYETKV
PasV-A1	MALFQDSISATSA--PSLDLPAARSNLAKAQSLLPLATAAKSNTHSHILTQS IKNYTNAI
Oscivirus	INLYSDSIKLSL--EDVDKTQLSMNLGEVRRLLSMSLKAGNTGYQTLKQALSNTYQAO
DHAV-1	AIMLALCDEHLCMLRTEKDYICEHNTRPKHQCLVEMVSGTLNQLQGISSARELAARLQHV
AsV-A1	VLSLAAADKHLVTLKADKAYATSKAARDYHLKITNEIID-LNAMDLGPPDRDLGTKIGQI
HPeV-1	CSILDYASDIIVESKDQSKMKTQDFYQRYSDCLAKFKPIMAI CFRSCHN-SISNTVYRLF
LV-1	ADVLDHASNIIKMKDPKEQRRASTISEYFEVLEQLKPIVSLCMKVAPSTKFSQVFRYI
PaV-A1	SNFMYTLNEHLKDCATTCNLRKREFRDKHKWLLSVLNRLTEGFTTYGVQNDITRALLDMR
SeAV-A1	SELLAAAEQLVLDVVNLAIPREVIEWARR-----SNILDKLSYAKKLSVNIPELDALVNKA
CaPdV-1	EYLELSYTFENGCNIDKSKVDEVLYFLKKMSVAANKIDDRHTVTLVNGLYNTYSKIKAKY
HHAV	KAIEEADEFICILQIQDVEKFEQYQKGVDLIQKLRVHSMQVDPNLMVHLSPLRDCIARV

BRAV-1	EPVT-----GRPEPVVVLVLRGKSGQGKSF	MANILASAI SRMLTGKPDSDVWSCP
FMDV-0	APSK-----SRPEPVVCLRGKSGQGKSF	LANVLAQAI SAHFTGRDTSVWYCP
CAV9	FKSK-----CRIEPVCLLLHGSPGAGKSV	ATNLIGRSLAEKLN---SSVYSLP
PV-1	FKSK-----HRIEPVCLLLHGSPGTGKSV	ATNLIARAIAEKEN---TSTYSLP
HRVB1	QR-----KRSEPVAVMIHGPPGTGKSI	TNFLARMITNES----DVYSLP
PSV-1	NMTR-----SRHEPVAMLIHGAPGTGKSL	ATEIIGRAIADKLDN--QRPYTLP
EMCV-1	DHAT-----ARCEPVVIVLRGDAGQGKSL	SSQIIAQAVSKTIFGR-QSVYSLP
TMEV	DHSV-----TRPEPVAVLVRGAAGQGKSV	TSQIIAQSVSKMAFGR-QSVYSMP
Mischivirus	TNNT-----PRMEPVVVVLRGKPGTGKSV	ASHILAQAVSKQMTGQ-QSVYSFP
HCoSV-A	S-DT-----SRPEPVVVVLRGKPGAGKSA	AATVMAAAVSKLLVGS-QSVYTLS
HuV-A1	PHEN-----SRQEPILIVLRGKPGQGKSV	AASMLAQMFHLSLGGK-PDYYSYN
PTV-1	PPDP-----TRPEPVVVVLRGAPGQGKSV	CSEMLARMLSYTLVGGK-SSYYAFN
ERBV-1	CYAY-----SRPEPVCILLGRAGQGKSV	AATVIAKAVSIVNTGK-ESVWTLF
SakV-A1	CNPQRTMS-----GTRPQPVVVYIHGAP	GVGKSLVASLLARTLAAKLTGPDFFYAPS
SaV-A1	SAISLVGTP-----GTRPEPLVVYLYG	PPGTGKSLLASLLASTLAQALSGDPNNYSPS
AiV-1	SQHRKQQT-----GPRPEPVVYLYGPP	GTGKSLLASLLAQTLSQLAGTPDDVYSPS
SiV-1	ASLGHNQF-----HQRPEPYVYVYIHG	PPGCGKSLMGSLLASRLAQALSGDPDDVYSPA
PasV-A1	ASQEALLA-----PPRPEPYVLYLYG	KPGSGKSVFAQALARTLAYHLCGDPESVYAPS
Oscivirus	NSLQRTIF-----AVRPEPVVYIYGG	PGSGKSVLAGLLARAISKALSGRADDIYAPS
DHAV-1	LNKLHQVNFEP	ELEWTHRPEPLGIWISGPGVVGKSLSNYIVKEIAK
AsV-A1	LNRLQSVTFDSVDAGSMRQEPLGIWISG	EPGCGKSLSHLIIKHLKEKKGFSV----FCN
HPeV-1	QELARIPNRISTNNDLRIEPIGIWIQ	EPGQGKSLTHTLSRQLQKSKCLNG---VFTN
LV-1	SEMMRVNVVRPANTDLTRLEPIGIWV	SEPGQGKSLFTHMLSTCLLKSCLNLEG---IYTN
PaV-A1	KSMLAVKLGQEQNTCAREEPLGVLLR	GEPGQGKSLMTHLLVRSVCNAMGWKVSSEVFSH
SeAV-A1	SLALRKVPATYVTPSHPRVEPLGVWLR	GAPGSGKSLMCKLARDVSLIKNSSV----FYH
CaPdV-1	NSRLY-----MERFEPVVIYLHGK	PGCGKSLASAEALAKAFARYFKLDFEECVYAS
HHAV	HQKLKLNLSIN-QAMVTRCEPVVYLYG	KRGGKSLTSLALATKICKHYGVEPEKNIYTK
	* : * : . * * * * :	
BRAV-1	-PDPTYFDGYRGQSVVIMDDLGNP	DGKDFKYFAQMVSSSTAFVVPMAALEDKGLTFTSPV
FMDV-0	-PDPDHF	DGYNQQTVVVIMDDLGNP
CAV9	-PDPDHF	DGYKQQA
PV-1	-PDPDHF	DGYKQQGVVIMDDLGNP
HRVB1	-PDPKHFDGYNQ	QKVVIMDDLGNP
PSV-1	-PDPKHFDGYNQ	QKVVIMDDLGNP
EMCV-1	-PDSDFFDGYNQ	FAAIMDDLGNP
TMEV	-PDSEYFDGYNQ	FVIMDDLGNP
Mischivirus	-PDCDHL	DGYTGQYAVVIMDDLGNP
HCoSV-A	-PDTEHMDG	YHGQFVTLIMDDLGNP
HuV-A1	-SSTNYFDG	YQQQPVVLIIDDLGQDP
PTV-1	-SATKHFDG	YKQQA
ERBV-1	-TDSDFFDG	YAGQNVVIIDDLGNP
SakV-A1	SADCQHYD	GYTGQPVHYIDDIGQD
SaV-A1	SPDCKFYD	GYSGQPVHYIDDIGQD
AiV-1	SASCEYFD	GYTGQTVHFIDDIGQD
SiV-1	SVSCEYD	GYRGQSVHYIDDVGGD
PasV-A1	SSDCAYD	GYAQQCVHYIDDVGGD
Oscivirus	SFGTDHF	DGYHQQT
DHAV-1	PTGSKHMD	GYVSQEIHFVDDFGQ
AsV-A1	PSGSDHMD	GYNGQEIHFVDDFGQ
HPeV-1	PTASEFMD	GYDNQDIHLIDDLGQ
LV-1	PTGSEFMD	GYIGQDIHIIDDAGQ
PaV-A1	PTSSEFFD	GYAGQPIHLIDDFGQ
SeAV-A1	PTGSNFFS	GYHGQYVHCIDDLGQ
CaPdV-1	PPASEYLD	GYGGHKIHLIDDLGQ
HHAV	PVASDYWD	GYSGQLVCIIDDIGQ
	. . * * : : * * * : : : . : * : * . : .	

BRAV-1	IIATTNLSDAFTPIITMACPEALQRRFHFHDYNLEAK--WKKGYH----LDVKRALQPTG--
FMDV-0	IIATTNLYSGFTPRMTMCPDALNRRFHFHDIVSAKDGYKINNK----LDI IKALEDTH--
CAV9	VLASTNAG--SINAPTVS DSRALARRFHFDMNIEVISMYSQNGKINMPMSVKTCDEECC--
PV-1	VLASTNSS--RITPPTVAHSDALARRFAFDVDIQVMGEYSKDGLKNMAMATEMCKNCHQ--
HRVB1	VLCSTNHS--LLAPPTISSLPAMNRRFFFDLDIVVHDNYKDAQGKLNVSKAFOPCNVNT--
PSV-1	VLASTNQH--ALTPRTIAEPDAINRRWFMNVDIHLKKEYKDDRGR--LDMSKCLPCKDCK--
EMCV-1	VVATTNLE--EFRPVTIAHYPAVERRI TFDYSVSAGPACMRTEAGCKVLDVEKAFRPIG--
TMEV	IVATTNLE--KFRPVTVAHYPAVDRRI TFDFTVTVTAGPHCKTPAG---MLDIEKAFDEIPG--
Mischivirus	IIATTNLA--AFAPVTVADPMAVERRI FLDLEVT PGVTCQINGK----LDLEAALEPIG--
HCoV-A	LIATTNLE--DFNPVTISDPRALDRRI TFDILVTPGSAATKNGK----LDLAAALKPDG--
HuV-A1	IIATTNLE--EFKPVTIADPGALQRRINFDFEVEAGQSYKTKAG---TLDLAKALEPTG--
PTV-1	LIANTNLE--SFNPITVSDPAAIKRRI FLDLTVEANRAYTKPDG---TLDLVRALQATG--
ERBV-1	IIATTNKNENFLPVTVSDQEAVTRRYWKVIDVSADDQYKTVDG---RLDYAKATQPTQ--
SakV-A1	IIITSNFS--GPNPRSVCQPALERRL IRLVAELGP--EPCSPAESVAPDG-----
SaV-A1	VIVTSNFF--GPNPRSARCVAALERRLH IRLNVTARD--GVAFSAAAALQPSNPP-----
AiV-1	IVVTSNFH--EPNERAARSMGALRRRVHLRINVT SNG--VPFDPTNALNPI PG-----
SiV-1	IIMTSNFF--EPNPRSRCPEALSRRRLRLRSVSP PRGPKHLDVTAALAPSGN-----
PasV-A1	IILTSNFS--EPNPRASRI PQALQRR LKCMIEIEPLSCPTQSNLHTLSSLPNQFNPETALR
Oscivirus	IIVTANFN--LPNYASAREPKALERRLHF KMFMGGS LNVD FACAPDG-----
DHAV-1	VVVTTNRR--DFTSCKLTDPDALERRFP IRLNIRPLQKYN--HGKRLDVATAMRDG-----
AsV-A1	VIATTNKN--EFDSTVLNDSGALRRRFP IRLHVRPHSFYSTQDGRDLNRAMKDG-----
HPeV-1	VVATTNKS--DFSSTVLQDSGALKRRFPY IMHIRAAKAYS--KAGKLNVSQAMAT-----
LV-1	VIATTNKE--DFTSMVLTDPAALERRFP FHLRIRAVASYS--RNNKLDVARSMAA-----
PaV-A1	VIATTNKS--DWSSRTL CAPGALKRRFP IYVTVRARRTLT--KNGLLDVNAHMSA-----
SeAV-A1	VIATTNMT--SFRTYTLTTPAALERRFP LVCDIVPKYSKP--NGTLNLN-----
CaPdV-1	IIATANFS--NPPDTASRDIGALRRRCKLCFEMTFAPDDGENTYKTEDSKLDVAAAFTP--
HHAV	IIATSNEWS--NPSPKTVYVKEAIDRRLHFKVEVKPASFFKNPHNDMLNVLAKTN-----
	:: .:* * : **
BRAV-1	--KPAANELFEEDYPLLNGQAVMFVAN-----KMC PAIDSAYELIEAVYAAVIERRDVAKV
FMDV-0	--TNPVAMFQYDCALLNGMAVEMKRMQQDMFKQPPLQNVYQLVQEV I DRVELHEKVSSH
CAV9	-----PVNFKKCCPLVCGKAIQFIDR-----RTQVRYSLDMLVTEMFREYNHRHSVGTAT
PV-1	-----PANFKRCCPLVCGKAIQLMDK-----SSRVRYSDVQITMI INERNRRSNIGNC
HRVB1	-----KIGNAKCCPFVCGKAVSFKDR-----STCSTYTLAQVYNHILEEDKRRRQVVDV
PSV-1	-----PTNFRKCNPLVCGKAI ILLDR-----KTQKNWTVDSAVTHLLEESERRKGFNLV
EMCV-1	--EAPLPCFQNNCLFLEKAGLQFRDN-----RSKEI ISLVEVIERAVSRIERKKKVLTT
TMEV	--SKPQLACFSADCP LLHKRGVMFTCN-----RTKTVYNLQQVVKMVNDTI TRKTENVKK
Mischivirus	---PAVGPFQRQDCELLHTAGLCFTDR-----RTRQQYSLYEVFQMV EERIKVKASVKKN
HCoV-A	---PGEHPYTSDCPI LHHTGLLLKNL-----RNNQTMNLKDLVDMIVKRIKHKKEVGNM
HuV-A1	---CSAPLHMVKADIIHLFSSACLKFKDR-----MARCECSLVGVYDRVMNSHKRRNDLANK
PTV-1	-KESQSP LLRQDHNILYSDCVAFKH-----GRHTLSFLEVFDMIKRELQRRQNVSNS
ERBV-1	-IPPELAVFKTHVPLLGALRDCQRTN---RSGARVLNLYDVISAICVEVDRREQLRSN
SakV-A1	---PSSKHFSSTPLTRFESIKLSWDQKSLFTSPENPKSLDELVDLVLELVARNSAISGD
SaV-A1	---SATRYCKFANPLTQFSMFNLAVDYKSVVLPNTPLTCFDELVDVFLSSLRDRASVNSL
AiV-1	---TQSKYFTAQTPLTLFQSNVRLDRDSIWTP--TFTNMDELVDAIVTRLDRSTGVSNS
SiV-1	---GPTKYFSADCAF LRFESFVLRSEMG-----APNFTHMDELVDYIMSQLDNTERNTA
PasV-A1	VDGPATRYFANDCPMLRFEAFRLTSNHG-----FKHADDIVRHVLDKVKNSGGISNA
Oscivirus	---IPMRYFKSGCPLLRSNGAIKESGSLVLP---CKFSDMDDVVELVLAEVKKRSLGLTM
DHAV-1	-----SLQGGACWERDIGQLG--LECWNPI NGQTLIDEIMSELQVRQEVASF
AsV-A1	-----DIDP--GCWEINVTG---RSCWQTLNWDILIEHEVEDELINRENINKE
HPeV-1	-----MSTGECWEVSKNG---RDWETLKLKDLVDKITIDYNERVKNYNA
LV-1	-----MADGSCWEYSTDGG---RAWKTLMSDELVKQITAVYTQRS DALMV
PaV-A1	-----VRDGAWEYTTNG-----YDWQPFVNDLAAEIIKQLEQRRESFQL
SeAV-A1	-----FDPHDCWKITCNG-----QEMCYMDLFLNLVLERLTEREKLHAD
CaPdV-1	-----DDDSMPDEYVGELTPFWN-----GKAVSLTRTGMAYN GPEKDCSFSLLEV
HHAV	-----DAIKDMSCVDLIMDG-----HNVSLMDLLSSLVMTVEIRKQNMTE

BRAV-1	GIVKQ-----
FMDV-O	PIFKQGENUSAQUAMAVIRUS
CAV9	LEALFQ-----
PV-1	MEALFQ-----
HRVB1	MSAIFQ-----
PSV-1	VDAIFQ-----
EMCV-1	VQTLVAQ-----
TMEV	MNSLVAQ-----
Mischivirus	LMALVFE-----
HCoSV-A	LDSLVAQ-----
HuV-A1	LVEIFNFQ-----
PTV-1	LTNLFQ-----
ERBV-1	LGGIFAQ-----
SakV-A1	LNSLIKQ-----
SaV-A1	LSGMVRTDVTRQ-----
AiV-1	LASLIRRQ-----
SiV-1	FRHLLPSTPKKQ-----
PasV-A1	LAALIPGVKPLARQQ-----
Oscivirus	FDDLVGQ-----
DHAV-1	MNQ-----
AsV-A1	FSQ-----
HPeV-1	WKQQLENQ-----
LV-1	WKRKLNTIRNE-----
PaV-A1	WNSFISQ-----
SeAV-A1	-----
CaPdV-1	FYKAIAYE-----
HHAV	FMELWSQ-----

FIGURE 4.15: Multiple sequence alignment of the amino acid sequences of 2C in several members of the *Picornaviridae* family using protein BLAST. The predicted amphipathic helix is highlighted in grey and boxed in red, the Walker A motif boxed in blue, Walker B motif boxed in yellow and motif C in boxed in red. Bovine rhinitis A virus 1 (BRAV-1), Foot-and-mouth disease virus O (FMDV-O), Seal aquamavirus A1 (SeAV-A1), Duck hepatitis A virus 1 (DHAV-1), Avisivirus A1 (AsV-A1), Encephalomyocarditis virus 1 (EMCV-1), Theiler's murine encephalomyelitis virus (TMEV), Human cosavirus A (HCoSV-A), Canine picodistrovirus 1 (CaPdV-1), Cocksackievirus A9 (CAV9), Poliovirus 1 (PV-1), Human rhinovirus 1B (HRVB1), Equine rhinitis B virus 1 (ERBV-1), Human hepatitis A virus (HHAV), Hunnivirus A1 (HuV-A1), Aichi virus 1 (AiV-1), Mischivirus A1, Oscivirus A1, Human parechovirus 1 (HPeV-1), Ljungan virus 1 (LV-1), Pasivirus A1 (PaV-A1), Passerivirus A1 (PasV-A1), Sakobuvirus A1 (SakV-A1), Salivirus A1 (SaV-A1), Porcine sapelovirus 1 (PSV-1), Sicinivirus A1 (SiV-1) and Porcine teschovirus 1 (PTV-1).

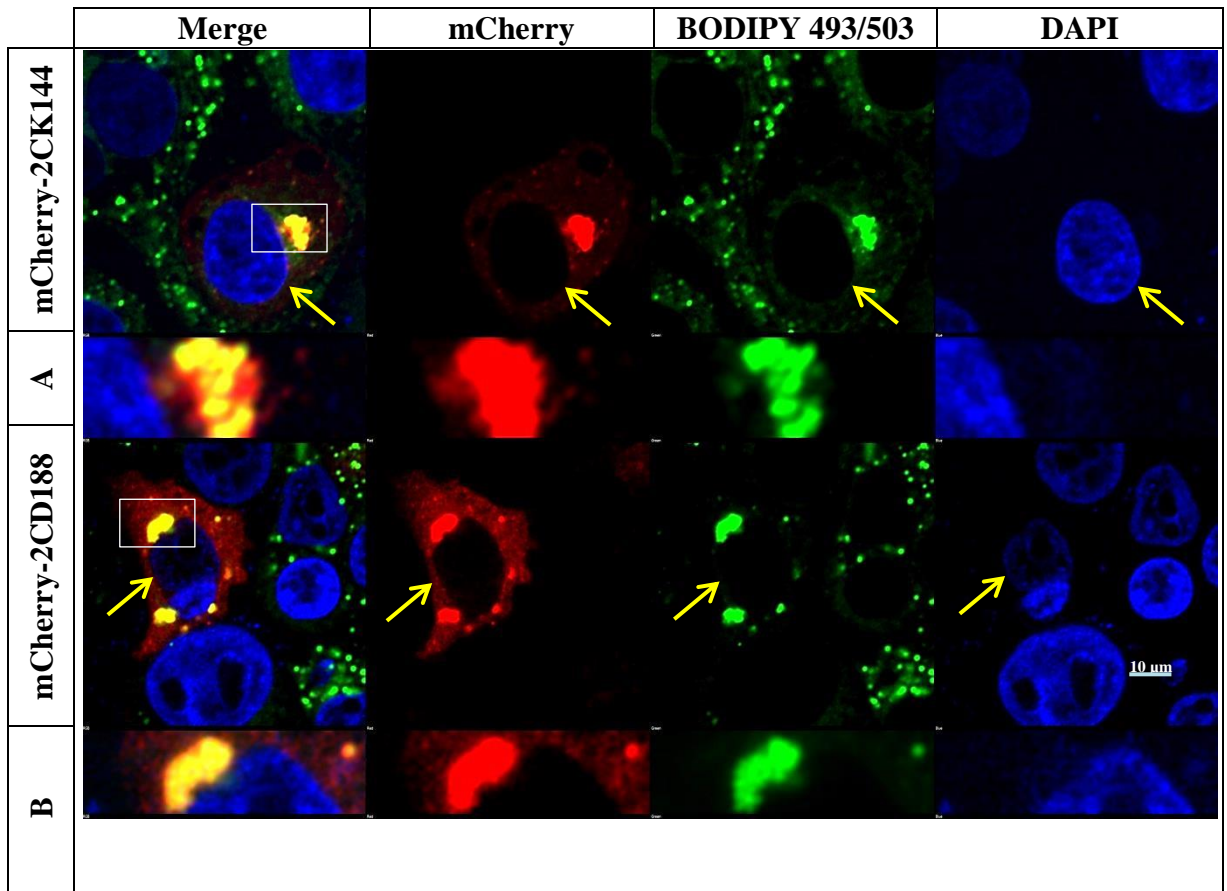


FIGURE 4.16: The effect of Walker A and Walker B mutations in HPeV1 2C on lipid droplets (LDs). GMK cells were grown on coverslips and transfected with mCherry-2C mutant K144 (pmChery-2CK) and D188 (pmChery-2CD) using Turbofect. Cells were fixed and stained with BODIPY 493/503 for 10 min at a final concentration of 10 mg/ml then cells were washed twice with PBS. The coverslips were mounted with hard set mounting medium with DAPI. Images were visualized using a Nikon A1 confocal microscope. The blue filter detects the nucleus, the red filter detects mCherry-2C K144 and mCherry-2CD188 and the green filter detects neutral lipids in LDs. A and B show the close-up images of the co-localisation. Yellow indicates overlap between the red and green images. The yellow arrows indicate transfected cells (which show an mCherry signal). mCherry-2CK144 and mCherry-2CD188 mutants still co-localises to LDs and this suggests that LDs does not depend on the NTPase activity of 2C. A and B show close-up images of areas marked with white boxes to illustrate the co-localisation. The scale bar shown is 10 μ m.

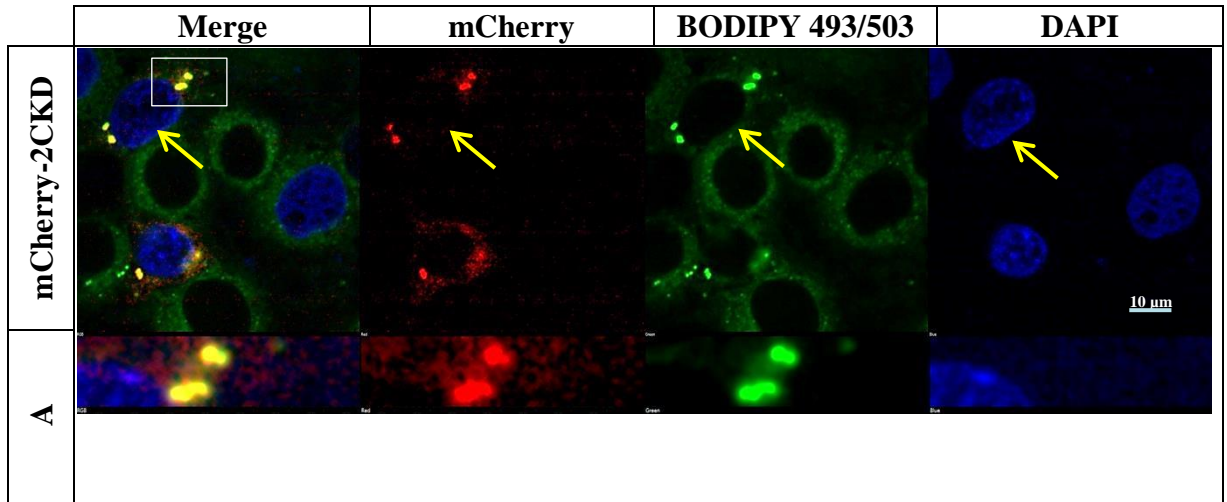


FIGURE 4.17: The effect of combining Walker A and Walker B mutations in HPeV1 2C on lipid droplets (LDs). GMK cells were grown on coverslips and transfected with mCherry-2C mutant KD (pmCherry-2CKD) using Turbofect. Cells were fixed and stained with BODIPY 493/503 for 10 min at a final concentration of 10 mg/ml then cells were washed twice with PBS. The coverslips were mounted with hard set mounting medium with DAPI. Images were visualized using a Nikon A1 confocal microscope. The blue filter detects the nucleus, the red filter detects mCherry-2CKD and the green filter detects neutral lipids in LDs. A shows the close-up images of the co-localisation. Yellow indicates overlap between the red and green images. The yellow arrow indicates a transfected cell (which show an mCherry signal). The mCherry-2CKD mutant still co-localises to LDs and this suggests that LD localisation of 2C does not depend on the NTPase activity. A shows close-up images of the co-localisation seen in the area marked with the white box. The scale bar shown is 10 μ m.

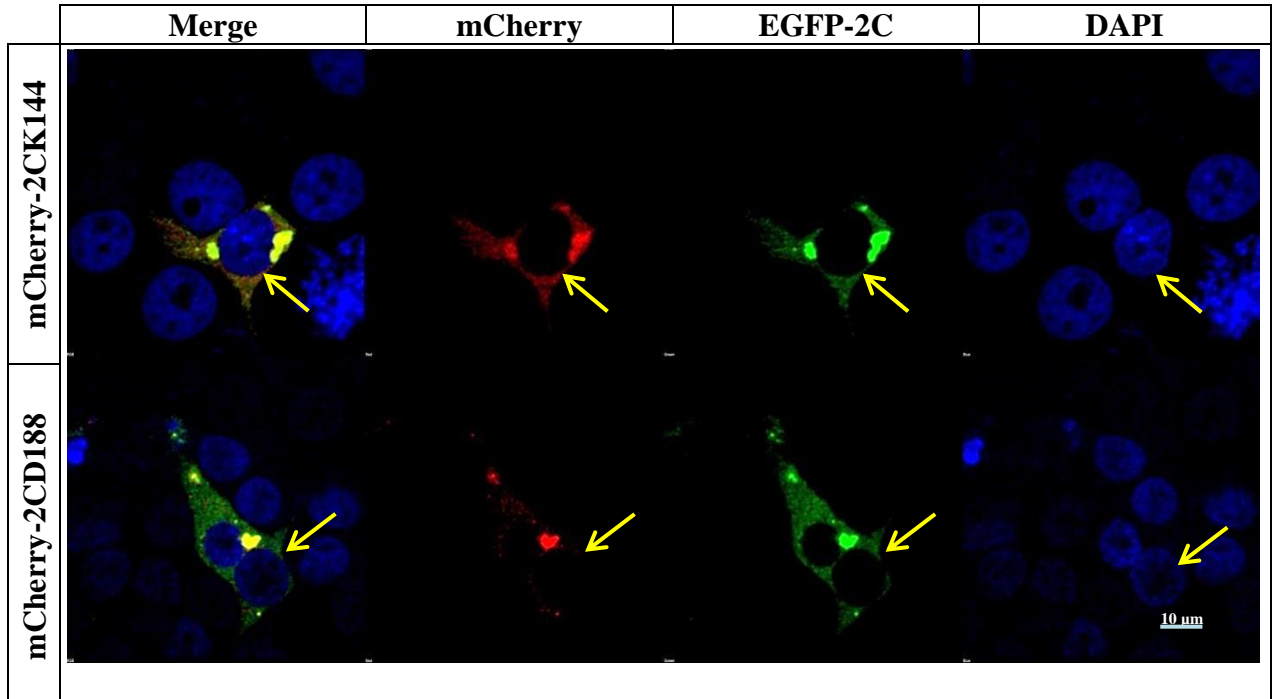
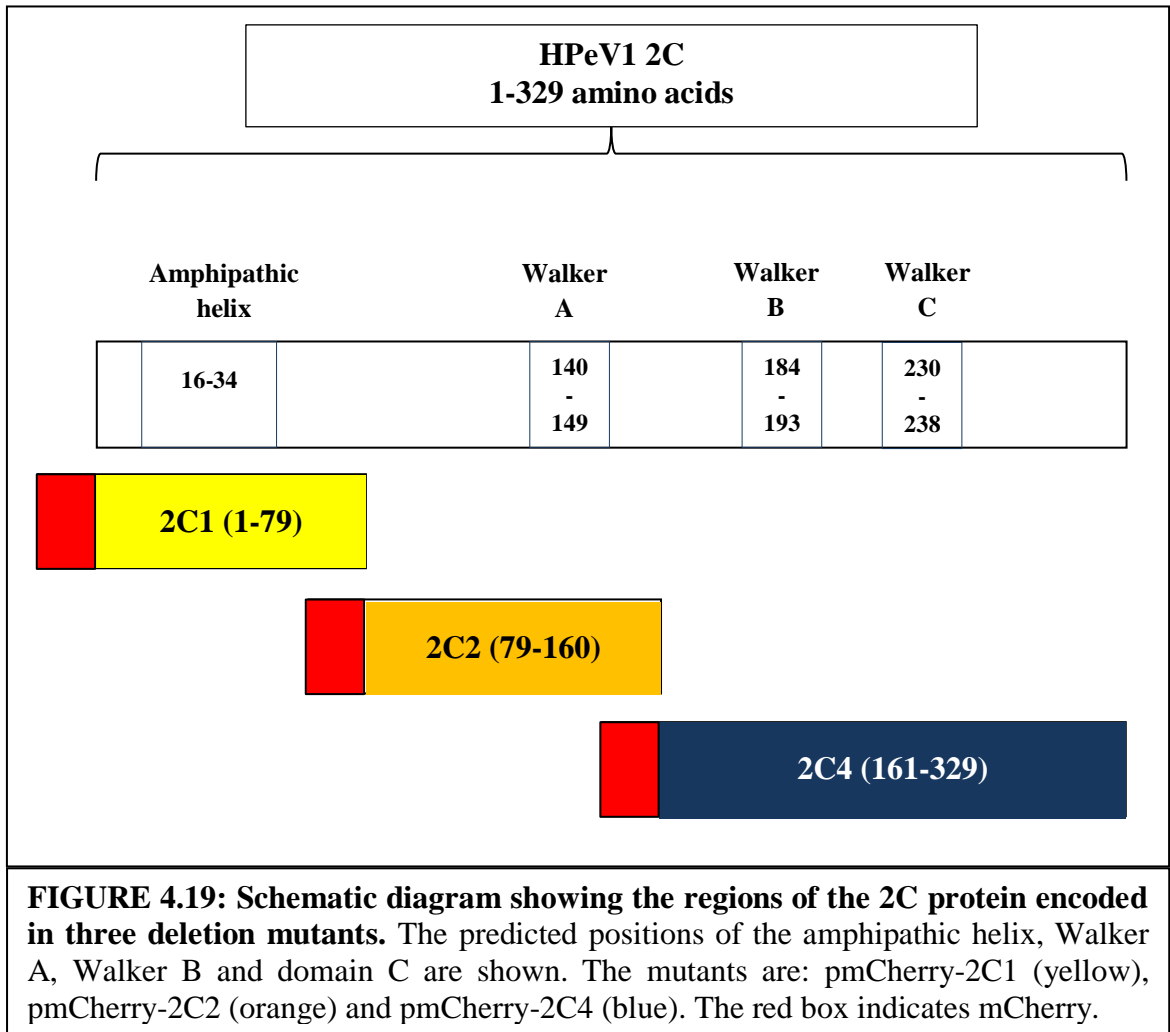


FIGURE 4.18: Co-transfection of pmCherry-2CK and pmCherry-2CD mutants with pEGFP-2C. GMK cells were grown on coverslips and co-transfected with with EGFP-2C and either mCherry-2C mutant K144 (pmChery-2CK) or D188 (pmCherry-2CD using Turbofect). The coverslips were mounted with hard set mounting medium with DAPI. Images were visualized using a Nikon A1 confocal microscope. The blue filter detects the nucleus, the red filter detects mCherry-2CK and mCherry-2CD and the green filter detects EGFP-2C. The yellow arrows indicate transfected cells (which show an mCherry and EGFP signals). mCherry-2CK144 and mCherry-2CD188 mutants co-localise to EGFP-2C. The scale bar shown is 10 μ m.



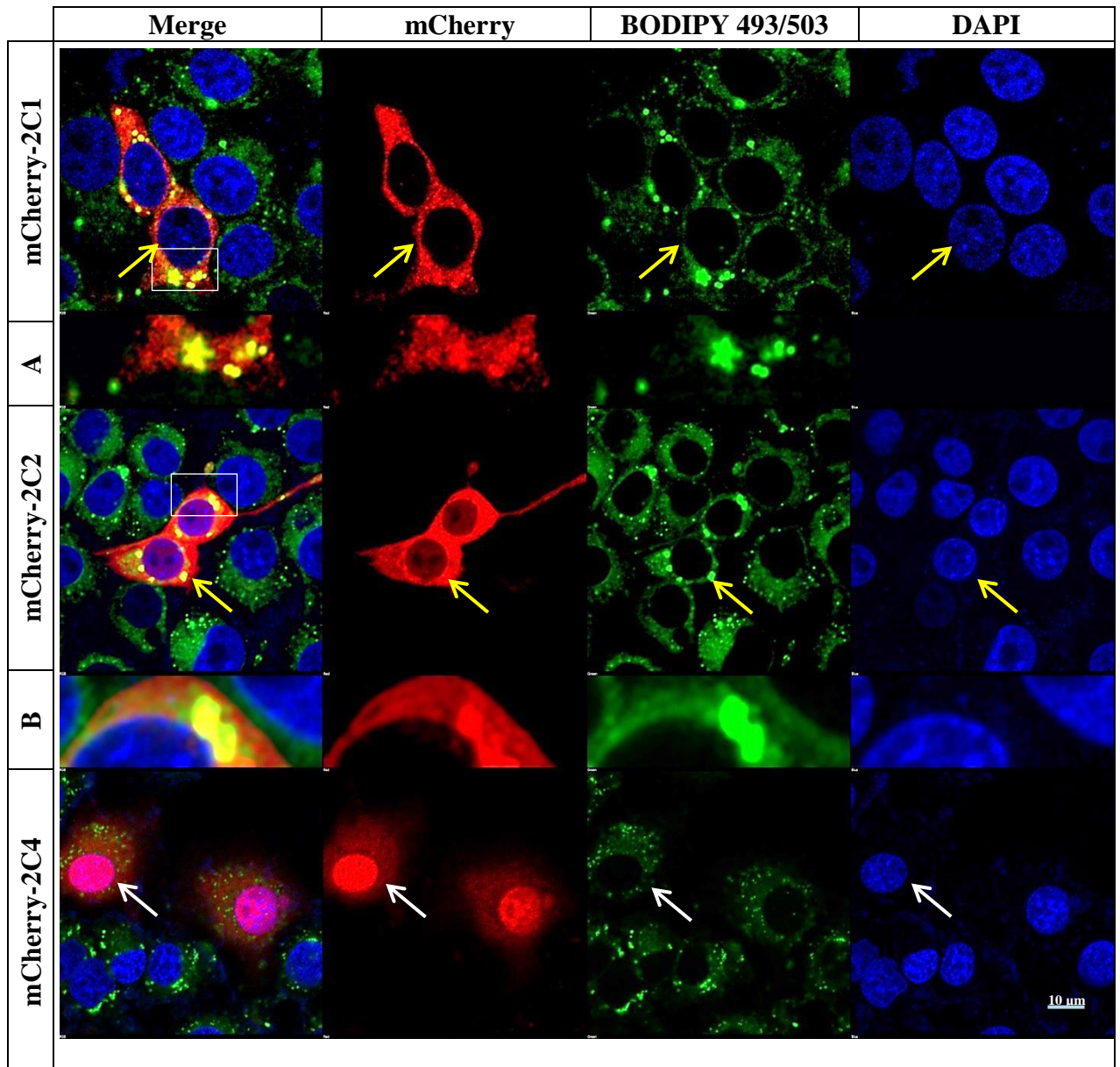


FIGURE 4.20: The distribution and effect of pmCherry-2C1, pmChery-C2 and pmCherry-2C4 deletion mutants on lipid droplets (LDs). GMK cells were grown on coverslips and transfected with pmCherry-2C1, pmCherry-2C2 or pmCherry-2C4 using Turbofect. Cells were fixed and stained with BODIPY 493/503 for 10 min at a final concentration of 10 mg/ml then cells were washed twice with PBS. The coverslips were mounted with hard set mounting medium with DAPI. Images were visualized using a Nikon A1 confocal microscope. The blue filter detects the nucleus, the red filter detects mCherry-2C1, mCherry-2C2 and mCherry-2C4 and the green filter detects neutral lipids in LDs. A and B show the close-up images of the co-localisation. Yellow indicates overlap between the red and green images. The arrows indicate transfected cells (which show an mCherry signal). mCherry-2C1 and mCherry-2C2 (yellow arrows) mutants partly co-localise to LDs and appear to cause them to aggregate. mCherry-2C4 (white arrow) has no aggregation effect on the LD staining compared to non-transfected cells in the field. A and B show close-up images of the co-localisation seen in the area marked with the white box. The scale bar shown is 10 μ m.

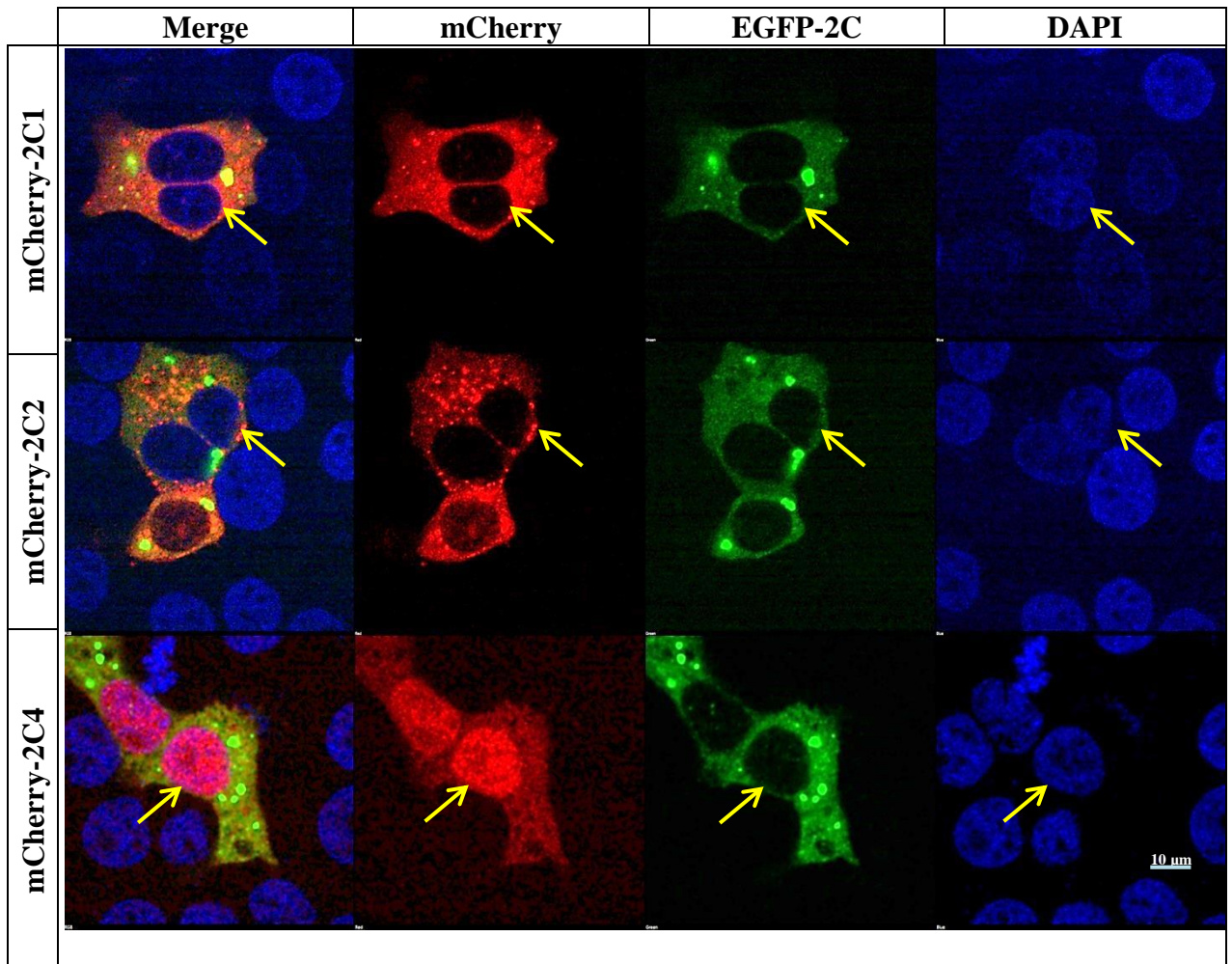


Figure 4.21: Co-transfection of pmCherry-2C1, pmCherry-2C2 and pmCherry-2C4 mutants with pEGFP-2C. GMK cells were grown on coverslips and co-transfected with pEGFP and either pmCherry-2C1, pmCherry-2C2 or pmCherry-2C4 using Turbofect. The coverslips were mounted with hard set mounting medium with DAPI. Images were visualized using a Nikon A1 confocal microscope. The blue filter detects the nucleus, the red filter detects mCherry-2C1, mCherry-2C2 and mCherry-2C4 and the green filter detects EGFP-2C. The yellow arrows indicate transfected cells (which show mCherry and EGFP signals). There is some similarity in the distribution between EGFP-2C and mCherry-2C1 or mCherry-2C2. There is no similarity between the distribution of EGFP-2C and mCherry-2C4. The scale bar shown is 10 μm .

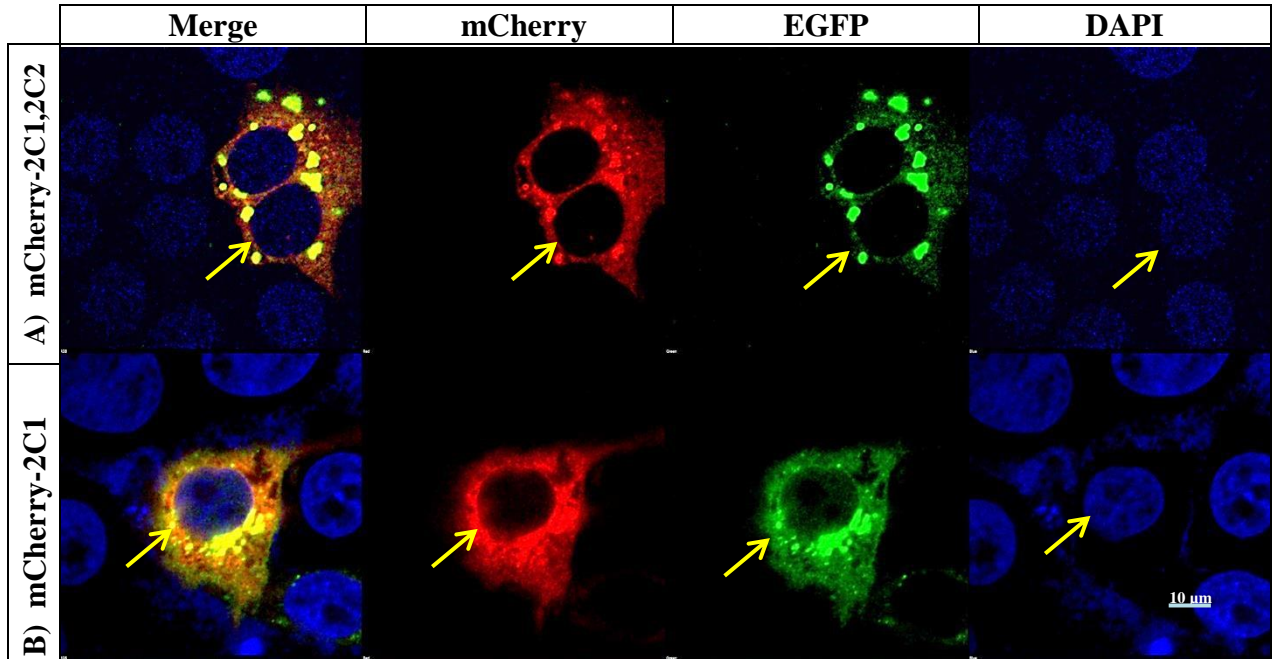


FIGURE 4.22: Co-transfection of pmCherry-2C1 and pmCherry-2C2 with pEGFP-2C and pmCherry-2C1 with pEGFP-2C2. GMK cells were grown on coverslips and co-transfected with A) pmCherry-2C1 plus pmCherry-2C2 with EGFP-2C B) mCherry-2C1 with EGFP-2C2, using Turbofect. The coverslips were mounted with hard set mounting medium with DAPI. Images were visualized using a Nikon A1 confocal microscope. The blue filter detects the nucleus, the red filter detects A) mCherry-2C1, 2C2 B) mCherry-2C1 and the green filter detects EGFP-2C2. The yellow arrows indicate transfected cells (which show mCherry and EGFP signals). A) mCherry-2C1 plus mCherry-2C2 mutants had a similar distribution of EGFP-2C. B) there is some similarity in the distribution between mCherry-2C1 and EGFP-2C2 mutants. The scale bar shown is 10 μm .

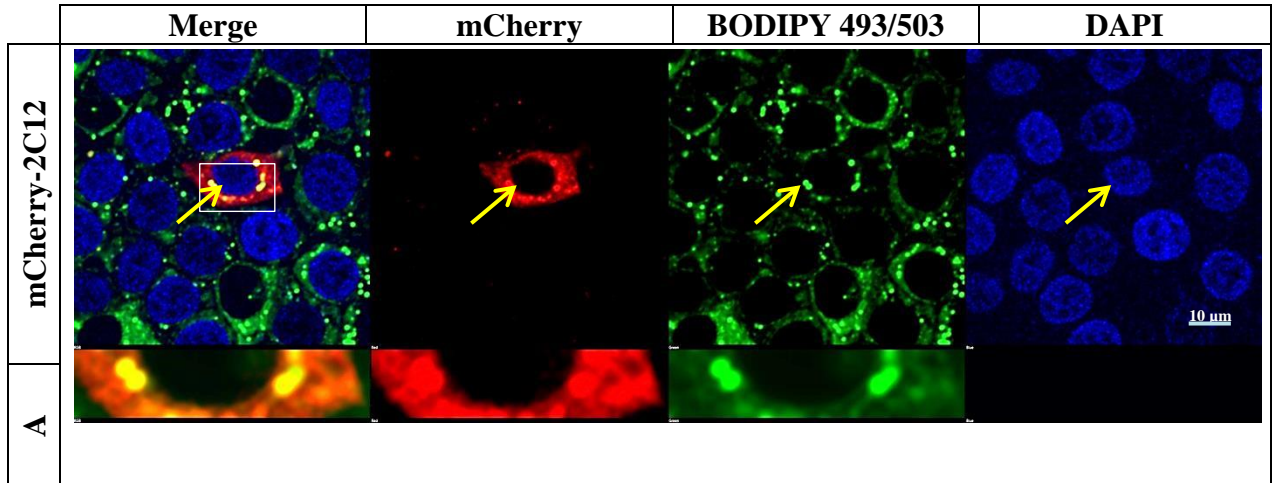


FIGURE 4.23: The effect of pmCherry-2C12 mutant on lipid droplets (LDs). GMK cells were grown on coverslips and transfected with pmCherry-2C12 using Turbofect. Cells were fixed and stained with BODIPY 493/503 for 10 min at a final concentration of 10 mg/ml then cells were washed twice with PBS. The coverslips were mounted with hard set mounting medium with DAPI. Images were visualized using a Nikon A1 confocal microscope. The blue filter detects the nucleus, the red filter detects mCherry-2C12 and the green filter detects neutral lipids in LDs. The yellow arrow indicates a transfected cell (which show an mCherry signal). mCherry-2C12 mutant mostly seems to co-localise to LDs. A shows close-up images of the co-localisation in the area marked by the white box. The scale bar shown is 10 μm .

4.4.4 Location of the LD-interacting region of 2C

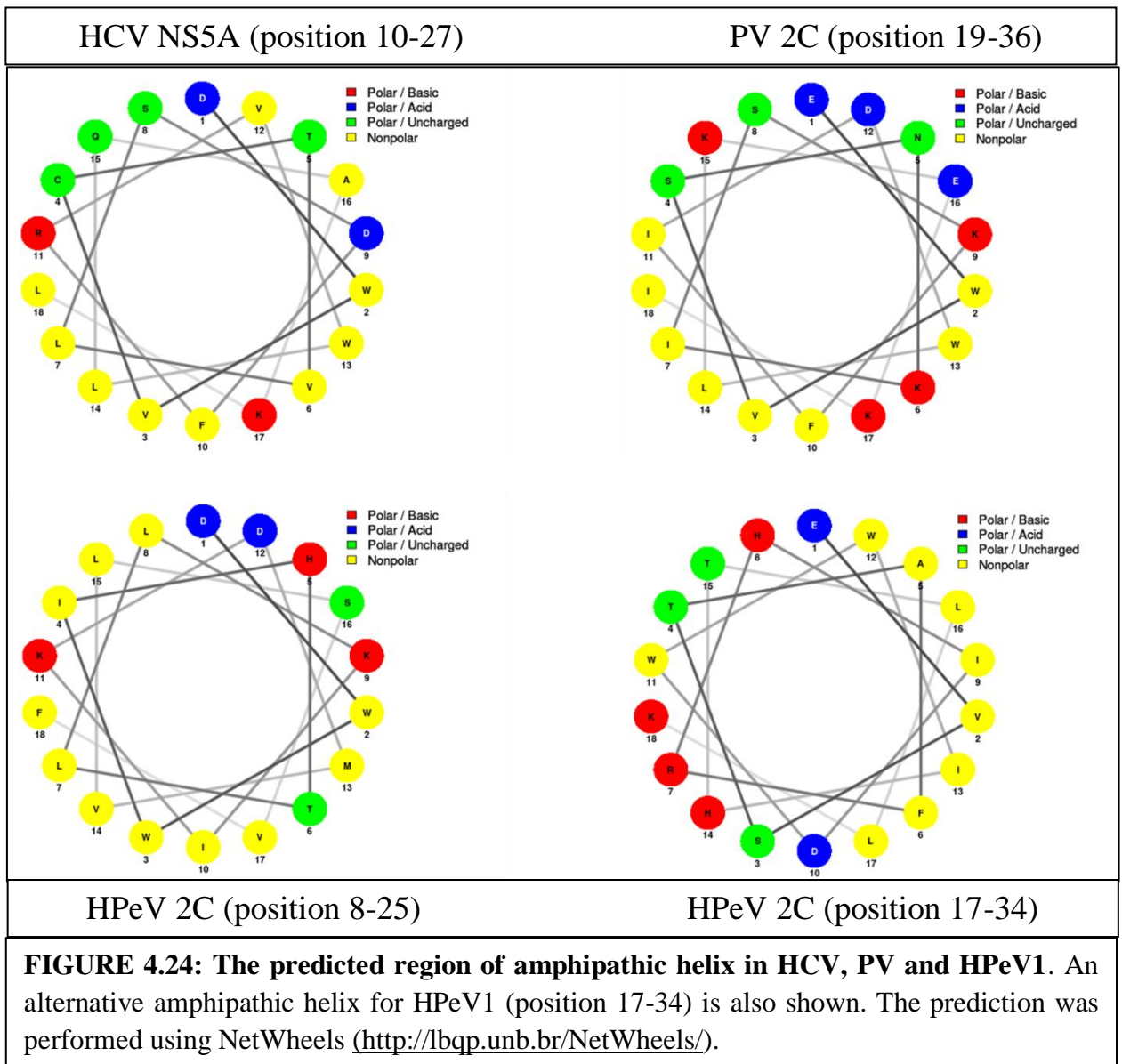
The N-terminal region of PV 2C (positions 19-36) was predicted to form an amphipathic helix, proposed to be responsible for its membrane binding property (Teterina *et al.*, 2006). This is remarkably similar in terms of the sequence and structure to an amphipathic helix in the N-terminal region of the NS5A protein of HCV (Figure 4.24). The ability to form an amphipathic helix seems to be conserved among all picornaviruses but the sequence similarity to HCV NS5A is not as great in other picornaviruses. Mutations in the helix in PV were shown to impair viral RNA synthesis, suggesting it has an important function (Teterina *et al.*, 2006). We found that the corresponding region (positions 17-34) in HPeV1 may form a similar structure, although a strong amphipathic helix can also be predicted between positions 8 and 25 (Figure 4.24).

The results on the localisation of the HPeV1 2C protein described above show that the region between positions 1-160, and not NTPase activity, is needed for localisation. To try to find which parts of the sequence are needed, 6 deletion mutants (Figure 4.25) were produced and transfected into GMK cells. The mutants are named from the start position e.g. 2C 7A contains 2C positions 7 to the C-terminus and was made as there is a conserved KXFN motif (position 4-7 in HPeV) in several 2C proteins from different picornaviruses (Figure 4.15). Mutants 2C 25A and 2C 53A remove the alternative amphipathic and alternative plus conserved amphipathic helices respectively.

mCherry-2C 7A and mCherry-2C 25A had a similar distribution to wild-type 2C (Figure 4.26) suggesting that the conserved motif and the alternative amphipathic helix do not play a role in LD localisation. LDs are still clustered in transfected cells. mCherry-2C 53A has the same localisation as the first two mutants and mCherry-2C 75A is very similar (Figure 4.27). The close up image of mCherry-2C 75A is a little different from the other mutants as some non-overlapping LD stain can be seen. To see if these mutants co-localise with wild-type mCherry-2C, we co-transfected the DNA constructs with pEGFP-2C (Figure 4.28). Both mutants have a

similar distribution to EGFP-2C, but mCherry-2C 75A seems to not precisely co-localise, suggesting that the 2C region from position 53 to 74 may have some role in the LD interaction. mCherry-2C 87A has a round foci distribution which is not related to LDs, while mCherry-2C 129A has an mCherry distribution with a lot of the protein localised in the nucleus (Figure 4.29). Neither of these mutants cluster the LDs, but LDs are still brighter than in the surrounding non-transfected cells. The results suggest that all the sequences needed to bind to structures in the cytoplasm are in the first 128 amino acids of 2C and that positions 75-86 are important in interacting with LDs.

Position 75-86 overlaps with sequences that can be predicted to form an amphipathic helix (position 74-91, Figure 4.30). This is in a larger region of 2C that is highly conserved between HPeV strains, but the HPeV sequences show some differences between strains. These differences are conserved in type and this suggests that a protein structure, not the sequence itself, is important. This is further evidence that an amphipathic helix forms (data not shown). In addition another *Parechovirus*, Ljungan virus, also appears to have an amphipathic helix at this position, even though the sequences making it up are mainly different from the HPeV sequences (Figure 4.30).



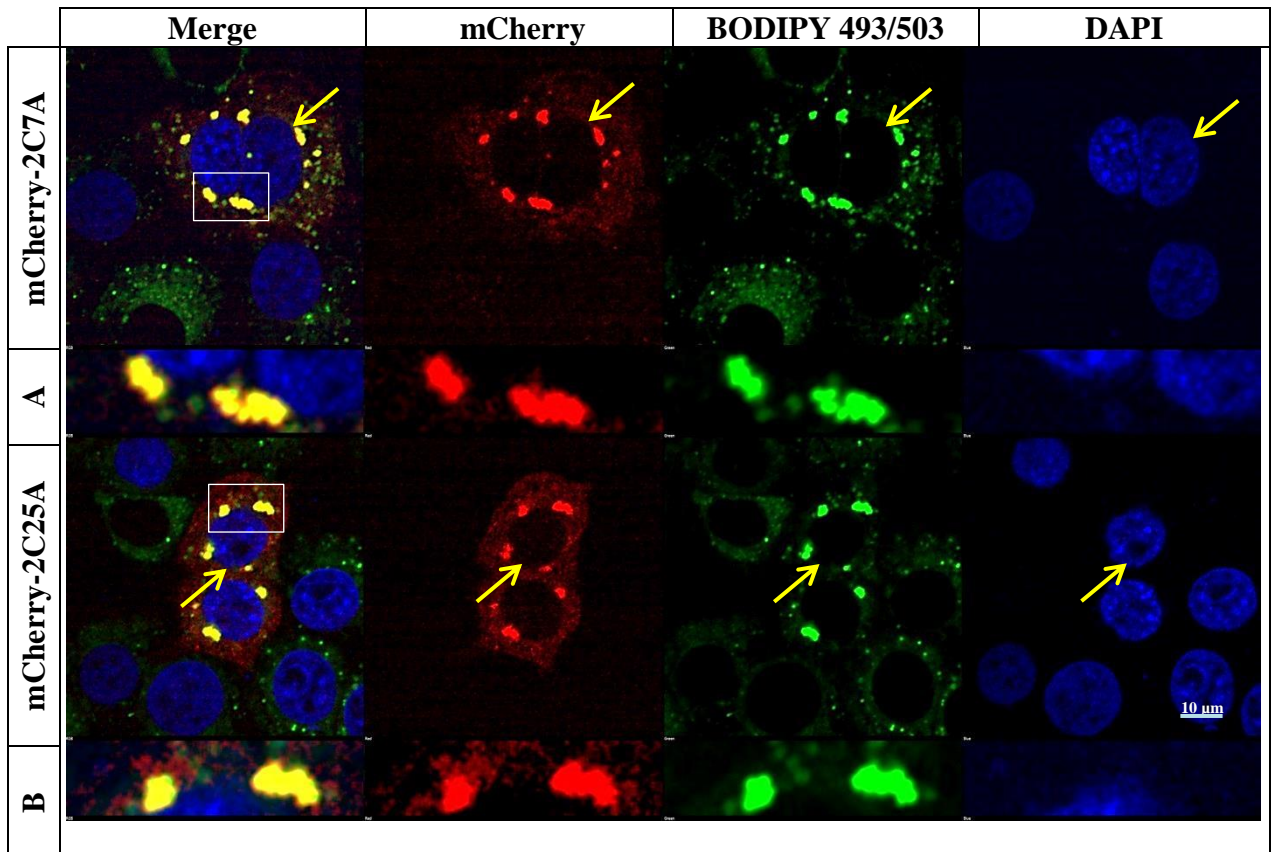


FIGURE 4.26: The effect of pmCherry-2C7A and pmCherry-2C25A mutants on lipid droplets (LDs) distribution. GMK cells were grown on coverslips and transfected with pmCherry-2C 7A and pmCherry-2C 25A using Turbofect. Cells were fixed, stained with BODIPY 493/503 for 10 min at a final concentration of 10 mg/ml, then cells were washed twice with PBS. The coverslips were mounted with hard set mounting medium containing DAPI. Images were visualised using a Nikon A1 confocal microscope. The blue filter detects the nucleus, the red filter detects mCherry and the green filter detects neutral lipids in LDs. A and B show close-up images of the co-localisation site. The yellow arrows indicate transfected cells (which show an mCherry signal). mCherry-2C7A and mCherry-2C25A mutants still co-localises with LDs. A and B show close-up images of the co-localisation seen in the area marked with the white box. The scale bar shown is 10 μ m.

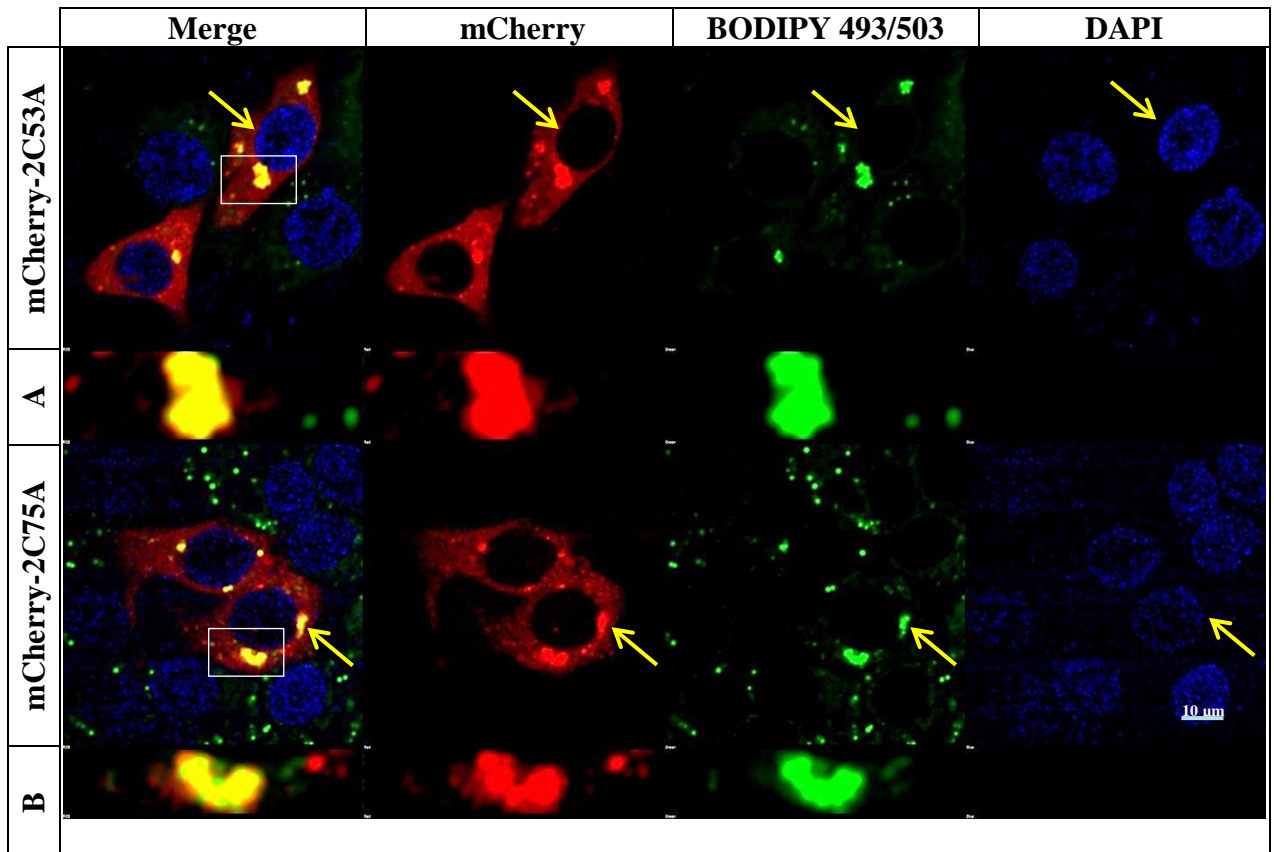


FIGURE 4.27: The effect of pmCherry-2C53A and pmCherry-2C75A mutants on lipid droplets (LDs) distribution. GMK cells were grown on coverslips and transfected with pmCherry-2C 53A and pmCherry-2C 75A using Turbofect. Cells were fixed, stained with BODIPY 493/503 for 10 min at a final concentration of 10 mg/ml, then cells were washed twice with PBS. The coverslips were mounted with hard set mounting medium containing DAPI. Images were visualised using a Nikon A1 confocal microscope. The blue filter detects the nucleus, the red filter detects mCherry and the green filter detects neutral lipids in LDs. A and B show close-up images of the co-localisation site. The yellow arrows indicate transfected cells (which show an mCherry signal). mCherry-2C53A and mCherry-2C75A mutants still co-localises with LDs. A and B show close-up images of the co-localisation seen in the area marked with the white box. The scale bar shown is 10 μ m.

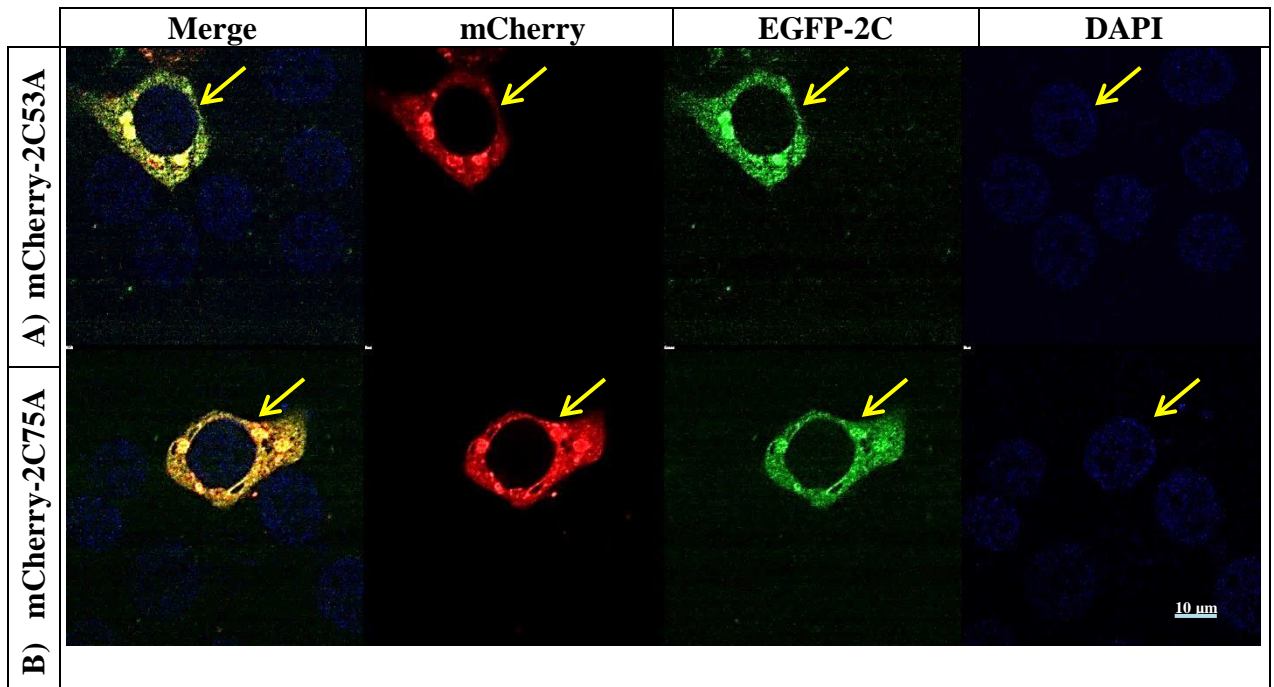


FIGURE 4.28: Co-transfection for pmCherry-2C53A and pmCherry-2C75A to pEGFP-2C. GMK cells were grown on coverslips and co-transfected with pEGFP-2C and A) pmCherry-2C53A or B) pmCherry-2C75A using Turbofect. Cells were fixed, then were washed twice with PBS. The coverslips were mounted with hard set mounting medium containing DAPI. Images were visualised using a Nikon A1 confocal microscope. The blue filter detects the nucleus, the red filter detects mCherry and the green filter detects EGFP. The yellow arrows indicate transfected cells (which show mCherry and EGFP signals). mCherry-2C53A and mCherry-2C75A mutants had a similar distribution to EGFP-2C. The scale bar shown is 10 μm .

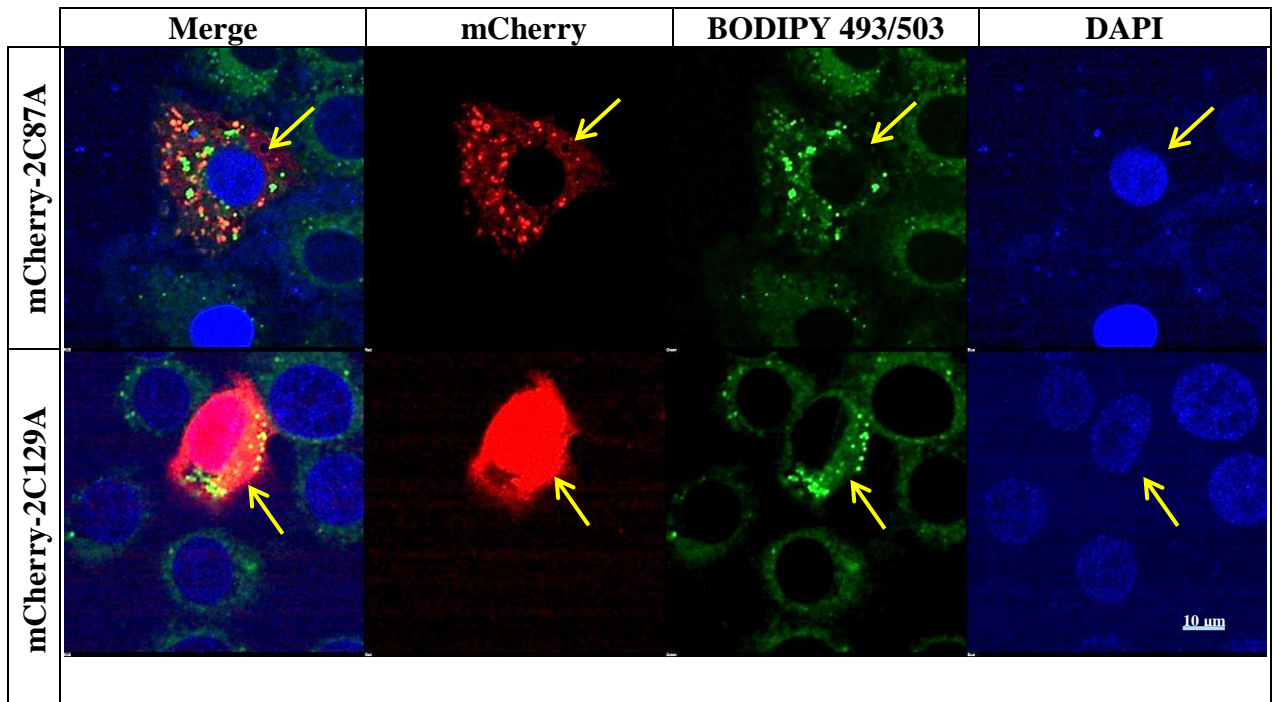
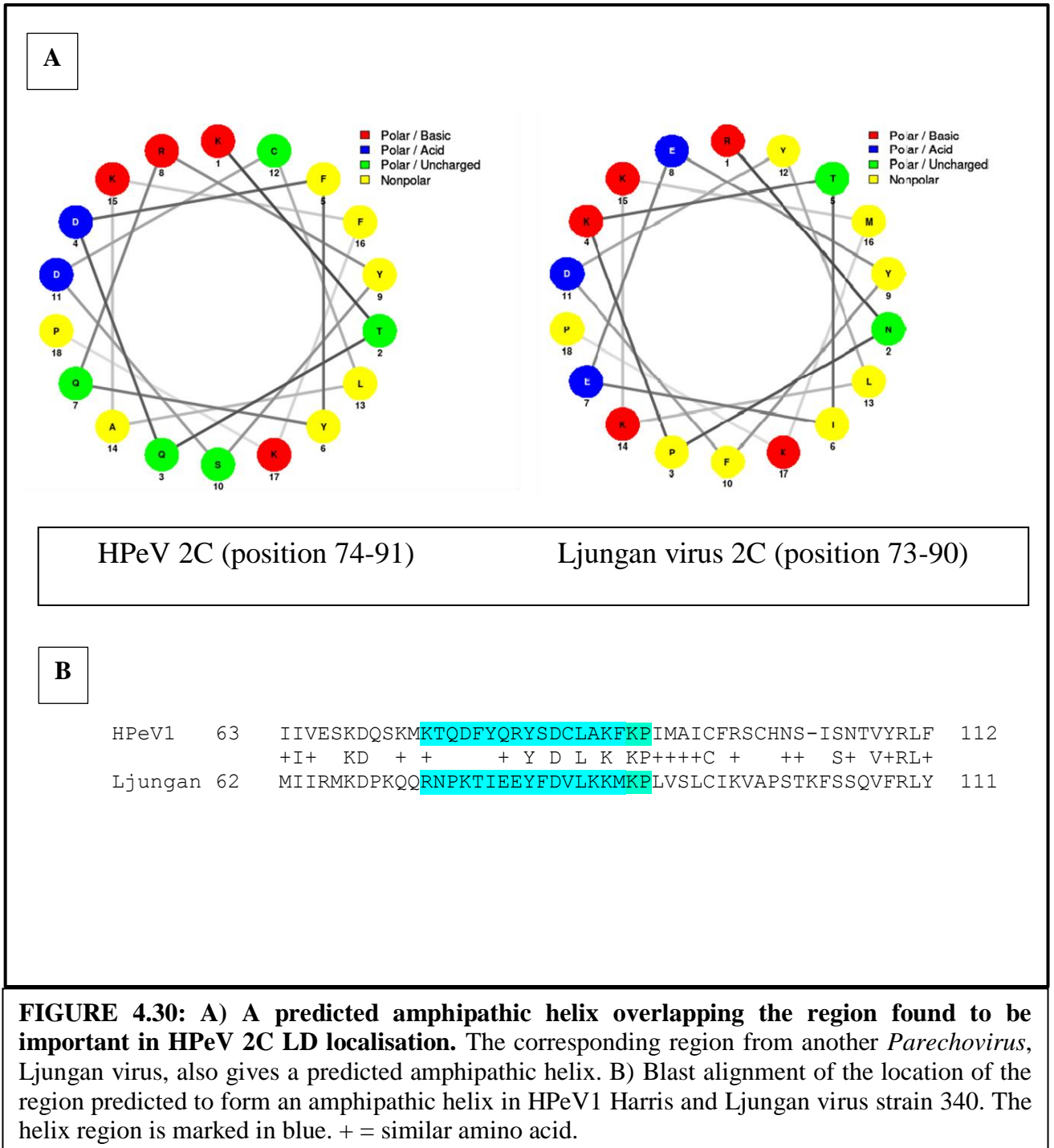


FIGURE 4.29: The effect of pmCherry-2C87A and pmCherry-2C129A mutants on lipid droplets (LDs) distribution. GMK cells were grown on coverslips and transfected with pmCherry-2C87A and pmCherry-2C 129A using Turbofect. Cells were fixed, stained with BODIPY 493/503 for 10 min at a final concentration of 10 mg/ml, then cells were washed twice with PBS. The coverslips were mounted with hard set mounting medium containing DAPI. Images were visualised using a Nikon A1 confocal microscope. The blue filter detects the nucleus, the red filter detects mCherry and the green filter detects neutral lipids in LDs. The yellow arrows indicate transfected cells (which show an mCherry signal). Neither mCherry-2C87A nor mCherry-2C129A mutants co-localise with LDs. The scale bar shown is 10 μm .



4.4.5 Cav1 and 2C of HPeV1

Caveolin-1 (Cav1) binds glycolipids and fatty acids and is thought to be engaged in intracellular lipid transport. Cav1 distributes in the caveolae and Golgi membranes under normal culture conditions, however when cells are loaded with lipids it translocates to the LD (Fujimoto *et al.*, 2008). To investigate if there was an interaction between 2C from HPeV1 and Cav1, we co-transfected pEGFP-2C and pmCherry-Cav1 into GMK cells. mCherry-Cav1 has a perinuclear localisation and does not co-localise with LDs (Figure 4.31). In addition, there is no co-localisation with EGFP-2C (Figure 4.32).

4.4.6 ADRP and 2C of HPeV1

ADRP is a protein found on the surface of LDs from the earliest time of their synthesis and helps to regulate lipid storage during LD formation. In addition, an increase in neutral lipid mass and LD accumulation occurs when ADRP is overexpressed. This slows down TAG turnover and simultaneously decreases TAG secretion in VLDL (Listenberger *et al.*, 2007). To provide further evidence that the 2C-induced cytoplasmic structures are related to LDs, an mCherry-ADRP construct was used. pmCherry-ADRP has a punctate distribution which partly co-localised to LDs (Figure 4.33). When mCherry-ADRP was co-transfected with pEGFP-2C or pEGFP-2BC some of the mCherry-ADRP concentrated into perinuclear spots which corresponded to EGFP-2C and EGFP-2BC fluorescence (Figure 4.34). This suggests that ADRP is recruited by 2C to these perinuclear spots and that they are modified/aggregated LDs.

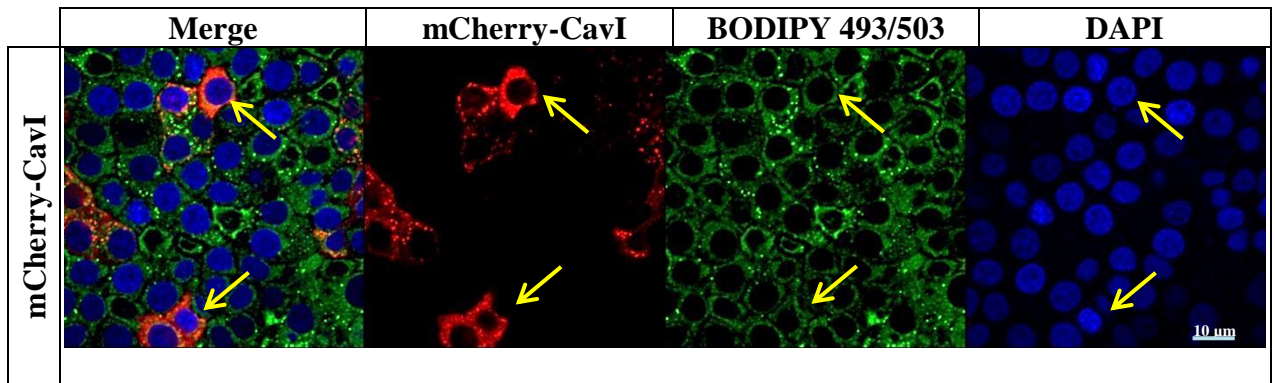


FIGURE 4.31: pmCherry-CavI and lipid droplets (LDs). GMK cells were grown on coverslips and transfected with pmCherry-Cav1 using Turbofect. Cells were fixed, stained with BODIPY 493/503 for 10 min at a final concentration of 10 mg/ml, then cells were washed twice with PBS. The coverslips were mounted with hard set mounting medium containing DAPI. Images were visualised using a Nikon A1 confocal microscope. The blue filter detects the nucleus, the red filter detects mCherry and the green filter detects neutral lipids in LDs. The yellow arrows indicate transfected cells (which show an mCherry signal). There is no co-localisation between mCherry CavI and LDs. The scale bar shown is 10 μ m.

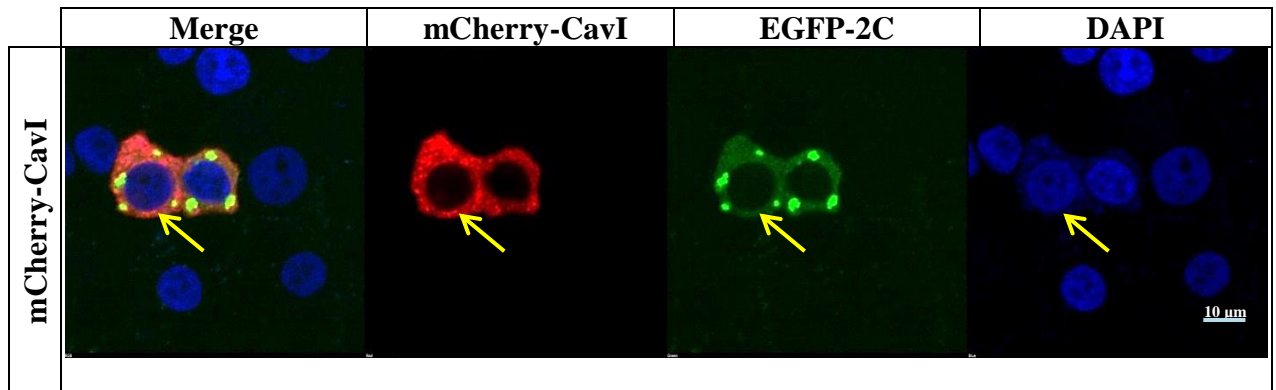


FIGURE 4.32: Co-transfection of pmCherry-Cav1 and pEGFP-2C. GMK cells were grown on coverslips and co-transfected with pEGFP-2C and pmCherry-Cav1 using Turbofect. Cells were fixed, then were washed twice with PBS. The coverslips were mounted with hard set mounting medium containing DAPI. Images were visualised using a Nikon A1 confocal microscope. The blue filter detects the nucleus, the red filter detects mCherry and the green filter detects EGFP. The yellow arrow indicate a transfected cell (which show mCherry and EGFP signals). There is no co-localisation between mCherry-CavI and EGFP-2C. The scale bar shown is 10 μm .

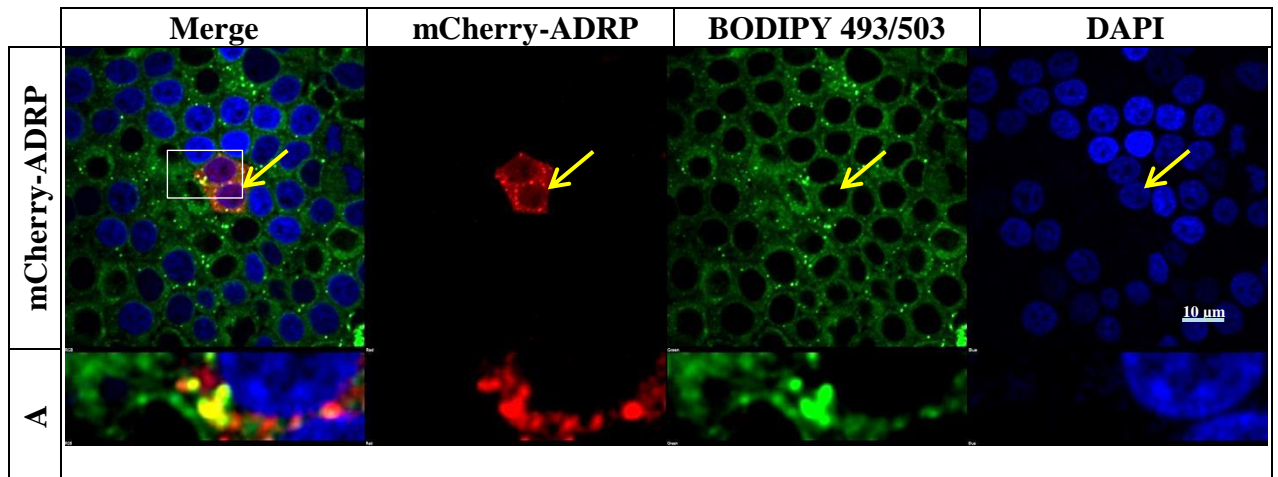


FIGURE 4.33: pmCherry-ADRP and lipid droplets (LDs). GMK cells were grown on coverslips and transfected with pmCherry-ADRP using Turbofect. Cells were fixed, stained with BODIPY 493/503 for 10 min at a final concentration of 10 mg/ml, then cells were washed twice with PBS. The coverslips were mounted with hard set mounting medium containing DAPI. Images were visualised using a Nikon A1 confocal microscope. The blue filter detects the nucleus, the red filter detects mCherry and the green filter detects neutral lipids in LDs. The yellow arrow indicates a transfected cell (which shows an mCherry signal). mCherry-ADRP partly co-localised with LDs. A shows close-up images of the co-localisation within the area marked with a white box. The scale bar shown is 10 μm .

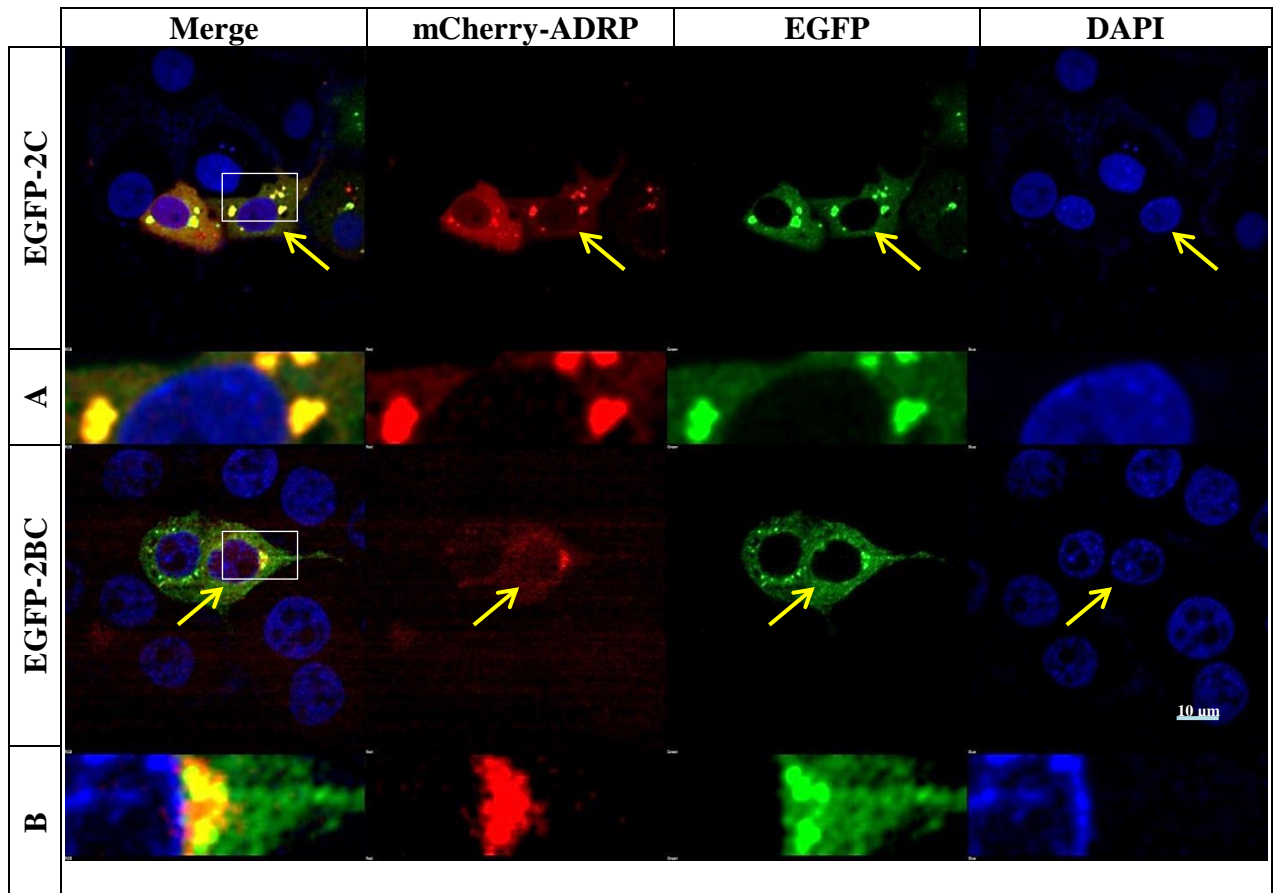


FIGURE 4.34: Co-transfection of pmCherry-ADRP and pEGFP-2C/pEGFP-2BC. GMK cells were grown on coverslips and co-transfected with pmCherry-ADRP and A. pEGFP-2C or B. pEGFP-2BC using Turbofect. Cells were fixed, then were washed twice with PBS. The coverslips were mounted with hard set mounting medium containing DAPI. Images were visualised using a Nikon A1 confocal microscope. The blue filter detects the nucleus, the red filter detects mCherry and the green filter detects EGFP. The yellow arrow indicates a transfected cell (which show mCherry and EGFP signals). mCherry-ADRP partly co-localised to EGFP-2C and EGFP-2BC. A and B show close-up images of the co-localisation in the areas marked with the white boxes. The scale bar shown is 10 μm .

4.5 Discussion

It has been shown that lipid synthesis and modifying enzymes are required in the replication of some positive sense RNA viruses. For example, phospholipid and/or sterol biosynthesis is required for efficient replication (Chukkapalli *et al.*, 2012).

In our work we saw only a slight effect on FAs in HPeV1-infected cells and in cells infected with CAV9. mCherry-2A of HPeV1 seemed to accumulate fatty acids (FAs) around the nuclei while there some co-localisation of FAs with mCherry-2B and -3A. In the case of mCherry-2C, some of the FA stain is located in foci and these correspond to the concentrations of 2C. The results suggest some interaction between HPeV proteins and FAs. It has been reported that in mock-infected cells FAs are mostly channelled to lipid droplets, while in cells infected with PV they are immediately utilized for highly upregulated PC synthesis. Poliovirus 2A protein stimulates FAs import (Nchoutmboube *et al.*, 2013). It would be interesting to investigate this in HPeV infection. Many other viruses use FAs during replication. Inhibition of FA synthesis inhibits HCV replication, maturation and release of HCV (Syed *et al.*, 2010). NS5B of HCV interacts with fatty acid synthase and contributes to HCV replication (Huang *et al.*, 2013). DENV infection controls fatty acid biosynthesis to increase lipid biogenesis to establish or expand its replications complex (Heaton *et al.*, 2010).

There was clear co-localisation between EGFP-2BC and mCherry-2C of HPeV1 with LDs and these proteins caused large foci or aggregates of LDs.

Several viruses seem to use or manipulate LDs during infection, but these organelles have been largely unstudied in picornavirus infections. HCV affects host lipid metabolism and induces LDs which then play a crucial role in viral replication and assembly (Fukasawa, 2010). HCV assembly occurs close to LDs (Vogt *et al.*, 2013). Dengue virus decreased LD number during infection due to autophagy-dependent lipolysis to release free fatty acid (Heaton and Randall,

2010; Herker and Ott, 2012). The C protein of Dengue virus (DENV) accumulates on the surface and localises to LDs (Herker and Ott, 2012; Liu *et al.*, 2010).

The rotavirus protein NSP4 contributes to LD metabolism using an autophagy pathway (Cheung *et al.*, 2010; Herker *et al.*, 2010). It would be interesting to study the role of LDs in HPeV and enterovirus infection as these seem affect LDs differently.

We focused our efforts on understanding the basis of the interaction between 2C and LDs. We find that ATPase activity is not needed for the interaction with LDs. Mutation of the equivalent active site amino acids in FMDV 2C completely abolished ATPase activity (Sweeney *et al.*, 2010) and gave non-viable viruses in poliovirus (Mirzayan and Wimmer, 1992; Teterina *et al.*, 1992).

If the ATPase activity of 2C is not involved in LD interactions, it is likely that regions which interact with membranes, such as the N-terminal amphipathic helix are involved. The poliovirus 2C N-terminus allows binding to cell membranes (Echeverri *et al.*, 1998; Echeverri and Dasgupta, 1995). To investigate which parts of HPeV1 2C may interact with LDs, 3 further mutants, 2C1(1-79), 2C2(79-160) and 2C4(161-329) were used. mCherry-2C1 and 2C2 partially co-localised to LDs. As the combination of the two mutants restores co-localisation with EGFP-2C, it is possible that there is an interaction between regions within the two mutant proteins which is necessary for efficient LD binding. A new mutant was produced fused to mCherry, mCherry-2C12, with positions 1-160 of 2C. The distribution of the new mutant seems to be punctate and mostly co-localise to LDs. The mutant seems to contain enough information to localise well with LDs but does not have the ability to aggregate LDs. This suggests that sequences in the second half of the protein could be involved. As this part of 2C is mainly the NTPase, which does not affect aggregation, it is unclear how aggregation occurs. A C-terminal cysteine-rich motif in the poliovirus 2C protein, located downstream of the NTPase domain, has been shown to bind zinc and be involved in RNA replication (Pfister *et al.*, 2000). HPeV 2C does

not have a similar motif, but it is possible that other motifs in this region could have critical roles independent of the NTPase activity.

Several more deletion mutants were produced and these suggested that amino acids 75-86 play an important role in the interaction. Looking at the HPeV1 sequence, these amino acids are part of an amphipathic helix which can be predicted. This is conserved in another *Parechovirus* species *Ljungan virus*. This is probably important in the LD localisation and this should be tested by making more precise mutants. The critical 75-86 region at the junction of the mCherry-2C1 (position 1-79) and mCherry-2C2 (79-160), which may explain why neither of these mutants fully localise to LDs.

Two proteins associated with LDs were also used. Caveolin 1 (Cav1) localises to LDs when over-expressed or when cells are treated with Brefeldin A (van Meer, 2001). mCherry-Cav1 did not co-localise to LDs or to EGFP-2C. The cells could be treated with Brefeldin A in future experiments to understand the relationship between 2C and LDs. Another protein, ADRP, is a key component of LDs (Listenberger et al., 2007). 2C concentrated the ADRP into strong foci which corresponded with 2C. This shows that the 2C-derived structures do contain LD markers and are probably aggregated LDs.

The best-studied virus with close ties to host LDs is HCV. In HCV-infected cells, the C protein localises to LDs, which may be involved in assembly. An amphipathic helix motif in C protein (D2 domain) has strong similarities to LD-binding domains. Localizing C to LDs involved triglyceride-synthesizing enzyme DGAT1. NS5A is also found in LDs and is thought to recruit viral RNA for encapsidation (Herker and Ott, 2012). HCV protein NS4B also targets LDs, using hydrophobic residues in amphipathic helices at the N- and C-termini (Tanaka *et al.*, 2013). Given that the N-terminal amphipathic helix is found in many picornavirus 2C proteins, it is surprising that it does not seem to play a role in LD association as it can be deleted without affecting

distribution. However, the identification of a putative amphipathic helix spanning the 75-86 region may suggest that HPeV 2C LD interactions also depend on an amphipathic helix.

HCV is an enveloped virus and so different from the naked picornavirus particle. LDs may not therefore play a similar role in assembly, but LDs could be involved in other processes such as RNA replication, although there is no overlap between HPeV replication complexes and LDs. The interaction between 2C and LDs should be investigated further to better understand how HPeVs replicate and possibly provide information for the development of antiviral agents. This will be further looked at in chapter 5.

CHAPTER FIVE
ANTIVIRAL DRUGS STUDY

5.1 Introduction

Using vaccines to prevent disease, or drugs to inhibit viral replication, are the two main strategies currently used to fight viral infections (van der Schaar et al., 2013). Vaccines are not useful for non-poliovirus enteroviruses as there are many virus serotypes and there are also several (16) HPeV serotypes. Despite decades of research on picornaviruses, there are no clinically-used antivirals for important enteroviruses/rhinoviruses or for parechoviruses (van der Schaar et al., 2013; Whitton et al., 2005; Zuo et al., 2016). New insights into the molecular biology of these viruses will hopefully open up new approaches to developing drugs (van der Linden *et al.*, 2015). Viral proteins have been the usual targets of antiviral drugs in the past and this approach had some successes in a few virus families. For example, viral proteins such as proteases, polymerases and integrases have been targets for classical antiviral agents. These antivirals do suffer from the problems of drug resistance, as many virus polymerases lack proof-reading mechanisms. Another approach is to target host factors that support viral replication, for example protein kinases involved in virus entry. These include serine/threonine kinase PAK1 for echoviruses, adenoviruses or vaccinia virus, as well as tyrosine kinases for coxsackievirus B3-RD (Jurgeit et al., 2010). It could be hypothesised that drug resistant mutants should be selected more rarely against a cellular target. While this is sometimes the case, in other cases resistant mutants have been produced relatively easily (Arita *et al.*, 2011; Geller *et al.*, 2007).

To select a cellular target for antiviral drugs we need to understand its role in the viral life cycle as well as identifying a target where drug resistant mutants cannot replicate efficiently in cells relevant to the development of the disease.

As we learn more about how picornaviruses replicate, potential cellular targets can be identified and useful drugs against some of these may already exist. Scanning large drug libraries for

molecules which have an effect on picornavirus replication has also given promising results recently (Gao *et al.*, 2015).

The work described in chapter 4 suggests that HPeV 2C interacts with LDs and this virus may also target lipid metabolism, as is being found for several other viruses (van der Schaar *et al.*, 2016). Many drugs target fatty acid biosynthesis, such as 5-tetradecyloxy-2-furoic acid (TOFA). TOFA inhibits the biosynthesis of fatty acids acetyl-CoA carboxylase (ACC) and has been shown to block replication of HCMV and influenza A virus. Treatment with trans-4-carboxy-5-octyl-3-methylene-butyrolactone (C75), an inhibitor of FASN (a key enzyme of the fatty acid biosynthetic pathway), also resulted in inhibition of the replication in HCMV, influenza A virus, DENV, yellow fever virus (YFV), WNV, HCV CVB3 and PV (Martin-Acebes *et al.*, 2013).

The aim of the work described in this chapter is to analyse the effect on HPeV replication of drugs known to target lipids/membranes, using CAV9 as a comparison. 4 drugs were used, Itraconazole, Brefeldin A, the DGAT inhibitor A922500 and betulinic acid.

5.1.1 Itraconazole

Itraconazole (ITZ, Figure 5.1) is an antifungal drug which is lipophilic. It inhibits CYP51, a cytochrome P450 required for sterol biosynthesis also has antiviral effects against HIV, cardioviruses, and HCV. It may also be a potential anti-cancer drug by affecting cholesterol trafficking (Shim *et al.*, 2016; Strating *et al.*, 2015). It was identified as an antiviral agent against rhinoviruses and enteroviruses in screens of the Food and Drug Administration (FDA)-approved drug library (Gao *et al.*, 2015; Shim *et al.*, 2016).

5.1.2 Brefeldin A

Brefeldin A (BFA, Figure 5.1) has been used to study membrane trafficking in eukaryotic cells and blocks ER to Golgi protein transport. BFA prevents membrane binding of COPI and formation of COPI-coated vesicles, while the formation of COPII-coated vesicles is not affected (Colanzi *et al.*, 2013; Wang *et al.*, 2012b) (Figure 5.1). BFA inhibits several enteroviruses,

including PV, SVDV and EV71 (Colanzi *et al.*, 2013; Vázquez-Calvo *et al.*, 2016; Wang *et al.*, 2012b).

5.1.3 Diacylglycerol acyltransferase inhibitor

Diacylglycerol acyltransferase (DGAT) enzymes are essential in LD biogenesis. DGAT1 and DGAT2 both localise to the ER, and DGAT1 is involved in LD formation (Herker *et al.*, 2010). A922500 (Figure 5.1) is a potent inhibitor of DGAT1 and inhibits HCV, DENV and rotavirus replication (Camus *et al.*, 2013; Crawford and Desselberger, 2016).

5.1.4 Betulinic acid

Betulinic acid (BetA, Figure 5.1) is a pentacyclic triterpenoid with anti-bacterial, anti-malarial, anti-inflammatory and anti-cancer activities. It also inhibits HSV-1, HIV and rotaviruses. DGAT1 is one of its targets (Crawford and Desselberger, 2016; Moghaddam *et al.*, 2012; Potze *et al.*, 2014).

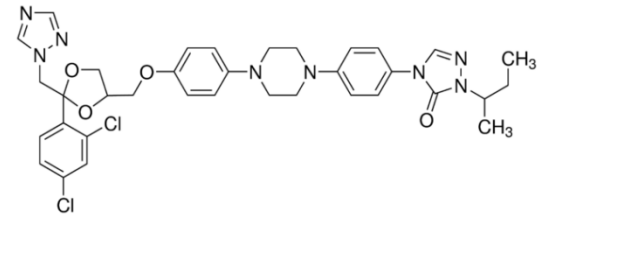
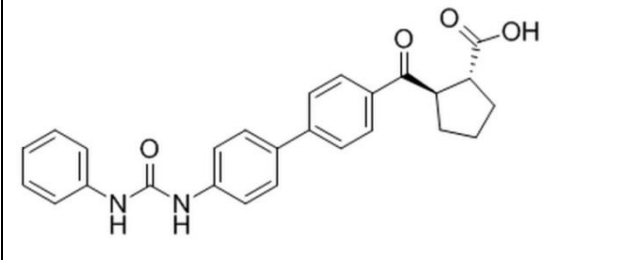
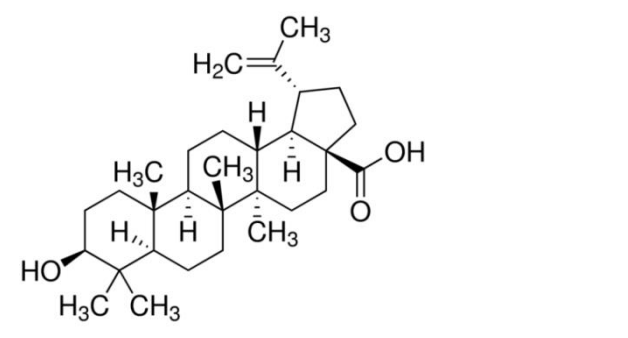
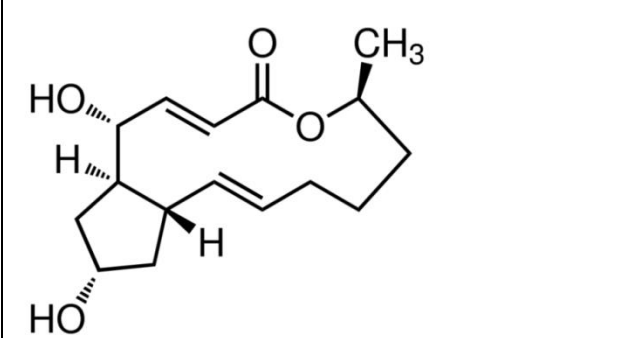
 <p>The chemical structure of Itraconazole features a central piperazine ring connected to two benzimidazole rings. One benzimidazole ring is substituted with a 4-chlorophenyl group, and the other is substituted with an isopropyl group. The piperazine ring is also substituted with a 4-(4-chlorophenyl)phenoxy group.</p>	 <p>The chemical structure of DGAT-1 Inhibitor, A 922500 consists of a benzamide group linked to a para-substituted benzene ring, which is further connected to another para-substituted benzene ring. This second benzene ring is attached to a cyclopentane ring, which has a carboxylic acid group and a methyl group attached to it.</p>
Itraconzol	DGAT-1 Inhibitor, A 922500
 <p>The chemical structure of Betulinic acid is a complex pentacyclic triterpene. It features a pentacyclic core with several methyl groups (H₃C) and a hydroxyl group (HO) attached. A side chain is attached to the core, containing a double bond (H₂C=CH-), a methyl group (CH₃), and a carboxylic acid group (COOH).</p>	 <p>The chemical structure of Brefeldin A is a complex pentacyclic triterpene. It features a pentacyclic core with several methyl groups (H₃C) and hydroxyl groups (HO) attached. A side chain is attached to the core, containing a double bond (C=C), a methyl group (CH₃), and a lactone ring (O-C=O).</p>
Betulinic acid	Brefeldin A

FIGURE 5.1: Chemical structure of drugs and inhibitor used in this study. Images were taken from <https://www.sigmaaldrich.com/united-kingdom.html>.

5.2 Immunofluorescence study

We first studied if there is any effect of these drugs on HPeV and CAV9. Cells were seeded in a 6 well plate containing glass coverslips 24 hours before the experiment. After 24 hours, 1.5 ml of the medium was removed and cells were treated with drugs for 30 min then were infected with 100 μ l CAV9 or HPeV1 (MOI 10) and were placed on a rocking platform for 45 minutes then incubated at 37°C incubator for 8 hours. Cells were fixed, followed by permeabilization and blocking. Primary antibody of dsRNA were added and kept overnight at 4°C. Alexa Fluor 488 secondary antibody was added and incubated for 2 hours at 4°C then were washed with PBS for 10 minutes. The coverslips were mounted with hard set mounting medium with DAPI and visualized using BX41 microscope. Infected cells were counted manually.

Cells were infected with HPeV1 or CAV9 and visualised by BX41 microscope and count the number of infected cells. In HPeV1, this number with cell treated with drugs seems to be less than that untreated cell (Figure 5.2). all four drugs affected the virus replication and DGAT inhibitor is the most effective drugs comparing to others and it reduced the infection rate up to two third (Figure 5.3). BetA and BFA reduce the number of infected cells to the half, where ITZ seem to be had less effect on HPeV1 but it reduced infection to the third.

BFA almost completely inhibit the CAV9 and image show few number of infected cell (Figure 5.2). DGAT inhibitor and BetA show less effective drugs with cells infected with CAV9 where the ITZ reduced the number of infected cells by two third (Figure 5.4)

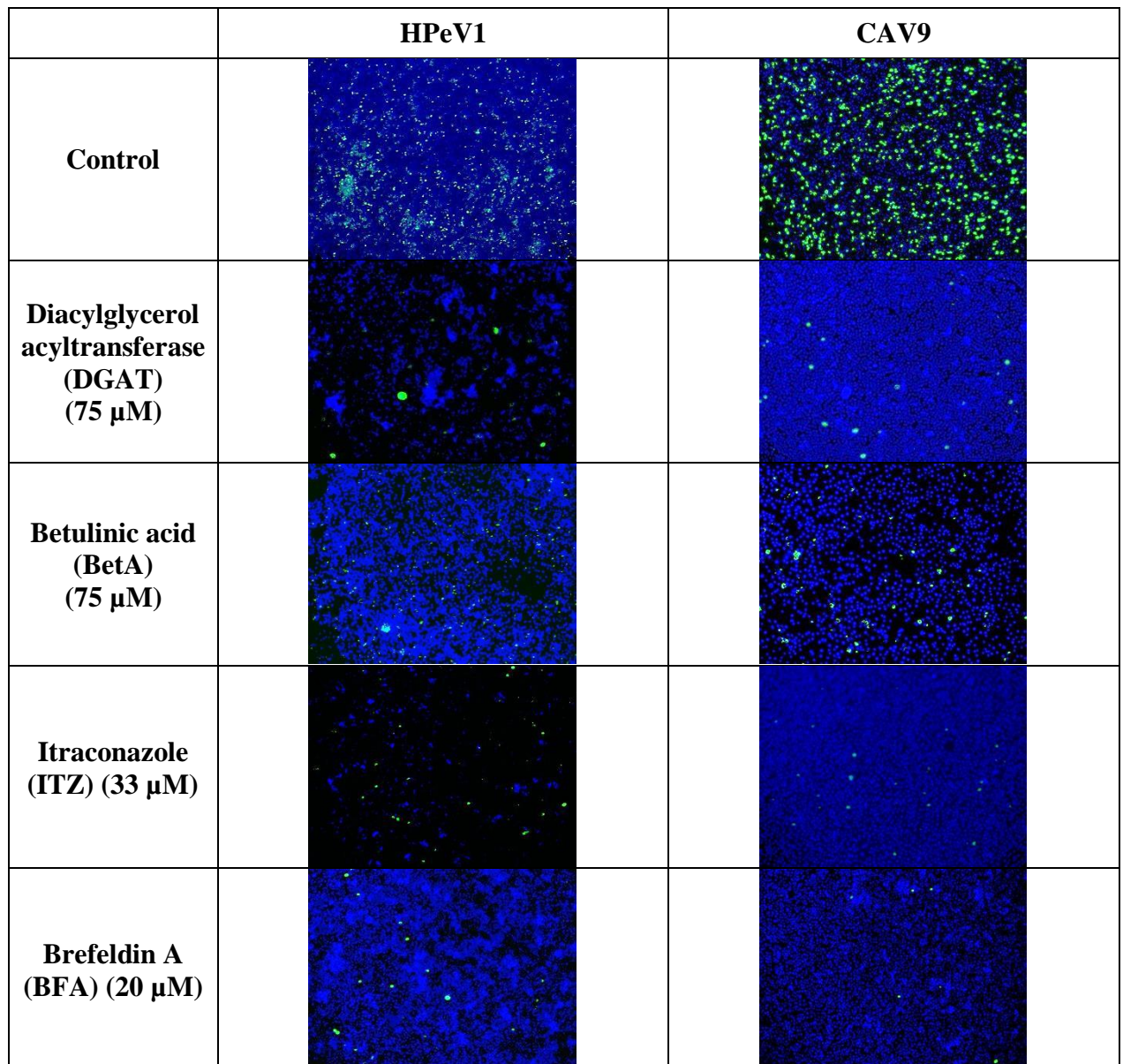


FIGURE 5.2: The effect of inhibitors on HPeV1 and CAV9 infection using immunofluorescence microscopy. HT29 or GMK cells were seeded in 6 well plate containing glass coverslips and were confluent before the start of the experiment. Cells were treated with the concentrations of the drugs shown for 30 min then were infected with HPeV1 or CAV9 (MOI 10) and incubated at 37°C for 8 hours. Then cells were fixed, permeabilized and blocked. A monoclonal antibody against dsRNA was used and recognised with secondary antibody labelled with Alexa Fluor 488. The coverslips were mounted with hard set mounting medium with DAPI. Images were visualized using BX41 microscope. A blue filter detects the nucleus and the green filter detects dsRNA in HPeV1 or CAV9 replication complexes. The blue/green merged image is shown.

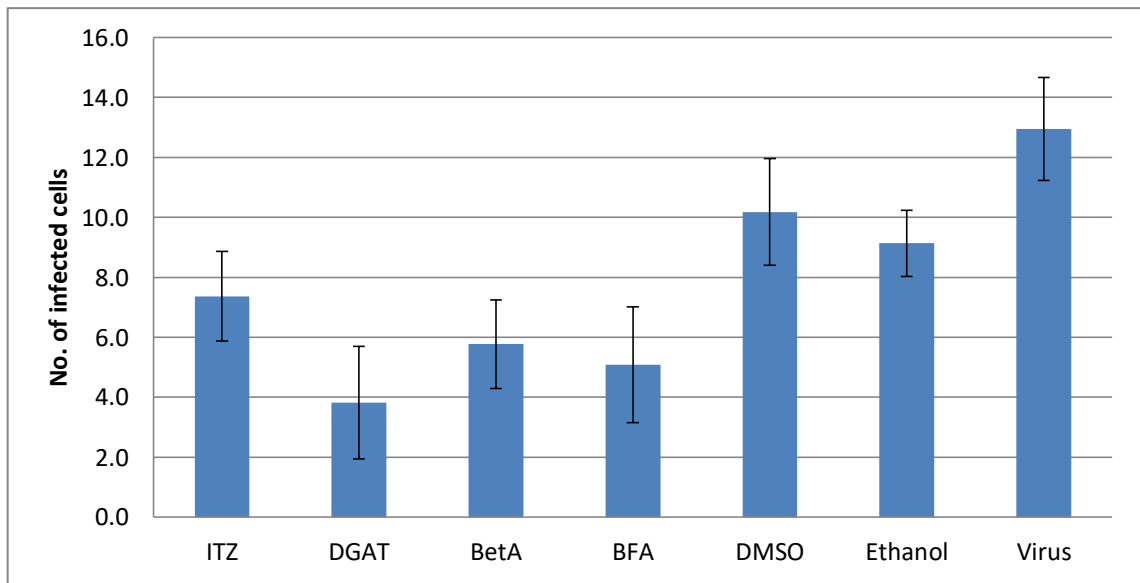


FIGURE 5.3: Bar chart showing the effect of drugs on HPeV infection. HT29 cells were treated with drugs, infected with HPeV1 and processed as described in Figure 5.2. The number of infected cells was then counted in 20 random fields and the average taken. Images were visualized using a BX41 microscope. (ITZ) Itraconazole, (BFA) Brefeldin A, (BetA) Betulinic acid and DGAT (inhibitor A922500). Error bars are standard deviations.

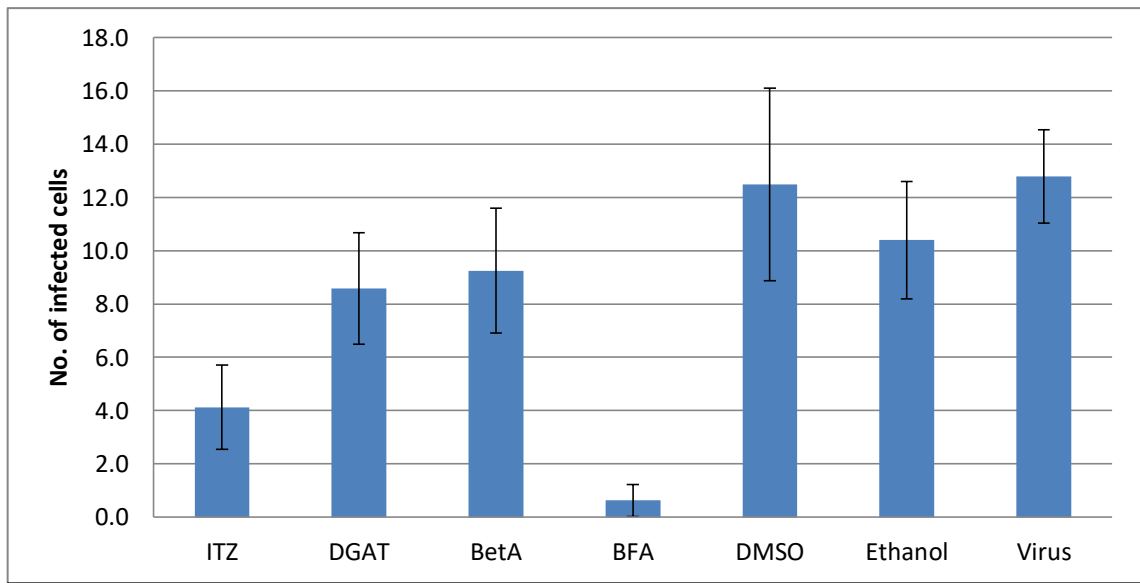


FIGURE 5.4: Bar chart showing the effect of drugs on CAV9 infection. GMK cells were treated with drugs, infected with CAV9 and processed as described in Figure 5.2. The number of infected cells was then counted in 20 random fields and the average taken. Images were visualized using a BX41 microscope. (ITZ) Itraconazole, (BFA) Brefeldin A, (BetA) Betulinic acid and DGAT (inhibitor A922500). Error bars are standard deviations.

5.3 Plaque assay

As an alternative method, after drug treatment the virus yield was determined by a standard plaque assay on cell monolayer. A trial shows that the HPeV1 plaques are much smaller than those seen for CAV9, but are visible and countable (Figure 5.5).

5.4 Screening study of drugs

A series of dilutions of the drugs or inhibitors in growth medium was prepared (Table 5.1) from DMSO (for ITZ, DGAT inhibitor and BetA) or ethanol (BFA) stocks. These all had the same concentration of the solvent and an equivalent concentration of the solvent was in growth medium was also prepared. Cells were incubated for 30 minutes before infection with one of the drug concentrations. Cells were then infected with 100 μ l CAV9 or HPeV1 (MOI 1) and were incubated in a 37°C incubator for 36 or 42 hours. Then cells were frozen and thawed three times and stored at -80°C before a plaque assay was performed to quantify the amount of virus produced by the cells. Examples of these plaques are shown in Figure 5.6 and 5.7.

The DGAT inhibitor reduced the viral titre of HPeV1 by more than 1.5 log₁₀ at the greatest concentration (75 mM) and this effect gradually reduced as lower concentrations were used. The effect of the DGAT inhibitor was less in cells infected with CAV9 and the viral titre was reduced by less than 1 log₁₀ (Figure 5.8). CAV9 was not affected by DGAT inhibitor at concentrations less than 25 μ M. There is little effect of BetA on both viruses and the reduction in viral titre was less than 1 log₁₀ (Figure 5.9). Similar results were found with ITZ (Figure 5.10). BFA had a large effect especially on CAV9 and it reduce the viral titre by almost 2 log₁₀. In HPeV1 it reduce the viral titre by approximately 1 log₁₀. In both viruses, a reduction was seen even at low concentrations (Figure 5.11).

Table 5.1: List of all concentration of drugs that used in this study									
Drugs	Concentration (μM)								
Itraconzol	33	10	3.3	1	0.33	0.1	.033	0.1	0.0033
DGAT-1 Inhibitor	75	25	7.5	2.5	0.75	0.25	0.075		
Betulinic acid	75	25	7.5	2.5	0.75	0.25	0.075		
Brefeldin A	20	15	10	5					
Itraconzol (Gao <i>et al.</i>, 2015) DGAT-1 Inhibitor A922500 (Camus <i>et al.</i>, 2013) Betulinic acid (Camus <i>et al.</i>, 2013) Brefeldin A (Maynell <i>et al.</i>, 1992)									

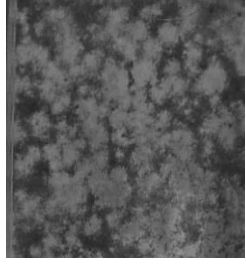
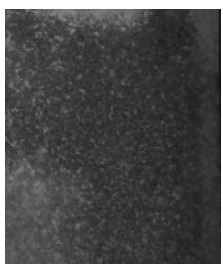
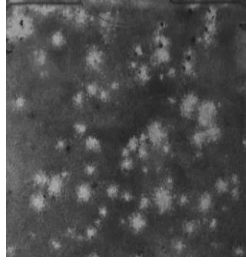
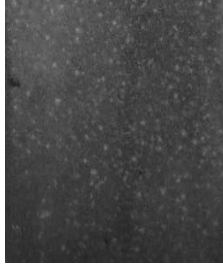
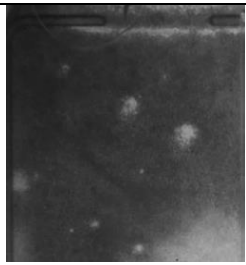
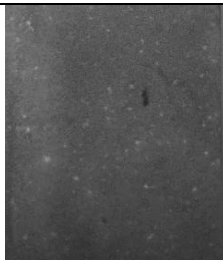
CAV9		10⁻² dilution		HPeV1
		10⁻³ dilution		
		10⁻⁴ dilution		

FIGURE 5.5: Plaque assays of CAV9 (GMK cells) and HPeV1 (HT29 cells). GMK and HT29 cell monolayers were infected with CAV9 or HPeV1, at the dilutions shown, for 45 min then the monolayer was covered with overlay medium containing 2% CMC and further cultured at 37°C under 5% CO₂ for 3-4 days. Then, the overlay medium was removed, and the cell monolayer was stained with 0.5% crystal violet.









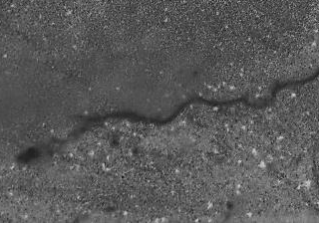
75 μM			Virus
25 μM			7.5 μM
2.5 μM			0.75 μM
0.25 μM			0.075 μM
DMSO			

FIGURE 5.6: An example of a plaque assay for HPeV1 treated with DGAT inhibitor A922500. A plaque assay was performed on HT29 cells as described in Figure 5.5. Samples were taken from cells pre-treated (30 minutes) with the drug at the concentrations shown, infected at MOI1 then incubated for 42 hours in the presence of the drug at the same concentration.

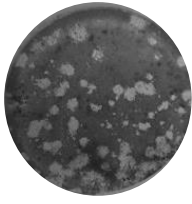
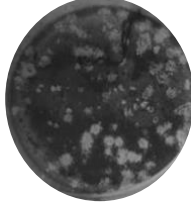
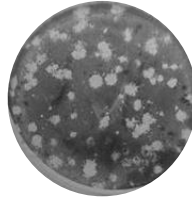
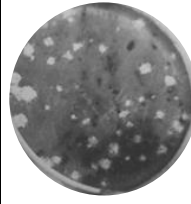
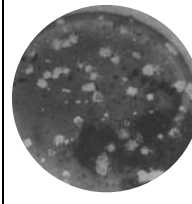
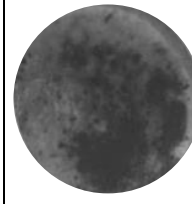

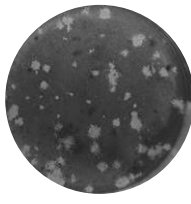
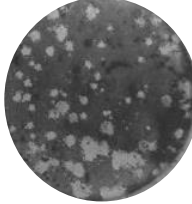
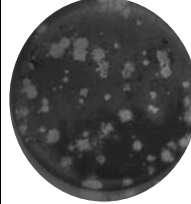
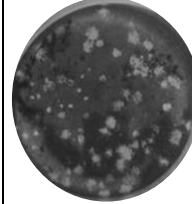
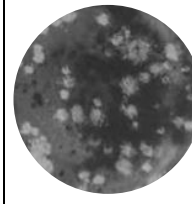
Virus	DMSO	2.5 μM	0.75 μM	0.0075 μM	Control
					
					
75 μM	25 μM	7.5 μM	0.25 μM	0.075 μM	0.025 μM

FIGURE 5.7: An example of a plaque assay for CAV9 treated with DGAT inhibitor A922500. Samples were taken from cells pre-treated (30 minutes) with the drug at the concentrations shown, infected at MOI1 then incubated for 36 hours in the presence of the drug at the same concentration.

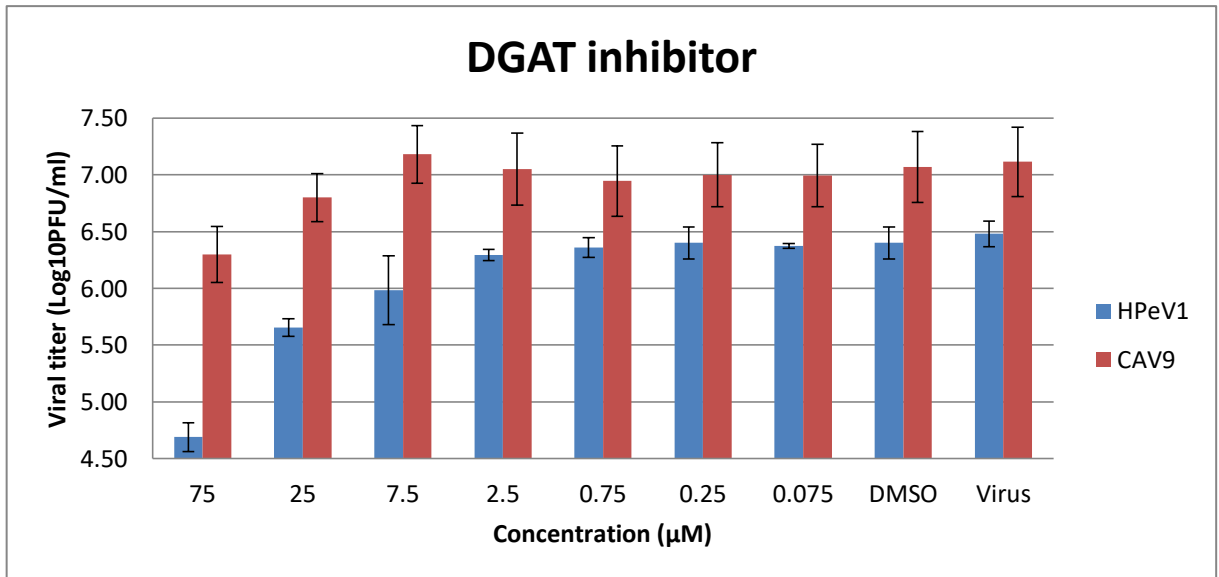


FIGURE 5.8: Bar chart of viral titres obtained when plaque assays were done to measure the amount of virus produced at different drug concentrations, when the DGAT inhibitor A922500 was used. Cells were pre-treated (30 minutes) with the drug at the concentrations shown, infected at MOI1 then incubated for 36 hours for CAV9 and 42 hours for HPeV1 in the presence of the drug at the same concentration. The samples were then freeze thawed and plaque assays were used to quantitate the amount of virus present. The experiment was performed three times and error bars are standard deviations.

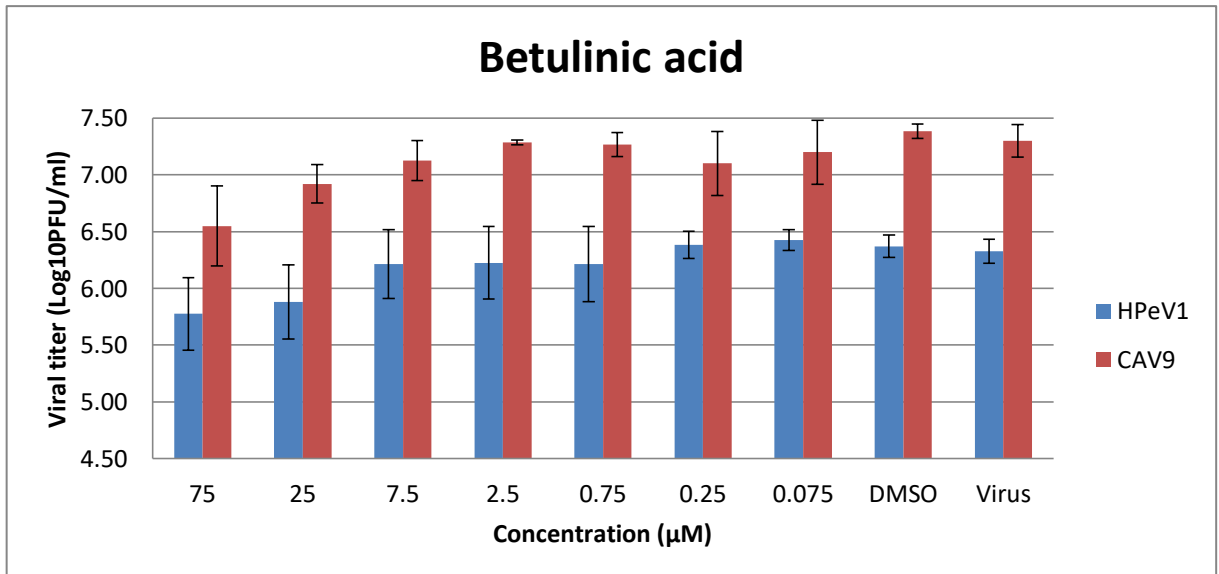


FIGURE 5.9: Bar chart of plaque assays done to measure the amount of virus produced at different drug concentrations, when the betulinic acid was used. Cells were pre-treated (30 minutes) with the drug at the concentrations shown, infected at MOI1 then incubated for 36 hours for CAV9 and 42 hours for HPeV1 in the presence of the drug at the same concentration. The samples were then freeze thawed and plaque assays were used to quantitate the amount of virus present. The experiment was performed three times and error bars are standard deviations.

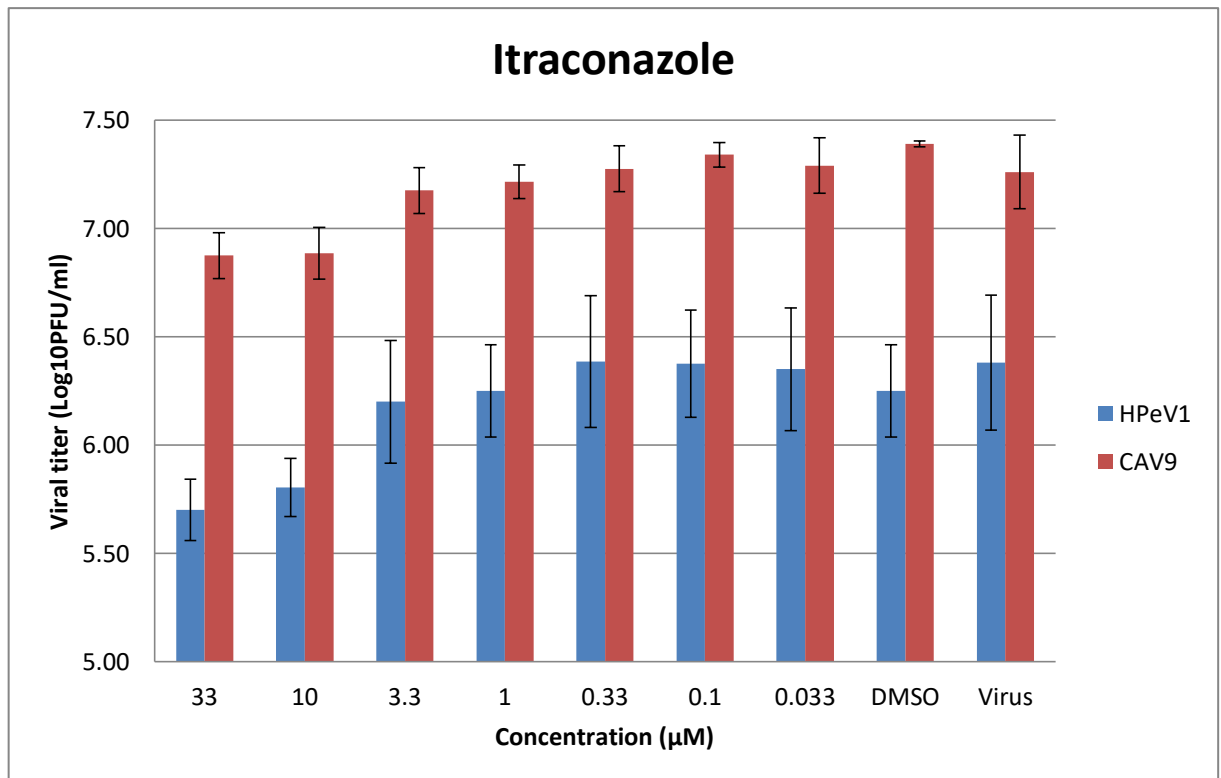


FIGURE 5.10: Bar chart of plaque assays done to measure the amount of virus produced at different drug concentrations, when Itraconazole was used. Cells were pre-treated (30 minutes) with the drug at the concentrations shown, infected at MOI1 then incubated for 36 hours for CAV9 and 42 hours for HPeV1 in the presence of the drug at the same concentration. The samples were then freeze thawed and plaque assays were used to quantitate the amount of virus present. The experiment was performed three times and error bars are standard deviations.

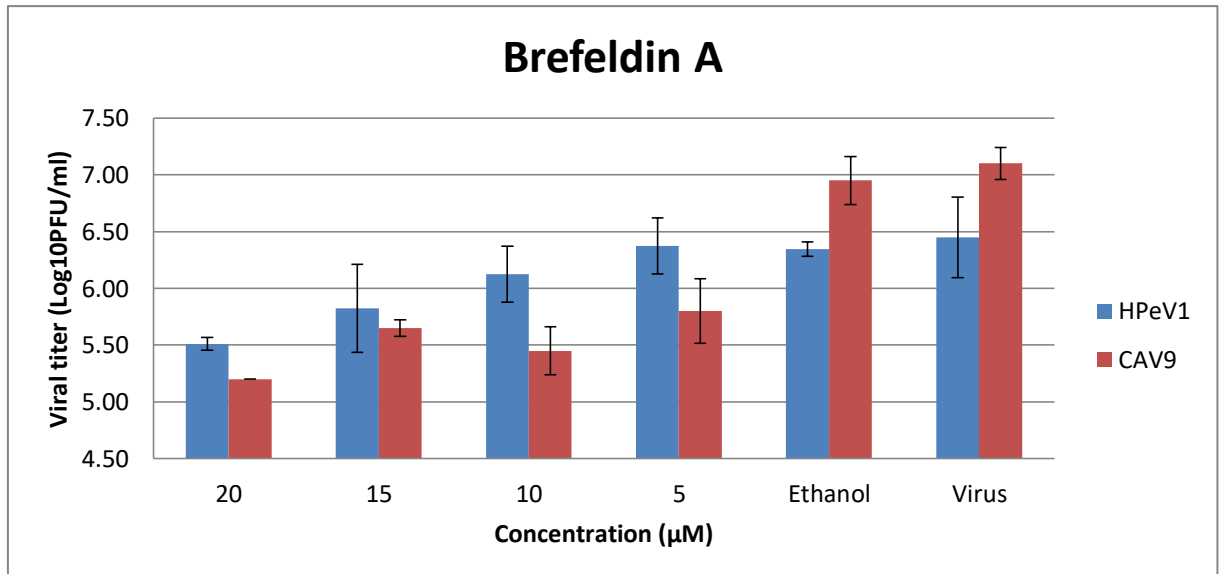


FIGURE 5.11: Bar chart of plaque assays done to measure the amount of virus produced at different drug concentrations, when Brefeldin A was used. Cells were pre-treated (30 minutes) with the drug at the concentrations shown, infected at MOI1 then incubated for 36 hours for CAV9 and 42 hours for HPeV1 hours in the presence of the drug at the same concentration. The samples were then freeze thawed and plaque assays were used to quantitate the amount of virus present. The experiment was performed three times and error bars are standard deviations.

5.5 Time-of-addition study

To identify the step(s) at which drugs suppresses virus infection, we analysed the drugs in a time-of-addition assay. The drug was added to one well which was the zero time point, and incubated for 30 minutes. Then all cell samples were infected with 100 μ l CAV9 or HPeV1 (MOI 10) and the drugs were added at 1, 3, 5 and 8 hours post- infection. The plate was incubated at 37°C incubators for (36 hours for CAV9 and 42 hours for HPeV1). The plate was frozen-then-thawed three times and a plaque assay was applied.

In HPeV1 the inhibitory effect of drugs on viral titre gradually decreased when the drug was added after infection for ITZ and BFA, suggesting that the replication steps affected occur through the replication cycle. The effect of both the DGAT inhibitors, A922500 and BetA reduced quite a lot when the drug was added after 5 hours, which suggests that they block a middle stage event in replication. Except BFA, the drugs did not have a great effect on CAV9 infection. BFA also seems to work mainly at an middle stage in replication. It seems that drugs do not function at an early (attachment or entry) or late (assembly or release) stage (Figure 5.10 and 5.11).

5.6 Attempts to generate drug resistant mutants

Passaging virus on cells line in the presence of the drugs or inhibitors to generate drug-resistant mutants was done. For each round of passaging, cells in 6 well plates were infected with (10 μ l of previous passaging for HPeV1 and 100 μ l of a 10^2 dilution of CAV9) in the presence of increasing concentrations of drugs or inhibitors. In the first round of infection 0.1 MOI was used. We started with the 0.075 μ M of DGAT and BetA and it was .033 μ M for ITZ. 7 passages were run and the 6 passage the plaque assay was run with and without drugs. In ITZ and BetA we did not find a resistant mutation with CAV9 (data not shown).

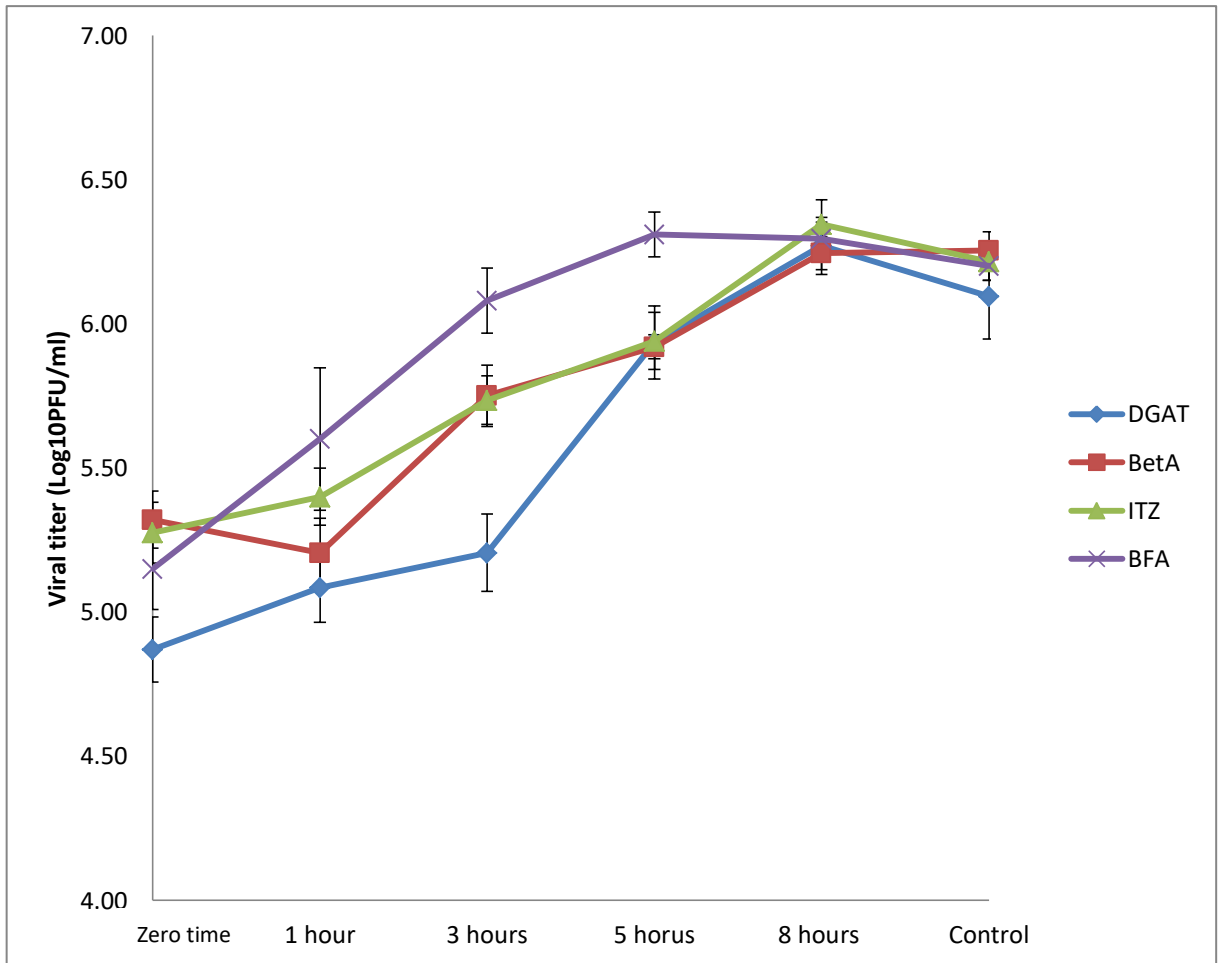


FIGURE 5.12: Graph of HPeV titre obtained after the drug shown was added at different times before (zero time) or after infection. The drug was added to one well which was the zero time point, and incubated for 30 minutes. Then all cell samples were infected with HPeV1 (MOI 1) and the drugs were added at 1, 3, 5 and 8 hours post-infection. The plate was then incubated for 42 hours. The plate was frozen-then-thawed three times and a plaque assay was applied. The experiment was done three times and error bars are standard deviations.

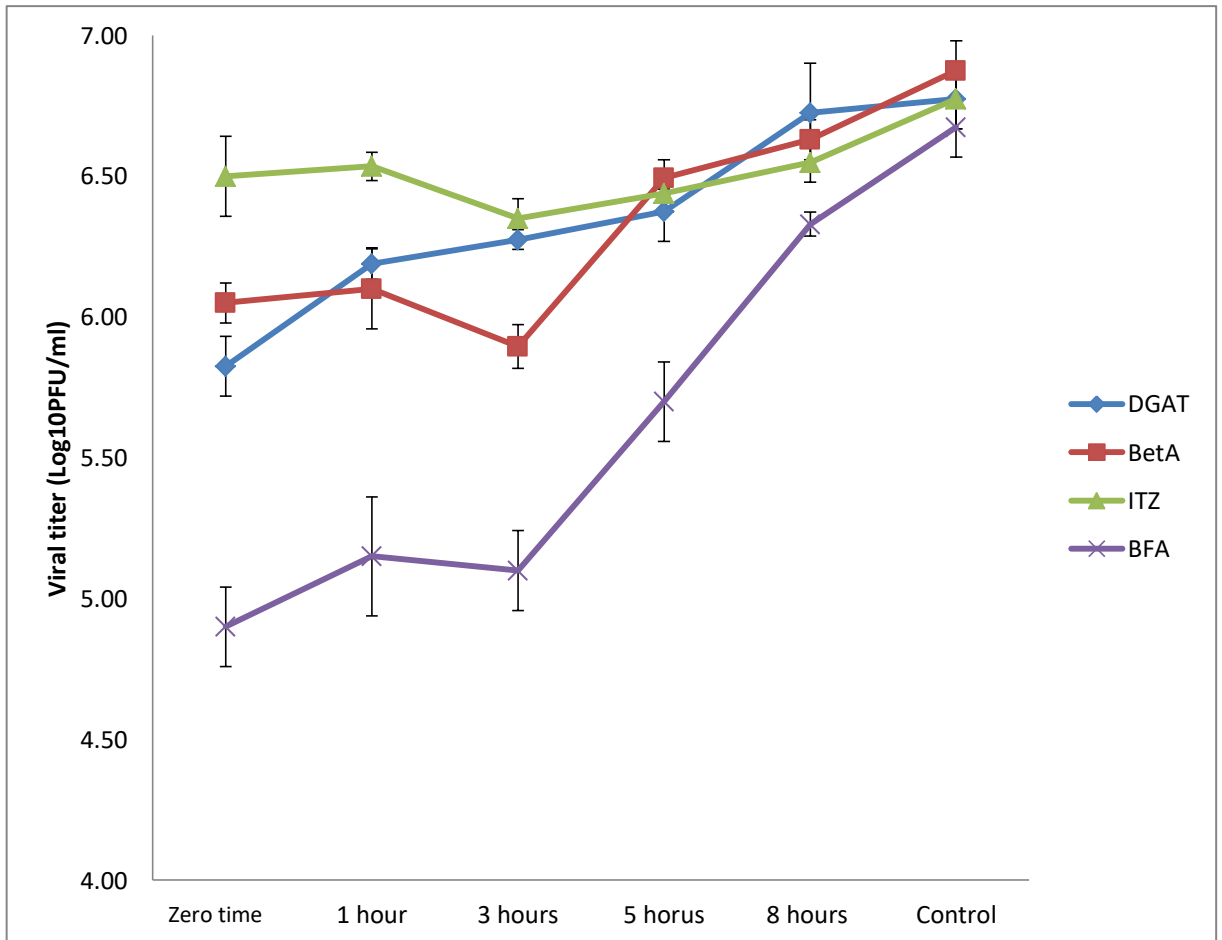


FIGURE 5.13: Graph of CAV9 titre obtained after drug was added at different times before (zero time) or after infection. The drug was added to one well which was the zero time point, and incubated for 30 minutes. Then all cell samples were infected with CAV9 (MOI 1) and the drugs were added at 1, 3, 5 and 8 hours post- infection. The plate was then incubated for 36 hours. The plate was frozen-then-thawed three times and a plaque assay was applied. The experiment was done three times and error bars are standard deviations.

5.7 Discussion

Generally for RNA viruses, drugs that target host factors are potentially at low risk of giving resistant viruses (van der Schaar *et al.*, 2013). Exploiting these host factors as targets could be a way of producing effective antiviral drugs. RNA virus replication is highly dependent on cellular membranes and lipid metabolism (van der Schaar *et al.*, 2016). Much research has been done in recent years to study drugs that target fatty acid biosynthesis or PI4KIII β . Examples of these drugs are TOFA, C75 and AL-9 (Martin-Acebes *et al.*, 2013).

Because we identified co-localisation of HPeV 2C with LDs, we were interested in testing drugs which may interfere with LDs to see if they inhibited HPeV infection. We investigated the effect of the DGAT inhibitor A922500 and also BetA, which has a number of effects on the cell, including inhibiting DGAT1 (Crawford and Desselberger, 2016). DGAT1 is important for LD development (Harris *et al.*, 2011). Another drug, ITZ, has a different mode of action, but this is also related to cellular lipids. It has been shown to target the oxysterol-binding protein, which shuttles cholesterol and PI4P between membranes, and ITZ can inhibit enterovirus replication (Strating *et al.*, 2015). It also inhibits cardiovirus replication, but not the aphthovirus equine rhinitis virus A. There was no information on its effect on HPeV replication and it was studied to find if it could also have an effect against this virus, which is genetically diverse from enteroviruses and cardioviruses. BFA was used as a control and because it has a potent effect on enteroviruses, but is reported to be only partially effective against HPeV (Gazina *et al.*, 2002).

In HPeV1, DGAT1 inhibitor A922500 was the most effective drug and gave a high level of blocking replication at 75 μ M. The other DGAT1 inhibitor, BetA, had a weaker effect. These drugs had less effect on CAV9, which could be related to the less clear effect of CAV9 infection and expression of CAV9 2C on LDs compared to HPeV. The findings suggest that A922500 could potentially be a useful drug against HPeV infections and that other compounds targeting LDs, or derivatives of A922500, could also be explored.

DGAT1 was shown to be required for HCV replication and this is blocked by knock-down of DGAT1 or by inhibitors (Herker *et al.*, 2010). Although DGAT1 plays a role in LD generation, this may not be directly related to HCV replication as in HCV-infected cells it recruits the core protein onto the surface of LDs and this plays a critical role in HCV infection. DGAT1 also forms a complex with the HCV NS5A protein and facilitates the interaction between these viral proteins (Camus *et al.*, 2013). Production of infectious viral particles of HCV is reduced in cells treated with the DGAT1 inhibitor A922500. The core protein still interacts with DGAT1 but cannot access LDs (Herker *et al.*, 2010). Rotavirus infection is affected by both A922500 and BetA, which both target DGAT1 (Crawford and Desselberger, 2016). How DGAT1 may be involved in HPeV replication is not yet clear, but A922500 could be a tool to investigate this.

ITZ showed antiviral activity against HRV, CVB3, EV-71, CAV16, poliovirus, cardioviruses and HCV (Shim *et al.*, 2016; Strating *et al.*, 2015). ITZ blocks intracellular cholesterol trafficking and so decreases the level of plasma membrane cholesterol. In addition, the antiviral activity of ITZ seems to be due to inhibiting oxysterol-binding protein (OSBP) in CVB3 and EV-71. Binding ITZ to OSBP blocked its cholesterol-shuttling function and inhibited cholesterol trafficking (Shim *et al.*, 2016; Strating *et al.*, 2015). Non-structural protein 3A was found to accumulate mutations in drug resistant EV-71. As expected, as CAV9 is very similar to CVB3, our results show some inhibition of CAV9. The effect is modest, but comparable to that shown by several enteroviruses (Shim *et al.*, 2016; Strating *et al.*, 2015).

The effect on HPeV1 is a novel observation. The inhibition is not as great as that shown by the DGAT1 inhibitor, but is greater than the effect of ITZ on CAV9. Again this suggests that ITZ could be potentially useful clinically. The advantage in using the well-established antifungal drug IZT or obesity therapy A922500, is that they have already been extensively tested for these different purposes, and found to be safe.

BFA inhibits the replication of several enteroviruses, including poliovirus, SVDV and EV-71 and so it is expected to inhibit CAV9 (Gazina *et al.*, 2002). It has been reported that HPeV is only partially resistant to BFA (Gazina *et al.*, 2002) and this is supported by the results we obtained, which show much less effect on HPeV1 than on CAV9. BFA inhibits enterovirus replication by targeting the cellular protein GBF1, a guanine nucleotide exchange factor for the small cellular GTPase Arf1, which in uninfected cells organizes the formation of COPI vesicles between *cis*-Golgi membranes and the endoplasmic reticulum (Belov *et al.*, 2008; Lanke *et al.*, 2009). BFA prevents the activated form of Arf1, Arf-GTP being formed from Arf-GDP by GBF1 (Szul *et al.*, 2007). It has been suggested that activated Arf1 is important for enterovirus replication, possibly to recruit other cellular factors needed for replication such as PI4KIII β (Hsu *et al.*, 2010). However, poliovirus 3A interacts with GBF1 and it may be this direct interaction that is needed for replication, by being involved in replication complex formation (Viktorova *et al.*, 2015). The normal cellular function of GBF1 seems to be inhibited at a much lower concentration of BFA than was poliovirus replication, suggesting that replication is not dependent on GBF1's Arf-GTP regeneration activity (Viktorova *et al.*, 2015).

Poliovirus variants resistant to BFA have been generated by 5 passages in the presence of increasing levels of BFA (0.1-1 μ g/ml), where the lowest concentration is sufficient to inhibit more than 90 % of virus production, to allow for the need for multiple mutations to achieve resistance, or simply by 10 serial passages in the presence of 2 μ g/ml BFA (Crotty *et al.*, 2004; Viktorova *et al.*, 2015). In both cases, resistant mutants were produced and show point mutations located in the 2C and 3A proteins, although the mutations observed are not the same. In similar work, a single amino acid change is seen in the 2C protein of SVDV (Crotty *et al.*, 2004; Vázquez-Calvo *et al.*, 2016; Viktorova *et al.*, 2015). It is known that 2C and 3A interact and it is likely that mutations giving BFA-resistance affect the same process, rather than that changes in 2C and 3A provide separate mechanisms of resistance. Interestingly, poliovirus easily generated

BFA-resistant mutants in HeLa cells, but it was impossible to select resistant viruses in Vero cells, although the virus grows well in both these cells in the absence of the drug (Viktorova *et al.*, 2015). Similarly, BFA-resistant mutants selected on HeLa cells were not resistant on Vero cells. This difference seems to be due to the lower availability of GBF1 in Vero cells. Vero cells are monkey cells, while HeLa cells are human, but other human cells also did not allow resistance to BFA, showing that this is not a species effect (Viktorova *et al.*, 2015).

To obtain more information on how the DGAT1 inhibitors A922500 and BetA, as well as ITZ, can block HPeV1 and CAV9 replication, we attempted to produce drug resistant mutants. These attempts were unsuccessful. 7 passages were performed with increasing concentrations of the drugs, as done in one of the poliovirus BFA experiments, where only 5 passages were performed and it was expected that this should allow mutants to be produced (Crotty *et al.*, 2004). There are several reasons why the experiment may have been unsuccessful. One is that none of the other drugs were as effective against the viruses as BFA was against CAV9, and this may have reduced the selective pressure. In addition, more care could have been taken to establish the optimal starting conditions for the passaging, so that a too high drug concentration was not used. Simply performing more passages may also have been eventually successful. A more interesting reason could be that, as for BFA on Vero cells, there was a cell-type restriction which did not allow resistant mutants to be generated (Viktorova *et al.*, 2015). This could be overcome by attempting a similar experiment with different cells. It could also be that it is not possible for mutants to be selected because the virus host cell target of the drug is essential and no virus mutants can adapt to different pathways, which would be the optimal scenario for a drug based on a cellular target.

The work on BFA, which targets the cellular target GBF1, shows that it can be easy, in the correct cells, for a virus to adapt to the presence of the drug and weakens the idea that a cell target may be less susceptible to selecting drug resistant mutants. However, as we find out more

about how viruses interact with the cell, we may be able to work out ways of reducing this possibility.

CHAPTER SIX
GENERAL DISCUSSION

Picornaviruses are non-enveloped, positive sense single-stranded RNA viruses which cause many diseases ranging from slight illness to fatal meningitis and encephalitis. There is no effective human vaccine for picornaviruses except for poliovirus and hepatitis A virus and no efficient drug treatment is currently available (van der Schaar et al., 2013). Human parechoviruses (HPeVs) can cause serious diseases but have been studied relatively little and are also genetically diverse from several picornaviruses. We therefore need to understand the details of virus replication, such as the changes to the host cell which occur during HPeV infection, which components of the secretory system are affected by infection and which virus proteins are needed to generate replication complexes to improve the opportunities to develop antiviral drugs (van der Linden et al., 2015). The aim of our studies was therefore to understand the effects of HPeV infection on the secretory system and the origin of HPeV replication complexes (chapter 3). During our work we discovered that not only does the HPeV 2C protein localise to lipid droplets (LDs) as previously reported (Krogerus et al. 2007), but it also aggregates these into large complexes. This led to a detailed study of this protein to find the basis of this aggregation and LD localisation (chapter 4). The possible involvement of LDs in HPeV replication then led to work to assess LDs as possible cellular targets for drugs against HPeV infection (chapter 5). The main findings are summarised below.

Studies of several different positive-strand RNA viruses have suggested the ER, Golgi, endosomes or lysosomes as sources for structures needed for replication (Salonen *et al.*, 2005; Suhy *et al.*, 2000). These membrane structures are used for several reasons, such as concentrating components needed for virus replication, holding replication complexes in place, and hiding dsRNA and so avoiding host defence mechanisms which respond to dsRNA (Miller and Krijnse-Locker, 2008; Sasaki et al., 2012). Some picornaviruses change the distribution of secretory pathway compartment and our results show that HPeV1 infection affects the ER, Golgi and ERGIC in the HT29 cell line. ER (PDI was used as the marker) almost completely

disappears in infected cells, while the number of spots of ERGIC-53 (ERGIC marker) is reduced. The Golgi (GM130 was used as a cis-Golgi marker) is also very much reduced by infection. We also found that infection with the *Enterovirus* CAV9 leads to reduction in staining and dispersal of the GM130 marker. The Golgi pattern seen in CAV9-infected cells is similar to that in previous work on enteroviruses (Cornell et al., 2006; Mousnier et al., 2014). In fact, disruption of the Golgi by infection seems to be a common feature for picornaviruses as several diverse picornaviruses have this effect (Gazina et al., 2002; Midgley et al., 2013). For another *Enterovirus*, rhinovirus 1A, it has been reported that disrupted Golgi membranes form virus replication complexes (Quiner and Jackson, 2010). We found for HPeV1 that there was no co-localisation between dsRNA, marking the site of replication, and GM130 marking the Golgi and this suggests that these viruses have a different requirement for Golgi material. However, previously it was reported that HPeV1 replication complexes show partial co-localisation with the trans-Golgi marker GalT (Krogerus et al., 2003). The rhinovirus 1A work used the Golgi cisternae marker Giantin (Quiner and Jackson, 2010). A wider panel of antibodies needs to be used to study the relationship between the Golgi and HPeV infection, as trans-Golgi and/or Golgi cisternae may be involved in replication complex formation, but not cis-Golgi.

A surprising finding was the almost complete loss of the ER in HPeV-infected cells. This is quite different from infection by two genetically distinct picornaviruses, FMDV and rhinovirus 1A, where there is no change seen in infected cells (Quiner and Jackson, 2010; Midgley et al., 2013; Wang et al., 2012). Infection by both these viruses causes some disruption of the ERGIC. The FMDV result is interpreted as showing an involvement of ER exit sites in formation of the virus replication complex. Diverting the normal flow of vesicles from the ER to ERGIC/Golgi would lead to a reduction in these compartments (Midgley et al., 2013). Our observation of almost complete loss of the ER may suggest that retrograde movement of vesicles from the Golgi/ERGIC to reform the ER, is disrupted, leading to less material in the ER. This is consistent

with the loss of COPI in HPeV-infected cells, as COPI coated vesicles are involved in retrograde traffic back to the ER (Gazina et al., 2002).

2B, 2BC/2C and 3A are the main non-structural proteins that affect the secretory pathway in picornaviruses. 2B, 2BC or 3A (but not 2C) of poliovirus disrupt protein trafficking and cell surface protein expression, while expression of 2B and 2C or of the 2BC precursor (but not 3A) is sufficient to inhibit trafficking between the ER and Golgi in FMDV (Sweeney et al., 2010; Midgely et al., 2013). In For HPeV1 we found that expression of 2C greatly affects all these compartments, giving similar results to the effects of infection. 3A also has an effect on some of them. 2C also had a major effect on lysosomes, suggesting that this protein is probably responsible for remodelling the secretory system in infected cells. There was some co-localisation of 2B with the ER and lysosomes and 3A with Golgi, ERGIC and lysosomes. We found a clear co-localisation between 2BC and 2C with LDs and these proteins caused large foci or aggregates of LDs.

When expressed individually, the non-structural proteins 2B and 3A had a similar reticular pattern in the cytoplasm, partially corresponding to ER (2B) or ERGIC and Golgi (3A). This is not surprising as both these proteins have transmembrane domains and amphipathic helices which locate them to membranes (Martinez-Gil et al., 2011). Surprisingly, 2A is found throughout the cell with no clear association with membranes although it is also predicted to have a transmembrane domain (Hughes and Stanway, 2000). 2C had the most distinctive distribution, large spots in the cytoplasm. This was suggested to be due to localisation to lipid droplets (LDs) (Krogerus et al., 2007). 2BC seemed to have a similar distribution but with a faint diffusion.

The interaction between 2C/2BC and LDs led us to study LDs further. Initially we investigated the effect of HPeV infection on lipids using BODIPY 500/510 C4-C9 long chain. There was little effect in HPeV-infected cells, and also in cells infected with CAV9 used as a comparison.

The non-structural proteins of HPeV1 were then used. Interestingly we found that 2A seems to accumulate fatty acids around the nuclei, while there is some co-localisation of FAs with 2B and 3A. In the case of 2C some of the fatty acid stain is located in foci and these correspond to the concentrations of 2C. This adds further weight to the idea that 2C is associating with fatty acid/lipid structures. It has been reported that inhibition of fatty acid synthesis inhibits HCV replication, maturation and release of HCV (Syed et al., 2010). NS5B of HCV interacts with fatty acid synthase and contributes to HCV replication (Huang et al., 2013).

We investigated the possible effect of HPeV1 and CAV9 on LD. In cells infected with HPeV, late in infection LDs become more prominent. In contrast LDs in CAV9-infected cells become less prominent later in infection. This suggests that replication of these viruses, belonging to different *Picornaviridae* genera, has a different requirement for LDs. We found that the ability of 2C to interact with LDs does not depend on the ATPase activity (Sweeney et al., 2010), nor on the N-terminal amphipathic helix found to be involved in membrane interactions in other picornaviruses (Echeverri and Dasgupta, 1995; Echeverri et al., 1998). Instead, we found that amino acids 75-86 of 2C play an important role in the LD localisation as deletion of amino acids 1-74 gives a mutant 2C which can localise to LDs, but deletion of 1-86 destroys this ability. This region is part of a novel amphipathic helix which is conserved in another *Parechovirus* species *Ljungan virus*.

Several viruses seem to use or manipulate LDs during infection, but these organelles have been largely unstudied in picornavirus infections. The best-studied virus with close ties to host LDs is HCV. In HCV-infected cells, the C protein localise to LDs which may be involved in assembly. HCV assembly occurs close to LDs (Vogt *et al.*, 2013). An amphipathic helix motif in C protein (D2 domain) has strong similarities to LD-binding domains (Herker and Ott, 2012).

Dengue virus decreased LD number during infection and due to autophagy-dependent lipolysis to release free fatty acid (Heaton and Randall, 2010; Herker and Ott, 2012). The C protein of

Dengue virus (DENV) accumulates on the surface and localises to LDs (Herker and Ott, 2012; Liu *et al.*, 2010). The rotavirus protein NSP4 contributes to LD metabolism using an autophagy pathway (Cheung *et al.*, 2010; Herker *et al.*, 2010). Several diverse viruses therefore exploit LDs during replication.

We investigated the effect of drugs which target lipid droplet formation and lipid homeostasis on HPeV replication. We demonstrated that drugs which target the enzyme DGAT1, which is involved in LD formation, have a potent effect on HPeV replication, but were less effective against CAV9. Our results suggest that blocking LD formation could be an important strategy for the treatment of HPeV infection. DGAT1 is a potential target for drugs against other viruses. DGAT1 forms a complex with the HCV NS5A protein and facilitates the interaction between these viral proteins (Camus *et al.*, 2013). Production of infectious viral particles of HCV is reduced with cells treated with the DGAT1 inhibitor A922500. Rotavirus infection is affected by both A922500 and BetA, which both target DGAT1 (Crawford and Desselberger, 2016). Our results add to the idea that drugs interfering with LDs could be useful antiviral agents.

Our results show that HPeV 2C is a major player in remodelling the secretory system and in interacting with LDs. Our drug studies showed that LDs are important in HPeV replication as drugs which target them inhibit the virus. The work described in this thesis therefore has potentially laid the foundations for the development of effective antiviral agents against these important human pathogens.

Future Work

The work has highlighted several differences between the intracellular events which occur in HPeV-infected cells and in cells infected with other viruses, such as enteroviruses and FMDV. HPeV infection has previously been shown have a different requirement for COPI coats from enteroviruses and coronaviruses (Gazina *et al.*, 2002). It is clear that these intracellular events need to be studied further to understand HPeV infection and develop useful drugs. Infection with

poliovirus or transfection of poliovirus 3A protein blocks ER-Golgi protein transport (Choe *et al.*, 2005; Richards *et al.*, 2014). PV proteins 2B protein localises to vesicles containing Sec13 and Sec31, both of which are components of the COPII vesicles. (den Boon *et al.*, 2010). The formation of enterovirus replication organelles also specifically requires COPI (Morosky *et al.*, 2016). Poliovirus 3A protein binds GBF1 and modulates recruitment of Arf1 effectors to favour phosphatidylinositol 4-kinase (PI4K) over COPI components. It may also inhibit ER-to-Golgi transport by stabilizing Arf1-GDP-GBF1 complexes, reducing the supply of Arf1-GTP for COPI coats. This creates membranes lacking COPI and enriched for PI4P, which promotes membrane binding of viral RNA-dependent RNA polymerases and formation of the viral replication complex (Midgley *et al.*, 2013; Pierini *et al.*, 2009). In FMDV, 2B plus 2C, or the 2BC precursor (but not 3A) can block trafficking of proteins between the ER and Golgi and their expression on the cell surface in FDMV (Sweeney *et al.*, 2010). The requirement of HPeV for molecules such as GBF1 and PI4K, as well as COPI and COPII coats needs to be studied further. This could be done using siRNA to knock-down the appropriate molecules and investigate the effect on virus replication. A wider panel of antibodies could also be useful, to probe the effect of infection on some of these molecules.

A major focus of the study was the HPeV 2C protein. In other picornaviruses this protein seems to have a number of different functions, including RNA binding, helicase activity and membrane rearrangement, and could be a useful target for new drugs (Ulferts *et al.*, 2016). One limitation in our studies is the lack of an antibody against HPeV 2C and generating a useful antibody will allow the location of 2C to be established in the infected cell, to find if it is present in replication complexes or demonstrate interactions with other proteins for instance. This cannot be achieved with EGFP/mCherry-2C as we find that expression of these prevents infection of the cell. Interactions with other molecules should also be probed by using mass spectrometry to identify

novel cellular proteins which interact with 2C and then explore how these may contribute to replication through co-localisation studies and siRNA knock-down.

LDs seem to be important for HPeV replication and their role should be studied more fully, again by siRNA knock-down of critical components, such as DGAT1 and ADRP. The interaction between HPeV 2C and LDs may involve a novel amphipathic helix in 2C, located between amino acids 74 and 91. This should be explored further to confirm if it sufficient to allow LD binding by producing shorter constructs and by finding the key amino acids by making point mutants, as done for the HCV NS4B amphipathic helix (Tanaka et al., 2013). As well as doing this by transfecting EGFP/mCherry constructs, point mutations should also be introduced into the virus to investigate the effect on replication.

The work in chapter 5 shows that drugs targeting LDs could be useful against HPeV infection and a wider panel of drugs which affect LDs and lipid metabolism in general should be tested to find more candidates (Crawford and Desselberger, 2016). Selection of drug resistant mutants against A922500 and BetA should be retried using different conditions, to confirm they cannot be produced or identify mutations which should give insights into how the drugs function.

These experiments should greatly increase our understanding of HPeV replication and lead to the identification of ways to treat infections by these important pathogens.

REFERENCES

- Acheson, N. H. (2007) Fundamentals of molecular virology. Danvers: John Wiley & Sons, Inc.
- Adams, M., Lefkowitz, E., King, A., Bamford, D., Breitbart, M., Davison, A., Ghabrial, S., Gorbalenya, A., Knowles, N. and Krell, P. (2015) Ratification vote on taxonomic proposals to the International Committee on Taxonomy of Viruses (2015). *Arch Virol*, **160**, 1837-50.
- Adams, M. J., King, A. M. and Carstens, E. B. (2013) Ratification vote on taxonomic proposals to the International Committee on Taxonomy of Viruses (2013). *Arch Virol*, **158**, 2023-30.
- Adams, M. J., Lefkowitz, E. J., King, A. M. and Carstens, E. B. (2014) Ratification vote on taxonomic proposals to the International Committee on Taxonomy of Viruses (2014). *Arch Virol*, **159**, 2831-41.
- Adams, M. J., Lefkowitz, E. J., King, A. M., Harrach, B., Harrison, R. L., Knowles, N. J., Kropinski, A. M., Krupovic, M., Kuhn, J. H., Mushegian, A. R., Nibert, M., Sabanadzovic, S., Sanfacon, H., Siddell, S. G., Simmonds, P., Varsani, A., Zerbini, F. M., Gorbalenya, A. E. and Davison, A. J. (2016) Ratification vote on taxonomic proposals to the International Committee on Taxonomy of Viruses (2016). *Arch Virol*, **161**, 2921-49.
- Adler J, Parmryd I. (2010) Quantifying colocalization by correlation: the Pearson correlation coefficient is superior to the Mander's overlap coefficient. *Cytometry A*, **77**, 733-42.
- Agnello, V., Abel, G., Elfahal, M., Knight, G. B. and Zhang, Q. X. (1999) Hepatitis C virus and other flaviviridae viruses enter cells via low density lipoprotein receptor. *Proc Natl Acad Sci U S A*, **96**, 12766-71.
- Al-Sunaidi, M., Williams, C. H., Hughes, P. J., Schnurr, D. P. and Stanway, G. (2007) Analysis of a new human parechovirus allows the definition of parechovirus types and the identification of RNA structural domains. *J Virol*, **81**, 1013-21.
- Appenzeller-Herzog, C. and Hauri, H.-P. (2006) The ER-Golgi intermediate compartment (ERGIC): in search of its identity and function. *J Cell Sci*, **119**, 2173-83.
- Arita, M., Kojima, H., Nagano, T., Okabe, T., Wakita, T. and Shimizu, H. (2011) Phosphatidylinositol 4-kinase III beta is a target of enviroxime-like compounds for antipoliiovirus activity. *J Virol*, **85**, 2364-72.
- Baker, A., Carrier, D. J., Schaedler, T., Waterham, Hans R., van Roermund, Carlo W. and Theodoulou, Frederica L. (2015) Peroxisomal ABC transporters: functions and mechanism. *Biochem Soc Trans*, **43**, 959-65.
- Banerjee, R., Weidman, M. K., Echeverri, A., Kundu, P. and Dasgupta, A. (2004) Regulation of poliovirus 3C protease by the 2C polypeptide. *J Virol*, **78**, 9243-56.
- Barlowe, C. and Helenius, A. (2016) Cargo Capture and Bulk Flow in the Early Secretory Pathway. *Annu Rev Cell Dev Biol*, **32**, 197-22
- Barrero-Villar, M., Barroso-González, J., Cabrero, J., Gordón-Alonso, M., Álvarez-Losada, S., Muñoz-Fernandez, M., Sánchez-Madrid, F. and Valenzuela-Fernández, A. (2008) PI4P5-kinase Ia is required for efficient HIV-1 entry and infection of T cells. *J Immunol*, **181**, 6882-88.
- Behnia, R. and Munro, S. (2005) Organelle identity and the signposts for membrane traffic. *Nature*, **438**, 597-604.
- Beller, M., Sztalryd, C., Southall, N., Bell, M., Jäckle, H., Auld, D. S. and Oliver, B. (2008) COPI complex is a regulator of lipid homeostasis. *PLoS Biol*, **6**, e292.
- Belov, G. A. (2014) Modulation of lipid synthesis and trafficking pathways by picornaviruses. *Curr Opin Virol*, **9**, 19-23.
- Belov, G. A., Feng, Q., Nikovics, K., Jackson, C. L. and Ehrenfeld, E. (2008) A critical role of a cellular membrane traffic protein in poliovirus RNA replication. *PLoS Pathog*, **4**, e1000216.
- Belsham, G. J. and Normann, P. (2008) Dynamics of picornavirus RNA replication within infected cells. *J Gen Virol*, **89**, 485-93.
- Benschop, K. S., de Vries, M., Minnaar, R. P., Stanway, G., van der Hoek, L., Wolthers, K. C. and Simmonds, P. (2010) Comprehensive full-length sequence analyses of human parechoviruses: diversity and recombination. *J Gen Virol*, **91**, 145-54.

- Benschop, K. S., Schinkel, J., Minnaar, R. P., Pajkrt, D., Spanjerberg, L., Kraakman, H. C., Berkhout, B., Zaaijer, H. L., Beld, M. G. and Wolthers, K. C. (2006) Human parechovirus infections in Dutch children and the association between serotype and disease severity. *Clin Infect Dis*, **42**, 204-10.
- Bianco, A., Reghellin, V., Donnici, L., Fenu, S., Alvarez, R., Baruffa, C., Peri, F., Pagani, M., Abrignani, S., Neddermann, P. and De Francesco, R. (2012) Metabolism of Phosphatidylinositol 4-Kinase III α -Dependent PI4P Is Subverted by HCV and Is Targeted by a 4-Anilino Quinazoline with Antiviral Activity. *PLoS Pathog*, **8**, e1002576.
- Bickel, P. E., Tansey, J. T. and Welte, M. A. (2009) PAT proteins, an ancient family of lipid droplet proteins that regulate cellular lipid stores. *Biochim Biophys Acta (BBA)*, **1791**, 419-40.
- Boivin, G., Abed, Y. and Boucher, F. D. (2005) Human parechovirus 3 and neonatal infections. *Emerg Infect Dis*, **11**, 103-05.
- Bonderoff, J. M., Larey, J. L. and Lloyd, R. E. (2008) Cleavage of poly(A)-binding protein by poliovirus 3C proteinase inhibits viral internal ribosome entry site-mediated translation. *J Virol*, **82**, 9389-99.
- Boonyakiat, Y., Hughes, P. J., Ghazi, F. and Stanway, G. (2001) Arginine-glycine-aspartic acid motif is critical for human parechovirus 1 entry. *J Virol*, **75**, 10000-4.
- Boros, A., Nemes, C., Pankovics, P., Kapusinszky, B., Delwart, E. and Reuter, G. (2012) Porcine teschovirus in wild boars in Hungary. *Arch Virol*, **157**, 1573-8.
- Bostrom, P., Andersson, L., Rutberg, M., Perman, J., Lidberg, U., Johansson, B. R., Fernandez-Rodriguez, J., Ericson, J., Nilsson, T., Boren, J. and Olofsson, S. O. (2007) SNARE proteins mediate fusion between cytosolic lipid droplets and are implicated in insulin sensitivity. *Nat Cell Biol*, **9**, 1286-93.
- Brocard, C. and Hartig, A. (2006) Peroxisome targeting signal 1: Is it really a simple tripeptide? *Biochim Biophys Acta (BBA)*, **1763**, 1565-73.
- Buenz, E. J. and Howe, C. L. (2006) Picornaviruses and cell death. *Trends Microbiol*, **14**, 28-36.
- Camus, G., Herker, E., Modi, A. A., Haas, J. T., Ramage, H. R., Farese, R. V., Jr. and Ott, M. (2013) Diacylglycerol acyltransferase-1 localizes hepatitis C virus NS5A protein to lipid droplets and enhances NS5A interaction with the viral capsid core. *J Biol Chem*, **288**, 9915-23.
- Carter, J. and Saunders, V. A. (2007) *Virology: principles and applications*. John Wiley & Sons.
- Cases, S., Smith, S. J., Zheng, Y.-W., Myers, H. M., Lear, S. R., Sande, E., Novak, S., Collins, C., Welch, C. B. and Lusis, A. J. (1998) Identification of a gene encoding an acyl CoA: diacylglycerol acyltransferase, a key enzyme in triacylglycerol synthesis. *Proc Natl Acad Sci U S A*, **95**, 13018-23.
- Chang, J. T., Yang, C. S., Chen, Y. S., Chen, B. C., Chiang, A. J., Chang, Y. H., Tsai, W. L., Lin, Y. S., Chao, D. and Chang, T. H. (2015) Genome and infection characteristics of human parechovirus type 1: the interplay between viral infection and type I interferon antiviral system. *PLoS One*, **10**, e0116158.
- Cherry, S., Kunte, A., Wang, H., Coyne, C., Rawson, R. B. and Perrimon, N. (2006) COPI activity coupled with fatty acid biosynthesis is required for viral replication. *PLoS Pathog*, **2**, e102.
- Cheung, W., Gill, M., Esposito, A., Kaminski, C. F., Courousse, N., Chwetzoff, S., Trugnan, G., Keshavan, N., Lever, A. and Desselberger, U. (2010) Rotaviruses associate with cellular lipid droplet components to replicate in viroplasm, and compounds disrupting or blocking lipid droplets inhibit viroplasm formation and viral replication. *J Virol*, **84**, 6782-98.
- Choe, S. S., Dodd, D. A. and Kirkegaard, K. (2005) Inhibition of cellular protein secretion by picornaviral 3A proteins. *Virology*, **337**, 18-29.
- Chukkapalli, V., Heaton, N. S. and Randall, G. (2012) Lipids at the interface of virus-host interactions. *Curr Opin Microbiol*, **15**, 512-8.
- Chukkapalli, V., Hogue, I. B., Boyko, V., Hu, W.-S. and Ono, A. (2008) Interaction between the Human Immunodeficiency Virus Type 1 Gag Matrix Domain and Phosphatidylinositol-(4,5)-Bisphosphate Is Essential for Efficient Gag Membrane Binding. *J Virol*, **82**, 2405-17.
- Colanzi, A., Grimaldi, G., Catara, G., Valente, C., Cericola, C., Liberali, P., Ronci, M., Lalioti, V. S., Bruno, A. and Beccari, A. R. (2013) Molecular mechanism and functional role of brefeldin A-mediated ADP-ribosylation of CtBP1/BARS. *Proc Natl Acad Sci U S A*, **110**, 9794-99.
- Cornell, C. T., Kiesses, W. B., Harkins, S. and Whitton, J. L. (2006) Inhibition of protein trafficking by coxsackievirus b3: multiple viral proteins target a single organelle. *J Virol*, **80**, 6637-47.

- Coyne, C. B. and Bergelson, J. M. (2006) Virus-induced Abl and Fyn kinase signals permit coxsackievirus entry through epithelial tight junctions. *Cell*, **124**, 119-31.
- Crawford, S. E. and Desselberger, U. (2016) Lipid droplets form complexes with viroplasm and are crucial for rotavirus replication. *Curr Opin Virol*, **19**, 11-15.
- Crotty, S., Saleh, M.-C., Gitlin, L., Beske, O. and Andino, R. (2004) The Poliovirus Replication Machinery Can Escape Inhibition by an Antiviral Drug That Targets a Host Cell Protein. *J Virol*, **78**, 3378-86.
- D'Arcangelo, J. G., Stahmer, K. R. and Miller, E. A. (2013) Vesicle-mediated export from the ER: COPII coat function and regulation. *Biochim Biophys Acta*, **1833**, 2464-72.
- de Jong, A. S., de Mattia, F., Van Dommelen, M. M., Lanke, K., Melchers, W. J., Willems, P. H. and van Kuppeveld, F. J. (2008) Functional analysis of picornavirus 2B proteins: effects on calcium homeostasis and intracellular protein trafficking. *J Virol*, **82**, 3782-90.
- De Palma, A. M., Vliegen, I., De Clercq, E. and Neyts, J. (2008) Selective inhibitors of picornavirus replication. *Med Res Rev*, **28**, 823-84.
- den Boon, J. A., Diaz, A. and Ahlquist, P. (2010) Cytoplasmic viral replication complexes. *Cell Host Microbe*, **8**, 77-85.
- Deszcz, L., Cencic, R., Sousa, C., Kuechler, E. and Skern, T. (2006) An antiviral peptide inhibitor that is active against picornavirus 2A proteinases but not cellular caspases. *J Virol*, **80**, 9619-27.
- Donnelly, M. L., Luke, G., Mehrotra, A., Li, X., Hughes, L. E., Gani, D. and Ryan, M. D. (2001) Analysis of the aphthovirus 2A/2B polyprotein 'cleavage' mechanism indicates not a proteolytic reaction, but a novel translational effect: a putative ribosomal 'skip'. *J Gen Virol*, **82**, 1013-25.
- Dorobantu, C. M., Ford-Siltz, L. A., Sittig, S. P., Lanke, K. H., Belov, G. A., van Kuppeveld, F. J. and van der Schaar, H. M. (2015) GBF1-and ACBD3-independent recruitment of PI4KIII β to replication sites by rhinovirus 3A proteins. *J Virol*, **89**, 1913-18.
- Dotzauer, A. and Kraemer, L. (2012) Innate and adaptive immune responses against picornaviruses and their counteractions: An overview. *World J Virol*, **1**, 91-107.
- Dunn, G., Klapsa, D., Wilton, T., Stone, L., Minor, P. D. and Martin, J. (2015) Twenty-eight years of poliovirus replication in an immunodeficient individual: Impact on the Global Polio Eradication Initiative. *PLoS Pathog*, **11**, e1005114.
- Dunn K. W. , Kamocka M. M. and McDonald John H. (2011) A practical guide to evaluating colocalization in biological microscopy. *Am J Physiol Cell Physiol*, **300**, 723-42
- Echeverri, A., Banerjee, R. and Dasgupta, A. (1998) Amino-terminal region of poliovirus 2C protein is sufficient for membrane binding. *Virus Res*, **54**, 217-23.
- Echeverri, A. C. and Dasgupta, A. (1995) Amino Terminal Regions of Poliovirus 2C Protein Mediate Membrane Binding. *Virology*, **208**, 540-53.
- English, A. R. and Voeltz, G. K. (2013) Endoplasmic reticulum structure and interconnections with other organelles. *Cold Spring Harb Perspect Biol*, **5**, a013227.
- Evans, D. J. and Almond, J. W. (1998) Cell receptors for picornaviruses as determinants of cell tropism and pathogenesis. *Trends Microbiol*, **6**, 198-202.
- Ewers, H. and Helenius, A. (2011) Lipid-mediated endocytosis. *Cold Spring Harb Perspect Biol*, **3**, a004721.
- Fan, P., Li, X., Sun, S., Su, W., An, D., Gao, F., Kong, W. and Jiang, C. (2015) Identification of a common epitope between enterovirus 71 and human MED25 proteins which may explain virus-associated neurological disease. *Viruses*, **7**, 1558-77.
- Filman, D. J., Syed, R., Chow, M., Macadam, A. J., Minor, P. D. and Hogle, J. M. (1989) Structural factors that control conformational transitions and serotype specificity in type 3 poliovirus. *Embo j*, **8**, 1567-79.
- Fry, E., Acharya, R. and Stuart, D. (1993) Methods used in the structure determination of foot-and-mouth disease virus. *Acta Crystallogr A*, **49 (Pt 1)**, 45-55.
- Fujimoto, T., Ohsaki, Y., Cheng, J., Suzuki, M. and Shinohara, Y. (2008) Lipid droplets: a classic organelle with new outfits. *Histochem Cell Biol*, **130**, 263-79.
- Fukasawa, M. (2010) Cellular lipid droplets and hepatitis C virus life cycle. *Biol Pharm Bull*, **33**, 355-9.
- Funston, G. M., Kallioinen, S. E., de Felipe, P., Ryan, M. D. and Iggo, R. D. (2008) Expression of heterologous genes in oncolytic adenoviruses using picornaviral 2A sequences that trigger ribosome skipping. *J Gen Virol*, **89**, 389-96.

- Gao, Q., Yuan, S., Zhang, C., Wang, Y., Wang, Y., He, G., Zhang, S., Altmeyer, R. and Zou, G. (2015) Discovery of itraconazole with broad-spectrum in vitro antienterovirus activity that targets nonstructural protein 3A. *Antimicrob Agents Chemother*, **59**, 2654-65.
- Garg, A. and Agarwal, A. K. (2009) Lipodystrophies: Disorders of adipose tissue biology. *Biochim Biophys Acta*, **1791**, 507-13.
- Gaunt, E. R., Zhang, Q., Cheung, W., Wakelam, M. J., Lever, A. M. and Desselberger, U. (2013) Lipidome analysis of rotavirus-infected cells confirms the close interaction of lipid droplets with viroplasms. *J Gen Virol*, **94**, 1576-86.
- Gazina, E. V., Mackenzie, J. M., Gorrell, R. J. and Anderson, D. A. (2002) Differential Requirements for COPI Coats in Formation of Replication Complexes among Three Genera of Picornaviridae. *J Virol*, **76**, 11113-22.
- Geller, R., Vignuzzi, M., Andino, R. and Frydman, J. (2007) Evolutionary constraints on chaperone-mediated folding provide an antiviral approach refractory to development of drug resistance. *Genes Dev*, **21**, 195-205.
- Ghazi, F., Hughes, P. J., Hyypia, T. and Stanway, G. (1998) Molecular analysis of human parechovirus type 2 (formerly echovirus 23). *J Gen Virol*, **79** (Pt 11), 2641-50.
- Gillon, A. D., Latham, C. F. and Miller, E. A. (2012) Vesicle-mediated ER export of proteins and lipids. *Biochim Biophys Acta*, **1821**, 1040-9.
- Glick, B. S. (2000) Organization of the Golgi apparatus. *Curr Opin Cell Biol*, **12**, 450-456.
- Glick, B. S., Elston, T. and Oster, G. (1997) A cisternal maturation mechanism can explain the asymmetry of the Golgi stack. *FEBS Lett*, **414**, 177-81.
- Glick, B. S. and Nakano, A. (2009) Membrane traffic within the Golgi apparatus. *Annu Rev Cell Dev Biol*, **25**, 113-32.
- Goldstaub, D., Gradi, A., Bercovitch, Z., Grosman, Z., Nophar, Y., Luria, S., Sonenberg, N. and Kahana, C. (2000) Poliovirus 2A Protease Induces Apoptotic Cell Death. *Mol Cell Biol*, **20**, 1271-77.
- Goodwin, S., Tuthill, T. J., Arias, A., Killington, R. A. and Rowlands, D. J. (2009) Foot-and-mouth disease virus assembly: processing of recombinant capsid precursor by exogenous protease induces self-assembly of pentamers in vitro in a myristoylation-dependent manner. *J Virol*, **83**, 11275-82.
- Gopalkrishna, V., Patil, P. R., Patil, G. P. and Chitambar, S. D. (2012) Circulation of multiple enterovirus serotypes causing hand, foot and mouth disease in India. *J Med Microbiol*, **61**, 420-5.
- Gower, T. L. and Graham, B. S. (2001) Antiviral activity of lovastatin against respiratory syncytial virus in vivo and in vitro. *Antimicrob Agents Chemother*, **45**, 1231-7.
- Grubman, M. J. and Baxt, B. (2004) Foot-and-mouth disease. *Clinical microbiology reviews*, **17**, 465-493.
- Guo, Y., Cordes, K. R., Farese, R. V. and Walther, T. C. (2009) Lipid droplets at a glance. *J Cell Sci*, **122**, 749-52.
- Harris, C. A., Haas, J. T., Streeper, R. S., Stone, S. J., Kumari, M., Yang, K., Han, X., Brownell, N., Gross, R. W., Zechner, R. and Farese, R. V., Jr. (2011) DGAT enzymes are required for triacylglycerol synthesis and lipid droplets in adipocytes. *J Lipid Res*, **52**, 657-67.
- Harris, J. R. and Racaniello, V. R. (2005) Amino acid changes in proteins 2B and 3A mediate rhinovirus type 39 growth in mouse cells. *J Virol*, **79**, 5363-73.
- Harvala, H., Calvert, J., Van Nguyen, D., Clasper, L., Gadsby, N., Molyneaux, P., Templeton, K., McWilliams Leitch, C. and Simmonds, P. (2014) Comparison of diagnostic clinical samples and environmental sampling for enterovirus and parechovirus surveillance in Scotland, 2010 to 2012. *Euro Surveill*, **19**, 14-22.
- Harvala, H., Robertson, I., McWilliam Leitch, E. C., Benschop, K., Wolthers, K. C., Templeton, K. and Simmonds, P. (2008) Epidemiology and clinical associations of human parechovirus respiratory infections. *J Clin Microbiol*, **46**, 3446-53.
- Hauri, H.-P., Kappeler, F., Andersson, H. and Appenzeller, C. (2000) ERGIC-53 and traffic in the secretory pathway. *J Cell Sci*, **113**, 587-96.
- Heaton, N. S., Perera, R., Berger, K. L., Khadka, S., Lacount, D. J., Kuhn, R. J. and Randall, G. (2010) Dengue virus nonstructural protein 3 redistributes fatty acid synthase to sites of viral replication and increases cellular fatty acid synthesis. *Proc Natl Acad Sci U S A*, **107**, 17345-50.

- Heaton, N. S. and Randall, G. (2010) Dengue virus-induced autophagy regulates lipid metabolism. *Cell Host Microbe*, **8**, 422-32.
- Heaton, N. S. and Randall, G. (2011) Multifaceted roles for lipids in viral infection. *Trends Microbiol*, **19**, 368-75.
- Heikkila, O., Susi, P., Stanway, G. and Hyypia, T. (2009) Integrin alphaVbeta6 is a high-affinity receptor for coxsackievirus A9. *J Gen Virol*, **90**, 197-204.
- Hendry, E., Hatanaka, H., Fry, E., Smyth, M., Tate, J., Stanway, G., Santti, J., Maaronen, M., Hyypia, T. and Stuart, D. (1999) The crystal structure of coxsackievirus A9: new insights into the uncoating mechanisms of enteroviruses. *Structure*, **7**, 1527-38.
- Herker, E., Harris, C., Hernandez, C., Carpentier, A., Kaehlcke, K., Rosenberg, A. R., Farese, R. V., Jr. and Ott, M. (2010) Efficient hepatitis C virus particle formation requires diacylglycerol acyltransferase-1. *Nat Med*, **16**, 1295-8.
- Herker, E. and Ott, M. (2012) Emerging role of lipid droplets in host/pathogen interactions. *J Biol Chem*, **287**, 2280-7.
- Hsu, N. Y., Ilnytska, O., Belov, G., Santiana, M., Chen, Y. H., Takvorian, P. M., Pau, C., van der Schaar, H., Kaushik-Basu, N., Balla, T., Cameron, C. E., Ehrenfeld, E., van Kuppeveld, F. J. and Altan-Bonnet, N. (2010) Viral reorganization of the secretory pathway generates distinct organelles for RNA replication. *Cell*, **141**, 799-811.
- Hu, Y. F., Yang, F., Du, J., Dong, J., Zhang, T., Wu, Z. Q., Xue, Y. and Jin, Q. (2011) Complete genome analysis of coxsackievirus A2, A4, A5, and A10 strains isolated from hand, foot, and mouth disease patients in China revealing frequent recombination of human enterovirus A. *J Clin Microbiol*, **49**, 2426-34.
- Huang, J.-T., Tseng, C.-P., Liao, M.-H., Lu, S.-C., Yeh, W.-Z., Sakamoto, N., Chen, C.-M. and Cheng, J.-C. (2013) Hepatitis C virus replication is modulated by the interaction of nonstructural protein NS5B and fatty acid synthase. *J Virol*, **87**, 4994-04.
- Hughes, P. J., Horsnell, C., Hyypiä, T. and Stanway, G. (1995) The coxsackievirus A9 RGD motif is not essential for virus viability. *J Virol*, **69**, 8035-40.
- Hughes, P. J. and Stanway, G. (2000) The 2A proteins of three diverse picornaviruses are related to each other and to the H-rev107 family of proteins involved in the control of cell proliferation. *J Gen Virol*, **81**, 201-7.
- Hyypiä, T., Horsnell, C., Maaronen, M., Khan, M., Kalkkinen, N., Auvinen, P., Kinnunen, L. and Stanway, G. (1992) A distinct picornavirus group identified by sequence analysis. *Proc Natl Acad Sci U S A*, **89**, 8847-51.
- Hyypia, T., Hovi, T., Knowles, N. J. and Stanway, G. (1997) Classification of enteroviruses based on molecular and biological properties. *J Gen Virol*, **78** (Pt 1), 1-11.
- Hyypia, T. and Stanway, G. (1993) Biology of coxsackie A viruses. *Adv Virus Res*, **42**, 343-373.
- Initiative, G. P. E. (2015) Polio Eradication and Endgame Midterm Review, July 2015. *Geneva, Switzerland: World Health Organization*.
- Inoue, T. and Tsai, B. (2013) How viruses use the endoplasmic reticulum for entry, replication, and assembly. *Cold Spring Harb Perspect Biol*, **5**, a013250.
- Irurzun, A., Perez, L. and Carrasco, L. (1992) Involvement of membrane traffic in the replication of poliovirus genomes: effects of brefeldin A. *Virology*, **191**, 166-75.
- Izquierdo-Useros, N., Lorizate, M., Contreras, F. X., Rodriguez-Plata, M. T., Glass, B., Erkizia, I., Prado, J. G., Casas, J., Fabriàs, G., Kräusslich, H.-G. and Martinez-Picado, J. (2012) Sialyllactose in Viral Membrane Gangliosides Is a Novel Molecular Recognition Pattern for Mature Dendritic Cell Capture of HIV-1. *PLoS Biol*, **10**, e1001315.
- Jackson, C. L. (2009) Mechanisms of transport through the Golgi complex. *J Cell Sci*, **122**, 443-52.
- Jackson, W. T., Giddings, T. H., Jr., Taylor, M. P., Mulinyawe, S., Rabinovitch, M., Kopito, R. R. and Kirkegaard, K. (2005) Subversion of cellular autophagosomal machinery by RNA viruses. *PLoS Biol*, **3**, e156.
- Jamal, S. M. and Belsham, G. J. (2013) Foot-and-mouth disease: past, present and future. *Vet Res*, **44**, 16-30.
- Jiang, P., Liu, Y., Ma, H. C., Paul, A. V. and Wimmer, E. (2014) Picornavirus morphogenesis. *Microbiol Mol Biol Rev*, **78**, 418-37.

- Joki-Korpela, P., Marjomäki, V., Krogerus, C., Heino, J. and Hyypiä, T. (2001) Entry of Human Parechovirus 1. *J Virol*, **75**, 1958-67.
- Ju, X., Yan, Y., Liu, Q., Li, N., Sheng, M., Zhang, L., Li, X., Liang, Z., Huang, F. and Liu, K. (2015) Neuraminidase of influenza A virus binds lysosome-associated membrane proteins directly and induces lysosome rupture. *J Virol*, **89**, 10347-58.
- Jurgeit, A., Moese, S., Roulin, P., Dorsch, A., Lotzerich, M., Lee, W. M. and Greber, U. F. (2010) An RNA replication-center assay for high content image-based quantifications of human rhinovirus and coxsackievirus infections. *Virology*, **7**, 264-77.
- Kalynych, S., Palkova, L. and Plevka, P. (2016) The Structure of Human Parechovirus 1 Reveals an Association of the RNA Genome with the Capsid. *J Virol*, **90**, 1377-86.
- Khatami, A., McMullan, B. J., Webber, M., Stewart, P., Francis, S., Timmers, K. J., Rodas, E., Druce, J., Mehta, B. and Sloggett, N. A. (2014) Sepsis-like disease in infants due to human parechovirus type 3 during an outbreak in Australia. *Clin Infect Dis*, **60**, 228-36.
- Khetsuriani, N., LaMonte-Fowlkes, A., Oberst, S., Pallansch, M. A., Control, C. f. D. and Prevention (2006) Enterovirus surveillance—United States, 1970–2005. *MMWR Surveill Summ*, **55**, 1-20.
- Kiener, T. K., Jia, Q., Lim, X. F., He, F., Meng, T., Chow, V. T. and Kwang, J. (2012) Characterization and specificity of the linear epitope of the enterovirus 71 VP2 protein. *Virology*, **9**, 55-66.
- Kim, S. S., Smith, T. J., Chapman, M. S., Rossmann, M. C., Pevear, D. C., Dutko, F. J., Felock, P. J., Diana, G. D. and McKinlay, M. A. (1989) Crystal structure of human rhinovirus serotype 1A (HRV1A). *J Mol Biol*, **210**, 91-111.
- Kitajima, M. and Gerba, C. P. (2015) Aichi virus 1: environmental occurrence and behavior. *Pathogens*, **4**, 256-68.
- Kitamura, N., Semler, B. L., Rothberg, P. G., Larsen, G. R., Adler, C. J., Dorner, A. J., Emini, E. A., Hanecak, R., Lee, J. J., van der Werf, S., Anderson, C. W. and Wimmer, E. (1981) Primary structure, gene organization and polypeptide expression of poliovirus RNA. *Nature*, **291**, 547-53.
- Klein, K. A. and Jackson, W. T. (2011) Human rhinovirus 2 induces the autophagic pathway and replicates more efficiently in autophagic cells. *J Virol*, **85**, 9651-54.
- Knowles, N. (2016) *The picornavirus home page* [Online]. Last accessed 07/08/2016.
- Knowles, N., Hovi, T., Hyypiä, T., King, A., Lindberg, A., Pallansch, M., Palmenberg, A., Simmonds, P., Skern, T. and Stanway, G. (2012) Picornaviridae. *Virus taxonomy: classification and nomenclature of viruses: ninth report of the international committee on taxonomy of viruses*, 855-80.
- Kolehmainen, P., Jääskeläinen, A., Blomqvist, S., Kallio-Kokko, H., Nuolivirta, K., Helminen, M., Roivainen, M., Lappalainen, M. and Tauriainen, S. (2014) Human parechovirus type 3 and 4 associated with severe infections in young children. *Pediatr Infect Dis J*, **33**, 1109-13.
- Krahmer, N., Farese, R. V. and Walther, T. C. (2013) Balancing the fat: lipid droplets and human disease. *EMBO Molecular Medicine*, **5**, 905-15.
- Krishnaswamy, S. and Rossmann, M. G. (1990) Structural refinement and analysis of Mengo virus. *J Mol Biol*, **211**, 803-44.
- Krogerus, C., Egger, D., Samuilova, O., Hyypia, T. and Bienz, K. (2003) Replication Complex of Human Parechovirus 1. *J Virol*, **77**, 8512-23.
- Krogerus, C., Samuilova, O., Poyry, T., Jokitalo, E. and Hyypia, T. (2007) Intracellular localization and effects of individually expressed human parechovirus 1 non-structural proteins. *J Gen Virol*, **88**, 831-41.
- Lanke, K. H., van der Schaar, H. M., Belov, G. A., Feng, Q., Duijsings, D., Jackson, C. L., Ehrenfeld, E. and van Kuppeveld, F. J. (2009) GBF1, a guanine nucleotide exchange factor for Arf, is crucial for coxsackievirus B3 RNA replication. *J Virol*, **83**, 11940-9.
- Landmann L. (2002) Deconvolution improves colocalization analysis of multiple fluorochromes in 3D confocal data sets more than filtering techniques. *J Microsc*, **208**, 134-47
- Le Lay, S., Hajdúch, E., Lindsay, M. R., Le Liepvre, X., Thiele, C., Ferre, P., Parton, R. G., Kurzchalia, T., Simons, K. and Dugail, I. (2006) Cholesterol-induced caveolin targeting to lipid droplets in adipocytes: a role for caveolar endocytosis. *Traffic*, **7**, 549-61.
- Lee, W. M., Ishikawa, M. and Ahlquist, P. (2001) Mutation of host delta9 fatty acid desaturase inhibits brome mosaic virus RNA replication between template recognition and RNA synthesis. *J Virol*, **75**, 2097-106.

- Lei, X., Sun, Z., Liu, X., Jin, Q., He, B. and Wang, J. (2011) Cleavage of the adaptor protein TRIF by enterovirus 71 3C inhibits antiviral responses mediated by Toll-like receptor 3. *J Virol*, **85**, 8811-8.
- Levy, H. C., Bostina, M., Filman, D. J. and Hogle, J. M. (2010) Catching a virus in the act of RNA release: a novel poliovirus uncoating intermediate characterized by cryo-electron microscopy. *J Virol*, **84**, 4426-41.
- Lewis, J. K., Bothner, B., Smith, T. J. and Siuzdak, G. (1998) Antiviral agent blocks breathing of the common cold virus. *Proc Natl Acad Sci U S A*, **95**, 6774-78.
- Li, C., Wang, J. C.-Y., Taylor, M. W. and Zlotnick, A. (2012) In vitro assembly of an empty picornavirus capsid follows a dodecahedral path. *J Virol*, **86**, 13062-69.
- Lin, J. Y., Chen, T. C., Weng, K. F., Chang, S. C., Chen, L. L. and Shih, S. R. (2009) Viral and host proteins involved in picornavirus life cycle. *J Biomed Sci*, **16**, 103-17.
- Listenberger, L. L., Ostermeyer-Fay, A. G., Goldberg, E. B., Brown, W. J. and Brown, D. A. (2007) Adipocyte differentiation-related protein reduces the lipid droplet association of adipose triglyceride lipase and slows triacylglycerol turnover. *J Lipid Res*, **48**, 2751-61.
- Liu, Y., Wang, C., Mueller, S., Paul, A. V., Wimmer, E. and Jiang, P. (2010) Direct interaction between two viral proteins, the nonstructural protein 2C and the capsid protein VP3, is required for enterovirus morphogenesis. *PLoS Pathog*, **6**, e1001066.
- Liu, Z., Guo, Z., Wang, G., Zhang, D., He, H., Li, G., Liu, Y., Higgins, D., Walsh, A., Shanahan-Prendergast, L. and Lu, J. (2009) Evaluation of the efficacy and safety of a statin/caffeine combination against H5N1, H3N2 and H1N1 virus infection in BALB/c mice. *Eur J Pharm Sci*, **38**, 215-23.
- Luzio, J. P., Pryor, P. R. and Bright, N. A. (2007) Lysosomes: fusion and function. *Nat Rev Mol Cell Biol*, **8**, 622-32.
- Mackenzie, J. M., Khromykh, A. A. and Parton, R. G. (2007) Cholesterol manipulation by West Nile virus perturbs the cellular immune response. *Cell Host Microbe*, **2**, 229-39.
- Martin-Acebes, M., Vazquez-Calvo, A., Caridi, F., Saiz, J.-C. and Sobrino, F. (2013) Lipid Involvement in Viral Infections: Present and Future Perspectives for the Design of Antiviral Strategies. In *Lipid metabolism*, 291– 22. Rijeka, Croatia.
- Martin-Acebes, M. A., Gonzalez-Magaldi, M., Sandvig, K., Sobrino, F. and Armas-Portela, R. (2007) Productive entry of type C foot-and-mouth disease virus into susceptible cultured cells requires clathrin and is dependent on the presence of plasma membrane cholesterol. *Virology*, **369**, 105-18.
- Martin, A. and Lemon, S. M. (2006) Hepatitis A virus: from discovery to vaccines. *Hepatology*, **43**.
- Maynell, L. A., Kirkegaard, K. and Klymkowsky, M. W. (1992) Inhibition of poliovirus RNA synthesis by brefeldin A. *J Virol*, **66**, 1985-94.
- Meester, I., Rosas-Taraco, A. G., Solís-Soto, J. M. and Salinas-Carmona, M. C. (2011) The roles of lipid droplets in human infectious disease. *Rev Port Cardiol*, **13**, 207-16.
- Meisen, I., Dzudzek, T., Ehrhardt, C., Ludwig, S., Mormann, M., Rosenbruck, R., Lumen, R., Kniep, B., Karch, H. and Muthing, J. (2012) The human H3N2 influenza viruses A/Victoria/3/75 and A/Hiroshima/52/2005 preferentially bind to alpha2-3-sialylated monosialogangliosides with fucosylated poly-N-acetyllactosaminyl chains. *Glycobiology*, **22**, 1055-76.
- Mercer, J., Schelhaas, M. and Helenius, A. (2010) Virus entry by endocytosis. *Annu Rev Biochem*, **79**, 803-33.
- Merilahti, P., Koskinen, S., Heikkila, O., Karelehto, E. and Susi, P. (2012) Endocytosis of integrin-binding human picornaviruses. *Adv Virol*, **2012**, 547530-39.
- Midgley, R., Moffat, K., Berryman, S., Hawes, P., Simpson, J., Fullen, D., Stephens, D. J., Burman, A. and Jackson, T. (2013) A role for endoplasmic reticulum exit sites in foot-and-mouth disease virus infection. *J Gen Virol*, **94**, 2636-46.
- Mihaila, R., Nedelcu, L., Fratila, O., Rezi, E. C., Domnariu, C., Ciuca, R., Zaharie, A. V., Olteanu, A., Bera, L., Deac, M. and Mihaila, R. (2009) Lovastatin and fluvastatin reduce viremia and the pro-inflammatory cytokines in the patients with chronic hepatitis C. *Hepatogastroenterology*, **56**, 1704-9.
- Miller, S. and Krijnse-Locker, J. (2008) Modification of intracellular membrane structures for virus replication. *Nat Rev Microbiol*, **6**, 363-74.

- Mirzayan, C. and Wimmer, E. (1992) Genetic analysis of an NTP-binding motif in poliovirus polypeptide 2C. *Virology*, **189**, 547-55.
- Moghaddam, M. G., Ahmad, F. B. H. and Samzadeh-Kermani, A. (2012) Biological activity of betulinic acid: a review. *Pharmacology & Pharmacy*, **3**, 119-23
- Morosky, S., Lennemann, N. J. and Coyne, C. B. (2016) BPIFB6 regulates secretory pathway trafficking and enterovirus replication. *J Virol*, **90**, 5098-107.
- Moscufo, N., Simons, J. and Chow, M. (1991) Myristoylation is important at multiple stages in poliovirus assembly. *J Virol*, **65**, 2372-80.
- Mousnier, A., Swieboda, D., Pinto, A., Guedan, A., Rogers, A. V., Walton, R., Johnston, S. L. and Solari, R. (2014a) Human rhinovirus 16 causes Golgi apparatus fragmentation without blocking protein secretion. *J Virol*, **88**, 11671-85.
- Mousnier, A., Swieboda, D., Pinto, A., Guedán, A., Rogers, A. V., Walton, R., Johnston, S. L. and Solari, R. (2014b) Human rhinovirus 16 causes Golgi apparatus fragmentation without blocking protein secretion. *J Virol*, **88**, 11671-85.
- Munger, J., Bennett, B. D., Parikh, A., Feng, X. J., McArdle, J., Rabitz, H. A., Shenk, T. and Rabinowitz, J. D. (2008) Systems-level metabolic flux profiling identifies fatty acid synthesis as a target for antiviral therapy. *Nat Biotechnol*, **26**, 1179-86.
- Nakamura, N., Wei, J. H. and Seemann, J. (2012) Modular organization of the mammalian Golgi apparatus. *Curr Opin Cell Biol*, **24**, 467-74.
- Nateri, A. S., Hughes, P. J. and Stanway, G. (2000) In vivo and in vitro identification of structural and sequence elements of the human parechovirus 5' untranslated region required for internal initiation. *J Virol*, **74**, 6269-77.
- Nayak, D. P., Balogun, R. A., Yamada, H., Zhou, Z. H. and Barman, S. (2009) Influenza virus morphogenesis and budding. *Virus Res*, **143**, 147-61.
- Nchoutmboube, J. A., Viktorova, E. G., Scott, A. J., Ford, L. A., Pei, Z., Watkins, P. A., Ernst, R. K. and Belov, G. A. (2013) Increased long chain acyl-Coa synthetase activity and fatty acid import is linked to membrane synthesis for development of picornavirus replication organelles. *PLoS Pathog*, **9**, e1003401.
- Nyquist, H. (1928) Certain topics in telegraph transmission theory. *American Institute of Electrical Engineers*, **47**, 617-44.
- Obara B, Jabeen A, Fernandez N and Laissue PP (2013) A novel method for quantified, superresolved, three-dimensional colocalisation of isotropic, fluorescent particles, *Histochem Cell Biol*, **139**, 391-402.
- Odendall, C. and Kagan, J. C. (2013) Peroxisomes and the antiviral responses of mammalian cells. *Subcell Biochem*, **69**, 67-75.
- Ohta, A. and Nishiyama, Y. (2011) Mitochondria and viruses. *Mitochondrion*, **11**, 1-12.
- Palmenberg, A., Neubauer, D. and Skern, T. (2010) Genome Organization and Encoded Proteins. *The Picornaviruses*. In: Ehrenfeld, E., Esteban, D., Roos, R.P. (Eds.), *The Picornaviruses*. ASM Press, Washington, DC, 3-17.
- Pan, X., Wilson, M., McConville, C., Arvanitis, T. N., Kauppinen, R. A. and Peet, A. C. (2012) The size of cytoplasmic lipid droplets varies between tumour cell lines of the nervous system: a 1H NMR spectroscopy study. *Magma*, **25**, 479-85.
- Pelletier, J. and Sonenberg, N. (1988) Internal initiation of translation of eukaryotic mRNA directed by a sequence derived from poliovirus RNA. *Nature*, **334**, 320-25.
- Perera, R., Riley, C., Isaac, G., Hopf-Jannasch, A. S., Moore, R. J., Weitz, K. W., Pasa-Tolic, L., Metz, T. O., Adamec, J. and Kuhn, R. J. (2012) Dengue Virus Infection Perturbs Lipid Homeostasis in Infected Mosquito Cells. *PLoS Pathog*, **8**, e1002584.
- Perttilä, J., Spuul, P. and Ahola, T. (2013) Early secretory pathway localization and lack of processing for hepatitis E virus replication protein pORF1. *J Gen Virol*, **94**, 807-16.
- Pestova, T. V., Hellen, C. U. and Shatsky, I. N. (1996) Canonical eukaryotic initiation factors determine initiation of translation by internal ribosomal entry. *Mol Cell Biol*, **16**, 6859-69.
- Pfister, T., Jones, K. W. and Wimmer, E. (2000) A Cysteine-Rich Motif in Poliovirus Protein 2CATPase Is Involved in RNA Replication and Binds Zinc In Vitro. *J Virol*, **74**, 334-43.
- Piccone, M. E., Rieder, E., Mason, P. W. and Grubman, M. J. (1995) The foot-and-mouth disease virus leader proteinase gene is not required for viral replication. *J Virol*, **69**, 5376-82.

- Pierini, R., Cottam, E., Roberts, R. and Wileman, T. (2009) Modulation of membrane traffic between endoplasmic reticulum, ERGIC and Golgi to generate compartments for the replication of bacteria and viruses. *Semin Cell Dev Biol*, **20**, 828-33.
- Poh, M. K., Shui, G., Xie, X., Shi, P. Y., Wenk, M. R. and Gu, F. (2012) U18666A, an intra-cellular cholesterol transport inhibitor, inhibits dengue virus entry and replication. *Antiviral Res*, **93**, 191-8.
- Pol, A., Gross, S. P. and Parton, R. G. (2014) Review: biogenesis of the multifunctional lipid droplet: lipids, proteins, and sites. *J Cell Biol*, **204**, 635-46.
- Potze, L., Mullauer, F. B., Colak, S., Kessler, J. H. and Medema, J. P. (2014) Betulinic acid-induced mitochondria-dependent cell death is counterbalanced by an autophagic salvage response. *Cell Death Dis*, **5**, e1169.
- Poulin, F. and Sonenberg, N. (2000) Mechanism of translation initiation in eukaryotes.
- Quiner, C. A. and Jackson, W. T. (2010) Fragmentation of the Golgi apparatus provides replication membranes for human rhinovirus 1A. *Virology*, **407**, 185-95.
- Rasmussen, A. L., Diamond, D. L., McDermott, J. E., Gao, X., Metz, T. O., Matzke, M. M., Carter, V. S., Belisle, S. E., Korth, M. J., Waters, K. M., Smith, R. D. and Katze, M. G. (2011) Systems virology identifies a mitochondrial fatty acid oxidation enzyme, dodecenoyl coenzyme A delta isomerase, required for hepatitis C virus replication and likely pathogenesis. *J Virol*, **85**, 11646-54.
- Raychaudhuri, S. and Prinz, W. A. (2008) Nonvesicular phospholipid transfer between peroxisomes and the endoplasmic reticulum. *Proc Natl Acad Sci U S A*, **105**, 15785-90.
- Reid, C. R., Airo, A. M. and Hobman, T. C. (2015) The Virus-Host Interplay: Biogenesis of +RNA Replication Complexes. *Viruses*, **7**, 4385-413.
- Reiss, S., Rebhan, I., Backes, P., Romero-Brey, I., Erfle, H., Matula, P., Kaderali, L., Poenisch, M., Blankenburg, H., Hiet, M.-S., Longerich, T., Diehl, S., Ramirez, F., Balla, T., Rohr, K., Kaul, A., Bühler, S., Pepperkok, R., Lengauer, T., Albrecht, M., Eils, R., Schirmacher, P., Lohmann, V. and Bartenschlager, R. (2011) Recruitment and activation of a lipid kinase by hepatitis C virus NS5A is essential for integrity of the membranous replication compartment. *Cell Host Microbe*, **9**, 32-45.
- Richards, A. L., Soares-Martins, J. A., Riddell, G. T. and Jackson, W. T. (2014) Generation of unique poliovirus RNA replication organelles. *MBio*, **5**, e00833-13.
- Rightsel, W. A., Dice, J. R., Mc, A. R., Timm, E. A., Mc, L. I., Jr., Dixon, G. J. and Schabel, F. M., Jr. (1961) Antiviral effect of guanidine. *Science*, **134**, 558-9.
- Robenek, H., Hofnagel, O., Buers, I., Robenek, M. J., Troyer, D. and Severs, N. J. (2006) Adipophilin-enriched domains in the ER membrane are sites of lipid droplet biogenesis. *J Cell Sci*, **119**, 4215-24.
- Romero-Brey, I. and Bartenschlager, R. (2016) Endoplasmic Reticulum: The Favorite Intracellular Niche for Viral Replication and Assembly. *Viruses*, **8**, 160-86.
- Rossmann, M. G. (2002) Picornavirus structure overview. In Semler B, Wimmer E (ed), *Molecular Biology of Picornavirus*. ASM Press, Washington, DC. 27-38.
- Rossmann, M. G., He, Y. and Kuhn, R. J. (2002) Picornavirus-receptor interactions. *Trends Microbiol*, **10**, 324-31.
- Saka, H. A. and Valdivia, R. (2012) Emerging roles for lipid droplets in immunity and host-pathogen interactions. *Annu Rev Cell Dev Biol*, **28**, 411-37.
- Salimi, A. (2015) *Investigation of the Localization and Role in Replication of Parechovirus Non-structural Proteins*. dissertation.: University of Essex.
- Salonen, A., Ahola, T. and Kääriäinen, L. (2005) Viral RNA Replication in Association with Cellular Membranes. *Curr Top Microbiol Immuno* **285**, 139-73.
- Sasaki, J., Ishikawa, K., Arita, M. and Taniguchi, K. (2012) ACBD3-mediated recruitment of PI4KB to picornavirus RNA replication sites. *EMBO J*, **31**, 754-66.
- Schlegel, A., Giddings, T. H., Ladinsky, M. S. and Kirkegaard, K. (1996) Cellular origin and ultrastructure of membranes induced during poliovirus infection. *J Virol*, **70**, 6576-88.
- Schlegel, R., Tralka, T. S., Willingham, M. C. and Pastan, I. (1983) Inhibition of VSV binding and infectivity by phosphatidylserine: is phosphatidylserine a VSV-binding site? *Cell*, **32**, 639-46.

- Schwarz, D. S. and Blower, M. D. (2016) The endoplasmic reticulum: structure, function and response to cellular signaling. *Cell Mol Life Sci*, **73**, 79-94.
- Seipelt, J., Guarne, A., Bergmann, E., James, M., Sommergruber, W., Fita, I. and Skern, T. (1999) The structures of picornaviral proteinases. *Virus Res*, **62**, 159-68.
- Seitsonen, J., Susi, P., Heikkilä, O., Sinkovits, R. S., Laurinmäki, P., Hyypia, T. and Butcher, S. J. (2010) Interaction of alphaVbeta3 and alphaVbeta6 integrins with human parechovirus 1. *J Virol*, **84**, 8509-19.
- Seo, J. Y., Yaneva, R., Hinson, E. R. and Cresswell, P. (2011) Human cytomegalovirus directly induces the antiviral protein viperin to enhance infectivity. *Science*, **332**, 1093-7.
- Shang, L., Xu, M. and Yin, Z. (2013) Antiviral drug discovery for the treatment of enterovirus 71 infections. *Antiviral Res*, **97**, 183-94.
- Shannon, C. E. (1949) Communication in the presence of noise. *Proceedings of the IRE*, **37**, 10-21.
- Sharp, T. M., Guix, S., Katayama, K., Crawford, S. E. and Estes, M. K. (2010) Inhibition of cellular protein secretion by norwalk virus nonstructural protein p22 requires a mimic of an endoplasmic reticulum export signal. *PLoS One*, **5**, e13130.
- Shim, A., Song, J.-H., Kwon, B.-E., Lee, J.-J., Ahn, J.-H., Kim, Y.-J., Rhee, K.-J., Chang, S.-Y., Cha, Y. and Lee, Y.-S. (2016) Therapeutic and prophylactic activity of itraconazole against human rhinovirus infection in a murine model. *Scientific reports*, **6**.
- Sieczkarski, S. B. and Whittaker, G. R. (2002) Dissecting virus entry via endocytosis. *J Gen Virol*, **83**, 1535-45.
- Stanway, G. (2013) Molecular biology and classification of enteroviruses. *Diabetes and Viruses*. Springer.
- Stanway, G. and Hyypia, T. (1999) Parechoviruses. *J Virol*, **73**, 5249-5254.
- Stanway, G., Joki-Korpela, P. and Hyypia, T. (2000) Human parechoviruses—biology and clinical significance. *Rev Med Virol*, **10**, 57-69.
- Stanway, G., Kalkkinen, N., Roivainen, M., Ghazi, F., Khan, M., Smyth, M., Meurman, O. and Hyypia, T. (1994) Molecular and biological characteristics of echovirus 22, a representative of a new picornavirus group. *J Virol*, **68**, 8232-38.
- Stephens, D. J., Lin-Marq, N., Pagano, A., Pepperkok, R. and Paccard, J.-P. (2000) COPI-coated ER-to-Golgi transport complexes segregate from COPII in close proximity to ER exit sites. *J Cell Sci*, **113**, 2177-85.
- Strating, J. R., van der Linden, L., Albulescu, L., Bigay, J., Arita, M., Delang, L., Leyssen, P., van der Schaar, H. M., Lanke, K. H., Thibaut, H. J., Ulferts, R., Drin, G., Schlinck, N., Wubbolts, R. W., Sever, N., Head, S. A., Liu, J. O., Beachy, P. A., De Matteis, M. A., Shair, M. D., Olkkonen, V. M., Neyts, J. and van Kuppeveld, F. J. (2015) Itraconazole inhibits enterovirus replication by targeting the oxysterol-binding protein. *Cell Rep*, **10**, 600-15.
- Suhy, D. A., Giddings, T. H., Jr. and Kirkegaard, K. (2000) Remodeling the endoplasmic reticulum by poliovirus infection and by individual viral proteins: an autophagy-like origin for virus-induced vesicles. *J Virol*, **74**, 8953-65.
- Suzuki, M., Shinohara, Y., Ohsaki, Y. and Fujimoto, T. (2011) Lipid droplets: size matters. *J Electron Microsc (Tokyo)*, **60 Suppl 1**, S101-16.
- Sweeney, T. R., Cisnetto, V., Bose, D., Bailey, M., Wilson, J. R., Zhang, X., Belsham, G. J. and Curry, S. (2010) Foot-and-mouth disease virus 2C is a hexameric AAA+ protein with a coordinated ATP hydrolysis mechanism. *J Biol Chem*, **285**, 24347-59.
- Syed, G. H., Amako, Y. and Siddiqui, A. (2010) Hepatitis C virus hijacks host lipid metabolism. *Trends in Endocrinology & Metabolism*, **21**, 33-40.
- Szul, T., Grabski, R., Lyons, S., Morohashi, Y., Shestopal, S., Lowe, M. and Sztul, E. (2007) Dissecting the role of the ARF guanine nucleotide exchange factor GBF1 in Golgi biogenesis and protein trafficking. *J Cell Sci*, **120**, 3929-40.
- Szul, T. and Sztul, E. (2011) COPII and COPI traffic at the ER-Golgi interface. *Physiology (Bethesda)*, **26**, 348-64.
- Takano, T., Tsukiyama-Kohara, K., Hayashi, M., Hirata, Y., Satoh, M., Tokunaga, Y., Tateno, C., Hayashi, Y., Hishima, T., Funata, N., Sudoh, M. and Kohara, M. (2011) Augmentation of DHCR24 expression by hepatitis C virus infection facilitates viral replication in hepatocytes. *J Hepatol*, **55**, 512-21.

- Tanaka, T., Kuroda, K., Ikeda, M., Wakita, T., Kato, N. and Makishima, M. (2013) Hepatitis C virus NS4B targets lipid droplets through hydrophobic residues in the amphipathic helices. *J Lipid Res*, **54**, 881-92.
- Teoule, F., Brisac, C., Pelletier, I., Vidalain, P. O., Jegouic, S., Mirabelli, C., Bessaud, M., Combelas, N., Autret, A., Tangy, F., Delpeyroux, F. and Blondel, B. (2013) The Golgi protein ACBD3, an interactor for poliovirus protein 3A, modulates poliovirus replication. *J Virol*, **87**, 11031-46.
- Teterina, N. L., Gorbalenya, A. E., Egger, D., Bienz, K. and Ehrenfeld, E. (1997) Poliovirus 2C protein determinants of membrane binding and rearrangements in mammalian cells. *J Virol*, **71**, 8962-72.
- Teterina, N. L., Gorbalenya, A. E., Egger, D., Bienz, K., Rinaudo, M. S. and Ehrenfeld, E. (2006) Testing the modularity of the N-terminal amphipathic helix conserved in picornavirus 2C proteins and hepatitis C NS5A protein. *Virology*, **344**, 453-67.
- Teterina, N. L., Kean, K. M., Gorbalenya, A. E., Agol, V. I. and Girard, M. (1992) Analysis of the functional significance of amino acid residues in the putative NTP-binding pattern of the poliovirus 2C protein. *J Gen Virol*, **73**, 1977-86.
- Teterina, N. L., Pinto, Y., Weaver, J. D., Jensen, K. S. and Ehrenfeld, E. (2011) Analysis of poliovirus protein 3A interactions with viral and cellular proteins in infected cells. *J Virol*, **85**, 4284-96.
- Tuthill, T. J., GropPELLI, E., Hogle, J. M. and Rowlands, D. J. (2010) Picornaviruses. *Curr Top Microbiol Immunol*, **343**, 43-89.
- Ulferts, R., de Boer, S.M., van der Linden, L., Bauer, L., Lyoo, H.R., Maté, M.J., Lichière, J., Canard, B., Lelieveld, D., Omta, W. and Egan, D., 2016. Screening of a Library of FDA-Approved Drugs Identifies Several Enterovirus Replication Inhibitors That Target Viral Protein 2C. *Antimicrob Agents Chemother*, **60**, 2627-38.
- van der Linden, L., Wolthers, K. C. and van Kuppeveld, F. J. (2015) Replication and Inhibitors of Enteroviruses and Parechoviruses. *Viruses*, **7**, 4529-62.
- van der Schaar, H. M., Dorobantu, C. M., Albulescu, L., Strating, J. R. and van Kuppeveld, F. J. (2016) Fat (al) attraction: picornaviruses usurp lipid transfer at membrane contact sites to create replication organelles. *Trends Microbiol*, **24**, 535-46.
- van der Schaar, H. M., Leyssen, P., Thibaut, H. J., de Palma, A., van der Linden, L., Lanke, K. H., Lacroix, C., Verbeken, E., Conrath, K., Macleod, A. M., Mitchell, D. R., Palmer, N. J., van de Poel, H., Andrews, M., Neyts, J. and van Kuppeveld, F. J. (2013) A novel, broad-spectrum inhibitor of enterovirus replication that targets host cell factor phosphatidylinositol 4-kinase IIIbeta. *Antimicrob Agents Chemother*, **57**, 4971-81.
- van Kuppeveld, F., van den Hurk, P., van der Vliet, W., Galama, J. and Melchers, W. (1997a) Chimeric coxsackie B3 virus genomes that express hybrid coxsackievirus-poliovirus 2B proteins: functional dissection of structural domains involved in RNA replication. *J Gen Virol*, **78**, 1833-40.
- van Kuppeveld, F. J., Hoenderop, J. G., Smeets, R. L., Willems, P. H., Dijkman, H. B., Galama, J. M. and Melchers, W. J. (1997b) Coxsackievirus protein 2B modifies endoplasmic reticulum membrane and plasma membrane permeability and facilitates virus release. *EMBO J*, **16**, 3519-3532.
- van Meer, G. (2001) Caveolin, Cholesterol, and Lipid Droplets? *J Cell Biol*, **152**, 29-34.
- Vázquez-Calvo, Á., Caridi, F., González-Magaldi, M., Saiz, J.-C., Sobrino, F. and Martin-Acebes, M. A. (2016) The Amino Acid Substitution Q65H in the 2C Protein of Swine Vesicular Disease Virus Confers Resistance to Golgi Disrupting Drugs. *Front Microbiol*, **7**, 612-23.
- Viktorova, E. G., Nchoutmboube, J., Ford-Siltz, L. A. and Belov, G. A. (2015) Cell-specific establishment of poliovirus resistance to an inhibitor targeting a cellular protein. *J Virol*, **89**, 4372-86.
- Vogt, D. A., Camus, G., Herker, E., Webster, B. R., Tsou, C. L., Greene, W. C., Yen, T. S. and Ott, M. (2013) Lipid droplet-binding protein TIP47 regulates hepatitis C Virus RNA replication through interaction with the viral NS5A protein. *PLoS Pathog*, **9**, e1003302.
- Walther, T. C. and Farese, R. V., Jr. (2012) Lipid droplets and cellular lipid metabolism. *Annu Rev Biochem*, **81**, 687-714.
- Wang, C. (2012) Functional analysis of poliovirus protein 2CATPase in viral RNA replication and encapsidation using alanine scanning mutagenesis. Doctoral dissertation, The Graduate School, Stony Brook University: Stony Brook, NY.

- Wang, C., Shan, T., Zheng, H., Tong, W., Chen, F., Hu, H., He, Q. and Tong, G. (2012a) Complete genome sequence of a novel human parechovirus. *J Virol*, **86**, 11945-6.
- Wang, J., Wu, Z. and Jin, Q. (2012b) COPI is required for enterovirus 71 replication. *PLoS One*, **7**, e38035.
- Wang, X., Ren, J., Gao, Q., Hu, Z., Sun, Y., Li, X., Rowlands, D. J., Yin, W., Wang, J., Stuart, D. I., Rao, Z. and Fry, E. E. (2015) Hepatitis A virus and the origins of picornaviruses. *Nature*, **517**, 85-8.
- Wanga, Q. M. and Chen, S. H. (2007) Human rhinovirus 3C protease as a potential target for the development of antiviral agents. *Curr Protein Pept Sci*, **8**, 19-27.
- Watson, P. and Stephens, D. J. (2005) ER-to-Golgi transport: form and formation of vesicular and tubular carriers. *Biochim Biophys Acta*, **1744**, 304-15.
- Wessels, E., Duijsings, D., Lanke, K. H., van Dooren, S. H., Jackson, C. L., Melchers, W. J. and van Kuppeveld, F. J. (2006) Effects of picornavirus 3A Proteins on Protein Transport and GBF1-dependent COP-I recruitment. *J Virol*, **80**, 11852-60.
- Whitton, J. L., Cornell, C. T. and Feuer, R. (2005) Host and virus determinants of picornavirus pathogenesis and tropism. *Nature Reviews Microbiology*, **3**, 765-776.
- Wilfling, F., Thiam, A. R., Olarte, M.-J., Wang, J., Beck, R., Gould, T. J., Allgeyer, E. S., Pincet, F., Bewersdorf, J. and Farese, R. V. (2014) Arf1/COPI machinery acts directly on lipid droplets and enables their connection to the ER for protein targeting. *Elife*, **3**, e01607.
- Williams, C. H., Kajander, T., Hyypia, T., Jackson, T., Sheppard, D. and Stanway, G. (2004) Integrin alpha v beta 6 is an RGD-dependent receptor for coxsackievirus A9. *J Virol*, **78**, 6967-73.
- Williams, C. H., Panayiotou, M., Girling, G. D., Peard, C. I., Oikarinen, S., Hyoty, H. and Stanway, G. (2009) Evolution and conservation in human parechovirus genomes. *J Gen Virol*, **90**, 1702-12.
- Wolins, N. E., Rubin, B. and Brasaemle, D. L. (2001) TIP47 associates with lipid droplets. *J Biol Chem*, **276**, 5101-8.
- Woo, P. C., Lau, S. K., Choi, G. K., Huang, Y., Teng, J. L., Tsoi, H.-W., Tse, H., Yeung, M. L., Chan, K.-H. and Jin, D.-Y. (2012) Natural occurrence and characterization of two internal ribosome entry site elements in a novel virus, canine picodistrovirus, in the picornavirus-like superfamily. *J Virol*, **86**, 2797-08.
- Xia, H., Wang, P., Wang, G. C., Yang, J., Sun, X., Wu, W., Qiu, Y., Shu, T., Zhao, X., Yin, L., Qin, C. F., Hu, Y. and Zhou, X. (2015) Human Enterovirus Nonstructural Protein 2CATPase Functions as Both an RNA Helicase and ATP-Independent RNA Chaperone. *PLoS Pathog*, **11**, e1005067.
- Yin, J., Liu, Y., Wimmer, E. and Paul, A. V. (2007) Complete protein linkage map between the P2 and P3 non-structural proteins of poliovirus. *J Gen Virol*, **88**, 2259-67.
- Ypma-Wong, M. F., Dewalt, P. G., Johnson, V. H., Lamb, J. G. and Semler, B. L. (1988) Protein 3CD is the major poliovirus proteinase responsible for cleavage of the P1 capsid precursor. *Virology*, **166**, 265-270.
- Zehmer, J. K., Huang, Y., Peng, G., Pu, J., Anderson, R. G. and Liu, P. (2009) A role for lipid droplets in inter-membrane lipid traffic. *Proteomics*, **9**, 914-21.
- Zhang, J., Diaz, A., Mao, L., Ahlquist, P. and Wang, X. (2012) Host acyl coenzyme A binding protein regulates replication complex assembly and activity of a positive-strand RNA virus. *J Virol*, **86**, 5110-21.
- Zuo, J., Kye, S., Quinn, K. K., Cooper, P., Damoiseaux, R. and Krogstad, P. (2016) Discovery of Structurally Diverse Small-Molecule Compounds with Broad Antiviral Activity against Enteroviruses. *Antimicrob Agents Chemother*, **60**, 1615-26.